MONASH University

Cellular and molecular basis of atmospheric hydrogen and carbon monoxide oxidation in mycobacteria

Paul Rodrigo Fule Cordero

B.Sc. Microbiology and M.Sc. Microbiology

University of Santo Tomas, Philippines

A thesis submitted for the degree of Doctor of Philosophy at

Monash University in 2020

School of Biological Sciences, Faculty of Science

Copyright notice

'I dedicate this thesis

to my mother, who taught me

resilience and determination

and

to my grandmother, who taught me

kindness and compassion'

Abstract

Mycobacteria are known for their ability to survive nutrient limitation by oxidizing atmospheric trace gases. In the genetically tractable soil actinobacterium *Mycobacterium smegmatis*, atmospheric H_2 oxidation has been extensively studied and the role of this process is now largely understood. H_2 oxidation in this organism is mediated by two uptake hydrogenases Huc and Hhy. These enzymes are upregulated during organic carbon limitation and enhance the survival of this organism. Despite this progress, it remains unclear how energy is conserved from H_2 oxidation and how the uptake hydrogenases are regulated. By contrast to H_2 oxidation, the physiological role of atmospheric CO oxidation in mycobacteria is unknown. It has been reported in other organisms that the enzyme mediating this process is upregulated during nutrient starvation. However, it has not yet been genetically or biochemically proven that atmospheric CO supports survival.

To address these knowledge gaps, this thesis investigated the following questions: (i) how are the uptake hydrogenases and H_2 oxidation integrated with the mycobacterial respiratory chain?; (ii) what roles do putative iron-sulfur proteins HucE and HhyE play in H_2 oxidation and mycobacterial survival?; (iii) how is H_2 uptake metabolism by Huc regulated?; and (iv) what is the physiological role of atmospheric CO oxidation in mycobacteria? These research questions will be addressed separately in four data chapters.

In the first results chapter, it is shown that although both Huc and Hhy mediate the oxidation of H_2, these enzymes have distinct roles in persistence and differentially interact with the respiratory chain. Whereas Huc is most active during the transition between exponential and stationary phase, Hhy is employed to scavenge atmospheric H_2 upon exhaustion of carbon sources, supporting long-term persistence. The electrons derived from the H_2 oxidation by both enzymes are transferred to the electron transport chain via the menaquinone pool. However, the uptake hydrogenases interact differentially with the terminal oxidases. Huc preferentially donates electrons to the cytochrome *bcc-aa*$_3$ complex, while Hhy donates electrons to both the cytochrome *bcc-aa*$_3$ and cytochrome *bd* complexes. In turn, atmospheric H_2 oxidation in the respiratory chain helps maintain proton-motive force when organic energy sources are limiting.

Following the findings from the previous chapter, it is unclear whether the electrons from H_2 oxidation are directly transferred to the menaquinone pool or via other physiological redox partners. The second data chapter reports two putative iron-sulfur proteins, HucE and HhyE, serve as potential redox partners of the uptake hydrogenases. HucE and HhyE are important

in the H$_2$ oxidation activities of Huc and Hhy, respectively, and both putative iron-sulfur proteins are integral for mycobacterial persistence. Deletion of *hucE* and *hhyE* resulted in the abolishment of hydrogenase activities and impaired the long-term survival of *M. smegmatis*. Considering their essentiality in H$_2$ oxidation, HucE and HhyE could serve as conduits between the hydrogenases and the menaquinone.

The regulation of Huc is studied in the third results chapter. This chapter shows that Huc is regulated via catabolite repression, mediated by the glycerol-responsive transcriptional regulator GylR. The absence of a functional GylR, either via a knockdown or a frameshift mutation, resulted in increased production and activity of Huc. This strongly suggests that GylR represses *huc* expression when the preferred energy substrate glycerol is abundant. However, electrophoretic mobility shift assays show that GylR does not bind to the *huc* promoter, indicating an indirect repression via a downstream regulator. Investigating the downstream regulator will be key to further our understanding of Huc regulation. Nevertheless, these findings show that H$_2$ metabolism is directly controlled by organic carbon levels and in turn energy availability.

Finally, the physiological role of mycobacterial CO oxidation was determined. The fourth data chapter reports that a form I CO-dehydrogenase is the sole CO-oxidizing enzyme in *M. smegmatis*. The synthesis of CO dehydrogenase is induced by organic carbon starvation and the enzyme enables aerobic respiration of atmospheric CO. Atmospheric CO oxidation also enhances survival, as indicated by the finding that the deletion of CO dehydrogenase reduced the survival of carbon-starved cells. With this, a persistence-centric model is proposed, where atmospheric CO is oxidized to provide energy during persistence in mycobacteria. The form I CO-dehydrogenase is found in diverse soil and marine bacteria, which may also use atmospheric CO to sustain persistence.

This thesis provides a comprehensive understanding of the biochemical and physiological basis of trace gas oxidation in mycobacteria, with significant ecological and medical implications. It adds to growing evidence that atmospheric H$_2$ and CO can be dependable energy sources for microorganisms living in nutrient-limited environments. These organisms can upregulate their hydrogenases and CO dehydrogenases in response to organic carbon starvation. In such conditions, the electrons provided by the oxidation of atmospheric trace gases can be used in the respiratory chain to help conserve energy for persistence. Likewise, mycobacterial pathogens may enhance their survival in host tissues by utilizing H$_2$ and CO. The findings in this thesis can provide a better understanding of how mycobacteria persist during latent infection and how we can better combat mycobacterial diseases.

Publications during enrolment

Published papers

- **Cordero PRF** & Bayly K, Leung PM, Huang C, Islam ZF, Schittenhelm RB, King GM, Greening C. (2019). Atmospheric carbon monoxide oxidation is a widespread mechanism supporting microbial survival. *The ISME Journal*, 13(11), 2868-2881.

- **Cordero PRF**, Grinter R, Hards K, Cryle MJ, Warr CG, Cook GM, Greening C. (2019). Two uptake hydrogenases differentially interact with the aerobic respiratory chain during mycobacterial growth and persistence. *Journal of Biological Chemistry*, 294(50), 18980-18991.

- Islam ZF & **Cordero PRF**, Greening C. (2019). Putative iron-sulfur proteins are required for hydrogen consumption and enhance survival of mycobacteria. *Frontiers in Microbiology*, 10(2749), 1-10.

- Islam ZF, **Cordero PRF**, Feng J, Chen Y, Bay SK, Gleadow RM, Jirapanjawat T, Gleadow RM, Carere CR, Stott MB, Chiri E, Greening C. (2019). Two Chloroflexi classes independently evolved the ability to persist on atmospheric hydrogen and carbon monoxide. *The ISME Journal*, 13(7), 1801-1813.

- Grinter R, Ney B, Brammananth R, Barlow C., **Cordero PRF**, Gillett DL, Izoré T, Cryle MJ, Harold LK, Cook GM, Taiaroa G, Williamson DA, Warden AC, Oakeshott JG, Taylor MC, Crellin PK, Jackson CJ, Schittenhelm RB, Coppel RL, Greening C. (2020). Cellular and structural basis of synthesis of the unique intermediate dehydro-F420-0 in mycobacteria. *mSystems*, 5(3), 1–14.

Manuscript in revision/preparation

- Bayly K & **Cordero PRF**, Huang C, Schittenhelm RB, Grinter R, Greening C. (2020). Mycobacteria tolerate carbon monoxide by remodeling their respiratory chain (in revision).

- **Cordero PRF**, Kropp A, Huang C, Schittenhelm RB, Grinter R, Greening C. (2020). Mycobacterial hydrogen metabolism is regulated by catabolite repression (in preparation).

Thesis including published works declaration

I hereby declare that this thesis contains no material which has been accepted for the award of any other degree or diploma at any university or equivalent institution and that, to the best of my knowledge and belief, this thesis contains no material previously published or written by another person, except where due reference is made in the text of the thesis.

This thesis includes three original papers published in peer reviewed journals. The core theme of the thesis is on the cellular and molecular basis of atmospheric trace gas oxidation in mycobacteria. The ideas, development and writing up of all the papers in the thesis were the principal responsibility of myself, the student, working within the School of Biological Sciences, Faculty of Science under the supervision of Associate Professor Chris Greening.

The inclusion of co-authors reflects the fact that the work came from active collaboration between researchers and acknowledges input into team-based research.

In the case of chapters 2, 3, 4, and 5, my contribution to the work involved the following:

Thesis Chapter	Publication Title	Status	Nature and % of student contribution	Co-author name(s) Nature and % of Co-author's contribution*	Co-author(s), Monash student Y/N*
2	Two uptake hydrogenases differentially interact with the aerobic respiratory chain during mycobacterial growth and persistence	Published	80% - design and execution of experiments, data analysis, writing draft, editing manuscript	1. Rhys Grinter – 6% - data analysis, writing draft, editing manuscript 2. Kiel Hards – 1% - provided reagents and tools 3. Max J. Cryle – 1% - supervision 4. Coral G. Warr – 1% - supervision 5. Gregory M. Cook – 1% - provided reagents and tools 6. Chris Greening – 10%, conceptualization, design, supervision, data analysis, writing	1-6 – No

				draft, editing manuscript	
3	Putative iron-sulfur proteins are required for hydrogen consumption and enhance survival of mycobacteria	Published	50% - design and execution of experiments, data analysis, writing draft, editing manuscript	1. Zahra F. Islam – 40% - design and execution of experiments, data analysis, writing draft, editing manuscript 2. Chris Greening - 10% - conceptualization, design, supervision, data analysis, editing manuscript	1 – Yes 2 – No
4	Mycobacterial hydrogen metabolism is regulated by catabolite repression	In preparation	70% - conceptualization, design and execution of experiments, data analysis, writing draft, editing manuscript	1. Ashleigh Kropp – 10% - design and execution of experiments 2. Cheng Huang – 3% - execution of experiments, data analysis 3. Ralf B. Schittenhelm – 1% 4. Rhys Grinter – 6% - conceptualization, design, data analysis 5. Chris Greening – 10% - conceptualization, design, supervision, data analysis, editing manuscript	1-5 – No
5	Atmospheric carbon monoxide oxidation is a widespread mechanism supporting microbial survival	Published	50% - design and execution of experiments, supervision of KB, data analysis, writing draft, editing manuscript	1. Katherine Bayly – 30% - execution of experiments, data analysis 2. Pok Man Leung – 5% - data analysis 3. Cheng Huang – 2% - execution of experiments, data analysis 4. Zahra F. Islam – 1% - provided reagents and tools	1,2,4 – Yes 3,5,6,7 – No

| | | | | 5. Ralf B. Schittenhelm – 1% - provided reagents and tools
6. Gary M. King – 1% - data analysis
7. Chris Greening – 10% - conceptualization, design, supervision, data analysis, editing manuscript | |

I have renumbered sections of submitted or published papers in order to generate a consistent presentation within the thesis.

Student name: Paul Rodrigo F. Cordero

Student signature: **Date:** 30/11/2020

I hereby certify that the above declaration correctly reflects the nature and extent of the student's and co-authors' contributions to this work. In instances where I am not the responsible author I have consulted with the responsible author to agree on the respective contributions of the authors.

Main Supervisor name: Associate Professor Chris Greening

Main Supervisor signature: **Date:** 30/11/2020

Acknowledgments

I am deeply thankful to my supervisor, Associate Professor Chris Greening, for the unwavering support throughout my PhD journey. He has always been a wonderful mentor who taught me to become a better researcher and provided me with great constructive feedbacks, moral and professional support during my presentations, and a source of motivation through tough times. I thank him for introducing me to various research collaborations and encouraging me to participate in scientific conferences, which helped me expand my knowledge and be integrated with the scientific community. He has been most instrumental for my development as a scientist; for this, I am tremendously grateful.

I am also very thankful to Associate Professor Max J. Cryle and Professor Coral G. Warr, who both co-supervised me and gave me invaluable advice in my research. My gratitude also extends to Dr. Rhys Grinter, whom I also consider a mentor and who helped me refine techniques in protein biochemistry. I also thank Professor Gregory M. Cook for the intellectual discussions and generously hosting my research visit in his lab in Otago, NZ, as well as Dr. Kiel Hards for teaching me how to use the microelectrode H_2 sensor. I also want to thank my PhD panel chair, Associate Professor Robert Bryson-Richardson, as well as panel members Dr. Jeremy Barr and Dr. Matthew Piper, for overseeing my milestone reviews and providing wonderful feedback to my research and professional development.

My PhD studies would not be possible without the financial support through a scholarship. I would like to thank Monash University for awarding me the following scholarships: Faculty of Science Dean's Postgraduate Research Scholarship (stipend) and Dean's International Postgraduate Research Scholarship (tuition and insurance) during my initial year of enrolment and Monash Graduate Scholarship for the subsequent years.

My research projects will also not be successful without the technical help of various researchers. I would like to thank our lab manager Thanavit (Tent) Jirapanjawat for his technical expertise and for overseeing the day-to-day operations of the lab which has been vital for the success of our experiments; Ashleigh Kropp for providing assistance in protein biochemistry experiments; Dr. Ralf B. Schittenhelm and Dr. Cheng (Enzo) Huang for their expertise in proteomics and mass spectrometry; Zahra F. Islam, Pok Man (Bob) Leung, Katherine Bayly, and David Gillett for amazing collaborations; and the members of the Greening lab for their camaraderie and creating a warm and positive workplace.

Finally, I am incredibly grateful to my family who has always been there in all of my endeavours, including my taking a PhD. I am thankful to my two wonderful sisters, Maria Pauline F. Cordero and Maria Pola C. Sevilla, who have been a great source of inspiration and most supportive; my mother, Gina F. Fule, who is a source of courage and has been most understanding; my grandmother, Susan F. Fule, who brings much joy and a source of wisdom; and my father, Pablito A. Cordero, Jr., who taught me humility and patience. Thank you very much.

Table of Contents

List of Tables

List of Figures

Abbreviations

ΔpH	chemical gradient component of PMF
$\Delta\psi$	electrical potential component of PMF
µg	microgram
µL	microliter
µM	micromolar
ACN	Acetonitrile
ADP	Adenosine diphosphate
ANOVA	Analysis of variance
ATP	Adenosine triphosphate
cAMP	3′,5′-cyclic Adenosine monophosphate
CBB	Calvin-Benson-Bassham cycle
CFU	Colony forming unit
CO	carbon monoxide
CRISPRi	Clustered Regularly Interspaced Short Palindromic Repeats interference
CRP	cAMP receptor protein
C_t	Cycle threshold
cyclic di-GMP	bis-(3′,5′)-cyclic dimeric Guanosine monophosphate
DEPC	Diethyl pyrocarbonate
e^-	electron
EMSA	Electrophoretic mobility shift assay
EPR	Electron paramagnetic resonance
FAD	Flavin adenine dinucleotide
fmol	femtomole
H^+	proton
H_2	molecular hydrogen
HdB	Hartmans de Bont minimal medium
HQNO	*N*-oxo-2-heptyl-4-hydroxyquinoline
kDa	Kilodalton
K_m	Michaelis constant, an index of enzyme affinity
LB	Lysogeny broth
mA	milliampere
mL	milliliter
MQ	Menaquinone
MQH_2	Menaquinol

MS	mass spectrometry
mV	millivolt
NAD^+	Nicotinamide adenine dinucleotide, oxidized form
NADH	NAD, reduced form
NBT	Nitroblue tetrazolium chloride
ng	nanogram
nM	nanomolar
PBS	Phosphate-buffered saline
PMF	Proton motive force
ppbv	parts per billion by volume
ppmv	parts per million by volume
qRT-PCR	Reverse transcriptase - quantitative polymerase chain reaction
rpm	Revolutions per minute
SDS-PAGE	Sodium dodecyl sulfate - polyacrylamide gel electrophoresis
sgRNA	single-guide ribonucleic acid
TCA	Tricarboxylic acid cycle
Tg	teragram
V	Volt
V_{max}	Maximum velocity, an index of enzyme reaction rate

Chapter 1

Introduction

1.1 Biogeochemical cycling of trace gases

This thesis focuses on mycobacterial metabolism of two trace gases, hydrogen (H_2) and carbon monoxide (CO). Biogeochemical cycles control the atmospheric consumption and production of H_2 and CO. It has recently been recognized that soil bacteria, including mycobacteria, contribute to these cycles by consuming these gases to sub-atmospheric levels.

1.1.1 Hydrogen

The global atmospheric hydrogen budget has been investigated since the 1970s, though the organisms and enzymes responsible for consuming atmospheric H_2 have only recently been identified [1–3]. Molecular hydrogen has a current atmospheric mixing ratio of 531 ppbv, with an estimated annual production between 76 and 107 Tg [4–6]. The atmospheric H_2 burden (i.e. total amount of a gas in the atmosphere) is ~155 Tg, and given that the total annual loss of H_2 is estimated to be 79 Tg, H_2 molecules are rapidly turned over with an average lifetime of about 2 years [4, 6]. This global H_2 budget is accountable to various geochemical, anthropogenic, and biological processes (**Figure 1.1**).

The largest sources of H_2 produced in the atmosphere are from geochemical processes and human activities, which account for around 90% of the total annual H_2 yield [4, 6]. Biological H_2 emission from soil and ocean contributes to a fraction of the global H_2 pool. On the other hand, soil accounts for about 80% of the annual atmospheric H_2 consumption globally and this has been attributed to microbial activities [4, 6, 7]. H_2-oxidizing bacteria must have adequately low thresholds (< 0.53 ppmv) and high affinities (K_m < 100 nM) to be able to consume H_2 at atmospheric concentrations [7, 8]. Conrad suggested that H_2 uptake activity is mostly due to cell-free soil hydrogenases (Conrad & Seiler, 1981). However, this notion has recently been overturned with the confirmation that some soil bacteria, including *Streptomyces avermitilis*, *Rhodococcus equi*, and *Mycobacterium smegmatis*, exhibit high affinity for H_2 [10–12]. These

microorganisms encode high-affinity hydrogenases, which are synthesized and active when they enter dormant states. The work of Greening and colleagues provided the first genetic confirmation of high-affinity hydrogenase activity (8, 11). The biochemical basis of this high-affinity hydrogenase activity is still unresolved. Investigating this will help define and understand the role of soil bacteria and their high-affinity hydrogenases in the biogeochemical cycle of H_2.
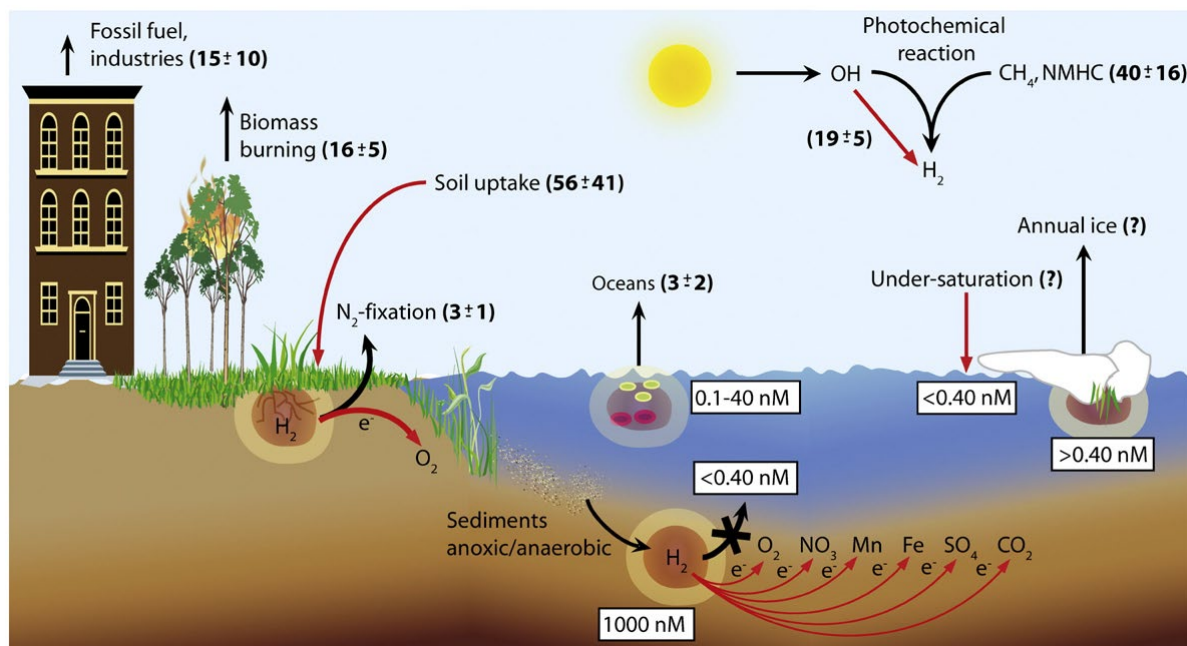
Figure 1.1. Biogeochemical cycle of atmospheric H_2. The diagram illustrates the different sources (black arrow) and sinks (red arrow) of H_2. The numbers represent the amount of H_2 produced and consumed each year in Tg (4); diagram adapted from (7).

1.1.2 Carbon monoxide

Carbon monoxide (CO) is one of the most abundant trace gases in the atmosphere. Every year, it is estimated that about 2600 Tg of CO is emitted globally (13). The concentration of CO varies spatially and temporally but on average, it has an atmospheric concentration of 90 ppbv (13).

Like atmospheric H_2, the global emission and consumption of atmospheric CO is mediated by various sources and sinks (**Figure 1.2**). Of the total CO emitted annually, about 60% comes from human activities while the remainder is accountable to natural processes (13). The anthropogenic sources of CO have been increasing over the years which can have broader environmental implications (14–16). These include motor vehicle combustion, other combustion of fossil fuels, and slash and burn deforestation, among others (14–16). The majority, about 85%, of the emitted CO is removed from the atmosphere by its reaction with OH radicals (13, 17). This is an important role of CO in tropospheric chemistry as it regulates OH radical levels in the atmosphere and it is estimated to remove more OH than methane does globally (18, 19). About 5% of the total CO emissions diffuse to the upper layer of the atmosphere (20). The remaining 10% or about 250 Tg of CO produced globally is taken up in the soil through microbial CO oxidation (13, 21). Microbial CO oxidizers directly remove CO from the atmosphere in soils in a process mediated by the enzyme form I carbon monoxide dehydrogenase (19). However, the physiological role of carbon monoxide dehydrogenase and atmospheric CO oxidation remains unclear.
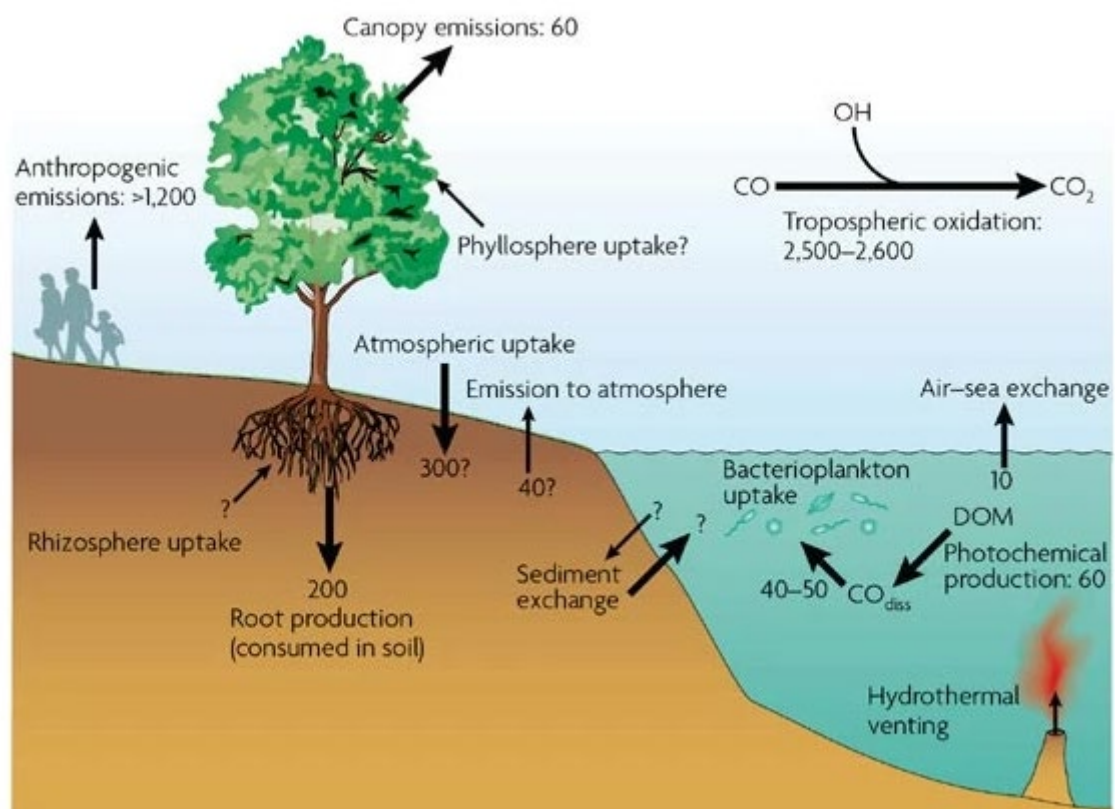
Figure 1.2. Biogeochemical cycle of atmospheric CO. The diagram illustrates various sources (production) and sinks (uptake) of CO. The numbers represent the amount of CO produced or consumed in Tg yr^{-1} (13); diagram adapted from (19).

1.2 Aerobic metabolism of trace gas in microorganisms

1.2.1 Aerobic hydrogen metabolism

Aerobic hydrogen-oxidizing bacteria, also known as "Knallgas" bacteria, utilize H_2 as an energy source through the oxyhydrogen reaction:

$$2 H_2 + O_2 \rightarrow 2 H_2O$$
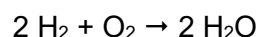
The first part of the reaction, which is catalyzed by various [NiFe]-hydrogenases, produces low-potential electrons (22). These electrons can be used for aerobic respiration and carbon fixation in many microorganisms (8, 23, 24).

Some aerobic bacteria grow chemolithoautotrophically on H_2 (22, 24). They use H_2 as source of energy and electrons, O_2 as the terminal electron acceptor, and CO_2 as source of carbon (22). Studies on pure cultures have shown that chemolithoautotrophy using H_2 can be an obligate trait (e.g. *Hydrogenobacter thermophilus* and *Hydrogenovibrio marinus*) (25, 26) or a facultative trait (e.g. *Bradyrhizobium japonicum* and *Rhodobacter capsulatus*) (27, 28). In some bacteria such as *Ralstonia eutropha*, H_2 can be co-metabolized with organic carbon for mixotrophic growth (22). In addition, studies on microbial communities lacking photosynthetic primary producers have shown the potential use of atmospheric H_2 to sustain chemolithoautotrophy (29, 30). In these environments, microbial communities in soil aerobically scavenge atmospheric concentrations of H_2, as well as CO, and mediate chemosynthetic fixation of atmospheric CO_2. These communities encode the high-affinity group 1h [NiFe]-hydrogenase (**see section 1.3.1**), type IE RuBisCO, and form I [MoCu]-carbon monoxide dehydrogenase (**see section 1.4.1**), which are determinants of trace gas

metabolism (29). Additionally, the group 2a [NiFe]-hydrogenase (**see section 1.3.1**) may also play a significant role in mediating atmospheric H_2 oxidation during mixotrophic growth (31).

Aside from supporting growth, an increasing number of studies show that H_2 can be used for microbial persistence (11, 12, 32–34). Upon depletion of organic electron donors, aerobic soil saprophytes scavenge atmospheric gases, including H_2, as energy source (8). These include microorganisms from phyla Acidobacteria, Actinobacteria, Chloroflexi, and Verrucomicrobia (11, 32, 33, 35). Respirometry studies have shown that H_2 oxidation in persisting cells is linked to the aerobic respiratory chain with O_2 as the terminal electron acceptor (11, 32). However, it is yet to be determined if the electrons from atmospheric H_2 oxidation are transferred to the respiratory chain. In addition, it has been consistently shown that high-affinity hydrogenases play an important role in microbial persistence (11, 33, 35). Previous studies report that high-affinity hydrogenases are upregulated during nutrient limitation and oxidation of atmospheric H_2 enhances long-term survival of mycobacteria and streptomycetes during starvation and hypoxia (11, 12, 34, 36). However, it remains unclear how high-affinity hydrogenases are integrated into the respiratory chain of such organisms and in turn how bacteria survive using atmospheric H_2.

1.2.2   Aerobic carbon monoxide metabolism

CO is a highly toxic gas for animals due to its ability to bind and inhibit enzymes of the respiratory chain (37, 38). However, for many microorganisms, CO can be a dependable source of energy. With a standard redox potential of -540 mV, CO provides extremely low potential electrons, making it an ideal energy source for CO-oxidizing bacteria (39). This group of microorganisms possesses form I [MoCu]-CO dehydrogenase that oxidizes CO to CO_2 in the following reaction (40).

$$CO + H_2O \rightarrow CO_2 + 2\ H^+ + 2\ e^-$$

Microorganisms can effectively harness the energy from this ubiquitous trace gas (19, 37). In oxygen-rich environments, taxonomically diverse bacteria can utilize CO both as energy and carbon source at elevated concentrations (19). This group of bacteria, referred to as carboxydotrophs, oxidize CO to yield electrons and CO_2. In the carboxydotroph *Oligotropha carboxidovorans*, the derived electrons reduce quinones and are likely relayed to CO-intensive terminal oxidases to reduce O_2 (41, 42). The electrons derived from CO oxidation can also be used to support CO_2 fixation into biomass via the Calvin-Benson-Bassham (CBB) cycle (43).

However, many aerobic CO-oxidizing bacteria are incapable of carboxydotrophic growth and instead are organoheterotrophs that use CO as a supplemental energy source (19, 44–46). For these carboxydovores, CO serves as an electron donor for the aerobic respiratory chain and they are adapted to oxidize CO at low concentrations (e.g. atmospheric levels) (19). It remains unclear how the electrons derived from CO oxidation are utilized by carboxydovores as there are only a limited number of studies in these microorganisms (44–47). Similar to H_2, the electrons derived from atmospheric CO oxidation may be used to maintain energy conservation during organic carbon starvation (19). However, it remains to be experimentally determined whether atmospheric CO oxidation can support microbial persistence.

1.2.3 Enzymes for H_2 and CO metabolism

Hydrogenase. The biological conversion of molecular hydrogen into electrons and protons, and its reverse reaction, is catalyzed by hydrogenases. These enzymes are categorized into three types, which have evolved independently to catalyze the same reaction: [NiFe]-hydrogenases, [FeFe]-hydrogenases, and [Fe]-hydrogenases (24, 48).

The most widely distributed type of hydrogenases, which can be found in almost every bacterial and archaeal phylum, are the [NiFe]-hydrogenases (49). They are commonly found in heterodimeric form wherein the large subunit contains the catalytic [NiFe] center, which is coordinated to cysteine residues, CO, and CN^- ligands (**Figure 1.3a**). The small subunit

usually harbors three iron-sulfur clusters, which conduct electrons between the catalytic center and the physiological redox partner of the hydrogenase. Another type of hydrogenases is the [FeFe]-hydrogenases, which are common in fermentative bacteria and are the only known type of hydrogenase found in eukaryotes to date. This group of hydrogenases is known to be highly sensitive to O_2 and has low substrate affinity but rapid turnover. The core domain of this hydrogenase, called the H-cluster, contains the [FeFe] metal center and a 4Fe-4S cluster bound to one of the irons of the metal center via a sulfhydryl bridge (**Figure 1.3b**). Like in [NiFe]-hydrogenases, in a remarkable example of convergent evolution, the catalytic metal center of [FeFe]-hydrogenases is coordinated to CO and CN^- ligands. (22, 24, 48, 50). The third type of hydrogenases are the [Fe]-hydrogenases. Originally discovered from *Methanothermobacter marburgensis* and only found in methanogens to date (49–51), this hydrogenase harbors no iron-sulfur cluster and has an Fe-guanylylpyrodinol (Fe-GP) cofactor in the catalytic center (**Figure 1.3c**). It catalyzes a reversible dehydrogenation of methylenetetrahydromethanopterin (methylene-H_4MPT), which serves as an intermediate during methanogenesis (51).
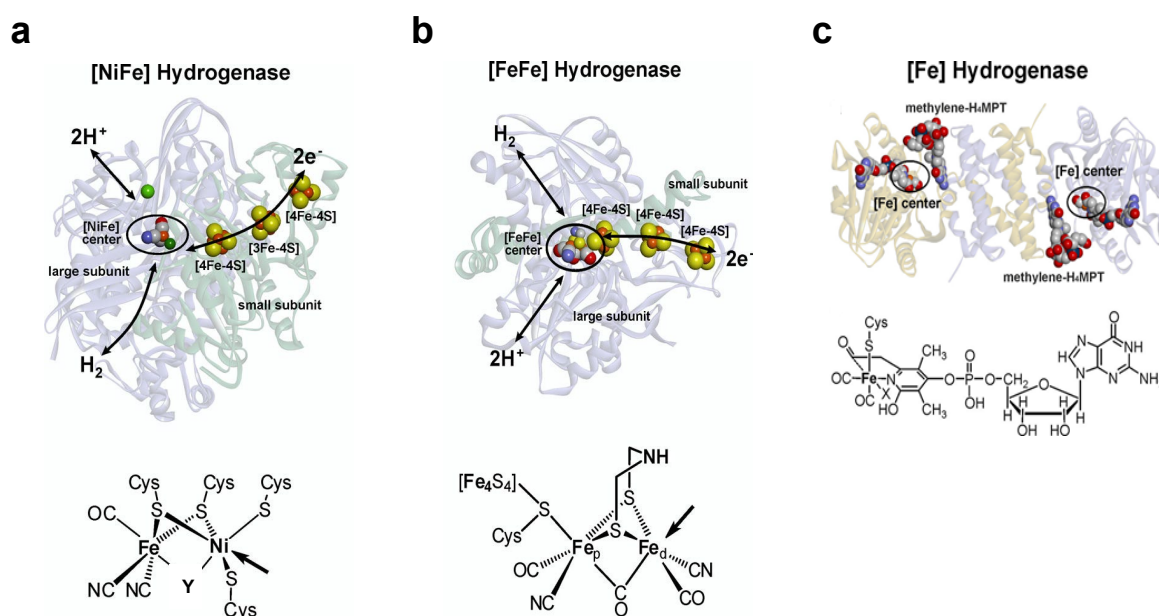
Figure 1.3. Representative structures of the three types of hydrogenases: a) [NiFe]-hydrogenase from *Desulfovibrio vulgaris*, **b)** [FeFe]-hydrogenase from *D. desulfuricans*, and **c)** [Fe]-hydrogenase from *Methanocaldococcus jannaschii.* The metallic catalytic centers

(encircled) are found buried deep in the enzyme. In **a)** [NiFe]-hydrogenase and **b)** [FeFe]-hydrogenase, shown are the iron-sulfur clusters (yellow and orange spheres) and the pathways for H_2 and proton transfer (green sphere is Mg^{2+}). Below the enzymes are the chemical structures of their active sites; the bridging ligand is marked by "Y" and the open metal coordination site are indicated by an arrow. The structure of the **c)** dimeric [Fe]-hydrogenase is depicted with the substrate, methylene-H4MPT. At the bottom is the chemical structure of the Fe-GP cofactor and the possible H_2-binding site is marked as "X". Adapted from (48).

Carbon monoxide dehydrogenase. CO dehydrogenase is the enzyme that catalyzes the oxidation of carbon monoxide (19). Both aerobic and anaerobic variants of this enzyme exist that differ in their metal ion center (19, 40, 52). In addition, they differ in their stability in air and the ability to reduce CO_2 (52).

The aerobic CO dehydrogenase contains a binuclear Mo–Cu center in which the Cu is ligated to a cofactor in the active site via a thiol group (**Figure 1.4a**) (53). This enzyme is a heterotrimer with two iron-sulfur clusters, a flavin adenine dinucleotide (FAD), and a molybdopterin cytosine dinucleotide cofactor (MCD) (53). [MoCu]-CO dehydrogenase is stable in air and is linked to the aerobic respiratory chain (19, 42, 53). Found in both carboxydotrophs and carboxydovores, the primary function of this enzyme is to liberate electrons from CO for the purpose of aerobic respiration and sometimes carbon fixation (19, 53, 54). By contrast, the anaerobic CO dehydrogenase has a Ni–Fe center in the active site and is extremely O_2-sensitive (52). This enzyme occurs either as mono-, bi-, or multifunctional complexes. The mono-functional [NiFe]-CO dehydrogenase has an exclusive function of oxidizing CO, while both the bi- and multifunctional complexes can additionally synthesize acetyl-CoA as part of supercomplexes with acetyl-CoA synthase (55–57). Through the Wood-Ljungdahl pathway, hydrogenotrophic methanogens and acetogens use the CO dehydrogenase unit of the complex to reduce CO_2 to CO (58–60). The CO is then utilized by acetyl-CoA synthase to produce acetyl-CoA, which can serve as precursor for other biosynthetic pathways (59, 60). CO can also be directly assimilated to acetyl-CoA and used

for carbon fixation when provided as sole carbon source (60, 61). [NiFe]-CO dehydrogenase typically has homodimeric subunits with the catalytic site containing a $[NiFe_4S_4]$-cluster (**Figure 1.4b**) (55). The cluster is a distorted heterocubane attached *in exo* to Fe(II). The Fe(II) ion is coordinated by a hydroxyl ligand in the state that is reactive with CO (62, 63).

a

b
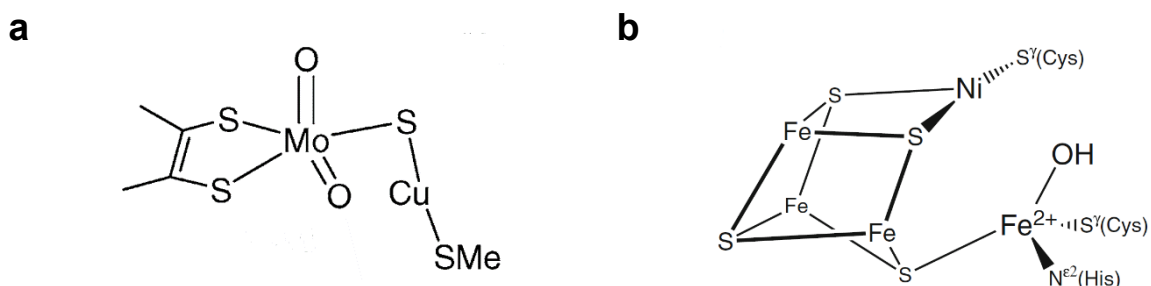
Figure 1.4. Metal center of the CO dehydrogenase active sites. a) Catalytic metal center of [MoCu]-CO dehydrogenase showing a µ-sulfido bond that bridges Mo and Cu. **b)** Catalytic center of [NiFe]-CO dehydrogenase depicting a heterocubane structure. Adapted from (55, 64).

1.2.4 Regulation of H_2 and CO metabolism

The expression of uptake hydrogenases is controlled by various signals and regulators. One way that microorganisms regulate hydrogenases is by sensing H_2. This involves regulatory hydrogenases that sense elevated concentrations of H_2 and activate a two-component system that activates the expression of uptake hydrogenase genes (65–68). In *R. eutropha*, this H_2-dependent expression of hydrogenase genes is mediated by three components: 1) the DNA-binding positive regulator HoxA, 2) histidine protein kinase HoxJ, and 3) the regulatory hydrogenase HoxBC (22, 66, 69, 70). In the absence of H_2, HoxJ auto-phosphorylates via its C-terminal kinase domain and transfers the phosphate group to response regulator HoxA (66). This renders HoxA inactive. When H_2 is present at elevated levels, it is detected by HoxBC, which then interacts with HoxJ via transfer of electrons to the N-terminal PAS domain of HoxJ (71). This interaction blocks the phosphoryl transfer from HoxJ to HoxA. The HoxA, in its non-phosphorylated form, activates the transcription of uptake hydrogenases (66, 69). A similar

regulatory system involving H_2 sensing is also employed by organisms such as *Rhodopseudomonas palustris*, *Rhodobacter capsulatus*, and *Bradyrhizobium japonicum* (65, 67, 72).

Another signal that is used for regulation of hydrogenase is O_2. For instance in *B. japonicum*, low oxygen tension activates the expression of hydrogenase through a series of signal transduction (68, 73, 74). Low O_2 levels are detected by the heme-binding domain of the transmembrane sensor FixL (73). This then triggers auto-phosphorylation of FixL at its C-terminal kinase followed by a phosphoryl transfer to FixJ. The phosphorylated FixJ activates the expression of *fixK2* and the product serves as an activator for the transcription of hydrogenase structural genes (75). Other organisms regulate expression of hydrogenase genes in response to O_2 level via the fumarate and nitrate reduction regulatory (FNR) protein that has an O_2-sensory and a regulatory DNA-binding domain (76–78). In *Enterobacteriaceae*, FNR activates *hya* and *hyb* expression during anaerobiosis, while *Thiocapsa roseopersicina* uses an FNR homolog to activate expression of hydrogenase genes (78–80). Two-component systems that respond to cellular redox state also regulates the expression of the genes encosing hydrogenases in some bacteria. For example, in *R. capsulatus*, RegB/RegA serves as a global redox regulator that prevents the cell from encountering reductive stress by regulating genes involved in lowering reductant levels (81). RegA is a transcriptional regulator that binds to the promoter of the hydrogenase gene operon and directly represses its expression (82). In *M. smegmatis*, expression of two hydrogenases is induced under hypoxia by the redox- and oxygen-sensing *dos* system (83, 84).

The availability of organic carbon sources also plays a part in regulating uptake hydrogenases. In previous studies on *Salmonella enterica*, the expression of the uptake hydrogenase 2 is repressed by glucose (80, 85). This is mediated by cAMP receptor protein (CRP) and in the absence of glucose, cAMP-CRP complex is formed and serves as an activator for the expression of hydrogenase 2 (85, 86). Similarly in *Escherichia coli*, catabolite repression by

glucose regulates the hydrogenase 2 (*hyb* operon), with the cAMP-CRP complex serving as an indirect regulator for the activation of the *hyb* operon expression (87). Additionally, expression of its hydrogenase 1 (*hya*) is also induced by carbon starvation where SigS transcription factor is instrumental in the induction of *hya* operon during carbon starvation (88, 89). *M. smegmatis* may also be employing catabolite repression to control the synthesis of its uptake hydrogenases. It has been previously shown that its hydrogenases are upregulated during carbon starvation and are highly active in the stationary phase (11, 36, 83). *M. smegmatis* may therefore directly regulate these hydrogenases in response to the availability of organic substrate. In these previous studies, glycerol is used as sole carbon source and may serve as a signal molecule that could repress the expression of hydrogenase genes. Studies are therefore needed to elucidate what role glycerol and catabolite repression play in regulating mycobacterial uptake hydrogenases, including which regulators are used to control the expression of hydrogenase genes.

With the aerobic CO dehydrogenase, little is known about its regulation. There is, however, evidence of a persistence-linked upregulation of this enzyme during carbon source depletion, as reported in five different bacteria (33, 36, 90–92). In addition, ecological studies using microbial communities have shown that CO is rapidly oxidized in ecosystems with low levels of organic carbon (29, 93, 94). Inferring from these findings, it is compelling to hypothesize that carbon availability may also play a role in the regulation of CO dehydrogenase. Studies are needed to determine the signals and regulators that control expression of this enzyme.

1.3   [NiFe]-Hydrogenase

1.3.1 Classification

The early classification by Vignais and co-workers identifies major lineages of [NiFe]-hydrogenases, but the recent work of Greening and co-workers reveals a more diverse classification of these hydrogenases (24, 49). Genomic and metagenomic surveys expand the

classification of [NiFe]-hydrogenases into 22 subgroups, which reflect the variety of their functions (**Figure 1.5**) (49). Two of these subgroups are the focus of much of this thesis, the group 1h and group 2a [NiFe]-hydrogenases, also known as Hhy and Huc hydrogenases.

Several lines of evidence show the group 1h [NiFe]-hydrogenases (Hhy; formerly group 5 [NiFe]-hydrogenases) have a significant role in the biogeochemical H_2 cycle and are the primary enzymatic mediators of atmospheric H_2 oxidation. Cellular studies indicate that, in contrast to other [NiFe]-hydrogenases, this enzyme has an exceptionally high affinity for H_2 ($K_{m(app)}$ of < 50 nM) (8, 11, 83, 95, 96). The kinetics of oxidation of atmospheric H_2 is near-identical between soil isolates harboring group 1h [NiFe]-hydrogenase and whole soil itself (96). Furthermore, it has been demonstrated that axenic soil with inoculated *Streptomyces* sp. PCB7 can oxidize atmospheric H_2 at a similar rate with that of the crude enzyme extract of the microorganism (95). Finally, in *M. smegmatis*, it has been demonstrated that knocking out the group 1h [NiFe]-hydrogenase limits atmospheric H_2 uptake (11). Genomic and metagenomic studies show these enzymes are ubiquitously distributed in soil environments and soil bacteria (8, 49, 95, 96). Group 2a [NiFe]-hydrogenases (Huc) are also widely distributed (31, 49). This group has originally been associated with Cyanobacteria where it is used to oxidize the H_2, which is a by-product of nitrogen fixation in diazotrophs (22, 97–99). However, a recent study reports that this group is much more broadly distributed, can mediate atmospheric H_2 oxidation in *M. smegmatis* (11), and supports mixotrophic growth of the carbon-fixing strains (31).
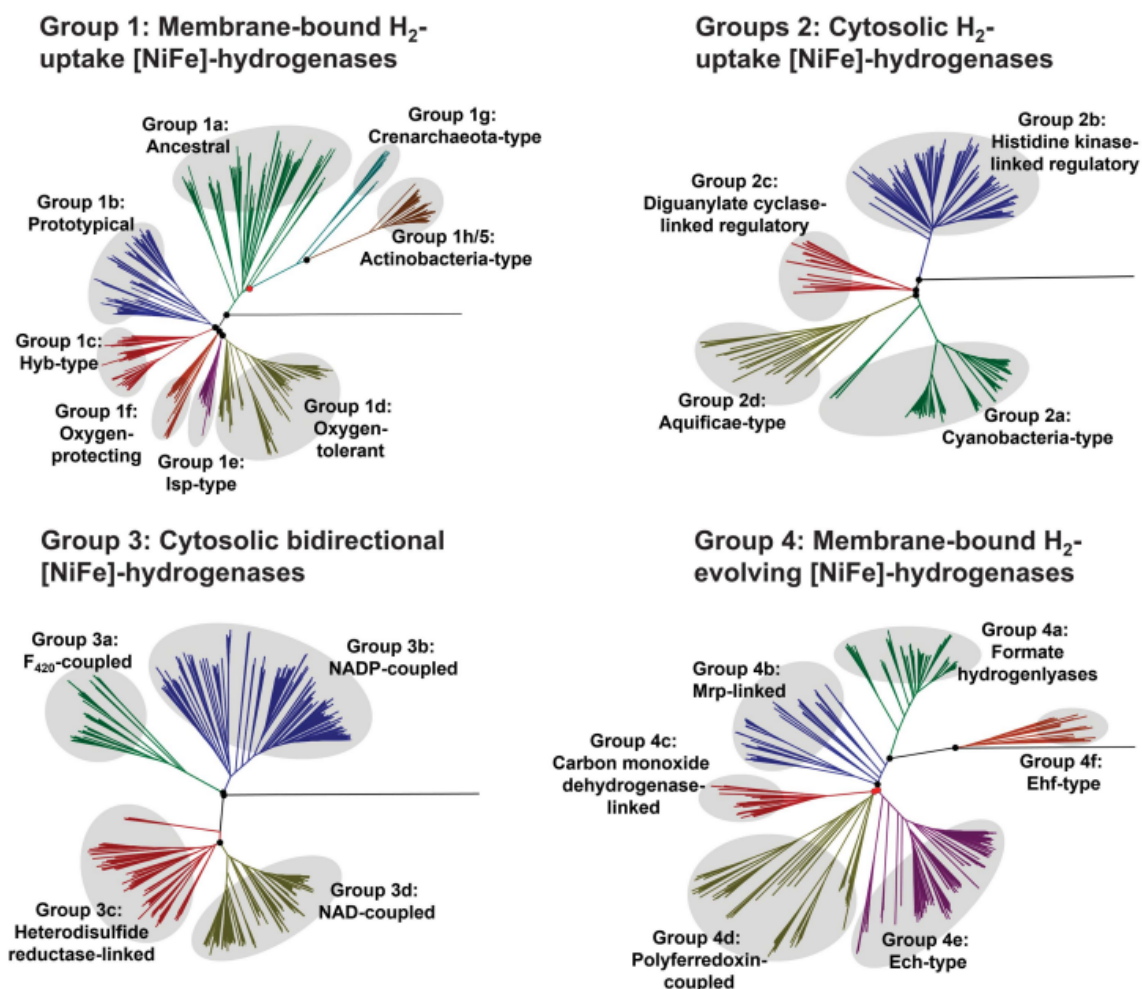
Figure 1.5. Phylogeny and classification of [NiFe]-hydrogenases with 22 distinct clades.

The expanded classification scheme has also revealed unexpected diversity of O_2-tolerant [NiFe]-hydrogenases. Oxygen-tolerant uptake hydrogenases include the groups 1d, 1h, and 2a [NiFe]-hydrogenases (100). Phylogenetic analysis has shown that these enzymes diverged from the deep-rooted oxygen-sensitive hydrogenases, suggesting that the divergence happened during the oxygenation of the Earth's atmosphere (49). There is evidence that multiple O_2-sensitive [NiFe]-hydrogenases convergently evolved into oxygen-tolerant variants and this, in turn, suggests that they have independently developed distinct mechanisms for O_2 tolerance (49).

1.3.2 Structure and catalysis

Crystal structures of many [NiFe]-hydrogenases have been solved and these give insight into the overall basic module and mechanism of the enzyme (101–110). The enzyme typically assembles as a heterodimer with the large subunit having a molecular mass of about 60 kDa and the small subunit with around 30 kDa. Each subunit contains cofators essential for catalysis and together they form an active [NiFe]-hydrogenase (48).
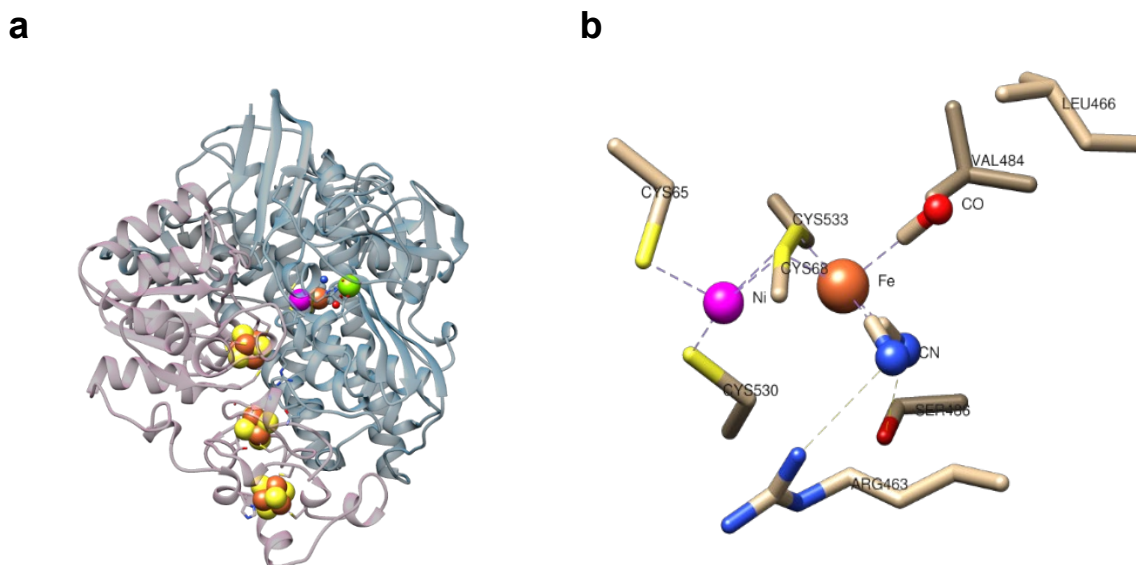
Figure 1.6. [NiFe]-hydrogenase from *D. gigas* (PDB entry 2FRV). a) Overall structure of the enzyme containing the catalytic [NiFe] center and a Mg for the proton transfer pathway in the large subunit (pale blue ribbons) and the iron-sulfur clusters in the small subunit (pale pink ribbons). **b)** The catalytic [NiFe] center coordinates to four cysteine residues and the iron coordinates to two CN and one CO. Figures are prepared using Chimera (University of California, San Francisco, USA).

In hydrogen-uptake metabolism, molecular hydrogen enters the enzyme via a gas channel (111). This channel is composed of hydrophobic amino acid residues that are traversed by the non-polar H_2 towards the catalytic center (112). The large subunit houses the catalytic site composed of a [NiFe]-cofactor (**Figure 1.6b**) (110). Three non-protein diatomic ligands are additionally coordinated to Fe: one CO ligand surrounded by hydrophobic amino acids and two CN^- ligands that form H-bonds to neighboring arginine and serine residues (102, 105, 110). These non-protein ligands have been postulated to maintain the redox state of Fe during

the catalytic cycle and serve as electron sinks during electron transfer (**Figure 1.6b**) (102). During the catalytic cycle, H_2 is heterolytically cleaved into H^+ and H^-. The [NiFe] metal center in active reduced state (Ni-R) (**Figure 1.7**) carries the H^- in the bridge between Ni(II) and Fe(II) and the H^+ is attached to a sulfur of the terminal Cys546, as illustrated in the subatomic resolution X-ray crystal structure of [NiFe]-hydrogenase of *Desulfovibrium vulgaris* Miyazaki F (113). Regeneration to the inactive oxidized state (Ni-A and Ni-B) is essential to enable the metal center to accept new H_2 to oxidize. This occurs when electrons in the hydride are transferred to the iron-sulfur electron transport system in the small subunit and the protons are released to the molecular surface (114, 115).
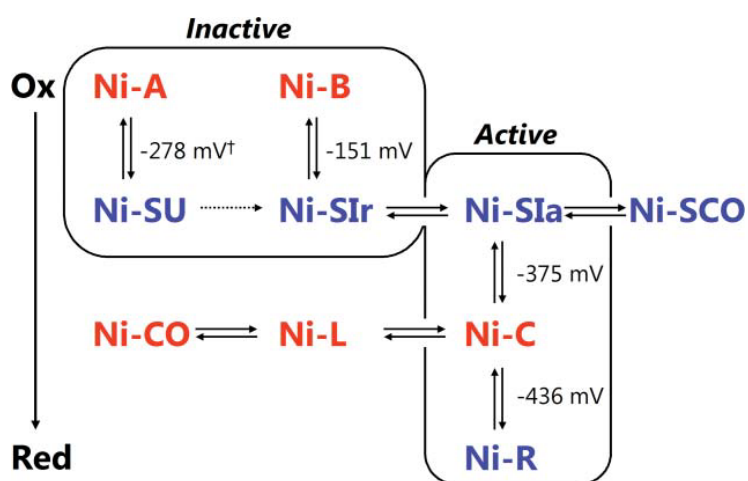
Figure 1.7. Different redox changes of the Ni center during the catalytic cycle. The EPR-detectable states and the EPR-silent states are shown in red and blue, respectively. Both Ni-A and Ni-B are in oxidized inactive states and do not participate in the catalytic cycle. Sequential one-electron reductions by external reducing agents lead to EPR-silent Ni-S forms which eventually results in the formation of the catalytically active Ni-C state. Ni-A (unready state), Ni-B (ready state), Ni-SU (EPR-silent unready state), Ni-SIr (EPR-silent ready state), Ni-SIa (EPR-silent active state), Ni-SCO (EPR-silent CO inhibited state), Ni-C (EPR-detectable reduced state), Ni-L (Light induced state), Ni-CO (EPR-detectable CO inhibited state), and Ni-R (EPR-silent reduced state), Adapted from (116).

After H_2 is split into protons and electrons, the electrons pass through a series of electron transport systems in the small subunit, which is comprised of three iron-sulfur [FeS] clusters situated proximally, medially, and distally to the [NiFe] center (**Figure 1.8a**) (103, 117). Variations from these compositions exist and, in some [NiFe]-hydrogenases, the composition of the proximal iron-sulfur cluster is thought to confer oxygen tolerance (101, 106, 107). The distal iron-sulfur cluster holds a coordination motif, usually 1His-3Cys, that enables the electron to be finally transferred to an external electron acceptor (118). The protons are believed to be transferred to the enzyme surface through a proton pathway at the C-terminal end of the large subunit, wherein a magnesium ion, internal water molecules, glutamate, and histidine residues are proposed to form the pathway (**Figure 1.8B**) (102, 103, 119).

a

b
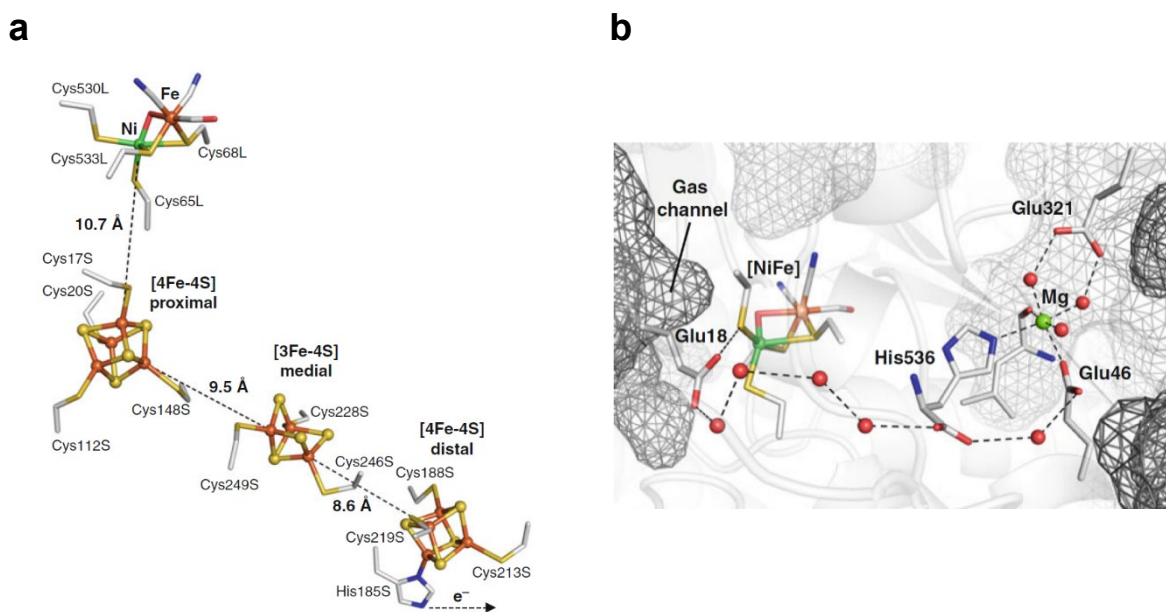
Figure 1.8. Pathways of the electrons and protons in the hydrogenase. a) Electron transfer pathway from the [NiFe] active site to the iron-sulfur clusters with the shortest distance. **b)** Putative proton transfer pathway in [NiFe]-hydrogenase of *D. gigas* through Mg^{2+}, GLU46, and GLU321 (pathway is indicated by dashed lines and water molecules are shown as red spheres). Adapted from (22).

1.3.3 Oxygen tolerance

Most [NiFe]-hydrogenases are inactivated by oxygen. In the presence of O_2, the active site is oxidized giving rise to a mixture of two inactive states, which depends on the nature of the oxygen ligand bridging the Ni and Fe in the active site; these inactive states are Ni-A (unready state, with possibly a peroxide-species bridging ligand) and Ni-B (ready state, with possibly a hydroxide bridging ligand) (116). These inactive forms of the catalytic site can be reactivated by exposure to H_2, wherein enzymes in the Ni-B state can be readily reactivated in a few seconds while the Ni-A state requires longer activation times of up to hours (116). For a hydrogenase to function in the presence of O_2, it is important that the Ni-A state is not formed and to continuously remove the oxygen species in the Ni-B state (120). These features can be found in O_2-tolerant [NiFe]-hydrogenases, which function in mixtures of H_2 and O_2 (22, 120).

Several studies have elucidated different mechanisms of O_2 tolerance in [NiFe]-hydrogenase. One mechanism has been ascribed to the structure of the proximal iron-sulfur cluster, which differs from that of the O_2-sensitive [NiFe]-hydrogenases (101, 106, 107, 121). O_2-sensitive [NiFe]-hydrogenases, such as groups 1a and 1b, typically have a proximal 4Fe-4S cluster coordinated to four cysteine residues (117, 122) (**Figure 1.9a, b**). By contrast, many characterized O_2-tolerant hydrogenases have varying composition and coordination of the proximal iron-sulfur cluster. This has been extensively studied in group 1d hydrogenases using electrochemical, spectroscopic, and structural techniques. The group 1d membrane-bound hydrogrnase (MBH) of *R. eutropha* has a unique proximal iron-sulfur cluster having 4Fe-3S composition coordinated to six cysteines (**Figure 1.9c**); this serves as an electronic switch wherein it functions as an electron acceptor when H_2 enters the active site and as an electron donor when O_2 is present (101). The cluster reductively detoxifies O_2 with four electrons and protons to water, thereby rapidly reactivating the [NiFe]-center from exposure to O_2 (101, 107). Thus, this enzyme is remarkably both a hydrogen oxidase and an oxygen reductase.
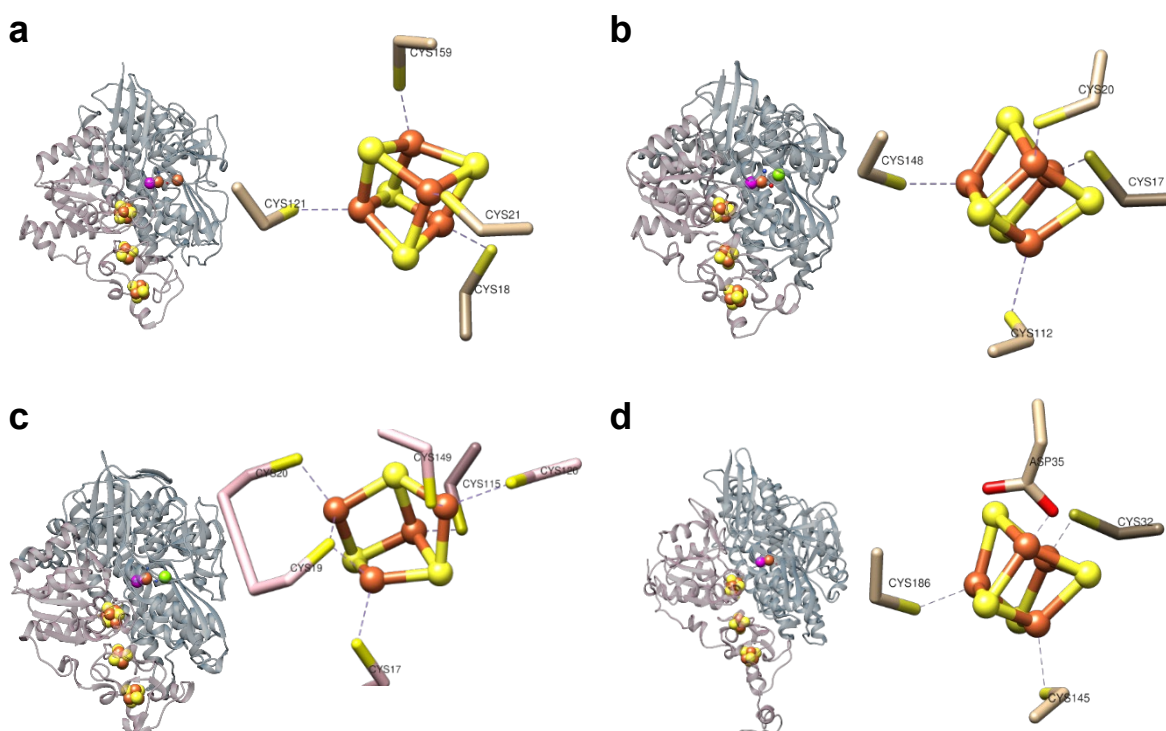
Figure 1.9. Structure of oxygen-sensitive [NiFe]-hydrogenases. Representative structures from **a)** group 1a [NiSeFe]-hydrogenase from *D. vulgaris* and **b)** group 1b [NiFe]-hydrogenase from *D. gigas*, as well as oxygen-tolerant **c)** group 1d and **d)** group 1h [NiFe]-hydrogenases from *R. eutropha*. The overall structures of the enzymes (left side) consist of the catalytic large subunit (pale blue ribbon) and the small subunit (pale pink ribbon) with three iron-sulfur clusters. A close up of their respective proximal iron sulfur clusters (right side) shows the oxygen-sensitive groups 1a and 1b have 4Fe-4S cluster composition coordinated to four cysteine residues. The oxygen-tolerant group 1d has 4Fe-3S composition coordinated to six cysteine residues and group 1h has 4Fe-4S composition coordinated to three cysteine and one aspartate residues. Figures are prepared using Chimera (University of California, San Francisco, USA).

O_2-tolerance has also been ascribed to the coordination of aspartate to the proximal 4Fe-4S cluster as opposed to cysteine-only coordination in the proximal cluster of many [NiFe]-hydrogenases (106). The group 1h actinobacterial-type hydrogenase (AH) from *R. eutropha* exhibits the typical 4Fe-4S cluster proximal to the catalytic center, but in contrast to O_2-sensitive [NiFe]-hydrogenases, the proximal cluster in AH is coordinated to one aspartate and three cysteine residues (**Figure 1.9d**). The electron-withdrawing carbonyl group in aspartate stabilizes a reduced state and contributes to a high redox potential of the proximal cluster (106). This high redox potential of the proximal iron-sulfur cluster is characteristic of other O_2-

tolerant [NiFe]-hydrogenases (123, 124). Although there are analogies between the oxygen-tolerance mechanisms of MBH (group 1d) and AH (group 1h), their mechanistic basis differs, reflecting the convergent evolution of these enzymes (49).

Other studies attribute tolerance to the physical exclusion of O_2 from the active site of the hydrogenase. In the group 2b regulatory hydrogenase (RH) of *R. eutropha,* the bulky side chains of isoleucine and phenylalanine in the gas channel restrict the entry of O_2 to the active site and only allow entry of the smaller H_2 molecule (125). In the oxidized state of the group 3d hydrogenase from *Hydrogenophilus thermoluteolus* (*Ht*-SH), Ni forms two extra coordinations to the carboxy group of a glutamate residue in addition to the four typical coordination bonds to cysteine residues (**Figure 1.10**). This extra coordination has been postulated to prevent O_2 from accessing the active site of the hydrogenase (108).
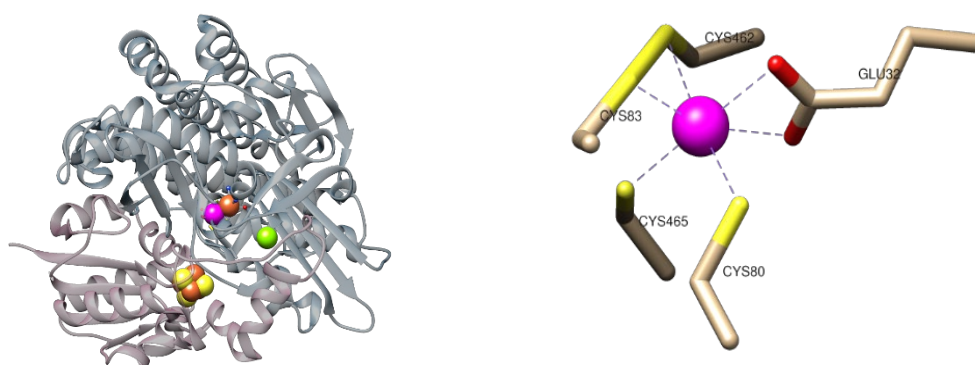
Figure 1.10. Structure of oxygen-tolerant group 3d [NiFe]-hydrogenase *from H. thermoluteolus*. The overall structure of the enzyme (left side) consists the large subunit (pale blue ribbon) and the small subunit (pale pink ribbon) with one 4Fe-4S cluster. A close-up view of the Ni (pink sphere) center (right side) shows coordination bonds to four cysteine residues and an additional bidentate coordination to GLU32. S (yellow sphere); Fe (orange sphere); Mg (green sphere). Figures are prepared using Chimera (University of California, San Francisco, USA).

1.4 d[MoCu]-CO dehydrogenase

1.4.1 Forms of the enzyme

The diversity of aerobic CO dehydrogenase was first revealed by King (126). Using phylogenetic analysis, he identified two distinct forms of [MoCu]-CO dehydrogenase based on the sequence of structural large subunit gene *coxL* (**Figure 1.11**) (126). Form I (originally called OMP clade: *Oligotropha*, *Mycobacterium*, and *Pseudomonas*) has been shown and characterized to oxidize CO. By contrast, Form II (originally called BMS clade: *Bradyrhizobium*, *Mesorhizobium*, and *Sinorhizobium*) seems to be non-functional and it is indicated that CO is not its physiological substrate (19, 126, 127). Since 2003, a number of environmental surveys of *coxL* sequences has been performed showing phylogenetic distinction between form I and form II. Microorganisms with *coxL* are found in agricultural and forest soils (128, 129), aquatic environments (46, 130, 131), volcano deposits (132, 133), and hot springs (134).
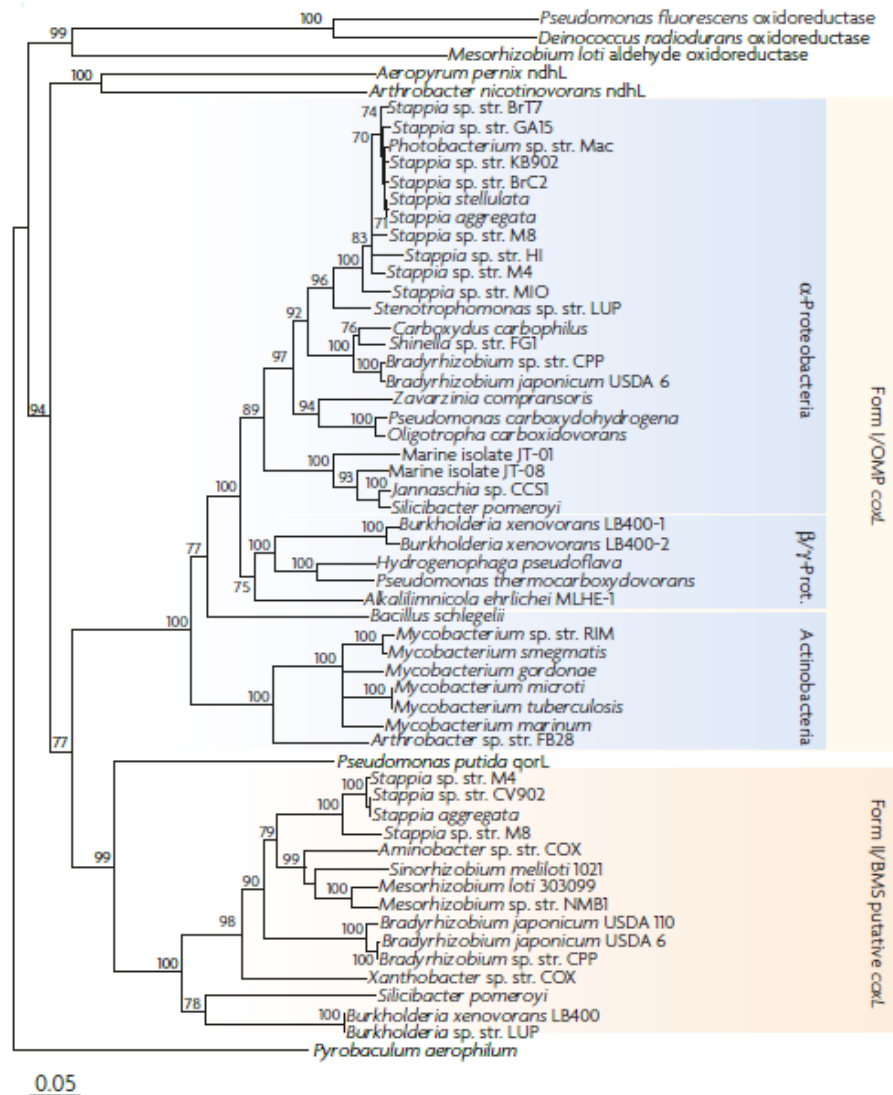
Figure 1.11. Phylogenetic analysis of the aerobic CO dehydrogenases. Form I (OMP: *Oligotropha*, *Mycobacterium*, and *Pseudomonas* clade) and form II (BMS: *Bradyrhizobium*, *Mesorhizobium*, and *Sinorhizobium*) putative coxL partially translated gene sequences. Adapted from (19).

Forms I and II [MoCu]-CO dehydrogenases have both similar and distinct features. Both forms contain three subunits, the iron-sulfur protein CoxS, flavoprotein CoxM, and catalytic subunit CoxL, with 40-50% sequence similarity between their two forms (135). In addition, the two forms share several amino acid motifs (126). The difference between form I and form II is apparent in their active sites. An AYXCSFR motif characterizes the form I CODH active site, whereas AYRGAGR characterizes form II (135) and other enzymes of the molybdenum

hydroxylase family (19). Another difference is found in the gene organization wherein the typical form II transcriptional order for structural genes is *coxS-coxL-coxM*, while in form I it is *coxM-coxS-coxL* (19). The true function of the putative form II [MoCu]-CO dehydrogenase remains unclear to date and is yet to be resolved.

1.4.2   Structure and catalysis

The first aerobic CO dehydrogenase from bacteria *O. carboxidovorans* was isolated in 1978 by Meyer and Schlegel, but it was not until 1999 when the first crystal structure was resolved by Dobbek and co-workers (43, 53). Active [MoCu]-CO dehydrogenase is composed of heterotrimeric structural subunits CoxLMS with respective sizes of 89, 30, and 18 kDa (**Figure 1.12a**) (53).

a   **b**
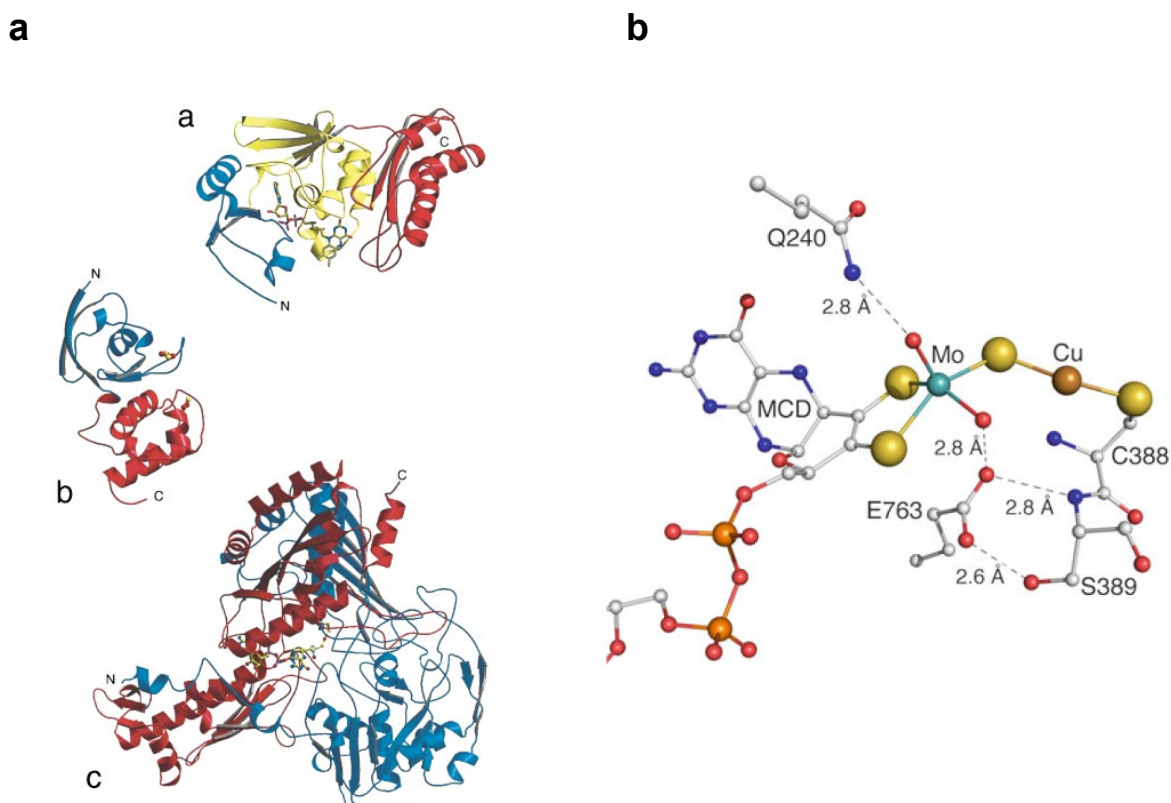
Figure 1.12. [MoCu]-CO dehydrogenase from *O. carboxidovorans.* a) The enzyme has three subunits (a) CoxM housing the FAD cofactor, (b) CoxS housing 2 x [2Fe2S] clusters, and (c) CoxL which has the [MoCu] active site. **b)** The catalytic center of the enzyme with the [MoCu] coordinated with the molybdopterin cytosine dinucleotide (MCD) cofactor. Adapted from (40, 54).

Several independent studies of the [MoCu]-CO dehydrogenase active site have enhanced understanding of its structure and reaction mechanism. The large subunit harbors the active site which has a binuclear [CuSMo(=O)2] metal cluster and a cofactor molybdopterin cytosine dinucleotide (MCD) (**Figure 1.12b**) (136–138). The metal cluster has a Cu ion that is bridged by a μ-sulfido ligand to the Mo-oxo group (53, 138). The whole cluster is covalently attached to the large subunit via the coordinate bond of the Cu ion with Cys388. The cofactor MCD is coordinated with a Mo ion and is non-covalently bound to the large subunit (136). The catalytic cycle is likely to start with the coordination of CO with Cu(I) ion, which activates the CO and thus allows the equatorial Mo-oxo ligand to perform a nucleophilic attack on CO (**Figure 1.13**) (64, 138–140). The transitional species isomerizes to form a thiocarbonate intermediate (64). As the release of CO_2 from the thiocarbonate intermediate is thermodynamically unfavorable, the intermediate is proposed to undergo rearrangement to lower the energy barrier (140). This supports the release of a CO and a two-electron transfer to Mo, thereby reducing Mo(VI) to Mo(IV). A water molecule finally binds to Mo and the release of two electrons and two protons regenerates the reactive center Mo(VI) for another cycle (64, 140).
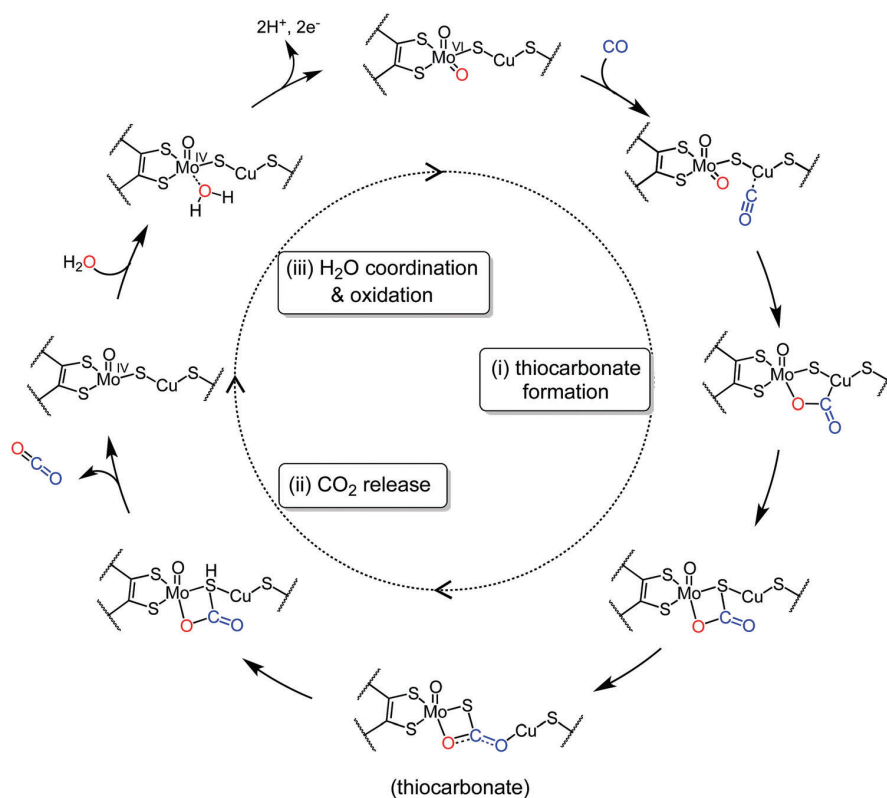
Figure 1.13. Catalytic cycle of [MoCu]-CO dehydrogenase. (i) The Mo-oxo group nucleophilically attacks the carbon of CO bound to Cu and undergoes isomerization to form a thiocarbonate intermediate; (ii) the thiocarbonate intermediate releases a free CO_2, transferring electrons to Mo; (iii) a water molecule coordinates to the Mo and with the transferred electrons, reduces; the CuSMo(=O)2 reactive species is regenerated by releasing two protons and two electrons. Adapted from (140).

The small and medium subunits of the enzyme house a series of redox-active cofactors that facilitate the transfer of electrons from the active site to an external electron acceptor (53, 138). The small subunit has C- and N-terminal domains containing one [2Fe–2S] cluster in each domain. The C-terminal domain harbors the [2Fe–2S] cluster proximal to the [MoCu]-MCD catalytic center while the N-terminal domain carries the distal [2Fe–2S] cluster. Adjacent to the distal [2Fe–2S] cluster is the cofactor flavin adenine dinucleotide (FAD) which is housed in the medium subunit via a non-covalent bond (53). The short distances between cofactors allow for a rapid electron transfer, flowing from the catalytic center in the large subunit, to the [2Fe–2S] clusters in the small subunit, and finally to FAD in the medium subunit (**Figure 1.14**) (40, 138). From FAD, the electrons can be directly transferred to an external acceptor such as quinones (42).

FAD
⇕ 8.7 Å
[2Fe2S]
⇕ 12.4 Å
[2Fe2S]
⇕ 14.6 Å
Cu,Mo-MCD
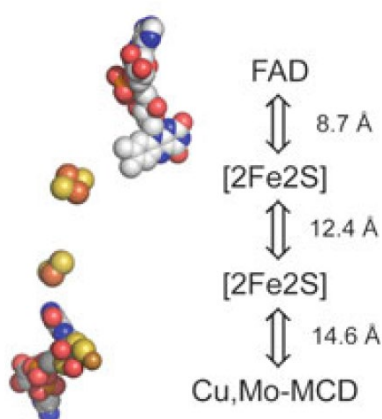
Figure 1.14. Flow path of the electrons in the [MoCu]-CO dehydrogenase. The electrons flow through the redox active sites of the cofactors that are separated by short distances. Adapted from (40).

1.5 *Mycobacterium* and its trace gas metabolism

1.5.1 *Mycobacterium* and oxidative phosphorylation

Mycobacterium is a medically and environmentally important genus within the phylum Actinobacteria. Mycobacteria are non-sporulating, non-motile rods characterized by having a thick cell envelope that is rich in mycolic acid which is attached to the cell wall through arabinogalactan (141–143). Member species are usually grouped according to their growth rate into rapid-growing mycobacteria such as *M. smegmatis* (~2.5 h doubling time) or slow-growing mycobacteria such as *M. leprae* (~12 days doubling time) (144). Many slow growers are causal agents of human and other animal diseases, including *M. tuberculosis* and *M. leprae*. On the other hand, many rapidly growing mycobacteria are common saprophytes that live in environmental habitats such as in soil, dust, freshwater, and seawater (142). These mycobacterial saprophytes have received much less attention than the medically relevant slow-growing species. For instance, *M. smegmatis* is often used as a model to understand *M. tuberculosis* and other mycobacterial pathogens, but it is increasingly realized that *M. smegmatis* has ecologically and biogeochemically important roles in its own, such as with respect to trace gas cycling.

Mycobacteria are typically obligate organoheterotrophs. They are obligate aerobes that require atmospheric oxygen for growth, although some like *M. bovis* are microaerophilic (143, 145). Some species, such as the pathogenic *M. tuberculosis*, have been shown to adapt to oxygen depletion *in vitro,* where they can survive through anaerobic respiratory processes, although they do not grow (146, 147). *M. smegmatis* has also been shown to persist under oxygen limitation by being able to promptly switch between hydrogen oxidation coupled to either oxygen or fumarate reduction, depending on electron acceptor availability, and fermentative hydrogen production (84). Mycobacteria are capable of utilizing a variety of energy sources. Organic compounds such as glycerol are well assimilated in many species

and some are even capable of utilizing uncommon substrates such as branched-chain, unsaturated, aromatic, and cyclic hydrocarbons (142, 148, 149). They have also been shown to oxidize H_2 or CO for electron sources to support persistence during carbon starvation and potentially mixotrophic growth (11, 36, 83, 150, 151). The flexibility to derive electrons from the catabolism of organic and inorganic substrates enables mycobacteria to generate ATP despite variations in resource availability. Some species, however, have lost the enzymes for the metabolism of these gases, like *M. tuberculosis* which lost hydrogenases and *M. leprae* and *M. ulcerans* which both lack CO dehydrogenase and hydrogenase.

Like many bacteria, mycobacteria employ oxidative phosphorylation as a mode to conserve energy (152). First described by Mitchell in his chemiosmotic theory, oxidative phosphorylation is a process that generates ATP from the electrochemical gradient across biological membranes that is driven by electron transfer through a series of membrane-bound complexes (153, 154). Generally, the electrons derived from the oxidation of carbon sources or alternative electron donors are carried by reducing equivalents such as NADH. These reducing equivalents then transfer the electrons to the membrane-bound complexes (e.g. NADH dehydrogenase), which in turn reduce quinone. In mycobacteria, menaquinones are the predominant quinones used as conduit in the electron transport chain in the membrane (143, 155). They transfer electrons to the terminal cytochrome oxidases, which reduce oxygen to water. The electron transfer between respiratory complexes drives proton translocation outside the cell. This proton translocation and the net consumption of protons in the cytoplasm create an electrochemical gradient across the membrane (152). This electrochemical gradient, also called the proton motive force (pmf), has two components: an electrical potential ($\Delta\psi$), resulting from the charge separation across the membrane and a chemical gradient of protons (ΔpH) (154). Mycobacteria usually grow in neutral pH and, under this condition, pmf is formed primarily as a function of $\Delta\psi$ (156). Because of the electrochemical gradient, protons can be pumped back to the cytoplasm via the F_1F_o-ATP synthase. In mycobacteria, the ATP synthase translocates three protons to the cytoplasm, which causes a 120° turn of the F_o c-ring. This is

deduced from the structure of F_o of *M. phlei*, which has 9 c-rings and that each c-ring translocates one proton (157). The 120° mechanical turn then powers the generation of one ATP from ADP and inorganic phosphate (Pi) (158).

1.5.2   Aerobic respiratory chain of *Mycobacterium*

The respiratory chain of *Mycobacterium* is branched wherein the terminal reduction of oxygen to water is catalyzed by either cytochrome *bcc-aa*$_3$ or cytochrome *bd* oxidase (152, 159). The cytochrome *bcc-aa*$_3$ is a supercomplex that contains equivalents of mitochondrial complex III, IV, and cytochrome *c* (159–161). The *bcc* complex translocates four protons out of the cytosol for every two electrons passing from menaquinol to cytochrome *c* ($4H^+/2e^-$), while the heme-copper containing *aa*$_3$-type cytochrome *c* oxidase is responsible for the terminal reduction of oxygen (159–161). For every two electrons transferred from the *aa*$_3$-type oxidase to oxygen, four protons are used in the cytoplasm to reduce oxygen to water and two are translocated into the periplasm ($2H^+/2e^-$). Overall, the stoichiometry of the protons pumped and electrons transferred by the cytochrome *bcc-aa*$_3$ is $6H^+/2e^-$ (152, 160, 161).

The other mycobacterial terminal oxidase is the cytochrome *bd* oxidase. It is a menaquinol-O_2 oxidoreductase that directly transfers electrons from menaquinol to oxygen (162). Although this cytochrome oxidase is bioenergetically less efficient, as it does not pump protons, it plays a crucial role during stressful conditions (152). At low oxygen saturation, it is found to be upregulated by more than 50-fold in *M. smegmatis*, which potentially enables the organism to respire micro-aerobically (36). In *E. coli*, the high affinity cytochrome *bd* oxidase scavenges oxygen at low concentrations (163), though it is unclear if this extends to *M. smegmatis*. It has been proposed that its potential high-affinity for oxygen could confer a selective advantage in low oxygen environments (164, 165). This oxidase has also been shown to be more tolerant to sulfide, peroxide, cyanide, and CO (164, 166–168). Additionally, cytochrome *bd* oxidase is reported to be crucial for mycobacterial survival during antibiotic inactivation of cytochrome

*bcc-aa*₃ complex (169, 170). Indeed, it has been shown that the loss in cytochrome *bcc-aa*₃ complex can be partially compensated by cytochrome *bd* oxidase (171).

The electrons that flow into the mycobacterial respiratory chain are usually derived from the oxidation of organic carbon sources during growth and from alternative organic and inorganic sources during starvation (152). In carbon-replete conditions, oxidation of organic carbon sources such as glucose or glycerol via central carbon metabolism (e.g. glycolysis and TCA cycle) produces reducing equivalents (e.g. NADH) (154). This compound is soluble in the cytoplasm and carries the electrons to the NADH dehydrogenase, of which mycobacteria have two types (172): the type I NADH dehydrogenase (homologous to mitochondrial Complex I) which translocates protons across the membrane to generate a proton motive force and the type II NADH dehydrogenase which does not pump proton but is essential for mycobacterial growth and survival (172–176). These NADH dehydrogenases couple NADH oxidation to menaquinone reduction (172). Another important complex in the mycobacterial respiratory chain is succinate dehydrogenase, which is homologous to mitochondrial Complex II. Most mycobacteria harbor two types of these enzymes: SDH1 is the primary aerobic succinate dehydrogenase while SDH2 is essential during hypoxia (177–179). As an integral part of the TCA cycle, succinate dehydrogenase bridges oxidative phosphorylation and central carbon metabolism by transferring two electrons to menaquinone from the oxidation of succinate (152, 177–179).

During carbon limitation and slow growth, mycobacteria utilize alternative carbon and energy sources. Amino acids such as proline can serve as both carbon and nitrogen sources (180). Proline is oxidized by proline dehydrogenase and is a crucial amino acid in cellular bioenergetics and redox control (180, 181). Inorganic substrates have also been increasingly recognized as important alternative energy sources during starvation. *Mycobacterium* has been shown to scavenge atmospheric H_2 during organic carbon depletion (11). This oxidation of atmospheric H_2 is catalyzed by high-affinity hydrogenases and produces two electrons that

can be transferred to the respiratory chain (83). Additionally, oxidation of CO is catalyzed by CO dehydrogenase and strong upregulation of the putative CO dehydrogenase during carbon limitation has been observed in *M. smegmatis* (36). However, direct evidence for the utilization of CO as an alternative energy source by the putative CO dehydrogenase during starvation is yet to be determined.

1.5.3   Mycobacterial persistence and trace gas metabolism

In response to environmental stresses such as nutrient starvation, bacteria generally transition into dormant forms such as spores to resist external pressures and reduce energy (182, 183). In the case of mycobacteria, they form resilient miniaturized persisting cells with reduced energy metabolism (184, 185). Nevertheless, persisting cells need some source of energy to maintain some basic cellular functions like membrane potential maintenance and macromolecular repair. Atmospheric trace gases can serve as alternative energy sources to provide this energy for maintenance (186).

In *M. smegmatis*, two [NiFe]-hydrogenases mediate an aerobic uptake of H_2 (11, 83), Huc (group 2a [NiFe]-hydrogenase) and Hhy (group 1h [NiFe]-hydrogenase) (83, 100). The genes associated with Huc and Hhy include the structural subunits (*hucSL* and *hhySL*), multiple genes involved in protein maturation (*hyp*), genes for putative iron-sulfur proteins (*hucE and hhyE*), and some hypothetical proteins (36, 83). The maturation proteins are pivotal in hydrogenase synthesis and they are proposed to perform different functions including insertion of Ni^{2+} into large subunit (HypA), Ni^{2+} binding/storage (HypB), transfer of $Fe\text{-}(CN^-)_2\text{-}(CO)$ moiety to large subunit (HypC and HypD), and biosynthesis of CN^- ligands (HypE and HypF) (36, 83). During carbon limitation, *M. smegmatis* mutants with only Huc as functioning hydrogenase oxidize H_2 to subatmospheric levels at rapid rates, suggesting Huc is the faster-acting hydrogenase. By contrast, variants with only functioning Hhy slowly oxidizes H_2 but oxidation continues at even lower H_2 concentration, suggesting Hhy has a higher affinity (11). Deletion of the genes encoding these hydrogenases show impairment in H_2 uptake and results

in poor survival, suggesting that H_2 is utilized as energy source to sustain cells during carbon limitation (11). These hydrogenases are proposed to physically and functionally interact with the membrane-bound respiratory chain (8). However, it is unclear how the electrons derived from H_2 oxidation are transferred to the electron transport chain. Moreover, it is yet to be determined if the electrons are fed into the menaquinone pool and ultimately to the terminal oxidases.

Atmospheric CO is another energy source that can be used by mycobacteria for aerobic respiration. In one study, stationary-phase *M. smegmatis* cells incubated aerobically have been shown to consume CO at sub-atmospheric mixing ratios (150). Like many mycobacteria, *M. smegmatis* encodes a putative [MoCu]-CO dehydrogenase that could be responsible for the observed CO oxidation in the study. However, a definitive proof for CO consumption by the putative [MoCu]-CO dehydrogenase has yet to be presented. In addition, the ability of *M. smegmatis* and *M. gordonae* to oxidize CO as an electron donor under low oxygen tension suggests a link between CO dehydrogenase and the high-affinity cytochrome *bd* oxidase (150). However, evidence that will directly connect CO oxidation with the mycobacterial respiratory chain, particularly with the terminal cytochrome oxidases, is still needed.

To date, we lack a systematic understanding of how the uptake hydrogenases and CO dehydrogenase of mycobacteria physically and functionally interact with the respiratory chain. Both *M. smegmatis* [NiFe]-hydrogenases are co-transcribed with putative iron-sulfur proteins, HhyE (MSMEG_2718) and HucE (MSMEG_2268) (83). These proteins could potentially serve as the immediate electron acceptors of the hydrogenases and bridge the electron transfer between the hydrogenases and the menaquinone pool (83). On the other hand, quinones are suggested to be the native electron acceptors for [MoCu]-CO dehydrogenase (42). However, this has only been demonstrated in *O. carboxidovorans* and *in vitro* using purified CO dehydrogenase. Physiological studies using mycobacterial whole cells will help ascertain

31

whether electrons are directly accepted by the menaquinone as conduit for the electron transport chain.

1.5.4 Comparing *Mycobacterium smegmatis* H$_2$ and CO metabolism with other model microorganisms

With Ralstonia eutropha. *R. eutropha* is a Betaproteobacterium that, like *M. smegmatis*, is capable of aerobically oxidizing H$_2$ using hydrogenases (22). *R. eutropha* has four hydrogenases encoded in a megaplasmid pHG1 with distinct roles: sensing of H$_2$ (regulatory hydrogenase), generating proton-motive force through H$_2$ oxidation (membrane-bound hydrogenase), and producing reducing equivalents for biosynthetic metabolism and carbon fixation (NAD$^+$-reducing hydrogenase) (187–189). In addition to these three, *R. eutropha* also possesses a functionally mysterious actinobacterial-type hydrogenase (AH) which is phylogenetically related to group 1h [NiFe]-hydrogenase, similar to the Hhy of *M. smegmatis* (49, 106). Both these hydrogenases are insensitive to oxygen (49, 106). Despite some of these similarities, the two microorganisms differ in how they metabolize H$_2$.

M. smegmatis is incapable of autotrophic growth as it does not have the genetic capacity to fix carbon. This is a striking contrast with *R. eutropha* that is capable of fixing carbon dioxide for chemolithoautotrophic growth (189). It oxidizes H$_2$ to produce reducing equivalents (NADH) using its NAD$^+$-reducing hydrogenase. The NADH is then used to reduce carbon dioxide in the Calvin-Benson-Bassham cycle for assimilation (189). Another difference between the two microorganisms is in their group 1h [NiFe]-hydrogenase. To date, only the *R. eutropha* AH from this group has been purified (106, 190). Although it is the first group 1h to have a solved crystal structure, and thus giving more insight to oxygen tolerance of hydrogenases, AH has low affinity for hydrogen (K_m of 3.6 μM) and has an extremely low activity (190). This contrasts with the high-affinity Hhy of *M. smegmatis* ($K_{m(app)}$ = 50 nM) that is capable of oxidizing subatmospheric concentrations of H$_2$ (11). The low affinity AH seems to suggest that it has little or no significance in atmospheric H$_2$ uptake. On the other hand, Hhy, with its high affinity,

is not only ecologically important but also physiologically relevant for the survival of *M. smegmatis* by scavenging atmospheric H_2 (11). Moreover, Hhy can be a good model to study the mechanism for high-affinity H_2 oxidation.

With Oligotropha carboxidovorans. *O. carboxidovorans* is an Alphaproteobacterium that encodes genes for a form I [MoCu]-CO dehydrogenase in a megaplasmid pHCG3 (126, 188). Genetic organization of the structural genes follows a *coxMSL* transcriptional order, similar to many CO oxidizers harboring the form I of the enzyme (126). The form I [MoCu]-CO dehydrogenase from *O. carboxidovorans* has been extensively investigated and has served as a model for various biochemical and physiological studies (42, 53, 64, 138). *O. carboxidovorans* grows on CO at high concentrations, a characteristic typical of carboxydotrophs (19). Consistent with this is that its CO dehydrogenase has low affinity for CO (K_m ~10 µM) (138). It uses its CO dehydrogenase to oxidize CO and as much as 16% of CO_2 produced from CO oxidation is assimilated in the cell (43). It encodes genes for the Calvin-Benson-Bassham cycle which allows for CO_2 assimilation (188).

By contrast, *M. smegmatis* is a carboxydovore that can also oxidize high levels of CO but is kinetically adapted to low levels (19). It lacks a gene cluster for carbon fixation that renders it incapable of autotrophic growth. However, an initial study demonstrates its ability to oxidize CO at environmentally relevant concentrations (150). This suggests that *M. smegmatis* CO dehydrogenase could have high affinity and gives insight into its role and importance in atmospheric CO consumption.

1.6   Thesis aims

Despite the extensive study on the genetic basis and physiological role of atmospheric H_2 oxidation in mycobacteria, current knowledge on the biochemical basis of atmospheric H_2 uptake is lacking. One fundamental question is how the uptake hydrogenases (Huc and Hhy)

of *M. smegmatis* are integrated to the aerobic respiratory chain. It is postulated that the electrons derived from H_2 oxidation are fed to the electron transport chain during carbon starvation to support persistence. This is based on previous findings that H_2 oxidation is strictly dependent on the presence of O_2 and that the uptake hydrogenases are inferred to be membrane-associated (11, 83). However, details of the physical association of Huc and Hhy with the membrane and their functional interactions with the respiratory chain have not been examined. For instance, it is unclear whether the hydrogenases are weakly or strongly connected to the membrane, or whether H_2 oxidation is coupled to O_2 reduction. Assuming the hydrogenases are linked to the aerobic respiratory chain, it also remains to be confirmed whether the electrons are transferred to the menaquinone pool or which of the two terminal cytochrome oxidases are the electrons fed into. A study is therefore needed to characterize the physical and functional interaction of the two hydrogenases with the mycobacterial respiratory chain.

Following up from the previous hypothesis, it is also interesting to know how the electrons will be transferred to the menaquinone. In most classes of respiratory uptake hydrogenases, a cytochrome *b* subunit transfers the electrons from H_2 oxidation to the quinone pool (191, 192). However, genes for such protein are not encoded in the *M. smegmatis* uptake hydrogenase operon. Instead, putative iron-sulfur proteins (tentatively annotated as HucE and HhyE) are encoded in the same operon together with the structural subunits of the hydrogenases (83). These putative iron-sulfur proteins could be the physiological redox partners that can serve as conduit between the hydrogenases and the menaquinone. Thus, it is pertinent to investigate the roles of HucE and HhyE in H_2 oxidation.

Another outstanding question is how the uptake hydrogenases are regulated. Previous studies show that their expression is low during exponential growth on glycerol and strongly upregulated when cells enter stationary phase upon carbon source depletion (11, 36). It is therefore hypothesized that *M. smegmatis* could be regulating its hydrogenases in response

to the availability of organic substrate. Signal molecules and regulators involved are needed to be identified. Some members of the *Enterobacteriaceae* family use cAMP-CRP to control the expression of hydrogenase genes (80, 85, 87) and similar regulators may be utilized by *M. smegmatis*. It is now compelling to examine if catabolite repression plays a role in regulating the mycobacterial uptake hydrogenases and which signals and regulators are used to control expression.

Lastly, the physiological role of atmospheric CO oxidation in mycobacteria, and carboxydovores in general, remains to be resolved. In other carboxydovores, it was initially proposed that CO oxidation primarily supports mixotrophic growth (19, 46, 193). However, a more recent study reports that CO neither stimulated growth nor influenced metabolite profiles in an alphaproteobacterial carboxydovore (47). We speculate that atmospheric CO oxidation is instead used by these organisms to persist during carbon starvation, similar to how atmospheric H_2 supports microbial survival during such condition (11, 33–35, 83, 96). However, it has not yet been genetically or biochemically proven that atmospheric CO supports survival. Inspecting the role of atmospheric CO oxidation using *M. smegmatis* as a model organism will help validate such hypothesis. Specifically, it needs to be examined whether (i) CO dehydrogenase is induced by organic carbon starvation, (ii) CO dehydrogenase mediates aerobic respiration of atmospheric CO, and (iii) atmospheric CO oxidation enhances survival of carbon-starved cells.

Considering these knowledge gaps, this thesis aims to determine:

1. how the uptake hydrogenases Huc and Hhy interact with the mycobacterial respiratory chain;

2. the roles of putative iron-sulfur proteins HucE and HhyE in H_2 oxidation and mycobacterial survival;

3. how catabolite repression regulates the mycobacterial hydrogenase Huc and H_2 uptake metabolism; and

4. the physiological role of CO dehydrogenase and atmospheric CO oxidation in mycobacteria and carboxydovores.

Each research objective will be addressed in four different chapters of this thesis.

Chapter 2

Two uptake hydrogenases differentially interact with the aerobic respiratory chain during mycobacterial growth and persistence

Paul R. F. Cordero[1], Rhys Grinter[1], Kiel Hards[2], Max J. Cryle[3], Coral G. Warr[1,4], Gregory M. Cook[2], Chris Greening[1] *

Form the [1] School of Biological Sciences, Monash University, Clayton, VIC 3800, Australia; [2] Department of Microbiology and Immunology, University of Otago, Dunedin, OTA 9016, New Zealand; [3] The Monash Biomedicine Discovery Institute, Department of Biochemistry and Molecular Biology, Monash University, Clayton, VIC 3800, Australia; [4] School of Medicine, University of Tasmania, Hobart, TAS 7000, Australia

* Correspondence can be addressed to Associate Professor Chris Greening (Chirs.Greening@monash.edu)

This chapter is a **published article in the Journal of Biological Chemistry**. I have contributed 80% to the paper. I performed all experiments and led the experimental design, data analysis, and paper drafting and editing. The sections in the article have been re-numbered to be consistent with the thesis format. Other authors contributed to study conceptualization and design (C.G.), data analysis (R.G., C.G.), methodological development (K.H., G.M.C.), and writing / editing (R.G., C.G.).

2.1 Abstract

To persist when nutrient sources are limited, aerobic soil bacteria metabolize atmospheric hydrogen (H_2). This process is the primary sink in the global H_2 cycle and supports the productivity of microbes in oligotrophic environments. H_2-metabolizing bacteria possess [NiFe] hydrogenases that oxidize H_2 to subatmospheric concentrations. The soil saprophyte *Mycobacterium smegmatis* has two such [NiFe] hydrogenases, designated Huc and Hhy, that belong to different phylogenetic subgroups. Both Huc and Hhy are oxygen-tolerant, oxidize H_2 to subatmospheric concentrations, and enhance bacterial survival during hypoxia and carbon limitation. Why does *M. smegmatis* require two hydrogenases with a seemingly similar function? In this work, we resolved this question by showing that Huc and Hhy are differentially expressed, localized, and integrated into the respiratory chain. Huc is active in late exponential and early stationary phases, supporting energy conservation during mixotrophic growth and transition into dormancy. In contrast, Hhy is most active during long-term persistence, providing energy for maintenance processes following carbon exhaustion. We also show that Huc and Hhy are obligately linked to the aerobic respiratory chain via the menaquinone pool and are differentially affected by respiratory uncouplers. Consistently, these two enzymes interacted differently with the respiratory terminal oxidases. Huc exclusively donated electrons to, and possibly physically associated with, the proton-pumping cytochrome *bcc–aa*$_3$ supercomplex. In contrast the more promiscuous Hhy also provided electrons to the cytochrome *bd* oxidase complex. These results indicate that, despite their similar characteristics, Huc and Hhy perform distinct functions during mycobacterial growth and survival.

2.2 Introduction

Earth's soils consume vast amounts of hydrogen (H_2) from the atmosphere (5, 194). Over the past decade, research by a number of groups has revealed that this net H_2 consumption is mediated by aerobic soil bacteria (12, 33–35, 96, 195). Based on this work, it has been

38

established that gas-scavenging bacteria are the major sink in the global H_2 cycle, responsible for the net consumption of ~70 million tons of H_2 each year and 80% of total atmospheric H_2 consumed (6, 7, 195, 196). In addition to its biogeochemical importance, it is increasingly realized that atmospheric H_2 oxidation is important for supporting the productivity and biodiversity of soil ecosystems (22, 29, 30, 49, 197–201). This process is thought to play a key role under oligotrophic conditions, where the majority of microbes exist in a non-replicative, persistent state (29, 202). As the energy requirements for persistence are approximately 1000-fold lower than for growing cells (203), the energy provided by atmospheric H_2 can theoretically sustain up to 10^8 cells per gram of soil (8).

The genetic basis of atmospheric H_2 oxidation has largely been elucidated. Two distinct subgroups of hydrogenase, namely the group 1h and 2a [NiFe]-hydrogenases, are known to oxidize H_2 to subatmospheric concentrations (11, 33, 96). The operons for these hydrogenases minimally encode the hydrogenase large subunit containing the H_2-activating catalytic center, the hydrogenase small subunit containing electron-relaying iron-sulfur clusters, and a putative iron-sulfur protein hypothesized to have a role in electron transfer (8, 83, 106, 190). Additional operons encode the maturation and accessory proteins required for hydrogenase function (49, 83). Increasing evidence suggests that hydrogenases capable of atmospheric H_2 oxidation are widely encoded in soil bacteria. Representatives of three dominant soil phyla, Actinobacteriota, Acidobacteriota, and Chloroflexota, have been experimentally shown to oxidize atmospheric H_2 (10–12, 33, 35, 96, 204). Moreover, genomic and metagenomic studies indicate that at least 13 other phyla possess hydrogenases from lineages known to support atmospheric H_2 oxidation (29, 32, 49, 201).

The saprophytic soil actinobacterium *Mycobacterium smegmatis* has served as a key model organism for these studies (11, 83, 84). In *M. smegmatis*, H_2 oxidation has been shown to be solely mediated by two oxygen-tolerant hydrogenases: the group 2a [NiFe]-hydrogenase Huc (also known as Hyd1 or cyanobacterial-type uptake hydrogenase) and the group 1h [NiFe]-

hydrogenase Hhy (also known as Hyd2 or actinobacterial-type uptake hydrogenase) (49, 83). These enzymes belong to distinct phylogenetic subgroups and their large subunits share less than 25% amino acid identity (49). Despite this, Huc and Hhy display striking similarities. Both enzymes oxidize H_2 to subatmospheric concentrations under ambient conditions (11) and both appear to be membrane-associated despite the lack of predicted transmembrane regions (11). Both Huc and Hhy are reported to be upregulated during stationary phase in response to both carbon and oxygen limitation (83). Consistently, Huc and Hhy deletion mutants show reduced growth yield and impaired long-term survival, suggesting that atmospheric H_2 oxidation supports energy and redox homeostasis (11, 36, 84). Nevertheless, some evidence suggests that these enzymes are not redundant. For reasons incompletely understood, significant survival phenotypes are observed for both single and double mutants (11, 83). In whole cells, the enzymes also exhibit distinct apparent kinetic parameters, with Hhy having higher affinity but lower activity for H_2 compared to Huc (11).

It remains to be understood if and how the hydrogenases of *M. smegmatis* are integrated into the respiratory chain. As an obligate aerobe, *M. smegmatis* depends on aerobic heterotrophic respiration to generate proton-motive force and synthesize ATP for growth (205). *M. smegmatis* possesses a branched respiratory chain terminating in one of two terminal oxidases, the cytochrome *bcc-aa₃* supercomplex or the cytochrome *bd* oxidase (152). The proton pumping cytochrome *bcc-aa₃* oxidase is the more efficient of these two complexes, leading to the efflux of six H^+ ions per electron pair received, and is the major complex utilized during aerobic growth (152, 161). The non-proton pumping cytochrome *bd* complex is less efficient, mediating the transport of two H^+ ions per electron pair, but is predicted to have a higher affinity for O_2 and is important during non-replicative persistence (36, 206–208). In actively growing *M. smegmatis*, electrons entering the respiratory chain are derived from heterotrophic substrates, and are donated to the respiratory chain by NADH largely via the non-proton pumping type II NADH dehydrogenase NDH-2 and succinate via the succinate dehydrogenase SDH1 (152). While *M. smegmatis* is strictly heterotrophic for replicative

growth, it was recently demonstrated that it is able to aerobically respire using CO at atmospheric concentrations during carbon-limited persistence through the actions of a carbon monoxide dehydrogenase (209). It has likewise been predicted that Huc and Hhy support survival during persistence by providing electrons derived from H_2 to the respiratory chain (11, 83). However, these studies were correlative and it remains to be definitively demonstrated that H_2 serves as a respiratory electron donor in this organism.

In this work, we addressed these knowledge gaps by comprehensively studying Huc and Hhy during different stages of mycobacterial growth and persistence. We show that Huc and Hhy are differentially expressed throughout growth and persistence and form distinct interactions with the membrane. In addition, we show both Huc and Hhy are obligately linked to the respiratory chain via the menaquinone pool but form distinct interactions with the terminal oxidases. These data demonstrate that H_2 oxidation in *M. smegmatis* provides electrons to the respiratory chain for mixotrophic growth via Huc and to energize persistence via Hhy. These findings represent a significant advance in our understanding of the role of high affinity hydrogenases in bacterial metabolism.

2.3   Materials and Methods

2.3.1   Bacterial strains and growth conditions

Mycobacterium smegmatis mc2155 and its derivatives were routinely grown in lysogeny broth (LB) agar plates supplemented with 0.05% (w/v) Tween 80 (LBT) (210). In broth culture, the strain was grown in either LBT or Hartmans de Bont (HdB) minimal medium supplemented with 0.2% (w/v) glycerol, 0.05% (w/v) tyloxapol, and 10 μM NiSO₄. Escherichia coli was maintained in LB agar plates and grown in LB broth (211). Selective LB or LBT media used for cloning experiments contained gentamycin at 5 μg mL-1 for M. smegmatis and 20 μg mL-1 for E. coli. Cultures were routinely incubated at 37°C, with rotary shaking at 150 rpm for

liquid cultures, unless otherwise specified. The strains of M. smegmatis (212, 213) and its derivatives and E. coli are listed in **Supplementary Table S4**.

2.3.2 Insertion of StrepII tags

To facilitate visualization of the hydrogenases in western blots, a StrepII tag was inserted at the C-terminal end of the small subunits of Huc (MSMEG_2262, *hucS*) and Hhy (MSMEG_2720, *hhyS*) through allelic exchange mutagenesis as described previously (205). Two allelic exchange constructs, *hucS*$_{StrepII}$ (2656 bp) and *hhyS*$_{StrepII}$ (3000 bp), were synthesized by GenScript. These were cloned into the SpeI site of the mycobacterial shuttle plasmid pX33 to yield the constructs pHuc-StrepII and pHhy-StrepII (**Supplementary Table S4**). The constructs were propagated in *E. coli* TOP10 and transformed into wild-type *M. smegmatis* mc^{2}155 cells by electroporation. Gentamycin was used in selective solid and liquid medium to propagate pX33. To allow for permissive temperature-sensitive vector replication, transformants were incubated on LBT gentamycin plates at 28°C until colonies were visible (5-7 days). Resultant catechol-positive colonies were subcultured onto fresh LBT gentamycin plates and incubated at 40°C for 3-5 days to facilitate integration of the recombinant plasmid, via flanking regions, into the chromosome. The second recombination event was facilitated by subculturing catechol-reactive and gentamycin-resistant colonies onto LBT agar plates supplemented with 10% sucrose (w/v) and incubating at 40°C for 3-5 days. Catechol-unreactive colonies were subsequently screened by PCR to distinguish wild-type revertants from Huc-StrepII and Hhy-StrepII mutants. Primers used for screening are listed in **Supplementary Table S5**.

2.3.3 Cellular fractionation for detection of Huc and Hhy

The untagged and StrepII-tagged Huc and Hhy were constitutively produced by growing *M. smegmatis* wild-type, Huc-only, Hhy-only, Huc-StrepII, and Hhy-StrepII strains in HdB with 0.2% glycerol as the sole carbon source (11, 210). Cells were grown at 37°C with agitation and harvested by centrifugation (15 min, 10,000 *g*, 4°C) after 1 day post-OD$_{max}$ (~3.0) for wild-type, Huc-only, and Huc-StrepII or 3 days post OD$_{max}$ (~3.0) for wild-type, Hhy-only, and Hhy-

StrepII. They were washed in lysis buffer (50 mM Tris-Cl, pH 8.0, 2 mM $MgCl_2$, 1 mM PMSF, 5 mg mL^{-1} lysozyme, 40 μg ml^{-1} DNase) and resuspended in the same buffer in a 1:5 cell mass to buffer ratio. The cell suspension was homogenized using a Dounce homogenizer and passed through a cell disruptor (40 Kpsi, four times; Constant Systems Ltd, model: One Shot series). After removal of unbroken cells by low-speed centrifugation (20 min, 8,000 g, 4°C), the whole-cell lysates of wild-type, Huc-only, and Hhy-only strains were used for activity staining. Cell lysates of Huc-StrepII and Hhy-StrepII strains were separated by ultracentrifugation (60 min, 150,000 g, 4°C) into cytosol and membrane fractions. Membrane was washed in lysis buffer and analyzed by western blot. Protein concentrations were measured by the bicinchoninic acid method against bovine serum albumin standards.

2.3.4 Hydrogenase activity staining

Twenty micrograms of each whole-cell lysates was loaded onto two native 7.5% (w/v) Bis-Tris polyacrylamide gels prepared as described elsewhere (214) and run in a Tris (25 mM)-glycine (192 mM) buffer (pH 8.3) alongside a protein standard (NativeMark Unstained Protein Standard, ThermoFisher Scientific) for 3 h at 25 mA. For total protein determination, gels were stained overnight at 4°C with gentle agitation using AcquaStain Protein Gel Stain (Bulldog Bio). To determine hydrogenase activity, a duplicate gel was incubated in 50 mM potassium phosphate buffer (pH 7.0) supplemented with 500 μM nitroblue tetrazolium chloride (NBT) in an anaerobic jar amended with an anaerobic gas mixture (5% H_2, 10% CO_2 85% N_2 v/v) overnight at room temperature. Bands present after incubation corresponded to hydrogenase activity. For blue native PAGE, lysates loaded onto native 7.5% (w/v) Bis-Tris polyacrylamide gels were run at 25 mA in a commercial buffer system consisting of anode NativePAGE™ Running Buffer (50 mM bisTris, 50 mM tricine, pH 6.8) and NativePAGE™ Light Blue Cathode buffer (50 mM bisTris, 50 mM tricine, 0.002% Coomassie Brilliant Blue G-250, pH 6.8) (ThermoFischer Scientific). After the run, gels were incubated either for total protein staining or hydrogenase activity staining, as described above.

2.3.5 Membrane solubilization and western blots

Membrane solubilization was performed by resuspending washed membranes (to a final protein concentration of 1 mg mL^{-1}) in solubilization buffer containing 50 mM Tris-Cl pH 8.0, 1 mM PMSF, and 5% (w/v) sodium cholate (215). The solutions were incubated at room temperature with gentle agitation for 3 h. Detergent-soluble proteins were separated from the insoluble material by ultracentrifugation. As a control, membrane was suspended in buffer without sodium cholate. Total proteins in the fractions were visualized in SDS-PAGE and Huc_StrepII and Hhy_StrepII by western blotting. For western blot, 20 µg total protein was loaded and ran on to Bolt™ 4-12% SDS polyacrylamide gels after boiling in Bolt™ SDS sample buffer and 50 mM dithiothreitol. The proteins in the gels were then transferred onto PVDF membrane using Trans-Blot® SD Semi-Dry Transfer Cell (Bio-Rad) set at 15 V for 60 m. Following transfer, the protein-containing PVDF membrane was blocked with 3% (w/v) bovine serum albumin in phosphate-buffered saline (PBS), pH 7.4 with 0.1% (v/v) Tween 20 (PBST). PVDF membrane was washed three times in 20 mL of PBST and finally resuspended in 10 mL of the same buffer. Strep-Tactin horse radish peroxidase (HRP) conjugate was then added at a 1:100,000 dilution. Peroxide-mediated chemiluminescence of luminol catalyzed by the HRP was developed according to manufacturer's specifications (Amersham ECL Prime detection reagent, GE Life Sciences) and the Strep-Tactin(HRP conjugated)–StrepII-tag complex was visualized in a Fusion Solo S (Fischer Biotech) chemiluminescence detector.

2.3.6 Gene expression analysis

For qRT-PCR analysis, five synchronized sets of biological triplicate cultures (30 mL) of wild-type *M. smegmatis* were grown in 125 mL aerated conical flasks. Each set of triplicates was quenched either at OD$_{600}$ 0.3, OD$_{600}$ 1.0, 1 day post-OD$_{max}$ (OD$_{600}$ ~3.0), 3 days post-OD$_{max}$ (OD$_{600}$ ~3.0), or 3 weeks post-OD$_{max}$ (OD$_{600}$ ~3.0) with 60 mL cold 3:2 glycerol:saline solution (-20°C). They were subsequently harvested by centrifugation (20,000 × g, 30 minutes, -9°C), resuspended in 1 mL cold 1:1 glycerol:saline solution (-20°C), and further centrifuged (20,000 × g, 30 minutes, -9°C). For cell lysis, pellets were resuspended in 1 mL TRIzol Reagent, mixed

with 0.1 mm zircon beads, and subjected to five cycles of bead-beating (4,000 rpm, 30 seconds) in a Biospec Mini-Beadbeater. Total RNA was subsequently extracted by phenol-chloroform extraction as per manufacturer's instructions (TRIzol Reagent User Guide, Thermo Fisher Scientific) and resuspended in diethylpyrocarbonate (DEPC)-treated water. RNA was treated with DNase using the TURBO DNA-free kit (Thermo Fisher Scientific) as per the manufacturer's instructions. cDNA was then synthesized using SuperScript III First-Strand Synthesis System for qRT-PCR (Thermo Fisher Scientific) with random hexamer primers as per the manufacturer's instructions. qPCR was used to quantify the levels of the target genes *hucL* (Huc) and *hhyL* (Hhy) and housekeeping gene *sigA* against amplicon standards of known concentration. All reactions were run in a single 96-well plate using the PowerUp SYBR Green Master Mix (Thermo Fisher Scientific) and LightCycler 480 Instrument (Roche) according to each manufacturers' instructions. A standard curve was created based on the cycle threshold (Ct) values of *hucL*, *hhyL*, and *sigA* amplicons that were serially diluted from 10^8 to 10 copies ($R^2 > 0.98$). The copy number of the genes in each sample was interpolated based on each standard curve and values were normalized to *sigA* expression. For each biological replicate, all samples, standards, and negative controls were run in technical duplicate. Primers used in this work are summarized in **Supplementary Table S5**.

2.3.7 Microrespiration measurements

Rates of H_2 oxidation or O_2 consumption were measured amperometrically according to previously established protocols (32, 83). For each set of measurements, either a Unisense H_2 microsensor or Unisense O_2 microsensor electrode were polarized at +800 mV or -800 mV, respectively, with a Unisense multimeter. The microsensors were calibrated with either H_2 or O_2 standards of known concentration. Gas-saturated phosphate-buffered saline (PBS; 137 mM NaCl, 2.7 mM KCl, 10 mM Na_2HPO_4 and 2 mM KH_2PO_4, pH 7.4) was prepared by bubbling the solution with 100% (v/v) of either H_2 or O_2 for 5 min. In uncoupler/inhibitor-untreated cells, H_2 oxidation was measured in 1.1 mL microrespiration assay chambers. These were amended with 0.9 mL cell suspensions of *M. smegmatis* wild-type or derivative

strains either at OD_{600} 0.3, OD_{600} 1.0, 1 day post-OD_{max} (OD_{600} ~3.0), 3 days post-OD_{max} (OD_{600} ~3.0), or 3 weeks post-OD_{max} (OD_{600} ~3.0), They were subsequently amended with 0.1 mL H_2-saturated PBS and 0.1 mL O_2-saturated PBS. Chambers were stirred at 250 rpm, room temperature. For cells at mid-stationary phase, following measurements of untreated cells, the assay mixtures were treated with either 10 µM nigericin, 10 µM valinomycin, 40 µM *N*-oxo-2-heptyl-4-hydroxyquinoline (HQNO) or 250 µM zinc azide before measurement. In O_2 consumption measurements, initial O_2 consumption without the addition of H_2 were measured in microrespiration assay chambers sequentially amended with 0.9 mL cell suspensions of *M. smegmatis* wild-type or derivative strains at mid-stationary phase (3 days post-OD_{max}) and 0.1 mL O_2-saturated PBS (0.1 mL) with stirring at 250 rpm, room temperature. After initial measurements, 0.1 mL of H_2-saturated PBS was added into the assay mixture and changes in O_2 concentrations were recorded. Additionally, O_2 consumption was measured in cytochrome *bcc-aa$_3$*-only strains treated with 250 µM zinc azide. In both H_2 and O_2 measurements, changes in concentrations were logged using Unisense Logger Software (Unisense, Denmark). Upon observing a linear change in either H_2 or O_2 concentration, rates of consumption were calculated over a period of 20 s and normalized against total protein concentration.

2.3.8 Mass spectrometry analysis

After hydrogenase activity staining, bands corresponding to Huc and Hhy activity were excised from the gel and destained with 50% acetonitrile (ACN) in 100 mM NH_4HCO_3 (ABC) (pH 8.5). The proteins were subsequently reduced with 10 mM DTT (Astral Thermo Fisher Scientific) and carbamidomethylated with 25 mM chloroacetamide (Sigma). The gel was then dehydrated with 100% ACN and rehydrated with digestion solution containing 10 ng µl^{-1} trypsin (Promega), 100 mM ABC, and 5% ACN. The gel was digested overnight at 37 °C, and tryptic peptides were extracted from the gel with 50% ACN-5% formic acid solution lyophilized in a vacuum concentrator, and purified using OMIX C18 Mini-Bed tips (Agilent Technologies) prior to LC-MS/MS analysis. Using a Dionex UltiMate 3000 RSLCnano system

equipped with a Dionex UltiMate 3000 RS autosampler, an Acclaim PepMap RSLC analytical column (75 μm × 50 cm, nanoViper, C18, 2 μm, 100 Å; Thermo Scientific), and an Acclaim PepMap 100 trap column (100 μm × 2 cm, nanoViper, C18, 5 μm, 100 Å; Thermo Scientific), the tryptic peptides were separated by increasing concentrations of 80% ACN/0.1% formic acid at a flow rate of 250 nL min^{-1} for 60 min and analyzed with a Orbitrap Fusion mass spectrometer (Thermo Scientific). The instrument was operated in data-dependent acquisition mode to automatically switch between full-scan MS and MS/MS acquisition. Each survey full scan (*m/z* 375–1575) was acquired in the Orbitrap with 70,000 resolution (at *m/z* 200) after accumulation of ions to a 1×10^6 target value with a maximum injection time of 54 ms. Dynamic exclusion was set to 60 s. The 20 most intense multiply charged ions (z ≥ 2) were sequentially isolated and fragmented in the collision cell by higher-energy collisional dissociation with a fixed injection time of 54 ms, 30,000 resolution, and automatic gain control target of 2×10^5. For assignment, the raw files were searched against the *M. smegmatis* database, containing 6717 entries, using Byonic v3.0.0 (ProteinMetrics). Database searching was performed with the following parameters: cysteine carbamidomethylation as a fixed modification, methionine oxidation and N-terminal acetylation as variable modifications, up to two missed cleavages permitted, mass tolerance of 10 ppm, and 1% protein false discovery rate for protein and peptide identification based on a decoy database. The *M. smegmatis* protein sequence database was downloaded from GenBank NCBI 2018. The raw mass spectrometry data have been deposited in Figshare (https://monash.figshare.com/projects/Hydrogenase/69578). File F1CH20190327_WT_Top.raw contains the raw data for the high-molecular-mass band corresponding to Huc activity. File F1CH20190327_WT_down.raw contains the raw data for the mid-sized molecular mass band corresponding to Hhy activity.

2.4   Results and Discussion

2.4.1   Mycobacterial hydrogenases are differentially expressed and active during growth and persistence

Previous work investigating the activity of Huc and Hhy in *M. smegmatis* showed they are induced in batch culture upon exhaustion of carbon sources (11). However, we lack a high-resolution understanding of the expression and activity of Huc and Hhy during mycobacterial growth and persistence. To address this question, we quantified Huc and Hhy gene expression using qPCR at different growth phases in batch liquid cultures. In exponentially growing, carbon replete cells (OD_{600} 0.3 and OD_{600} 1.0 cultures), transcript levels for *hucL* (the Huc large subunit) were relatively low; however, as carbon sources became exhausted *hucL* expression increased, with maximum expression observed at 1 day post-OD_{max} (OD_{600} ~3.0). Subsequently, at 3 days post-OD_{max} (OD_{600} ~3.0) as cells endured prolonged carbon-limitation, expression levels of *hucL* declined significantly (**Figure 2.1a**). In contrast, expression of *hhyL* (the Hhy large subunit) remained low during exponential growth, before rapidly increasing by 57-fold when cells reached carbon-limited stationary phase and remained at high levels into late stationary phase (**Figure 2.1b**).

Next, we determined the rate of H_2 oxidation of wild-type *M. smegmatis* and mutant strains containing only Huc or Hhy at different stages of growth and persistence in liquid batch culture. H_2 oxidation rates in the Huc-only strain correlated well with gene expression levels; levels of H_2 oxidation were relatively low during early exponential growth (OD_{600} 0.3) and increased during late exponential phase (OD_{600} 1.0), before peaking at 1 day post-OD_{max} and declining rapidly thereafter (**Figure 2.1c**). The rapid decline in transcript levels and activity of Huc during stationary phase suggests tight regulation of this enzyme. In contrast, the activity of Hhy was low during exponential growth (OD_{600} 0.3 and 1.0), increased slightly at 1 and 3 days post-OD_{max}, and increasing markedly during prolonged persistence, with high levels of activity observed at 3 weeks post-OD_{max} (**Figure 2.1d**). A notable lag was observed between the

increase of transcript levels and Hhy activity during stationary phase, suggesting post-transcriptional regulation of this hydrogenase. The H_2 oxidation activity profile of the wild-type strain in these assays are the same as the sum of the activity of Huc and Hhy only mutants, confirming that Huc and Hhy are functioning normally in the mutant background (**Figure 2.1e**). Additionally, a mutant strain lacking both Huc and Hhy did not consume H_2, confirming that Huc and Hhy are solely responsible for H_2 oxidation (**Figure 2.1f**).

These data provide a clear picture of the differential regulation of Huc and Hhy, hinted at by previous studies (83). Huc is expressed by *M. smegmatis* during the transition from growth to persistence, allowing cells to grow mixotrophically on atmospheric H_2 and, where available, higher concentrations produced through abiotic or biotic processes (e.g. fermentation, nitrogen fixation) (216). Subsequently, as cells commit to persistence due to carbon starvation, Hhy is expressed and supplies energy from atmospheric H_2 to meet maintenance needs.
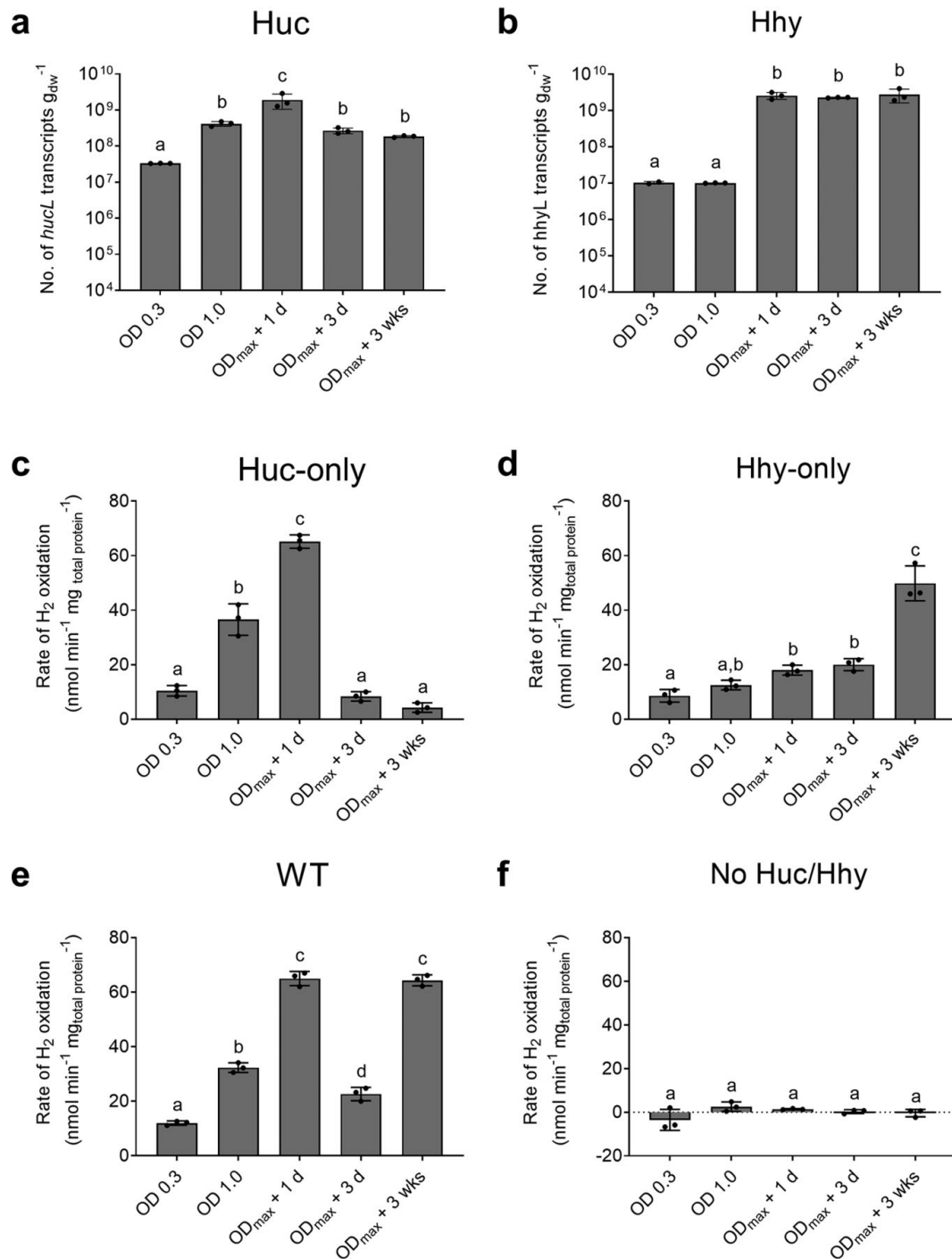
Figure 2.1. Differential expression and activity of Huc and Hhy. Normalized number of transcripts of the large subunit gene of **a)** Huc (*hucL*) and **b)** Hhy (*hhyL*) in wild-type cultures. Cultures were harvested during either carbon-replete conditions, i.e. OD_{600} 0.3 and OD_{600} 1.0, or carbon-limited conditions, i.e. 1 d post-OD_{max} (OD_{600} ~3.0), 3 d post-OD_{max} (OD_{600} ~3.0), and 3 wks post-OD_{max} (OD_{600} ~3.0). Absolute transcript levels were determined through qRT-PCR and normalized to the housekeeping gene *sigA*. Rates of H_2 oxidation of whole cells of **c)** Huc-only, **d)** Hhy-only, **e)** wild-type, and **f)** no Huc/Hhy (triple hydrogenase deletion) strains of *M. smegmatis*. Activities were measured amperometrically using a hydrogen microelectrode under

50

carbon-replete and carbon-limited conditions. All values labeled with different letters are statistically significant based on one-way ANOVA.

2.4.2 Mycobacterial hydrogenases differentially associate with the membrane, with Huc potentially forming a supercomplex with the cytochrome *bcc–aa*$_3$ oxidase

To directly attribute the H_2 oxidation activity in our cellular assays to Huc and Hhy, we separated cell lysates of wild-type and hydrogenase mutant strains using native-PAGE and detected hydrogenase activity by zymographic staining (**Figure 2.2a**). A high molecular weight species and a low-MW weight band exhibiting H_2 oxidation activity was detected at 1 day post-OD_{max} in wild-type and Huc-only cultures, but not in the Hhy-only strain. We determined the size of the high-MW species to be >700 kDa and the low-MW band to be >66 kDa, via blue native-PAGE (**Supplementary Figure S1**). In contrast, at 3 days post-OD_{max}, a mid-sized molecular weight H_2 oxidizing species was present in wild-type and Hhy-only cultures, but was absent from the Huc-only strain (**Figure 2.2a**). These high and mid-sized molecular weight bands from the wild-type strain were excised and proteins present were identified by mass spectrometry. The high-molecular-mass band yielded peptides corresponding to Huc (**Supplementary Table S1 and S2**), whereas the mid-sized molecular mass band yielded peptides corresponding to Hhy (**Supplementary Table S1 and S3**) These data correlate well with the activity of Huc and Hhy observed in our cellular assays, confirming Huc is the dominant hydrogenase during the transition from growth to dormancy and Hhy is more active during prolonged persistence.

The difference in size between Huc and Hhy activity observed on the native gel is striking. The slow migration of Huc may be due to the formation of an oligomer containing multiple Huc subunits or other unidentified proteins. To test this hypothesis, we interrogated the mass spectrometry data for likely Huc interacting partners. Intriguingly, components of the cytochrome *bcc–aa*$_3$ oxidase supercomplex were detected in the Huc sample with a high probability and coverage, demonstrating that they are prevalent in this region of the gel

alongside various other proteins (**Supplementary Table S1 and S2; Figure S2**). It was shown previously that H_2 oxidation in *M. smegmatis* is oxygen dependent, suggesting that Huc and Hhy activity are obligately linked to respiratory chain (11). As cytochrome *bcc-aa$_3$* is a large supercomplex (217), association with Huc could account for the high-MW of Huc activity on the native gel, while placing the hydrogenase in an ideal position to donate electrons to this complex.
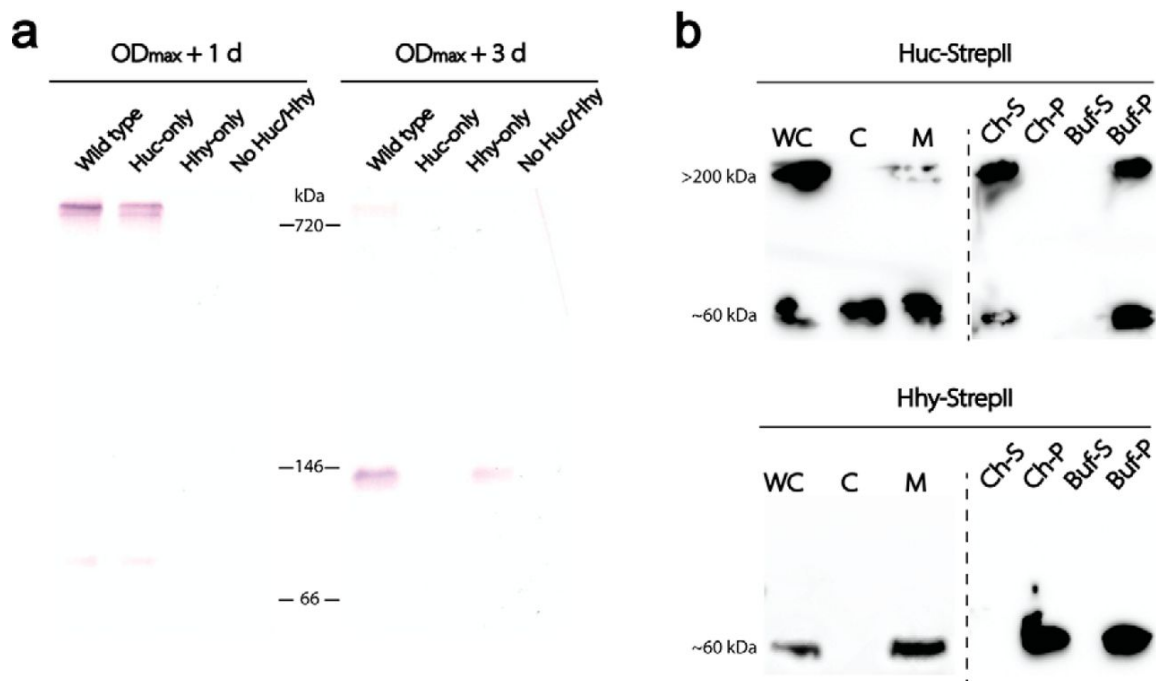
Figure 2.2. Activity and physical association of Huc and Hhy in cell extracts. a) Differential native activity staining of Huc and Hhy in whole-cell lysates of different *M. smegmatis* strains harvested at 1 d post-OD$_{max}$ (OD$_{600}$ ~3.0) and 3 d post-OD$_{max}$ (OD$_{600}$ ~3.0). **b)** Localization of StrepII-tagged Huc (Huc-StrepII) and Hhy (Hhy-StrepII) in different cellular fractions by western blot (left of dotted lines): WC – whole-cell lysates; C – cytosol; M – membrane. Huc-StrepII was harvested at 1 d post-OD$_{max}$ (OD$_{600}$ ~3.0) and Hhy-StrepII 3 d post-OD$_{max}$ (OD$_{600}$ ~3.0). Membranes containing Huc-StrepII and Hhy-StrepII solubilized in 5% sodium cholate at 22 °C for 3 h (right of dotted line). Huc-StrepII and Hhy-StrepII in the cholate-soluble (Ch-S) and cholate-insoluble fractions (Ch-P) are visualized by western blot. Solubilization controls incubated under identical conditions minus cholate are shown, supernatant (Buf-S) and pellet (Buf-P).

Previous work indicated Huc and Hhy were membrane-associated despite lacking obvious transmembrane regions or signal peptides (11). To interrogate the nature of this membrane association, we fractionated cells into lysates, cytosols, and membranes and detected the hydrogenases by western blotting chromosomally StrepII-tagged variants of Huc and Hhy. Two bands corresponding to Huc were detected by western blot in *M. smegmatis* whole cells, with sizes of ~60 and >200 kDa. Upon cell fractionation, the ~60 kDa band was observed in both cytoplasmic and membrane fractions, while the >200 kDa band was only observed in the membrane fraction (**Figure 2.2b**). Interaction of Huc with the membrane was disrupted by 5% sodium cholate, with both bands partitioning to the soluble phase (**Figure 2.2b**). In contrast, a single ~60 kDa band corresponding to Hhy was observed in the whole cell lysate and membrane fractions but was absent from the cytoplasmic fraction. The interaction between Hhy and the cell membrane was not disrupted by the addition of 5% sodium cholate, suggesting it forms a strong interaction with the membrane relative to Huc and implies different mechanisms are responsible for their membrane association **(Figure 2.2b)**. Both Huc and Hhy are predicted to form heterotetramers, consisting of two large and small subunits with a molecular weight of >200 kDa (83, 106). This is consistent with the bands observed via western blot, with the >200 kDa species observed for Huc representing an intact tetramer, with the ~60 kDa species representing partial disassociation of this complex.

2.4.3   Mycobacterial hydrogenases are coupled to the respiratory chain and interact differentially with the terminal cytochrome oxidases

Although it is known that O_2 is required for H_2 oxidation by Huc and Hhy in *M. smegmatis* (11, 195), it had not been determined whether these enzymes support the reduction of O_2 through coupling to the respiratory chain. To resolve this question, we amperometrically monitored the H_2 and O_2 consumption in carbon-limited *M. smegmatis* cells (3 days post-OD_{max}) following sequential spiking with H_2 and O_2 saturated buffer (**Figure 2.3a**). In H_2 oxidation measurement, upon spiking cells with H_2 only, oxidation (0.31 µM min^{-1}) was observed due to ambient levels of O_2 present in solution. When O_2-saturated buffer was subsequently added, the rate of H_2

oxidation increased markedly (1.2 µM min^{-1}) (**Figure 2.3a**). In O$_2$ consumption measurements, cells that were initially spiked with O$_2$ minimally consumed O$_2$ (0.01 µM min^{-1}). However, with the subsequent addition of H$_2$, the cells consumed O$_2$ at approximately half the rate observed for H$_2$ oxidation (0.51 µM min^{-1}) (**Figure 2.3a**). This rate is consistent with the expected stoichiometry of H$_2$-dependent aerobic respiration (H$_2$ + ½ O$_2 \rightarrow$ H$_2$O). These data directly link H$_2$ oxidation to O$_2$ consumption, providing strong experimental evidence that electrons derived from H$_2$ support respiratory reduction of O$_2$ in *M. smegmatis*.

Having established that H$_2$ oxidation directly supports O$_2$ reduction in *M. smegmatis*, we next sought to determine which of the two terminal oxidases were utilized for this process. To achieve this, we monitored the rate of H$_2$ oxidation and O$_2$ consumption in wild-type, Huc-only, and Hhy-only strains, as well as mutant strains possessing either cytochrome *bcc-aa$_3$* or *bd* oxidase as the sole terminal respiratory complex. Given the loss of both terminal oxidases is lethal in *M. smegmatis* (169)*,* we utilized zinc azide, a selective inhibitor of cytochrome *bcc-aa$_3$* oxidase (218), to assess the effects of loss of both terminal oxidases on H$_2$ oxidation. As expected from our initial experiments at 3 days post-OD$_{max}$ (**Figure 2.1**), the H$_2$ oxidation rate of the Hhy-only mutant was 3-fold higher than the Huc-only strain (**Figure 2.3b**). H$_2$ oxidation was also observed in the cytochrome *bcc-aa$_3$* oxidase only strain, showing the complex receives electrons from H$_2$ oxidation. However, this activity was 3-fold lower than observed for wild-type cells, suggesting that cytochrome *bd* complex also receives electrons from H$_2$ oxidation at 3 days post-OD$_{max}$ (**Figure 2.3b**). In striking contrast, H$_2$ oxidation in the cytochrome *bd* only strain was 6.3-fold greater than wild type (**Figure 2.3b**). This may be due to an increase in the amount of hydrogenases present in the cells or deregulation of their activity, due to metabolic remodeling to cope with the loss of the proton pumping cytochrome *bcc-aa$_3$* oxidase (161). The O$_2$ consumption for the wild-type and Huc- and Hhy-only strains, when spiked with H$_2$, fit approximately with the 2:1 stoichiometry observed in our initial experiment (**Figure 2.3c**). However, O$_2$ consumption of either oxidase mutants in the presence of H$_2$ was significantly higher than wild-type and did not conform to a 2:1 ratio (**Figure 2.3c**),

suggesting H_2 is co-metabolized with other substrates (e.g. carbon reserves). Taken together, these data show that both terminal oxidase complexes accept electrons from H_2 oxidation.

Next, we probed the specifics of coupling between Huc and Hhy and the terminal oxidases, by inhibiting the cytochrome *bcc-aa$_3$* complex with zinc azide. In wild-type cells, the addition of azide led to a 4.6-fold reduction in H_2 oxidation, demonstrating that hydrogenase activity is primarily coupled to the cytochrome *bcc-aa$_3$* complex at 3 days post-OD_{max}. For the Huc-only strain, the addition of zinc azide largely abolished H_2 oxidation (8.4-fold reduction), suggesting that Huc is obligately coupled to the cytochrome *bcc-aa$_3$* complex (**Figure 2.3b)**. In contrast, only a 1.5-fold reduction in Hhy activity was observed; this demonstrates that while Hhy utilizes the cytochrome *bcc-aa$_3$* oxidase, it is promiscuous and can also donate electrons to the alternative cytochrome *bd* complex (**Figure 2.3b**). The addition of azide to the cytochrome *bcc-aa$_3$* only strain led to near complete inhibition of H_2 oxidation (10.5-fold decrease) and O_2 consumption (22.9-fold decrease) (**Figure 2.3c**). This confirms that Huc and Hhy require an active terminal oxidase to oxidize H_2, and thus are obligately coupled to the respiratory chain. The high level of H_2 oxidation observed in the cytochrome *bd* only strain was unchanged by azide treatment, which is expected given this complex is unaffected by azide inhibition (218).
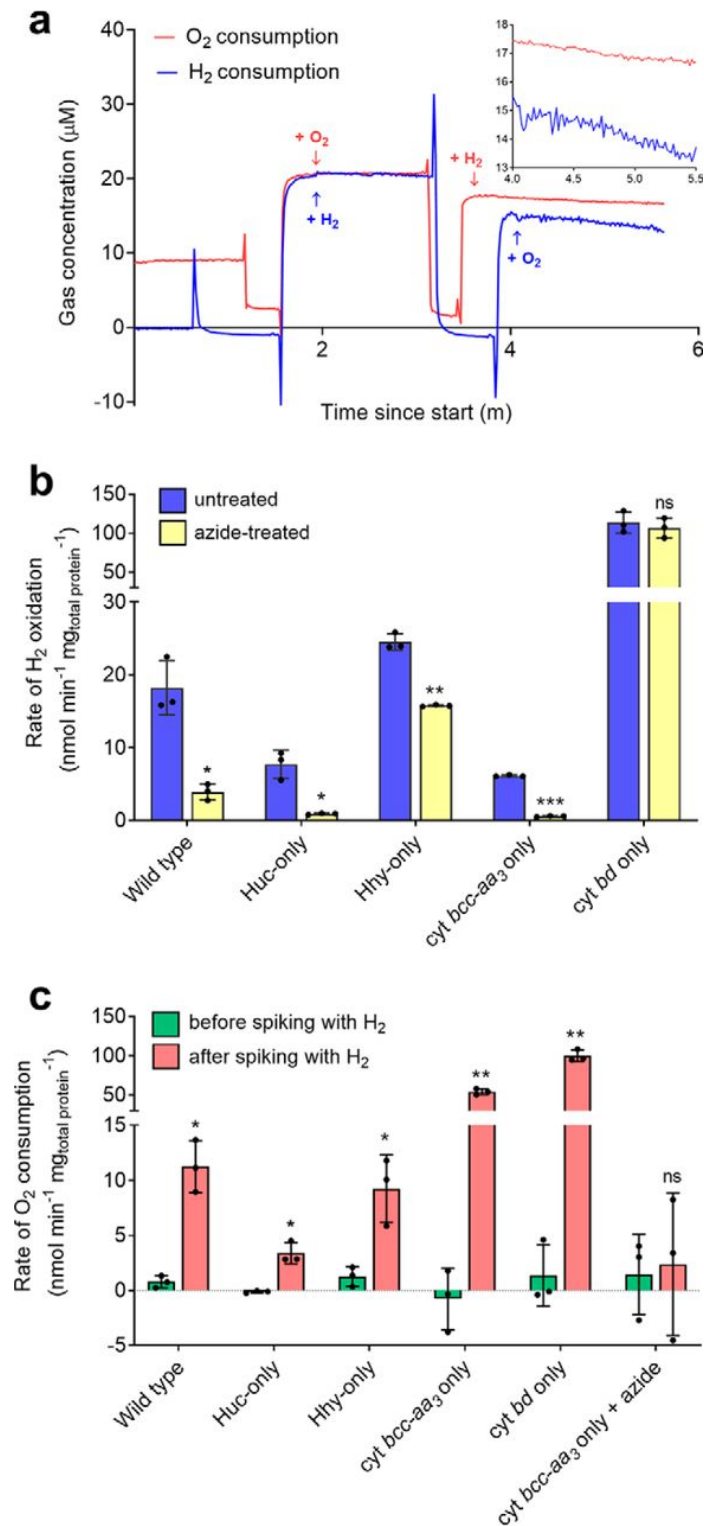
Figure 2.3. Interaction of Huc and Hhy with the terminal cytochrome oxidases. H_2 and O_2 consumption of whole cells from carbon-limited cultures (3 d post OD_{max} ~3.0) of wild-type, hydrogenase, and cytochrome oxidase mutant strains. **a)** Representative raw electrode traces of H_2 and O_2 consumption by carbon-limited wild-type *M. smegmatis* cultures. The top right inset shows an enlarged view of H_2 and O_2 consumption. H_2 oxidation is dependent on the

presence of O_2 and likewise, O_2 is not consumed without addition of H_2 as an electron source. **b)** The rate of H_2 uptake by whole cells before and after treatment with the cytochrome oxidase inhibitor zinc azide (250 μM). **c)** O_2 consumption in the same set of strains was measured using an oxygen microelectrode before and after addition of H_2. Values with asterisks indicate activity rates that are significantly different from the untreated whole cells based on student's t-test (* p ≤ 0.05; ** p ≤ 0.01; *** p ≤ 0.001; ns – not significant).

2.4.4 Huc and Hhy transfer electrons into the respiratory chain via the quinone pool

Having firmly established that Huc and Hhy activity is coupled to terminal oxidase activity under the conditions tested, we sought to better understand this relationship. To do so, we measured H_2 oxidation of the wild-type, Huc-only, and Hhy-only strains in the presence of selective respiratory chain inhibitors and uncouplers. First, we tested whether the electrons generated by Hhy and Huc are transferred to the electron carrier menaquinone, which donates electrons to both terminal oxidases in mycobacteria (219). To do so, we tested the effect of HQNO, a competitive inhibitor of quinone-binding (218, 220), on H_2 oxidation in our wild-type, Huc- and Hhy-only strains. Addition of HQNO led to a 8.6-fold and 10.4-fold decrease in H_2 oxidation by the Huc- and Hhy-only mutants respectively, demonstrating transport of electrons generated by these enzymes occurs via the menaquinone pool (**Figure 2.4a, b**). There was a 2.5-fold decrease in the activity of wild-type cells treated with HQNO, confirming that H_2 oxidation is also menaquinone dependent in a non-mutant background (**Figure 2.4c**).

Next, we tested the effect of valinomycin on H_2 oxidation. Valinomycin is an ionophore that binds K^+. It forms a positively charged complex, specifically transporting K^+ ions across the cellular membrane along the electrical gradient, collapsing the electrical potential component of the proton-motive force (PMF) in respiratory bacteria (221). In *M. smegmatis* at an external pH above 5, the majority of the PMF is driven by electrical potential (156); thus addition of valinomycin under our assay conditions (pH 5.8) leads to a dramatic reduction in the PMF. Huc and Hhy exhibited strikingly different responses to valinomycin. Valinomycin reduced H_2 oxidation by 20-fold in the Huc-only strain, but increased oxidation by 1.3-fold in the Hhy-only

and wild-type strains, compared to untreated cells (**Figure 2.4**). The near complete loss of Huc activity due to valinomycin treatment indicates this enzyme is energy-dependent, requiring the largely intact PMF to function; this may indicate that the complex is obligately associated with the proton-translocating cytochrome *bcc-aa*$_3$ supercomplex. Conversely, the increase in Hhy activity demonstrates that this enzyme does not require the PMF, with the increase in H$_2$ oxidation possibly resulting from increased metabolic flux as the cells attempt to maintain their membrane potential.

Next, we tested the effect of nigericin on H$_2$ oxidation. Nigericin is an ionophore which acts as an antiporter of K$^+$ and H$^+$ ions and is uncharged in its ion bound forms (221). In our assay, nigericin leads to the net efflux of K$^+$ ions from and influx of H$^+$ ions into the cell, dissipating the proton gradient but not affecting membrane potential. The experimentally determined pH of the external media in our assay was 5.8. Under these conditions, ΔpH across the membrane accounts for approximately one-third of the PMF in *M. smegmatis* (156). Thus, the addition of nigericin will lead to a significant net influx of protons and acidification of the cytoplasm, shifting the equilibrium for H$_2$ towards reduction. Addition of nigericin inhibited H$_2$ oxidation to a moderate degree in our assay. Wild-type and Huc-only strains exhibited a ~1.5-fold decrease in activity, whereas Hhy activity was reduced 2.3-fold (**Figure 2.4**). This inhibition of both hydrogenases may be attributed to cytoplasmic acidification or direct inhibition of these enzymes by nigericin. The inhibitory effect of nigericin towards Hhy is in contrast with the stimulatory effect of valinomycin on this enzyme. This possibly results from the fact that valinomycin directly diminishes the PMF but nigericin does not, or it may be a consequence of a more complicated secondary effect on cellular metabolism.
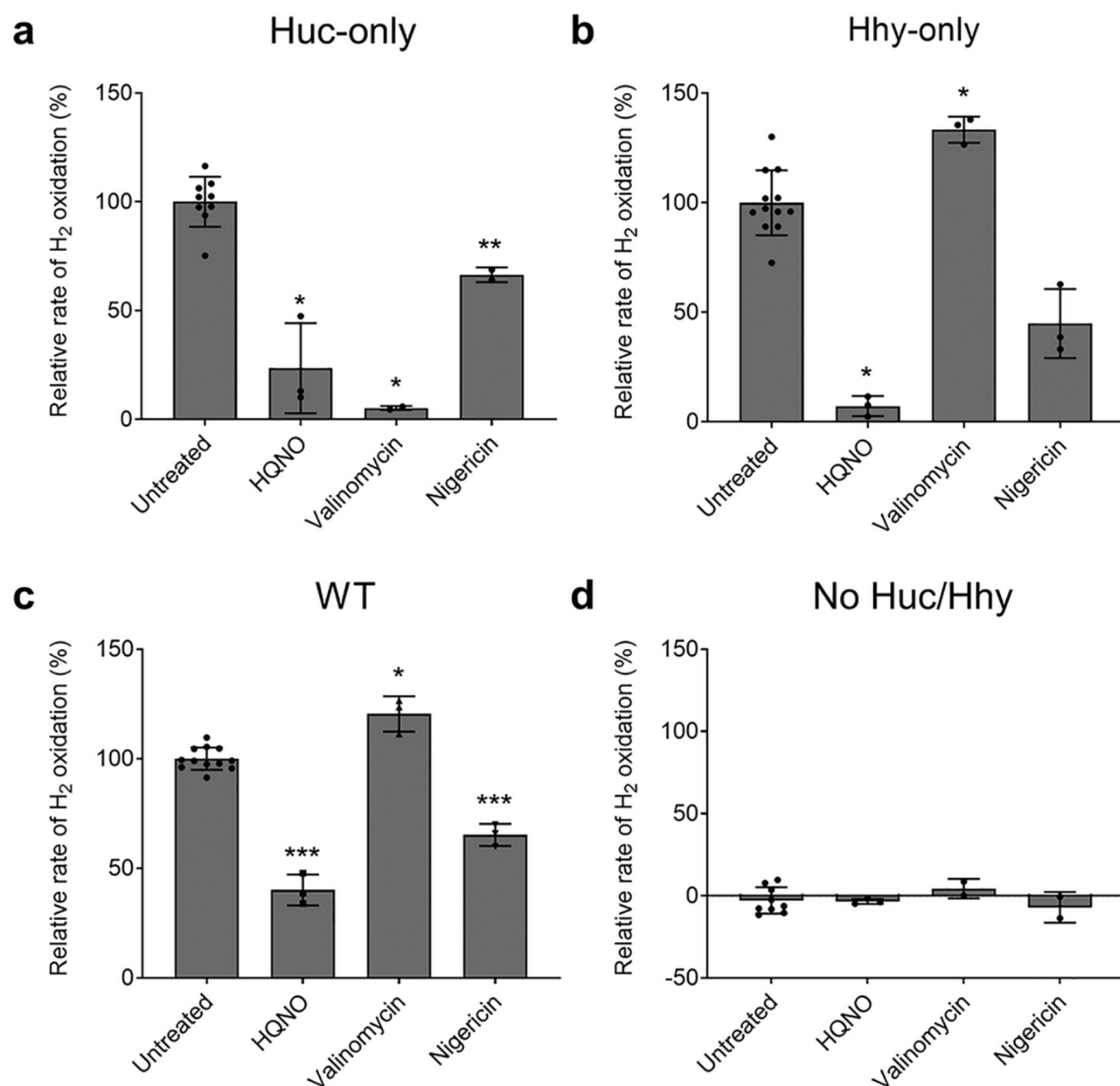
Figure 2.4. Inhibition of Huc and Hhy coupling to the electron transport chain. H_2 oxidation rates of **a)** Huc-only, **b)** Hhy-only, **c)** wild-type, and **d)** no Huc/Hhy (triple hydrogenase deletion) cultures were measured using a hydrogen microelectrode before and after treatment with different respiratory chain uncouplers and inhibitors: HQNO (40 µM), valinomycin (10 µM), nigericin (10 µM). Rates were normalized to mg total protein and expressed as percentage relative to the average rate of untreated cells. Cultures during carbon limitation (3 d post OD_{max} ~3.0) were used. Values with asterisks indicate activity rates that are significantly different from the untreated whole cells based on student's t-test (* $p \leq 0.05$; ** $p \leq 0.01$; *** $p \leq 0.001$)

2.4.5 A model of the integration of hydrogenases in the mycobacterial respiratory chain

Based on the findings from our work we propose a model for integration of Huc and Hhy into the mycobacterial respiratory chain, which we outline in **Figure 2.5**. Our data show that both Huc and Hhy are obligately coupled to O_2 reduction via the terminal oxidases of the respiratory chain. Huc preferentially donates electrons to the cytochrome *bcc-aa*$_3$ complex, while Hhy donates electrons both to cytochrome *bcc-aa*$_3$ and cytochrome *bd* complexes. Both enzymes are membrane associated, positioning them for the transfer of electrons produced by H_2 oxidation to the respiratory chain. The size of Huc and its co-migration with the cytochrome *bcc-aa*$_3$ complex on a native gel suggest that Huc association with the membrane may be mediated by protein-protein interactions, possibly with the terminal oxidase. Inhibition of Huc and Hhy activity due to blocking of menaquinone binding by HQNO shows that electrons from these enzymes are transferred to the terminal oxidases via this cofactor. It remains to be resolved whether electron transfer to menaquinone is directly mediated by the hydrogenases or through an intermediate protein, for example the FeS proteins co-transcribed with the hydrogenase large and small subunits in the *huc* and *hhy* operons (83). Collapse of the PMF by valinomycin treatment leads to near complete inhibition of Huc activity, but enhancement of Hhy activity. This suggests a distinct relationship exists between these enzymes and the PMF, with Huc requiring an intact PMF, potentially due to its obligate coupling to the cytochrome *bcc-aa*$_3$ complex.

Our data also demonstrates that Huc and Hhy are differentially regulated during mycobacterial growth and persistence. The tightly controlled expression and activity of Huc during the transition between growth and dormancy suggests that it oxidizes H_2 mixotrophically as heterotrophic energy sources become scarce. The proton-motive force generated by Huc, through obligate interaction with the cytochrome *bcc–aa*$_3$ complex, may help to energize the cell during the transition to dormancy. Expression of *hhyL*, the gene encoding the large Hhy subunit, is upregulated at the cessation of cell division. However, high levels of Hhy-mediated

H$_2$ oxidation are only observed several weeks into dormancy. This suggests that the enzyme primarily functions to meet maintenance needs during persistence, a role that is further supported by its promiscuous utilization of cytochrome *bd* oxidase. The observed lag between *hhyL* transcription and Hhy activity suggests that regulation of this hydrogenase also occurs downstream of transcription. This possibly provides flexibility to *M. smegmatis* by not committing to synthesis of this resource-intensive protein immediately upon exhaustion of carbon-derived energy sources but allowing rapid deployment of Hhy if resources remain scarce.
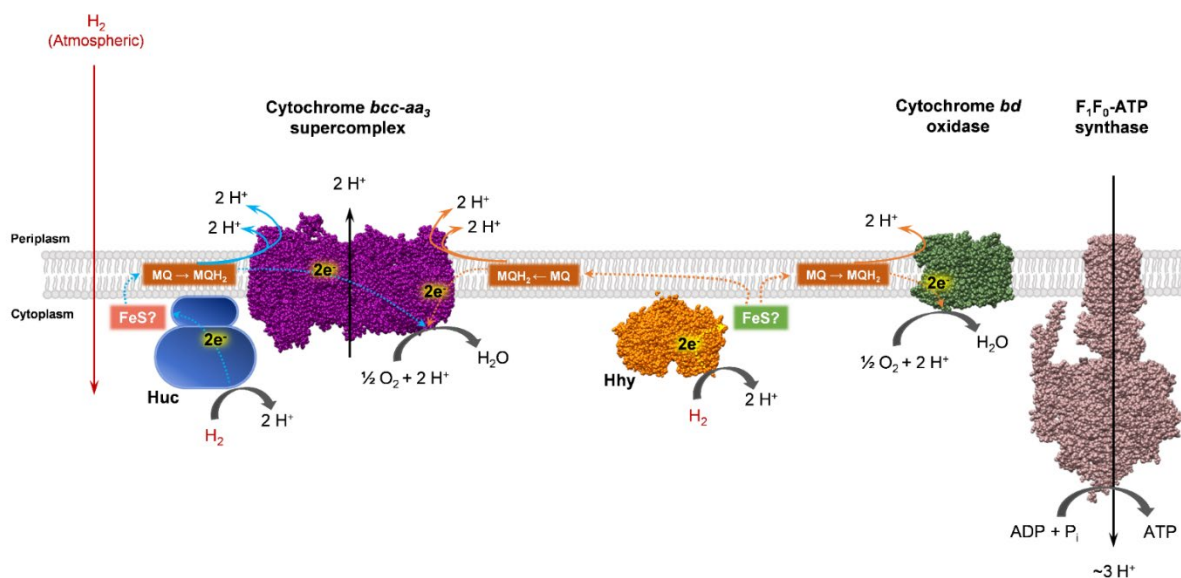
Figure 2.5. Huc and Hhy differentially energize the mycobacterial respiratory chain during carbon starvation. Both Huc and Hhy oxidize H$_2$ to two H$^+$ and two e$^-$. The electrons are used to reduce membrane-soluble menaquinone (MQ) to menaquinol (MQH$_2$). It is possible that the genetically associated iron-sulfur proteins (FeS) HucE (MSMEG_2268) and HhyE (MSMEG_2718) relay electrons from the hydrogenase to the menaquinone pool. Huc-reduced MQH$_2$ transfers electrons exclusively to the cytochrome *bcc-aa*$_3$ supercomplex, where they are transferred to the terminal electron acceptor O$_2$, yielding H$_2$O and resulting in efflux of 6 H$^+$ from the cell. Under starvation or hypoxia, Hhy-derived MQH$_2$ transfers electrons to either cytochrome *bcc-aa*$_3$ or the alternate cytochrome *bd* complex. This results in the efflux of six H$^+$ or two H$^+$ from the cell, respectively, together with the reduction of O$_2$ to H$_2$O. The proton gradient generated by H$_2$ oxidation maintains membrane potential and allows generation of ATP via F$_1$F$_o$-ATP synthase.

Although this work provides the basis for understanding how Huc and Hhy are regulated and integrated into cellular metabolism, further investigation is required to fully understand the mechanisms that regulate these enzymes and the biochemistry of their H_2 oxidation. For example, what are the regulatory pathways that allow the cell to rapidly switch on Huc when resources become scarce and then off again as *M. smegmatis* commits to dormancy? Analogously, how do non-replicating *M. smegmatis* cells regulate transcription and then activity of Hhy during a state of resource limitation? In addition, the data we present suggests physical interactions between Huc and respiratory chain components. Purification of both Huc and Hhy from their native context in the *M. smegmatis* cell will likely provide insight into the protein-protein interactions that mediate electron transfer from these enzymes. Furthermore, purification of these complexes, combined with structural and spectroscopic analysis, will likely provide insight into the mechanisms that underpin the high H_2 affinity and O_2 tolerance of Huc and Hhy. In conjunction with this study, these data will provide a richer picture of how mycobacteria consume H_2 during growth and persistence.

2.5   Footnotes

Ralf Schittenhelm and Dr. Cheng Huang of the Monash Proteomic and Metabolic Facility for performing MS analyses.

The authors declare that they have no conflicts of interest.

Chapter 3

Putative iron-sulfur proteins are required for hydrogen consumption and enhance survival of mycobacteria

Zahra F. Islam[1] & Paul R. F. Cordero[1], Chris Greening[1]*

Form the [1] School of Biological Sciences, Monash University, Clayton, VIC 3800, Australia

* Correspondence can be addressed to Associate Professor Chris Greening
(Chirs.Greening@monash.edu)

This chapter is an edited version of the **published paper in Frontiers Microbiology**, where I am a co-first author. I made an equal contribution to the published manuscript, including performing experiments (mutant strain construction, complementation, respirometry measurements, activity staining), designing experiments, analyzing data, and drafting and editing the paper. For this thesis, the chapter has been edited to reflect the sections of the paper that I contributed, focusing on the biochemistry and physiology aspect of the putative iron-sulfur proteins, such that my contribution is 50%. Other authors contributed to study conceptualization and design (C.G.), mutant strain construction (Z.F.I.), physiological analysis (Z.F.I.), data analysis (Z.F.I.., C.G.), and writing / editing (R.G., C.G.).

3.1   Abstract

Aerobic soil bacteria persist by scavenging molecular hydrogen (H_2) from the atmosphere. This key process is the primary sink in the biogeochemical hydrogen cycle and supports the productivity of oligotrophic ecosystems. In *Mycobacterium smegmatis*, atmospheric H_2 oxidation is catalyzed by two phylogenetically distinct [NiFe]-hydrogenases, Huc (group 2a) and Hhy (group 1h). However, it is currently unresolved how these enzymes transfer electrons derived from H_2 oxidation into the aerobic respiratory chain. In this work, we used genetic approaches to confirm that two related putative iron-sulfur cluster proteins encoded on the hydrogenase structural operons, HucE and HhyE, are required for H_2 consumption in *M. smegmatis*. H_2 oxidation was reduced when the genes encoding these proteins were deleted individually and was eliminated when they were deleted in combination. In turn, the growth yield and long-term survival of these deletion strains was modestly but significantly reduced compared to the parent strain. In both biochemical and phenotypic assays, the mutant strains lacking the putative iron-sulfur proteins phenocopied those of hydrogenase structural subunit mutants. We hypothesize that these proteins mediate electron transfer between the catalytic subunits of the hydrogenases and the menaquinone pool of the *M. smegmatis* respiratory chain; however, other roles (e.g. in maturation) are also plausible and further work is required to resolve their role. The conserved nature of these proteins within most Hhy- or Huc-encoding organisms suggests that these proteins are important determinants of atmospheric H_2 oxidation.

3.2   Introduction

Over the last decade, various studies have revealed that aerobic bacteria conserve energy during persistence through aerobic respiration of atmospheric hydrogen (H_2) (12, 33–35, 96, 195). This process is now recognized to be important for biogeochemical and ecological reasons. Gas-scavenging soil bacteria serve as the primary sink in the global hydrogen cycle and are responsible for the net consumption of approximately 70 million tonnes of H_2 each

year (6, 11, 96, 196). More recently, it has been inferred that this process supports the productivity and biodiversity of various ecosystems, especially low-carbon soils (29, 30, 49, 197–200, 216). Atmospheric H_2 oxidation appears to be a widespread trait among soil bacteria. To date, bacteria from three phyla have been experimentally shown to oxidize atmospheric H_2, Actinobacteriota (10–12), Acidobacteriota (35, 204), and Chloroflexota (33). However, genomic and metagenomic studies have indicated at least 13 other phyla encode enzymes that can mediate this process (32, 49, 201).

The genetic basis and physiological role of atmospheric H_2 oxidation is now largely understood. This process has been most comprehensively studied in the genetically tractable soil actinobacterium *Mycobacterium smegmatis* (222). In this organism, atmospheric H_2 oxidation is mediated by two membrane-bound, oxygen-tolerant hydrogenases, Huc (group 2a [NiFe]-hydrogenase, also known as Hyd1 or cyanobacterial-type uptake hydrogenase) and Hhy (group 1h [NiFe]-hydrogenase, also known as Hyd2 or actinobacterial-type uptake hydrogenase) (83). Additionally, *M. smegmatis* encodes a third [NiFe]-hydrogenase, Hyh (Hyd3), which mediates fermentative H_2 production during hypoxia (84). Both H_2-oxidizing hydrogenases contain a large subunit containing the [NiFe] active site (HucL, HhyL) and a small subunit containing three iron-sulfur clusters (HucS, HhyS), as well as potential additional subunits (83, 223). These two hydrogenases are upregulated in stationary-phase cells, including in response to organic carbon limitation (36, 83). Consistently, when the structural subunits of these hydrogenases are deleted, strains show reduced growth yield and impaired long-term survival during starvation (11, 36, 83). Similar findings have been made in *Streptomyces avermitilis*; the sole hydrogenase of this organism, Hhy, is exclusively expressed in exospores and strains lacking this enzyme exhibit severe survival defects (34, 96). Given these findings, it is proposed that bacteria shift from growing on organic compounds to persisting on atmospheric trace gases. Indeed, theoretical calculations indicate that the energy derived from atmospheric H_2 oxidation (0.53 ppmv) can sustain the maintenance of 10^7 to 10^8 cells per gram of soil (21).

Despite this progress, little is currently known about the biochemical basis of atmospheric H_2 oxidation. One outstanding question is how electrons derived from H_2 oxidation are transferred to the respiratory chain. Most classes of respiratory uptake hydrogenases are predicted to be co-transcribed with a cytochrome *b* subunit (49, 100). For example, such subunits interact with the prototypical oxygen-tolerant hydrogenases (group 1d [NiFe]-hydrogenases) of *Escherichia coli* and *Ralstonia eutropha*; they anchor the hydrogenase to the membrane and transfer electrons from the hydrogenase small subunit to the quinone pool (191, 192). However, we did not detect equivalent proteins in the operons encoding the structural subunits of Huc (MSMEG_2261–2270) or Hhy (MSMEG_2722 – 2718) in *M. smegmatis* (**Figure 3.1**) (83). Putative iron-sulfur proteins, tentatively annotated as HucE (MSMEG_2268) and HhyE (MSMEG_2718), were encoded downstream of the hydrogenase structural subunits and may potentially fulfill this role instead (11, 83). In this work, we characterized the effects of deleting these genes on hydrogenase activity, growth, and survival in *M. smegmatis*.

3.3 Materials and Methods

3.3.1 Bacterial strains and growth conditions

All bacterial strains and plasmids used in this study are listed in (**Supplementary Table S6**). *Escherichia coli* TOP10 was maintained on lysogeny broth (LB) agar plates (10 g L^{-1} tryptone, 5 g L^{-1} NaCl, 5 g L^{-1} yeast extract, 15 g L^{-1} agar), while *Mycobacterium smegmatis* mc^{2}155 (212). and derived mutants were maintained on LB agar plates supplemented with 0.05% (w/v) Tween 80 (LBT). For broth culture, *E. coli* was grown in LB. *M. smegmatis* was grown in either LBT or in Hartmans de Bont (HdB) minimal medium (224) supplemented with 0.2% (w/v) glycerol. In all cases, liquid cultures were grown in rotary incubators at 37°C with agitation (200 rpm).
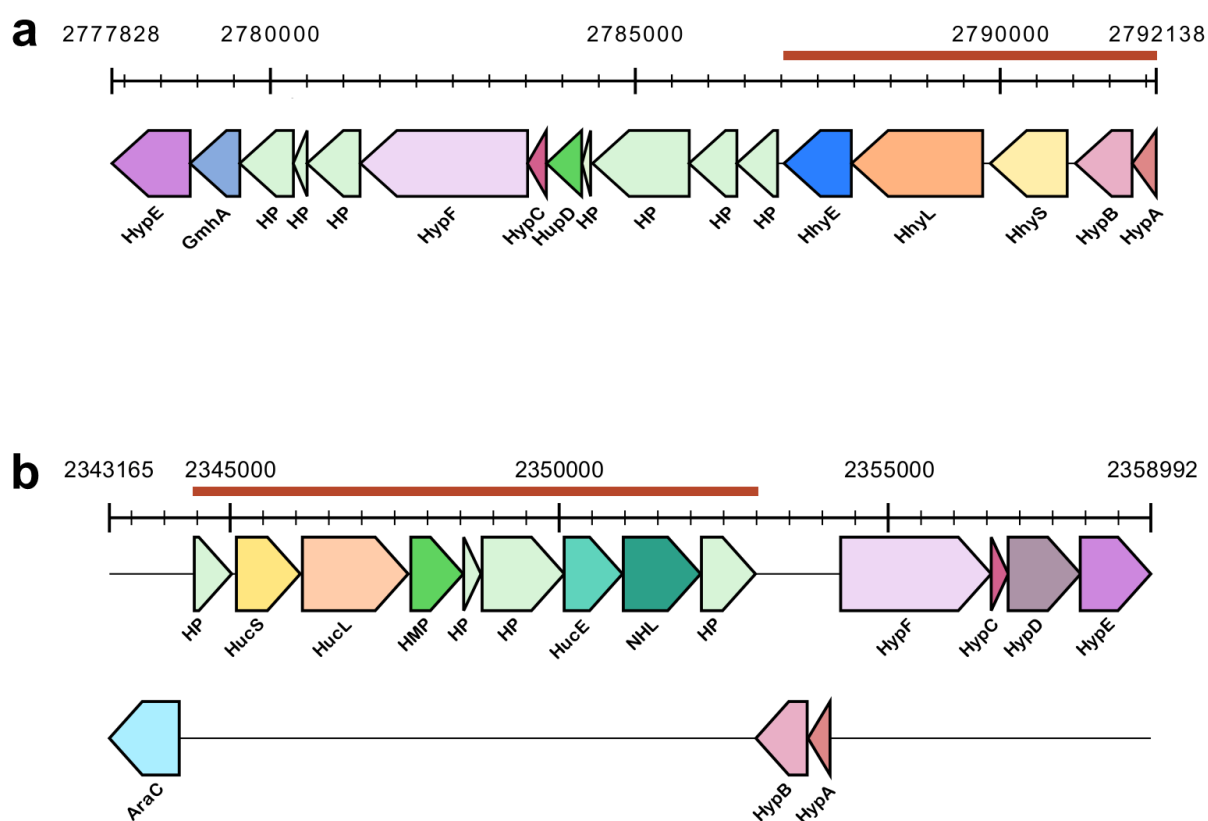
Figure 3.1. Genes associated with Huc and Hhy in *Mycobacterium smegmatis*. a) Organisation of the genes associated with the group 1h [NiFe]-hydrogenase, Hhy. **b)** Organisation of the genes associated with the group 2a [NiFe]-hydrogenase, Huc. Abbreviations: HMP = hydrogenase maturation protease; NHL = NHL repeat protein; GmhA = phosphoheptose isomerase homolog; AraC = arabinose regulatory protein homolog. The length of the genes is shown to scale. The red line is used to denote genes that are transcribed in operons, as verified by previous RT-PCR studies (83). Figure credit: Zahra Islam.

3.3.2   Mutant Strain Construction

Allelic exchange mutagenesis was used to produce markerless deletions of the genes encoding two putative iron-sulfur proteins, *hucE* (MSMEG_2268) and *hhyE* (MSMEG_2718) (**Supplementary Figure S3**). Briefly, a fragment containing fused left and right flanks of the MSMEG_2268 (1800 bp) and MSMEG_2718 (3098 bp) genes were synthesized by GenScript. These fragments were cloned into the *Spe*I site of the mycobacterial shuttle plasmid pX33 (210) to yield the constructs pX33-*huc*E and pX33-*hhy*E (**Supplementary Table**

S6). These constructs were propagated in *E. coli* TOP10 and transformed into wild-type *M. smegmatis* mc^{2}155 cells by electroporation. Gentamycin (5 µg mL^{-1} for *M. smegmatis* or 20 µg mL^{-1} for *E. coli*) was used in selective solid and liquid medium to propagate pX33. Creation of the double iron-sulfur cluster mutant (Δ*hucE*Δ*hhyE*) was achieved by transformation of Δ*hhyE* electrocompetent *M. smegmatis* mc^{2}155 with the pX33-*huc*E construct. Briefly, to allow for permissive temperature-sensitive vector replication, transformants were incubated on LBT gentamicin plates at 28°C until colonies were visible (5–7 days). Resultant catechol-positive colonies were subcultured onto fresh LBT gentamicin plates and incubated at 40°C for 3–5 days to facilitate integration of the recombinant plasmid flanks into the chromosome. The second recombination event was facilitated by subculturing catechol-reactive and gentamicin-resistant colonies onto LBT agar plates supplemented with 10% sucrose (w/v) and incubating at 40°C for 3–5 days. Catechol-unreactive colonies were subsequently screened by PCR to discern wild-type revertants from Δ*hucE*, Δ*hhyE* and Δ*hucE*Δ*hhyE* mutants. Primers used for the generation of mutants and for screening are listed in **Supplementary Table S7**.

3.3.3   Complementation Vector Construction

The genes for the putative iron-sulfur proteins were amplified by PCR and the resulting fragments were cloned into the constitutive expression plasmid pMV261 via *Pst*I/*Hin*dIII site for *hucE* and *Bam*HI/*Hin*dIII site for *hhyE* (225) to yield the constructs pMV*hucE* and pMV*hhyE* (**Supplementary Table S6**). Sequence fidelity of the genes was verified through Sanger sequencing and insertion of the genes into the vector was confirmed through restriction-digestion analysis (**Supplementary Figure S4**). The plasmid constructs were propagated in *E. coli* DH5α and transformed into *M. smegmatis* cells by electroporation. Vector pMV*hucE* was transformed into *M. smegmatis* wild-type and Δ*hucE* strains, while pMV*hhyE* was transformed into wild type and Δ*hhyE* mutant. In addition, an empty pMV261 was transformed into wild-type, Δ*hucE*, and Δ*hhyE* strains. These seven *M. smegmatis* strains were used for complementation experiments in respirometry and activity

staining. Kanamycin (20 μg mL^{-1} for *M. smegmatis* or 50 μg mL^{-1} for *E. coli*) was used in selective solid and liquid medium to propagate pMV261. Primers used for the generation of the constructs are listed in **Supplementary Table S7**.

3.3.4 Respirometry Measurements

Cultures of wild-type, derived mutants, and complemented mutant strains of *M. smegmatis* were grown in 125 mL aerated conical flasks containing 30 mL HdB medium supplemented with 0.2% glycerol. Respirometry measurements were performed with mid-stationary phase cells, i.e., 72 h post OD$_{max}$ (~3.0). A Unisense H$_2$ microsensor electrode was polarized at + 800 mV for 1 h using a Unisense multimeter and calibrated against standards of known H$_2$ concentration. Gas-saturated PBS was prepared by bubbling the solution with 100% (v/v) of either H$_2$ or O$_2$ for 5 min. The 1.1 mL microrespiration assay chambers were sequentially amended with stationary-phase cultures (0.9 mL, OD$_{600}$ = 3.0), H$_2$-saturated PBS (0.1 mL), and O$_2$-saturated PBS (0.1 mL). Chambers were stirred at 250 rpm, 37°C. Changes in H$_2$ concentration were recorded using Unisense Logger Software, and upon observing a linear change in H$_2$ concentration, rates of consumption were calculated over a period of 20 s, which corresponds to the most linear uptake of hydrogen by the cells. Oxidation rates were normalized against total protein concentration, which was determined by the bicinchoninic acid method (226) with bovine serum albumin standards.

3.3.5 Activity staining

Cultures of wild-type, derived mutants, and complemented mutant strains of *M. smegmatis* were grown in 2.5 L aerated conical flasks containing 500 mL HdB medium supplemented with 0.2% glycerol. For Huc activity staining, cultures of wild-type, Δ*hucS*, Δ*hucE*, Δ*hucS*Δ*hhyL*, Δ*hucE*Δ*hhyE*, and complemented Δ*hucE* and wild-type *M. smegmatis* (either with empty pMV261 or complementation vector pMV*hucE*) were harvested by centrifugation (10,000 × *g*, 10 min, 4°C) at early-stationary phase (24 h post OD$_{max}$, ~3.0) (223). For Hhy activity staining, cultures of wild-type, Δ*hhyL*, Δ*hhyE*, Δ*hucS*Δ*hhyL*,

70

Δ*hucE*Δ*hhyE*, and complemented Δ*hhyE* and wild-type *M. smegmatis* (either with empty pMV261 or complementation vector pMV*hhyE*) were harvested by centrifugation at mid-stationary phase (72 h post OD_{max}, ~3.0) (223). Harvested cultures were washed in phosphate-buffered saline solution (PBS; 137 mM NaCl, 2.7 mM KCl, 10 mM Na_2HPO_4, 2 mM KH_2PO_4, pH 7.4), and resuspended in 16 mL lysis buffer (50 mM Tris-Cl, pH 8.0, 1 mM PMSF, 2 mM $MgCl_2$, 5 mg mL^{-1} lysozyme, 40 µg mL^{-1} DNase, 10% glycerol). Resultant cell suspensions were passed through a Constant Systems cell disruptor (40,000 psi, four times), with unbroken cells removed by centrifugation (10,000 × g, 20 min, 4°C) to yield whole-cell lysates. Protein concentration was determined using a bicinchoninic acid assay with bovine serum albumin standards. Next, 20 µg of each whole-cell lysate was loaded onto two native 7.5% (w/v) Bis-Tris polyacrylamide gels prepared as described elsewhere (214) and run alongside a protein standard (NativeMark Unstained Protein Standard, Thermo Fisher Scientific) for 1.5 h at 25 mA. One gel was stained overnight at 4°C with gentle agitation using AcquaStain Protein Gel Stain (Bulldog Bio) for total protein determination. The other gel was incubated for hydrogenase activity staining in 50 mM potassium phosphate buffer (pH 7.0) supplemented with 500 µM nitroblue tetrazolium chloride (NBT) in an anaerobic jar amended with an anaerobic gas mixture (5% H_2, 10% CO_2, 85% N_2 v/v) overnight at room temperature.

3.3.6 Growth and survival assays

Cultures of wild type and derived mutants of *M. smegmatis* were inoculated into 125 mL conical flasks containing 30 mL LBT medium (initial OD_{600} of 0.001), in six biological replicates. Growth was monitored by measuring optical density at 600 nm (1 cm cuvettes; Eppendorf BioSpectrometer Basic); when OD_{600} was above 0.5, cultures were diluted ten-fold in LBT before measurement. Specific growth rate during mid-exponential growth was calculated for each replicate using GraphPad Prism (non-linear regression, exponential growth equation, least squares fit). The long-term survival of the cultures was determined by counting colony forming units (CFU mL^{-1}) of cultures 21 days post-OD_{max}. Cultures were serially diluted in HdB

containing no carbon source and spotted on to agar plates in technical quadruplicates. After incubation at 37°C for 3 days, the resultant colonies were counted.

3.4   Results

3.4.1   HucE and HhyE are essential for H_2 oxidation in *Mycobacterium smegmatis*

We used allelic exchange mutagenesis to generate markerless single and double mutants of the *hucE* and *hhyE* genes in *M. smegmatis*, i.e., Δ*hucE*, Δ*hhyE*, and Δ*hucE*Δ*hhyE.* Gene deletion was confirmed by PCR targeting chromosomal sequences adjacent to the flanking regions used for homologous recombination (**Supplementary Figure S3**). Assays were used to compare H_2 oxidation of these strains with the wild-type strain and strains containing previously generated deletions of the hydrogenase structural subunits, i.e., Δ*hucS*, Δ*hhyL*, and Δ*hucS*Δ*hhyL*, that lack hydrogenase activity (11, 36, 83).

We first used a H_2 electrode to measure rates of aerobic H_2 respiration mediated by whole cells of each strain. There were significant differences in the rate of H_2 oxidation for all deletion strains compared to the wild type (**Figure 3.2a**). Loss of *hucE* and *hhyE* resulted in rate reductions of 1.8-fold and 8.4-fold, respectively; such reductions were statistically indistinguishable from those observed in the mutants of the hydrogenase structural subunits *hucS* and *hhyL*. Deletion of both iron-sulfur proteins (Δ*hucE*Δ*hhyE*) or both hydrogenase structural subunits (Δ*hucS*Δ*hhyL*) caused complete cessation of H_2 oxidation, highlighting that these two hydrogenases are solely responsible for H_2 oxidation and that the putative iron-sulfur proteins are indispensable for this process. The low-level negative rates in Δ*hucE*Δ*hhyE* and Δ*hucS*Δ*hhyL* strains most likely reflect drift of the electrode rather than actual H_2 production by Hyh (Hyd3), since this hydrogenase is only upregulated during hypoxia (83). We successfully complemented the Δ*hucE* and Δ*hhyE* strains by reintroducing the *hucE* and *hhyE* genes on the episomal plasmid pMV261 (225) (**Figure 3.2b**); in contrast, introducing the empty vector caused no effect and neither did introducing the complementation

vectors in a wild-type background. This restoration of Huc and Hhy activities in complemented iron-sulfur protein deletion mutants strongly indicate that HucE and HhyE are essential for H_2 oxidation. Moreover, the similarity in H_2 oxidation rates between the strains containing deletions of the catalytic subunits, compared to the putative iron-sulfur proteins, is consistent with HucE and HhyE being functionally linked with the Huc and Hhy hydrogenases, respectively.

A

B
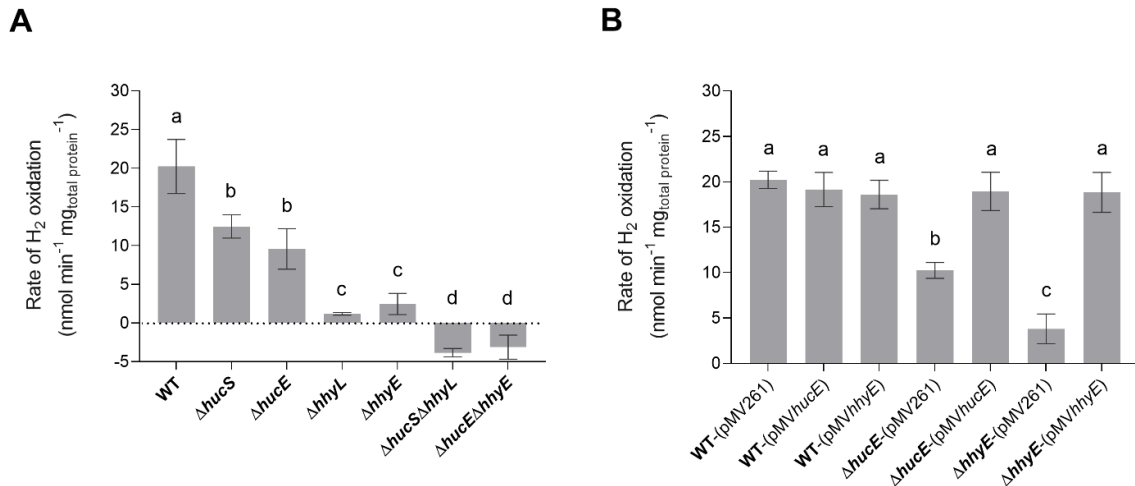
Figure 3.2. **Hydrogen oxidation by wild-type, derived mutants, and complemented mutant strains of _M. smegmatis._** H_2 uptake by whole cells in mid-stationary phase (72 h post $OD_{max} \sim 3.0$) was measured amperometrically using a Unisense H_2 electrode. **a)** Comparison of the rates of H_2 oxidation between wild-type, single and double mutants of the iron-sulfur proteins (_ΔhucE_, _ΔhhyE_, _ΔhucEΔhhyE_), and single and double mutants of hydrogenase structural subunits (_ΔhucS_, _ΔhhyL_, _ΔhucSΔhhyL_). **b)** Rates of H_2 oxidation in _ΔhucE_ and _ΔhhyE_ strains complemented with expression of _hucE_ and _hhyE_, respectively. Controls include wild-type, _ΔhucE_, and _ΔhhyE_ strains transformed with empty vector pMV261 and wild-type strain transformed with complementation vectors pMV_hucE_ and pMV_hhyE_. Error bars show standard deviations of three biological replicates and values labeled with different letters are significantly different ($p < 0.05$) based on a one-way ANOVA.

In an interrelated assay, we performed activity staining of the Huc and Hhy hydrogenases using whole-cell lysates of wild-type and deletion mutant strains, with and without the complementation vectors, in the presence of the artificial electron acceptor nitroblue tetrazolium chloride. In the Huc activity staining gel (**Figure 3.3a**), three bands were observed

in the whole-cell lysates of wild-type strains, with or without complementation vectors: the top high-MW band, middle mid-MW band, and bottom low-MW band. Both the high-MW and low-MW bands correspond to Huc activity (223) and these bands were not observed in strains lacking either *hucS* or *hucE*. However, Huc activity was restored when the Δ*hucE* strain was complemented by episomal expression of *hucE*. For Hhy activity staining (**Figure 3.3b**), a mid-sized MW band was observed in all wild-type strains. This band, which is the same middle band observed in the Huc activity stain (**Figure 3.3a**), corresponds to Hhy activity (11, 223). No Hhy staining was detected with the loss of either *hhyL* or *hhyE*, but complementation of the Δ*hhyE* strain with *hhyE* restored Hhy activity. The similarity in the staining bands observed between Δ*hucS* and Δ*hucE* strains or between Δ*hhyL* and Δ*hhyE* indicate that the putative iron-sulfur proteins HucE and HhyE, like their respective hydrogenase core subunits HucS and HhyL, are important for hydrogenase activity. The artificial electron acceptor cannot compensate for the loss of HucE/HhyE and neither can HucE for HhyE nor HhyE for HucE. This further supports the model that HucE and HhyE form a functional association with Huc and Hhy, respectively.
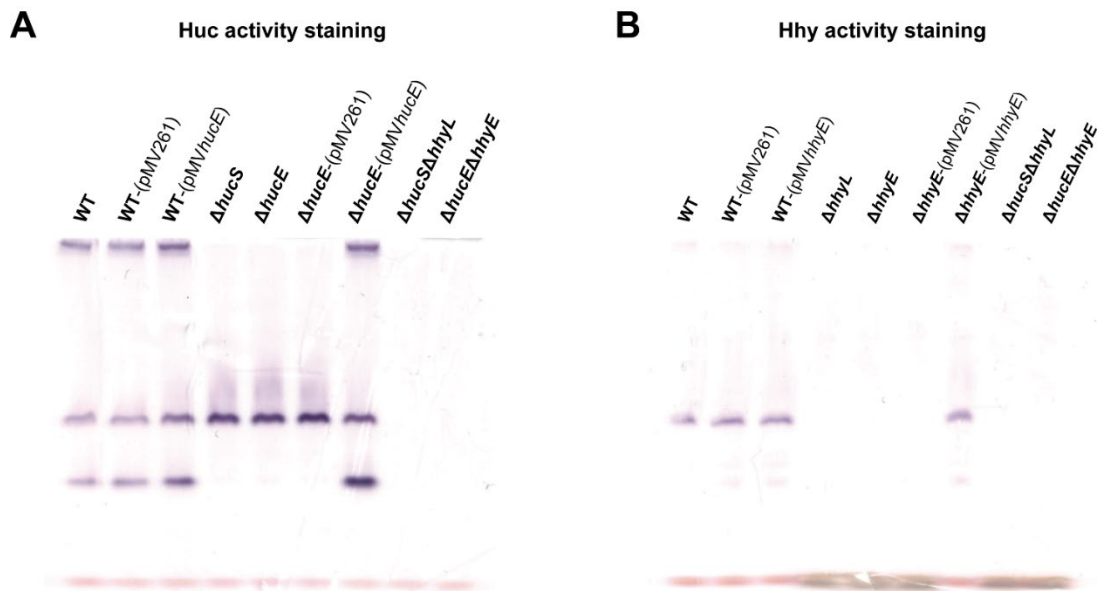
Figure 3.3. Hydrogenase activity staining in wild-type, derived mutants, and complemented mutant strains of *M. smegmatis.* Whole-cell lysates were used for zymographic staining of H_2 uptake in a H_2-rich atmosphere with nitroblue tetrazolium as artificial electron acceptor. **a)** Huc activity staining of cultures of wild-type, Δ*hucS*, Δ*hucE*, Δ*hucS*Δ*hhyL*,

Δ*hucE*Δ*hhyE*, and complemented Δ*hucE* and wild-type *M. smegmatis* (either with empty pMV261 or complementation vector pMV*hucE*) harvested at early-stationary phase (24 h post $OD_{max} \sim 3.0$). **b)** Hhy activity staining of cultures of wild-type, Δ*hhyL*, Δ*hhyE*, Δ*hucS*Δ*hhyL*, Δ*hucE*Δ*hhyE*, and complemented Δ*hhyE* and wild-type *M. smegmatis* (either with empty pMV261 or complementation vector pMV*hhyE*) harvested at mid-stationary phase (72 h post $OD_{max} \sim 3.0$). The original gels and Coomassie stain are shown in **Supplementary Figure S5**.

3.4.2   HucE and HhyE mutant strains have significant growth and survival defects

Previous genetic studies have shown that the hydrogenases modestly increase growth yield and long-term survival of *M. smegmatis* (36, 195). We therefore tested whether these findings extended to the putative iron-sulfur proteins by analyzing the growth rate, growth yield, and long-term survival of the seven aforementioned strains when cultured aerobically on rich media (LBT). In line with previous findings (11, 83, 195), no significant differences in specific growth rate were observed between the strains (**Figure 3.4a**). However, there was a 10% reduction in the specific growth yield of the HhyE mutant compared to the wild-type strain ($OD_{maxwt} = 4.19 \pm 0.21$; OD_{max} Δ*hhyE* = 3.81 ± 0.09; *p* = 0.008) (**Figure 3.4b**). This phenotype extended to the double mutant strain (Δ*hucE*Δ*hhyE*) and again phenocopied single and double mutants lacking the *hhyL* gene.

We also tested whether the strains were defective in long-term survival by counting colonies of aerobic cultures 21 days following OD_{max}. There were significant reductions in the survival of most strains compared to the wild-type (**Figure 3.4c**). Cell counts were approximately two-fold lower for the Δ*hhyE* and Δ*hhyL* strains (*p* < 0.02), and four-fold lower for the double mutant strains (*p* < 0.002), relative to the wild-type. These findings agree with previous reports that atmospheric H_2 oxidation by the hydrogenases enables *M. smegmatis* to survive energy starvation (195) and further supports that the putative iron-sulfur proteins contribute to this function. For reasons currently unclear, no phenotypes were observed for the Δ*hucE* strain.
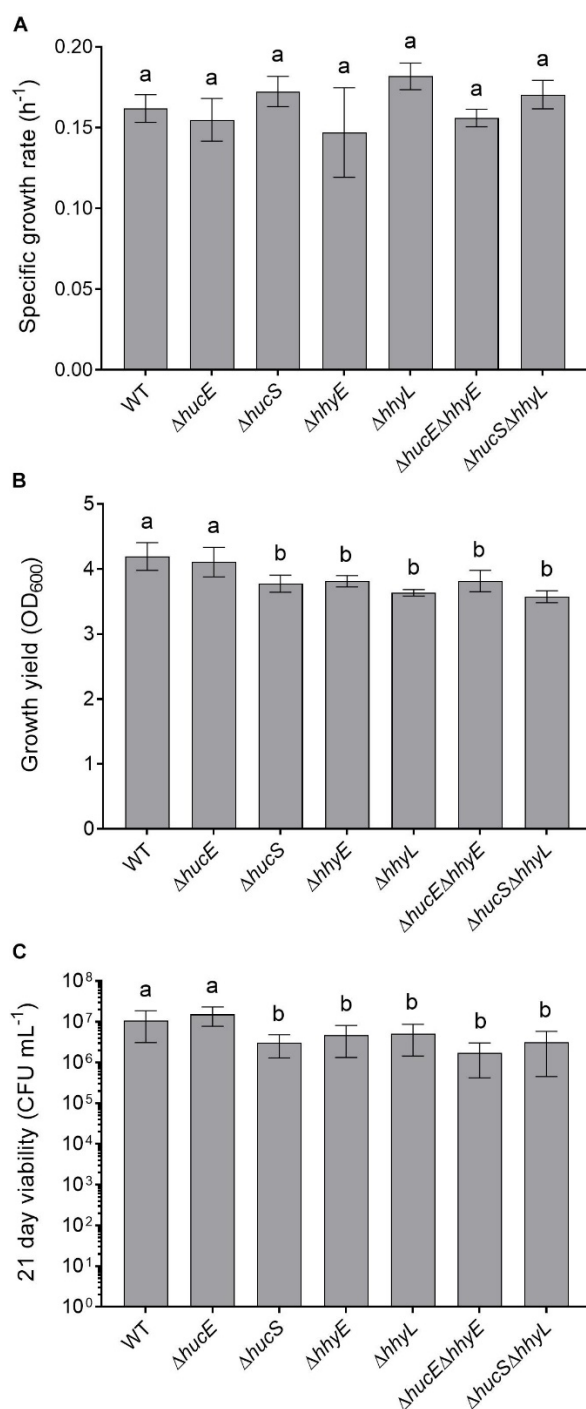
Figure 3.4. Comparison of growth and survival between wild-type and mutant strains of _M. smegmatis._ Seven strains were grown on lysogeny broth supplemented with Tween80 (LBT): wild-type, single and double mutants of the iron-sulfur proteins (Δ_hucE_, Δ_hhyE_, Δ_hucE_Δ_hhyE_), and single and double mutants of hydrogenase structural subunits (Δ_hucS_, Δ_hhyL_, Δ_hucS_Δ_hhyL_). **a)** Specific growth rate (μ) during exponential phase. **b)** Final growth yield (OD$_{max}$) at 24 h post-stationary phase. **c)** Long-term survival (CFU mL^{-1}) at 21 days post-stationary phase. Error bars show standard deviations of six biological replicates. Values labeled with different letters are significantly different ($p < 0.05$) based on a one-way ANOVA. Experiment performed by Zahra Islam.

76

3.5   Discussion

In summary, this study shows that HucE and HhyE are required for the enzymatic activity and physiological function of the mycobacterial uptake hydrogenases. Strains lacking these proteins showed no hydrogenase activity in either amperometric or zymographic assays. Furthermore, the *hhyE* mutant exhibited growth and survival phenotypes similar to those of the hydrogenase structural subunit *hhyL* mutant (36, 195); as with the structural subunit mutants, these phenotypes are relatively minor, likely reflecting the numerous survival mechanisms present in *M. smegmatis* such as the ability to persist on carbon monoxide (223). Despite some sequence similarity between the two proteins, they are non-redundant, as there was no compensation in hydrogenase activity in the single mutant strains.

This study lends some support to the hypothesis that these proteins serve as the immediate electron acceptors for the group 2a and group 1h [NiFe]-hydrogenases. There are broadly five lines of evidence that support this hypothesis: (i) the presence of highly conserved motifs for binding iron-sulfur clusters (33), (ii) the essentiality of these proteins for the function of these hydrogenases, (iii) their association with the structural rather than maturation operons of the hydrogenases (83), (iv) co-localization of HhyL, HhyS, and HhyE subunits on native polyacrylamide gels (223), and (v) their genomic association with hydrogenases that lack known electron transfer subunits (e.g., cytochrome *b* subunits) (**Supplementary Figure S6**). With the respect to the latter point, it is interesting that these proteins are conserved in Cyanobacteria, given the immediate electron acceptors of their uptake hydrogenases have long remained enigmatic (99). It is also notable that HucE proteins encode the signature motifs of a Rieske iron-sulfur cluster (227). Given their unusual ligands, these clusters have a higher standard redox potential (E_o' > −150 mV) than most iron-sulfur clusters (e.g., ferredoxins) (228). They would therefore be well-poised to accept the relatively high-potential electrons derived from atmospheric H_2 and transfer them to menaquinone. Consistently, zymographic studies suggest that the high-affinity hydrogenases operate at higher redox potential than

prototypical hydrogenases, given they are reactive with the nitroblue tetrazolium (E_o' = −80 mV) but not viologen compounds (E_o' = −360 mV) (11, 229).

While this study demonstrates HucE and HhyE are important for mycobacterial hydrogenase activity, further work is ultimately needed to resolve their respective function. While a role in electron transfer is most plausible, we have not demonstrated that these proteins interact with the hydrogenases and it is notable that the artificial electron acceptor nitroblue tetrazolium chloride cannot compensate for their absence. In this regard, other roles are also possible and compatible with the available evidence, for example as specific assembly factors and/or structural scaffolds for the hydrogenases. For example, it has been demonstrated that a rubredoxin-related protein is important for aerobic maturation of the group 1d [NiFe]-hydrogenase in *R. eutropha* (230). Furthermore, it is possible that other hypothetical proteins downstream of HucE and HhyE may also serve as electron acceptor candidates, in particular MSMEG_2717 that shares homology to PHG067, the proposed electron acceptor of *R. eutropha* (190). Biochemical studies, including studying the redox chemistry of these proteins and their interactions with the as-yet-unpurified hydrogenases, are now required to distinguish these possibilities and develop a sophisticated understanding of their function.

3.6   Footnotes

Supplementary Information: The supplementary material for this chapter can be found in **Appendix B.**

Chapter 4

Mycobacterial hydrogen metabolism is regulated by catabolite repression

Paul R. F. Cordero[1], Ashleigh Kropp[1], Cheng Huang[2], Ralf B. Schittenhelm[2], Rhys Grinter[1]*, Chris Greening[1]*

Form the [1] Department of Microbiology, Monash Biomedicine Discovery Institute, Monash University, Clayton, VIC 3800, Australia; [2] Monash Biomedical Proteomics Facility and Department of Biochemistry, Monash Biomedicine Discovery Institute, Monash University, Clayton, VIC 3800, Australia

* Correspondence can be addressed to Associate Professor Chris Greening (Chirs.Greening@monash.edu) or Dr. Rhys Grinter (Rhys.Grinter@monash.edu)

This chapter has yet to be submitted for publication. I contributed 70% to this chapter, including performing most experiments (knockout and knockdown strain construction, activity profiles, growth curves, aspects of EMSA and proteomic analysis), designing experiments, analyzing data, and drafting and editing the manuscript. Other authors contributed to performing EMSAs (A.K.), proteomic analyses (C.H., C.G.), study conceptualization and design (R.G., C.G.), and paper editing (C.G.).

4.1   Abstract

Mycobacterial uptake hydrogenases are upregulated during carbon starvation and hydrogen metabolism is most active during stationary phase. However, the regulators controlling their expression under starvation remain unresolved. In this study, we demonstrate that the glycerol-inducible regulator GylR serves to regulate synthesis and activity of the hydrogenase Huc in *Mycobacterium smegmatis*. We compared *huc* expression and the activity of its product between the wild-type strain and two strains lacking *gylR* due to a CRISPRi-mediated knockdown and a spontaneous frameshift mutation. Whereas Huc was most active in early stationary phase in the wild-type strain, Huc was active throughout exponential and stationary phase in both the *gylR* knockdown and mutant strains. This is consistent with the proteomic data which showed significant increase in Huc production in the absence of GylR during both growth phases. The specific growth rate of wild type *M. smegmatis* (k = 0.24 ± 0.025 h^{-1}) was sevenfold higher than the *gylR* knockdown (k = 0.035 ± 0.002 h^{-1}) and mutant (k = 0.032 ± 0.002 h^{-1}) strains when grown in glycerol, suggesting the importance of GylR in glycerol catabolism. In contrast, when grown in other organic substrates such as glucose, succinate, or acetate, there was no noticeable difference in the Huc activity profile and specific growth rate among the three strains. Altogether, this strongly indicates that GylR regulates Huc production in response to the availability of the preferred growth substrate glycerol, consistent with a catabolite repression model. However, electromobility shift assays (EMSAs) showed the GylR protein does not specifically bind to *huc* promoter DNA, suggesting it indirectly controls *huc* expression via a downstream transcription factor. An increase in production of some candidate regulators was detected in the proteomes of both the *gylR* knockdown and mutant strains, providing targets for further genetic studies. Based on the results, we propose a model for Huc regulation: GylR serves as a sensor protein for glycerol that represses *huc* expression through the as-of-yet unidentified downstream regulator when the organic substrate is abundant and allows for *huc* expression when the substrate is depleted.

4.2   Introduction

Bacteria from the genus *Mycobacterium* have the ability to survive prolonged starvation for their organic growth substrates (11, 36). One key strategy they use is by oxidizing atmospheric trace gases such as molecular hydrogen (H_2) (8, 11, 35, 83, 186, 223). *Mycobacterium smegmatis* oxidizes atmospheric H_2 using two distinct uptake hydrogenases Huc and Hhy. Although both enzymes can oxidize low levels of H_2, they are from distinct phylogenetic lineages and differ in genetic organization, expression profiles, kinetic behavior, and respiratory chain integration (11, 49, 83, 223). Whereas Hhy is most active and expressed during late stationary phase of growth, Huc is highly expressed and active during the transition between late exponential and early stationary phase (223). These enzymes have been also shown to differentially integrate with the aerobic respiratory chain during organic carbon limitation. They provide electrons derived from H_2 oxidation to the electron transport chain, with Huc preferentially donating electrons to the cytochrome *bcc-aa*$_3$ complex, while Hhy donates electrons both to the cytochrome *bcc-aa*$_3$ and cytochrome *bd* complexes. (223). Although the uptake hydrogenases are known to be upregulated and active during carbon starvation (11, 223), the regulators of their expression remain unclear.

There are multiple signals and regulators that control hydrogenase synthesis in different organisms (22, 68, 222). These hydrogenases are regulated for microorganisms to adapt to the changing environmental and cellular pressures (222). For instance in various bacteria capable of aerobic hydrogenotrophic growth, for example *Ralstonia eutropha*, the presence of H_2 is detected by regulatory [NiFe]-hydrogenase HoxBC and the signal is transduced to the two-component regulatory system HoxJ/HoxA (65–67, 69, 72, 187). Another strategy is to regulate the expression of hydrogenase genes in response to redox state or oxidant levels, for example through oxygen-sensing FNR in *Enterobacteriaceae* (76–80), the redox-sensing RegB/RegA system in *Rhodobacter capsulatus* (82), or the oxygen- and redox-sensing DosST/DosR system in *Mycobacterium smegmatis* (36, 84). Hydrogenases expression can

also be subject to catabolite repression in response to organic carbon availability. For instance in *Salmonella enterica* serovar Typhimurium, expression of the uptake hydrogenase Hyb is repressed by glucose which is mediated by cAMP receptor protein (CRP) (80, 85). In the absence of glucose, adenylate cyclase produces cyclic AMP (cAMP) and the cAMP-CRP complex serves as an activator for the expression of hydrogenase isoenzyme 2 (85, 86). Similarly in *E. coli*, catabolite repression by glucose plays a pivotal role in the regulation of Hyb, with the cAMP-CRP complex acting as indirect regulator for the activation of *hyb* operon expression (87). Expression of its other uptake hydrogenase, Hya, seems to also respond to carbon starvation with the SigS sigma factor inducing *hya* operon during carbon starvation (88, 89).

In *M. smegmatis,* catabolite repression may also play a role in regulating its uptake hydrogenases. Through several studies, it has been demonstrated that hydrogenase gene expression is low during growth on glycerol and strongly induced when cells enter stationary phase due to carbon starvation (11, 36, 223). However, it is unknown whether this expression is directly influenced by the availability of organic substrates or instead responds indirectly through starvation-induced changes in cellular growth rate, redox state, or other parameters. One possibility is that mycobacteria directly sense glycerol and in turn represses the expression of hydrogenase genes in response to availability of the carbon source through a catabolite repression system. Consistently, GylR is a glycerol-responsive transcriptional regulator known to activate the expression of *glpFKD* operon for glycerol metabolism in *M. smegmatis* (231). The presence of glycerol is detected by GylR and this causes a change in its quaternary structure, from GylR homotetramers to homodimers. The homotetramers are the most abundant form in low glycerol levels, while the homodimers are dominant when glycerol level is high (231). Although both forms are able to bind to the *gylR-glpF* intergenic regions (IR1-IR3) of the *glpFKD* promoter, the GylR dimers have higher probability of binding to the IR3, which is crucial for recruiting RNA polymerase to the promoter and

activating *glpFKD* expression (231). In *Streptomyces coelicolor*, it was shown that GylR mediates both substrate induction and glucose (catabolite) repression of *gylCABX* operon (232). GylR serves as a negative regulator for the operon and glycerol 3-phosphate (G3P) is its inducer molecule (232). In *E. coli*, GlpR (GylR homolog) represses *glpTQ* and *glpABC*, which are genes implicated in antibiotic resistance (233, 234). In a similar manner, GylR and glycerol could regulate uptake hydrogenases in mycobacteria through catabolite repression. In this study, we show that GylR and glycerol regulate expression of Huc. Based on evidence from gene knockdowns, shotgun proteomics, activity measurements, and electromobility shift assays (EMSAs), we propose a model where glycerol sensing controls the expression of hydrogenase genes via GylR and a thus far unidentified downstream transcription factor.

4.3   Materials and Methods

4.3.1   Bacterial strains and culture conditions

The strains of *Mycobacterium smegmatis* and *Escherichia coli* are listed in **Supplementary Table S8**. *M. smegmatis* mc^{2}155 and its derived strains (*gylR* mutant and *gylR* knockdown) were routinely grown in lysogeny broth (LB) agar plates supplemented with 0.05% (w/v) Tween 80 (LBT) (210). In broth culture, the *M. smegmatis* strains were grown in either LBT or Hartmans de Bont (HdB) minimal medium supplemented with 0.05% (w/v) tyloxapol, 10 µM NiSO$_4$, and 0.2% carbon source (glycerol, glucose, succinate, or acetate). *E. coli* was maintained in LB agar plates and grown in LB broth (211). Selective LB or LBT media used for cloning experiments contained kanamycin at 20 µg mL^{-1} for *M. smegmatis* and 50 µg mL^{-1} for *E. coli*. Cultures were routinely incubated at 37°C, with rotary shaking at 150 rpm for liquid cultures, unless otherwise specified.

4.3.2 Spontaneous isolation and characterization of *gylR* frameshift mutant

A *gylR* mutant was spontaneously isolated over the course of experiments to characterize the differential activities of the two *M. smegmatis* uptake hydrogenases (223). This mutant was analyzed by whole-genome sequencing (Peter Doherty Institute, University of Melbourne). Genomic analysis revealed that it harbors a frameshift (from Leu154) in the transcriptional regulator GylR.

4.3.3 Creating plasmid construct for CRISPR interference

Plasmids and oligonucleotides used in this study can be found in **Supplementary Table S8 and S9**. To achieve a knockdown of *gylR* (MSMEG_6757), a single guide RNA (sgRNA) was designed to target the non-template strand within the open reading frame of *gylR* (235). A 21-bp sequence immediately 5' to the 5'-NNGGAAC-3' protospacer adjacent motif (PAM) located within the template strand was used to target the repression of *gylR*. This 21-bp sequence was designated as the forward oligonucleotide (msmeg6757_KD1_fwd) and its complementary sequence was the reverse oligonucleotide (msmeg6757_KD1_rev). A 5'-GGGA-3' was added to the forward oligonucleotide and 5'-AAAC-3' to the reverse oligonucleotide in order to make overhang sticky ends for cloning. The oligonucleotides were synthesized (IDT, Australia) and annealed through the following setting: 50 µL reaction containing 20 µM each of oligonucleotides and T4 ligase buffer (NEB); heating at 95°C for 5 min followed by cooling to 25°C at a ramp rate of $0.1°C\ s^{-1}$. Next, cloning of the annealed oligonucleotides into pLJR962 was done through Golden Gate cloning as described previously (235). Briefly, a 10 µL single-pot reaction was set up containing T4 DNA ligase (200 U) and T4 ligase buffer (NEB), *BsmB*I (5 U, NEB), pLR962 (25 ng), and annealed oligonucleotides (1 µM). The reaction was incubated in 30 cycles of digestion (42°C, 5 min) and ligation (16°C, 5 min) to yield the pLJR962_KDgylR construct (**Supplementary Figure S7a**). This construct now harbors the *gylR*-targeting sgRNA with the nuclease-dead Cas9 gene (dCas9) and both can be induced with anhydrotetracycline (aTc). The construct was propagated in *E. coli* DH5α and after sequence verification, was transformed into wild type *M. smegmatis* mc^{2}155. The

resultant colonies were screened by PCR using primers pljr962_multi_SapI_fwd and pljr962_multi_SapI_rev (**Supplementary Figure S7b**). *M. smegmatis* harboring the pLJR962_KDgylR was designated as *M. smegmatis gylR* knockdown and was used for Huc activity assay, growth curve experiments, and proteomics.

4.3.4 Huc activity staining

Cultures of wild type and derived strains of *M. smegmatis* were grown in 125 mL aerated conical flasks containing 30 mL HdB medium supplemented with either 0.2% glycerol, 0.2% glucose, 0.2% succinate, or 0.2% acetate. At the start of incubation, 300 ng mL^{-1} aTc was added to the *M. smegmatis gylR* knockdown cultures to initiate repression of *gylR*. Cells were harvested by centrifugation (10,000 × g, 10 min, 4°C) at exponential phase (OD$_{600}$ ~0.8 and ~1.5) and stationary phase (OD$_{max}$ and 1 d post OD$_{max}$) (223). Harvested cultures were washed in phosphate-buffered saline solution (PBS; 137 mM NaCl, 2.7 mM KCl, 10 mM Na$_2$HPO$_4$, 2 mM KH$_2$PO$_4$, pH 7.4), and resuspended in 2 mL lysis buffer (50 mM Tris-Cl, pH 8.0, Roche cOmplete™ Protease Inhibitor Cocktail, 2 mM MgCl$_2$, 5 mg mL^{-1} lysozyme, 40 µg mL^{-1} DNase). The cell suspensions were passed through a Constant Systems cell disruptor (40,000 psi, four times), and the unbroken cells were removed by centrifugation (8,000 × g, 2 min, 4°C) to yield whole-cell lysates. Protein concentration was determined using a bicinchoninic acid assay with bovine serum albumin standards (226). Twenty micrograms of each lysate was loaded onto native 7.5% (w/v) Bis-Tris polyacrylamide gels prepared as described previously (214) and run alongside a protein standard (NativeMark Unstained Protein Standard, Thermo Fisher Scientific) for 1.5 h at 25 mA. Next, the gels were incubated for hydrogenase activity staining in 50 mM potassium phosphate buffer (pH 7.0) supplemented with 500 µM nitroblue tetrazolium chloride (NBT) in an anaerobic jar amended with an anaerobic gas mixture (7% H$_2$, 7% CO$_2$, 86% N$_2$ v/v) overnight at room temperature (11).

4.3.5 Shotgun proteome analysis

For shotgun proteome analysis, 30 mL cultures of *M. smegmatis* wild type, *gylR* mutant, and *gylR* knockdown strains (induced with 300 ng mL^{-1} aTc upon inoculation) were grown in triplicate in 125 mL aerated conical flasks containing HdB medium supplemented with 0.2% glycerol. Cultures were quenched at exponential phase (OD$_{600}$ ~1.5) and stationary phase (1 d post OD$_{max}$ ~3.0) with 60 mL cold 3:2 glycerol:saline solution (−20 °C). They were subsequently harvested by centrifugation (4,800 × *g*, 30 min, −9 °C), further quenched with 1 mL cold 1:1 glycerol:saline solution (−20 °C), and pelleted by centrifugation. After final quenching, the cell pellets were washed in ice-cold PBS. To lyse the cell pellets and denature proteins, the pellets were resuspended in lysis buffer (50 mM Tris-HCl, pH 8.0, 2 mM MgCl$_2$, lysozyme, DNase) supplemented with SDS to a final concentration of 4% They were boiled at 95 °C for 10 min and sonicated in a Bioruptor (Diagenode) using 20 cycles of '30 s on' followed by '30 s off'. The lysates were clarified by centrifugation (14,000 × *g*, 10 mins, room temperature). Protein concentration was confirmed using the bicinchoninic acid assay kit (Thermo Fisher Scientific) and equal amounts of protein were processed from the strains in exponential and stationary phase for downstream analyses. After removal of SDS by chloroform/methanol precipitation, the proteins were proteolytically digested with trypsin (Promega) and purified using OMIX C18 Mini-Bed tips (Agilent Technologies) prior to LC-MS/MS analysis. Using a Dionex UltiMate 3000 RSL Cnano system equipped with a Dionex UltiMate 3000 RS autosampler, the samples were loaded via an Acclaim PepMap 100 trap column (100 µm × 2 cm, nanoViper, C18, 5 µm, 100 Å; Thermo Scientific) onto an Acclaim PepMap RSLC analytical column (75 µm × 50 cm, nanoViper, C18, 2 µm, 100 Å; Thermo Scientific). The peptides were separated by increasing concentrations of buffer B (80% acetonitrile/0.1% formic acid) for 158 min and analyzed with an Orbitrap Fusion Tribrid mass spectrometer (Thermo Scientific) operated in data-dependent acquisition mode using in-house, LFQ-optimized parameters. Acquired .raw files were analyzed with MaxQuant (236) to globally identify and quantify proteins across conditions. Data visualization and statistical analyses were performed in Perseus (237).

4.3.6 Growth assay

Cultures of wild type and derived mutants of *M. smegmatis* were inoculated into 125 mL conical flasks containing 30 mL HdB medium supplemented with either 0.2% glycerol (initial OD_{600} = 0.0125), 0.2% glucose, 0.2% succinate, or 0.2% acetate (initial OD_{600} = 0.009) in three biological replicates. At the start of incubation, 300 ng mL^{-1} aTc was added to the *M. smegmatis gylR* knockdown cultures to initiate repression of *gylR*. Growth was monitored by measuring the optical density at 600 nm (1 cm cuvettes; Eppendorf BioSpectrometer Basic). When OD_{600} was above 0.5, cultures were diluted ten-fold in HdB before measurement. Specific growth rate during exponential growth was calculated using GraphPad Prism (non-linear regression, exponential growth equation, least squares fit).

4.3.7 Electrophoretic mobility shift assay

The binding of GylR to the *huc* promoter was investigated through electrophoretic mobility shift assays using DIG Gel Shift Kit, 2nd Generation (Roche). A 454-bp *huc* promoter (83) was amplified using primers hucp_fw and hucp_rev. In addition, a 306-bp *glpFKD* promoter (231) was amplified using glpp_fw and glpp_rev primers. The amplified products were purified, concentrated, and labelled with digoxigenin (DIG) at the 5' end according to the manufacturer's protocol (Roche). Next, DNA-protein reactions (20 µl) were set up containing 0, 25, or 75 ng purified GylR protein and either 310 fmol DIG-labelled *huc* promoter or 310 fmol DIG-labelled *glpFKD* promoter in binding buffer (20 mM HEPES, pH 7.6, 1 mM EDTA, 10 mM $(NH_4)_2SO_4$, 1 mM DTT, 0.2% (w/v) Tween 20, 30 mM KCl). The reaction mixtures were incubated for 15 min at room temperature. Next, a 5% non-denaturing polyacrylamide gel, prepared as per manufacturer's protocol (Roche), was pre-run for 60 min at 6-18 mA in 0.5 × TBE buffer (44.5 mM Tris, 44.5 mM boric acid, 1 mM EDTA, pH 8.0). After pre-run, the DNA-protein reaction mixtures were loaded onto the gel and was run at 6-15 mA until the dye front was two-thirds down the gel. This was followed by contact transfer, as described by manufacturer's protocol

(Roche), to a NYLM-RO nylon membrane (Roche). DIG-labelled free DNA and DNA–protein complexes were detected according to the manufacturer's protocol (Roche).

4.4   Results

4.4.1   GylR represses Huc activity in *M. smegmatis* in response to glycerol availability

To characterize the regulation of the *M. smegmatis* uptake hydrogenase Huc, we measured its activity by zymographic staining during different stages of growth and persistence on Hartmans de Bont minimal medium with glycerol as the carbon and energy source. Consistent with previous observations, Huc activity was minimal in the wild-type strain during mid-exponential growth and peaked during the transition from exponential to stationary phase, resulting in intense bands at both medium and high molecular weight (**Figure 4.1a**)**.** However, we recovered a mutant strain in which Huc is highly active during both exponential and stationary phase, indicating the loss of a repressor (**Figure 4.1a**). Whole-genome sequencing confirmed this strain had a frameshift in the *gylR* gene, a glycerol-responsive transcription factor that is frequently subject to spontaneous mutations in *M. smegmatis* (231, 238) .

To validate that this phenotype is caused by the mutation in *gylR*, we created a knockdown of this gene using CRISPR interference (CRISPRi) and characterized its role in *huc* expression and hydrogen metabolism. In CRISPRi, the expression of the target gene is repressed (knocked-down) by the dCas9-sgRNA complex and this repression can be induced with anhydrotetracycline (aTc) (239). In the *gylR*-knockdown strain, Huc production during early stationary phase (1d post OD_{max} ~3.0) increased in a dose-dependent manner in response to increasing concentrations of aTc (50-500 ng mL^{-1}) (**Figure 4.1b; Supplementary Table S10**). In addition, in contrast to the wild-type, Huc activity was observed at high levels in the aTc-supplemented knockdown strains at each phase, from early exponential phase (OD 0.8) up until early stationary phase (1d post OD_{max} ~3.0), (**Figure 4.1a**). This activity phenotype was similar to *M. smegmatis gylR* mutant and was highly distinct from the wild type (**Figure 4.1a**).

The overproduction of Huc in the absence of a functional GylR, whether through its gene mutation or knockdown, strongly suggests that this regulator represses *huc* expression.
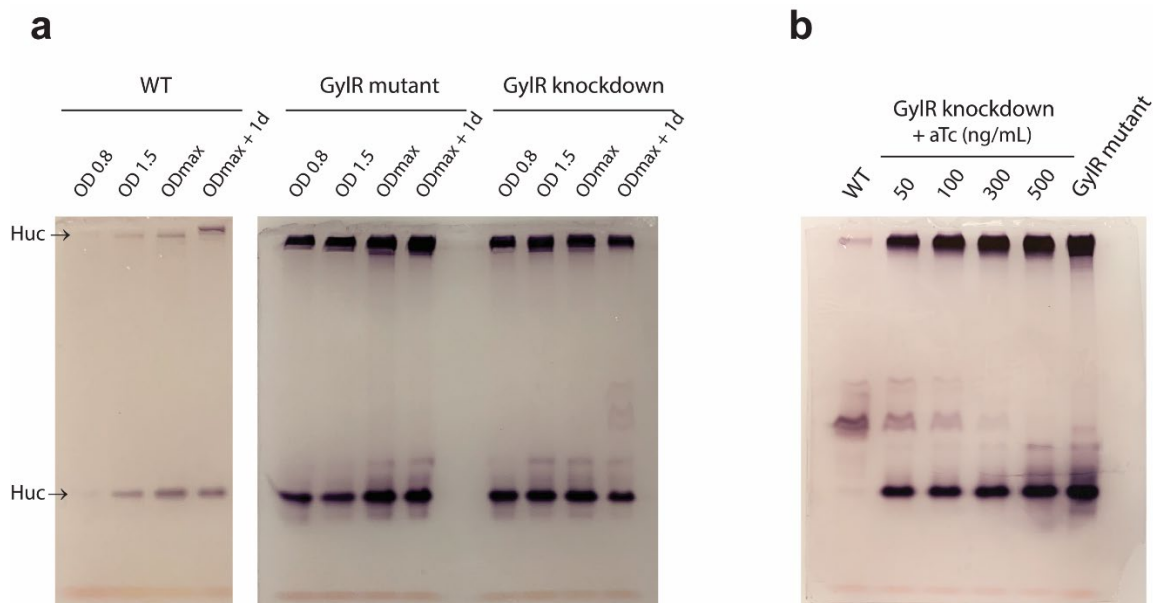
Figure 4.1. Huc activity staining of *M. smegmatis* wild type and derived strains grown in glycerol. *M. smegmatis* strains include wild type (WT), *gylR* -frameshift mutant (*gylR* mutant), and *gylR* knockdown strain. **a)** Huc activity stains (medium and high MW bands pointed by arrows) of strains grown in HdB with 0.2% glycerol at different stages of growth, from exponential (OD 0.8 and OD 1.5) to stationary phase (OD$_{max}$ ~3.0 and OD$_{max}$ + 1d). **b)** Induction of *gylR* knockdown with different concentrations of anhydrotetracycline (aTc); strains were grown in HdB with 0.2% glycerol at OD$_{max}$ + 1d.

4.4.2 Proteomics confirms hydrogenase production is increased in the absence of GylR

We performed comparative shotgun proteomics to confirm if the observed increase in activity of Huc in the *gylR* mutant and knockdown cells was due to overproduction of this enzyme. To do this, the wild type, *gylR* mutant, *gylR* knockdown *M. smegmatis* were grown on glycerol as sole carbon source. They were harvested at exponential phase (OD$_{600}$ ~1.5) and at stationary phase (1 d post OD$_{max}$ ~ 3.0) and the proteomes of either the *gylR* mutant or knockdown strain were compared with that of wild type for each growth phase (**Figure 4.2**). In the *gylR*

knockdown strain, GylR was significantly less abundant (17-fold, $p < 0.001$) compared to the wild type, in both growth phases (**Figure 4.2a, b**). This affirms that aTc did knockdown *gylR* expression and production throughout the growth of the strain.

The proteomic analysis suggested GylR regulates production of Huc as expected. The structural subunits of Huc (HucL and HucS) were significantly more abundant ($p < 0.001$) in the *gylR* knockdown compared to the wild type. During exponential growth, HucL and HucS production increased by 9.7- and 89-fold respectively, while in stationary phase production of both subunits increased by 5.7-fold. Similarly, in the mutant strain, HucL and HucS were significantly more abundant in both exponential (by 16- and 204-fold) and stationary phase (by 9.7- and 11-fold) (**Figure 4.2c, d**). The strong induction of Huc in the absence of GylR indicates that GylR is involved in regulating *huc* transcription. This regulation by GylR seems to be specific to Huc as the structural subunits of the other enzymes for trace gas oxidation (i.e. Hhy and CO dehydrogenase Cox) were not significantly different. Moreover, the pronounced upregulation of Huc in both the *gylR* mutant or knockdown strain suggests the enzyme is directly regulated by catabolite repression, as opposed to indirect effects such as on growth rate which would be expected to induce Hhy and Cox too (36). The enzymes for glycerol catabolism were also significantly less abundant ($p < 0.001$) in the *gylR* mutant and knockdown strain. Levels of both the glycerol kinase and glycerol 3-phosphate dehydrogenase were decreased by at least 34-fold in exponential phase and by more than 3.5-fold in stationary phase. This corroborates with previous findings that GylR is an activator of the *glpFKD* operon (231).
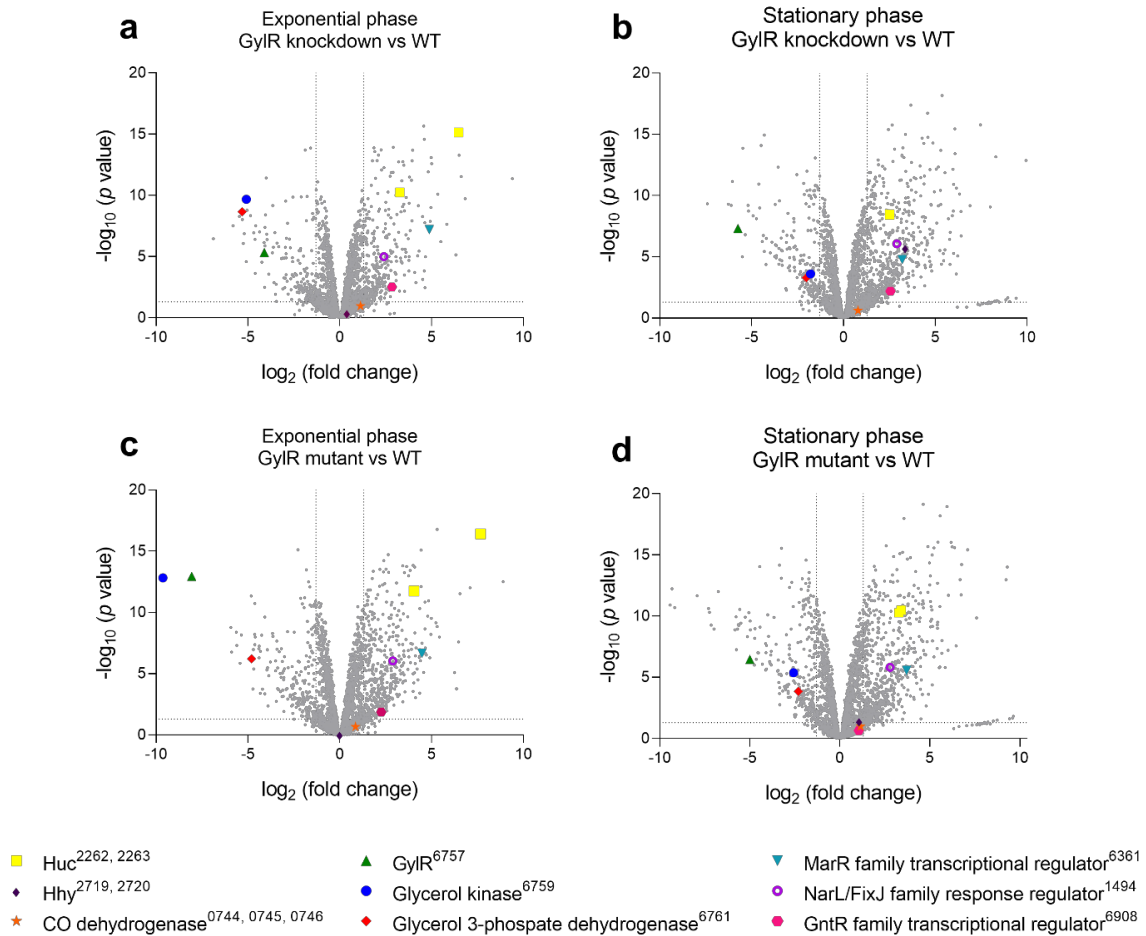
Figure 4.2. Volcano plots showing relative change in protein abundance in *gylR* knockdown and mutant compared with wild type *M. smegmatis*. Cells were grown on glycerol as sole carbon source at exponential phase (OD_{600} ~1.5) and stationary phase (1 d post OD_{max} ~ 3.0). The proteome of *gylR* knockdown was compared with wild type (WT) in **a)** exponential and **b)** stationary phase as well as the proteome of *gylR* -frameshift mutant with wild type in **c)** exponential and **d)** stationary phase. Fold change was determined for each growth phase by dividing the relative abundance of each protein in three *gylR* knockdown/mutant proteomes with that in the three wild type proteomes (biological replicates). Each protein is represented by a gray dot. Structural subunits of selected metabolic enzymes and regulators are highlighted and their locus numbers are shown in superscript in the legend. Note that the Huc subunits in panel **b** are on top of each other as they have very similar $\log_2$ fold change (2.52 and 2.51) and $-\log_{10}$ *p* value (8.49 and 8.43).

4.4.3 GylR is vital for growth on glycerol but inessential for growth on other organic substrates

To see how other organic substrates would influence Huc activity in different growth phases of the *gylR* mutant and GylR knockdown strains, we grew these strains in minimal medium containing either glucose, succinate, or acetate as sole carbon source. The growth of the three *M. smegmatis* strains were monitored to see how GylR could affect growth on glycerol and on other organic substrates. When grown in glycerol, both the *gylR* mutant and *gylR* knockdown strains grew at a much slower rate (k = 0.032 ± 0.002 h^{-1} and 0.035 ± 0.003 h^{-1}, respectively) than the wild-type (0.24 ± 0.025 h^{-1}) (**Figure 4.3a**). In contrast, there was no difference in the growth of the three strains when grown in either glucose, succinate, or acetate (**Figure 4.3b**). The inability of the *gylR*-knockdown and mutant strains to efficiently grow on glycerol is consistent with the specific role of GylR in activating genes for glycerol uptake in response to glycerol (231). This also provides further support that GylR is a sensor specific to glycerol, which could serve as the signal molecule in regulating *huc* expression and activity.

The activity staining of Huc was compared between cells grown on glucose, succinate, or acetate as sole carbon source. While significant Huc activity was observed in mid-exponential and early stationary phase cells, there was no difference in Huc activity among the wild type, *gylR* mutant, and *gylR* knockdown strains (**Figure 4.3c; Supplementary Table S10**). In addition, the strong Huc activity phenotype was not observed in the three strains when grown in glucose, succinate, or acetate. This is in contrast to the strong activity of Huc seen in the *gylR* mutant and knockdown strains grown in glycerol **Figure 4.1a**). Moreover, when the three strains were grown in either glucose or acetate, there was more pronounced Huc activity in early stationary phase than in mid-exponential (**Figure 4.3c**), similar to the staining profile observed in wild type grown in glycerol (**Figure 4.1a**). That the knockdown or mutation of *gylR* affects Huc regulation only when cells are grown in glycerol is concordant with GylR being a reported glycerol sensor. Taken together, these results are consistent with a catabolite repression model of Huc regulation.
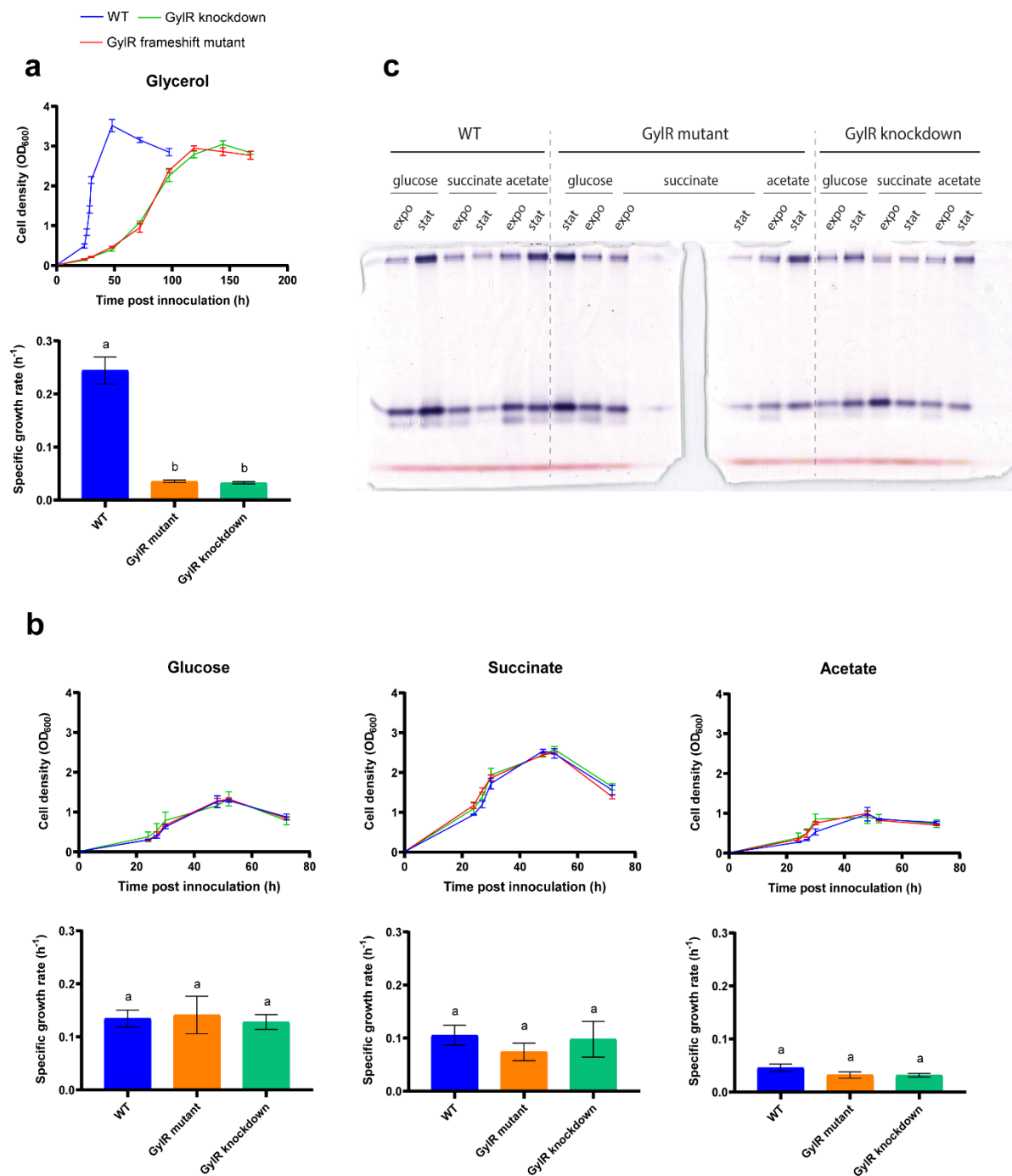
Figure 4.3. Growth and Huc activity of *M. smegmatis* wild type and derived strains in different organic substrates. a) Growth curve and corresponding specific growth rate of wild type (WT), *gylR*-frameshift mutant (*gylR* mutant), and *gylR* knockdown strain cultured in HdB with 0.2% glycerol. **b)** Growth curve and corresponding specific growth rate of the strains in HdB with either 0.2% glucose, 0.2% succinate, or 0.2% acetate. All values labeled with different letters are statistically significant (p <0.0001) based on one-way ANOVA. **c)** Huc activity stains

of the three strains grown in either 0.2% glucose, 0.2% succinate, or 0.2% acetate at OD 1.2 (succinate) or OD 0.5 (acetate, glucose) (expo) and OD_{max} + 1d (stat).

GylR does not directly repress transcription at the *huc* promoter

To detect whether GylR interacted with the *huc* promoter, electrophoretic mobility shift assays (EMSA) were performed using the purified GylR protein and 454-bp *huc* promoter. No shift in mobility of *huc* promoter was detected with increasing amounts of GylR (0, 25, 75 ng) (**Figure 4.4**). This was in contrast to the control *glpFKD* promoter DNA, which shifted in response to increasing amounts of GylR. These results suggest that GylR does not bind to the *huc* promoter and hence indirectly represses *huc* expression. It is worth noting, however, that these assays were performed in the absence of glycerol-3-phosphate (G3P). G3P was previously reported to enhance GylR binding and RNA polymerase recruitment to the *glpFKD* promoter (231), and may also facilitate DNA binding in the *huc* promoter. Nonetheless based on the results, GylR could instead be acting on a downstream regulator, which in turn could be directly regulating Huc.

Some regulators that were significantly upregulated in the *gylR* knockdown strain could serve as candidate downstream regulators (**Figure 4.2**). These include a transcriptional regulator from the MarR family, which is involved in regulating various genes for cellular stress responses, antibiotic resistance, and virulence (240, 241); a response regulator from the NarL/FixJ family, which include regulators for osmo-sensing, nitrate assimilation, and expression of hydrogenase in response to oxygen levels (75, 242, 243); and a transcriptional regulator from the GntR family, which include regulators involved in catabolite repression and metabolism of various organic substrates (244–246). Any of these upregulated regulators could directly activate the expression of the *huc* operon. Other possible candidates are the regulators that were downregulated, which could serve as a direct repressor of *huc* operon.
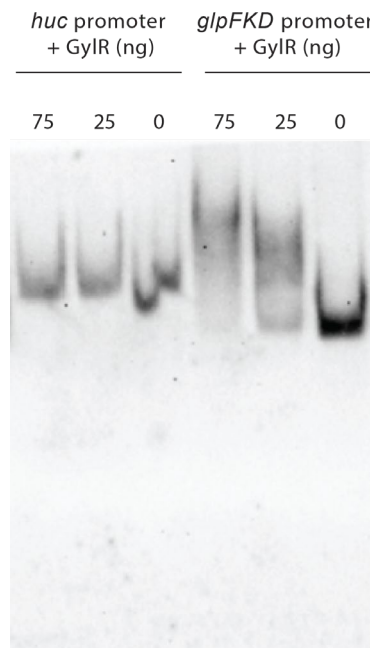
Figure 4.4. Electrophoretic mobility shift assays. Purified GylR protein at different amounts (0, 25, or 75 ng) were incubated with DIG-labelled *huc* promoter (454 bp; 310 fmol) or DIG-labelled *glpFKD* promoter (positive control; 306 bp; 310 fmol). DIG-labelled DNA was detected by chemiluminescence (Roche) and mobility shifts indicate DNA-protein interaction. Experiment performed by Ashleigh Kropp.

4.5   Discussion

Here we show catabolite repression regulates hydrogenase gene expression and activity in *M. smegmatis*. The knockdown or mutation of the regulator protein GylR resulted in the overproduction of Huc. This was only observed when cells were grown on glycerol as sole carbon source and not on other organic substrates. Moreover, the growth of *gylR* -knockdown and mutant strains on glycerol were impaired, growing seven times more slowly than the wild type. In turn, this provokes the model that GylR responds to glycerol availability and represses *huc* expression when available. Several lines of evidence now strongly support such a model: (i) upregulation of uptake hydrogenases Huc and Hhy during carbon limitation (11, 36); (ii) highly active uptake hydrogenases during persistence when cells are starved of glycerol (11, 223); and (iii) strongly increased *huc* expression and activity in the absence of a functional glycerol-responsive regulator GylR. This study therefore shows a regulator serves to link the organic carbon levels to hydrogenase gene expression.

An alternative explanation for our findings is that slow growth on glycerol contributes to the upregulation of hydrogenase gene expression. A similar observation was previously reported in wild type *M. smegmatis*, wherein uptake hydrogenases were upregulated in slow-growing cells (36). However, the slow growth of the *gylR* -knockdown and mutant strains is unlikely to primarily account for the very strong activity of Huc observed, and instead this likely reflects a disruption in catabolite repression pathways. Indeed, Huc activity in exponentially growing cells in the strains unable to synthesize GylR greatly exceeded activity of the wild-type strain during stationary phase (**Figure 4.1a**). Likewise, only moderate Huc activity was observed even on substrates that support slow growth (i.e. acetate) and there was no significant induction of other trace gas oxidation enzymes known to be activated at extremely slow growth rates (36). Furthermore, the role of GylR as a catabolite repressor is well-established in both mycobacteria and streptomycetes (232, 247), though not linked to hydrogenase production and activity until now.

Although this study presented how GylR and catabolite repression control hydrogen metabolism, an outstanding question still needs to be addressed: which key regulator does GylR feed into? It is likely that GylR is acting on a downstream regulator, given that it does not directly bind to the Huc promoter as indicated by EMSA results (**Figure 4.4**). In *E. coli* and *S. coelicolor*, GylR is a repressor that, in the absence of glycerol, exerts negative control on the operon for glycerol catabolism (232, 248). In *M. smegmatis* however, GylR is a glycerol-responsive sensor that activates the expression of the *glpFKD* operon (231). When glycerol is abundant, the GylR homodimeric form (231) could modify the expression or activity of a downstream transcription activator or repressor that could control the *huc* promoter. In addition, the pronounced Huc activity in the stationary phase than in the exponential phase when grown in substrates such as glucose or acetate in both wild-type and *gylR* knockdown/mutant backgrounds also suggests that Huc is more broadly regulated in response to the availability of organic carbon sources. Would *M. smegmatis* also exhibit very strong Huc activity in the absence of the regulatory genes for the catabolism of these organic substrates?

If this is the case, there may be a common transcription factor that these regulatory proteins, including GylR, are feeding into. This further reinforces the idea that a downstream regulator is directly regulating the *huc* promoter when organic carbon sources are replete. The proteomic data provides some possible candidates for this downstream regulator, as suggested by the upregulation of various regulators in the *gylR* -knockdown and mutant proteomes. Further investigations are needed to identify which key transcriptional regulator does GylR, and probably other carbon catabolite regulators, is feeding into in order to regulate Huc.

4.6 Footnotes

Chapter 5

Atmospheric carbon monoxide oxidation is a widespread mechanism supporting microbial survival

Paul R. F. Cordero[1] & Katherine Bayly[1], Pok Man Leung[1], Cheng Huang[2], Zahra F. Islam[1], Ralf B. Schittenhelm[2], Gary M. King[3], Chris Greening[1*]

Form the [1] School of Biological Sciences, Monash University, Clayton, VIC 3800, Australia; [2] Monash Biomedical Proteomics Facility and Department of Biochemistry, Monash Biomedicine Discovery Institute, Monash University, Clayton, VIC 3800, Australia; [3] School of Biological Sciences, Louisiana State University, Baton Rouge, LA 70803, USA

* Correspondence can be addressed to Associate Professor Chris Greening (Chirs.Greening@monash.edu)

This chapter is a **published article in the ISME Journal**, where I am co-first author and contributed 50% of the work. The majority of the experiments where performed by me and Katherine Bayly, who was an Honours student that I directly supervised on a day-to-day basis. Experiments performed by me include knockout construction, cultures for shotgun proteomics, activity staining, respirometry measurements, and sequence analysis. Experiments done together with Katherine Bayly are gene expression analysis, growth and survival assays, and glycerol quantification. I also led the data analysis, paper drafting, and manuscript editing. Other authors contributed to study conception and design (C.G.), metagenomic analysis (P.M.L., G.M.K., C.G.), proteomic analysis (C.H., R.B.S.), and paper writing and editing (C.G.).

5.1 Abstract

Carbon monoxide (CO) is a ubiquitous atmospheric trace gas produced by natural and anthropogenic sources. Some aerobic bacteria can oxidize atmospheric CO and, collectively, they account for the net loss of ~250 teragrams of CO from the atmosphere each year. However, the physiological role, genetic basis, and ecological distribution of this process remain incompletely resolved. In this work, we addressed these knowledge gaps through culture-based and culture-independent work. We confirmed through shotgun proteomic and transcriptional analysis that the genetically tractable aerobic soil actinobacterium *Mycobacterium smegmatis* upregulates the expression of a form I molydenum–copper carbon monoxide dehydrogenase by 50-fold when exhausted for organic carbon substrates. Whole-cell biochemical assays in wild-type and mutant backgrounds confirmed that this organism aerobically respires CO, including at sub-atmospheric concentrations, using the enzyme. Contrary to current paradigms on CO oxidation, the enzyme did not support chemolithoautotrophic growth and was dispensable for CO detoxification. However, it significantly enhanced long-term survival, suggesting that atmospheric CO serves as a supplemental energy source during organic carbon starvation. Phylogenetic analysis indicated that atmospheric CO oxidation is widespread and an ancestral trait of CO dehydrogenases. Homologous enzymes are encoded by 685 sequenced species of bacteria and archaea, including from seven dominant soil phyla, and we confirmed genes encoding this enzyme are abundant and expressed in terrestrial and marine environments. On this basis, we propose a new survival-centric model for the evolution of aerobic CO oxidation and conclude that, like atmospheric H_2, atmospheric CO is a major energy source supporting persistence of aerobic heterotrophic bacteria in deprived or changeable environments.

5.2   Introduction

Carbon monoxide (CO) is a chemically reactive trace gas that is produced through natural processes and anthropogenic pollution. The average global mixing ratio of this gas is ~90 ppbv in the troposphere (lower atmosphere), though this concentration greatly varies across time and space, with levels particularly high in urban areas (13, 249–251). Currently, human activity is responsible for ~60% of emissions, with the remainder attributable to natural processes (13). Counteracting these emissions, CO is rapidly removed from the atmosphere (lifetime of 2 months) by two major processes: geochemical oxidation by atmospheric hydroxyl radicals (85%) and biological oxidation by soil microorganisms (10%) (13, 252). Soil microorganisms account for the net consumption of ~250 teragrams of atmospheric CO (13, 252, 253); on a molar basis, this amount is seven times higher than the amount of methane consumed by soil bacteria (254). Aerobic CO-oxidizing microorganisms are also abundant in the oceans; while oceans are a minor source of atmospheric CO overall (255, 256), this reflects that substantial amounts of the gas are produced photochemically within the water column and the majority is oxidized by marine bacteria before it is emitted to the atmosphere (257).

Aerobic CO-oxidizing microorganisms are traditionally categorized into two major groups, the carboxydotrophs and carboxydovores (19). The better studied of the two groups, carboxydotrophs grow chemolithoautotrophically with CO as the sole energy and carbon source when present at elevated concentrations. To date, this process has been reported in 11 bacterial genera from four classes (**Supplementary Table S11**): Alphaproteobacteria (43, 44, 258, 259), Gammaproteobacteria (44, 150, 258, 260, 261), Actinobacteria (3, 262, 263), and Bacilli (264). Genetic and biochemical studies on the model alphaproteobacterial carboxydotroph *Oligotropha carboxidovorans* have demonstrated that form I carbon monoxide dehydrogenases mediate aerobic CO oxidation (53, 136, 265). The catalytic subunit of this heterotrimeric enzyme (CoxL) contains a molybdenum–copper center that specifically binds and hydroxylates CO (53, 136). In such organisms, electrons derived from CO oxidation

are relayed through both the aerobic respiratory chain to support ATP generation and the Calvin–Benson cycle to support CO_2 fixation (19, 266). With some exceptions (262), these CO dehydrogenases have a high catalytic rate but exhibit low-affinity for their substrate ($K_m > 400$ nM) (267). Thus, carboxydotrophs can grow in specific environments with elevated CO concentrations, but often cannot oxidize atmospheric CO (19, 21).

Carboxydovores are a broader group of bacteria and archaea adapted to oxidize CO at lower concentrations, including atmospheric levels, in a wide range of environments. These bacteria can oxidize CO but, in contrast to carboxydotrophs, require organic carbon for growth (19, 126). Carboxydovores have now been cultured from some 31 bacterial and archaeal genera to date (**Supplementary Table S11**), spanning classes Alphaproteobacteria (46, 47, 126, 127), Gammaproteobacteria (126, 268–271), Actinobacteria (90, 150, 151, 272, 273), Bacilli (274), Thermomicrobia (33, 274–276), Ktedonobacteria (275, 277), Deinococcota (274), Thermoprotei (278, 279), and Halobacteria (269, 280). Carboxydovores are also thought to use form I CO dehydrogenases, but usually encode slower-acting, higher-affinity enzymes. In contrast to carboxydotrophs, carboxydovores usually lack a complete Calvin–Benson cycle, suggesting they can support aerobic respiration, but not carbon fixation, using CO (19). A related enzyme family (tentatively annotated as form II CO dehydrogenases) was also proposed to mediate CO oxidation in carboxydovores (19, 126, 129), but recent studies suggest CO is not their physiological substrate (127).

The physiological role of CO oxidation in carboxydovores has remained unclear. It was originally thought that such microorganisms oxidize CO primarily to support mixotrophic growth (46, 126), but a recent study focused on the alphaproteobacterial carboxydovore *Ruegeria pomeroyi* showed that CO neither stimulated growth nor influenced metabolite profiles (47). We recently developed an alternative explanation: consumption of atmospheric CO enables carboxydovores to survive carbon limitation (8, 29, 33). This hypothesis is inspired by studies showing atmospheric H_2 oxidation enhances survival (33–

36, 84, 96, 195). In support of this, CO dehydrogenases have been shown to be upregulated by five different bacteria during carbon limitation (33, 36, 90–92) and atmospheric CO is consumed by stationary-phase cells (33, 193). Moreover, ecological studies have shown that CO is rapidly oxidized in ecosystems containing low organic carbon (29, 93, 94). However, in contrast to atmospheric H_2 (11, 34, 36, 84, 195), it has not yet been genetically or biochemically proven that atmospheric CO supports survival. To address this, we studied CO oxidation in *Mycobacterium smegmatis*, a genetically tractable representative of a globally abundant soil actinobacterial genus (281, 282). This organism encodes a form I CO dehydrogenase and six other putative enzymes from the wider molybdenum-containing hydroxylase superfamily, but lacks a form II CO dehydrogenase (126, 150). We show, through proteomic, genetic, and biochemical analyses, that its CO dehydrogenase is (i) strongly induced by organic carbon starvation, (ii) mediates aerobic respiration of atmospheric CO, and (iii) enhances survival of carbon-starved cells. On this basis, we confirm that atmospheric CO supports microbial survival and, with support from genomic, metagenomic, and metatranscriptomic analyses, propose a survival-centric model for the evolution and ecology of carboxydovores.

5.3   Materials and Methods

5.3.1   Bacterial strains and growth conditions

Supplementary Table S17 lists the bacterial strains and plasmids used in this study. *Mycobacterium smegmatis* mc²155 (212) and the derived strain Δ*coxL* were maintained on lysogeny broth (LB) agar plates supplemented with 0.05% (w/v) Tween80. For broth culture, *M. smegmatis* was grown on Hartmans de Bont minimal medium (224) supplemented with 0.05% (w/v) tyloxapol and 5.8 mM glycerol. *Escherichia coli* TOP10 cells were maintained on LB agar plates and grown in LB broth. Liquid cultures of both *M. smegmatis* and *E. coli* were incubated on a rotary shaker at 200 rpm, 37 °C unless otherwise

specified. Selective LB or LBT media used for cloning experiments contained gentamycin at 5 µg mL^{-1} for *M. smegmatis* and 20 µg mL^{-1} for *E. coli*.

5.3.2 Mutant construction

A markerless deletion of the *coxL* gene (MSMEG_0746) was constructed by allelic exchange mutagenesis. Briefly, a 2245 bp fragment containing the fused left and right flanks of the MSMEG_0746 gene was synthesized by GenScript. This fragment was cloned into the *Spe*I site of the mycobacterial shuttle plasmid pX33 (210) with *E. coli* TOP10 and transformed into *M. smegmatis* mc^{2}155 electrocompetent cells. To allow for temperature-sensitive vector replication, the transformants were incubated on LBT-gentamycin agar at 28 °C for 5 days until colonies were visible. Catechol-reactive colonies were sub-cultured on to LBT-gentamycin agar plates incubated at 40 °C for 3 days to facilitate the first recombination of the *coxL* flanks into the chromosome. To allow the second recombination and removal of the backbone vector to occur, colonies that were gentamycin-resistant and catechol-reactive were sub-cultured in LBT-sucrose agar and incubated at 40 °C for 3 days. The resultant colonies were screened by PCR to discriminate Δ*coxL* mutants from wild-type revertants (**Supplementary Figure S8**). Whole-genome sequencing (Peter Doherty Institute, University of Melbourne) confirmed *coxL* was deleted and no other SNPs were present in the Δ*coxL* strain. **Supplementary Table S18** lists the cloning and screening primers used in this study.

5.3.3 Shotgun proteome analysis

For shotgun proteome analysis, 500 mL cultures of *M. smegmatis* were grown in triplicate in 2.5 L aerated conical flasks. Cells were harvested at mid-exponential phase (OD$_{600}$ ~ 0.25) and mid-stationary phase (72 h post OD$_{max}$ ~ 0.9) by centrifugation (10,000 × *g*, 10 min, 4 °C). They were subsequently washed in phosphate-buffered saline (PBS; 137 mM NaCl, 2.7 mM KCl, 10 mM Na$_2$HPO$_4$ and 2 mM KH$_2$PO$_4$, pH 7.4), recentrifuged, and resuspended in 8 mL lysis buffer (50 mM Tris-HCl, pH 8.0, 1 mM PMSF, 2 mM MgCl$_2$, 5 mg mL^{-1} lysozyme, 1 mg

DNase). The resultant suspension was then lysed by passage through a Constant Systems cell disruptor (40,000 psi, four times), with unbroken cells removed by centrifugation (10,000 × g, 20 min, 4 °C). To denature proteins, lysates were supplemented with 20% SDS to a final concentration of 4%, boiled at 95 °C for 10 min, and sonicated in a Bioruptor (Diagenode) using 20 cycles of '30 s on' followed by '30 s off'. The lysates were clarified by centrifugation (14,000 × g, 10 mins, room temperature). Protein concentration was confirmed using the bicinchoninic acid assay kit (Thermo Fisher Scientific) and equal amounts of protein were processed from both exponential and stationary phase samples for downstream analyses. After removal of SDS by chloroform/methanol precipitation, the proteins were proteolytically digested with trypsin (Promega) and purified using OMIX C18 Mini-Bed tips (Agilent Technologies) prior to LC-MS/MS analysis. Using a Dionex UltiMate 3000 RSL Cnano system equipped with a Dionex UltiMate 3000 RS autosampler, the samples were loaded via an Acclaim PepMap 100 trap column (100 μm × 2 cm, nanoViper, C18, 5 μm, 100 Å; Thermo Scientific) onto an Acclaim PepMap RSLC analytical column (75 μm × 50 cm, nanoViper, C18, 2 μm, 100 Å; Thermo Scientific). The peptides were separated by increasing concentrations of buffer B (80% acetonitrile/0.1% formic acid) for 158 min and analyzed with an Orbitrap Fusion Tribrid mass spectrometer (Thermo Scientific) operated in data-dependent acquisition mode using in-house, LFQ-optimized parameters. Acquired.raw files were analyzed with MaxQuant (236) to globally identify and quantify proteins across the two conditions. Data visualization and statistical analyses were performed in Perseus (237).

5.3.4 Activity staining

For CO dehydrogenase activity staining, 500 mL cultures of wild-type and Δ*coxL M. smegmatis* were grown to mid-stationary phase (72 h post OD_{max} ~ 0.9) in 2.5 L aerated conical flasks. Cells were harvested by centrifugation, resuspended in lysis buffer, and lysed with a cell disruptor as described above. Following removal of unlysed cells by centrifugation (10,000 × g, 20 min, 4 °C), the whole-cell lysates were fractionated into cytosols and membranes by ultracentrifugation (150,000 × g, 60 min, 4 °C). The protein concentration of the

lysates, cytosols, and membranes was determined using the bicinchoninic acid assay (226) against bovine serum albumin standards. Next, 20 μg protein from each fraction was loaded onto native Bis-Tris polyacrylamide gels (7.5% w/v running gel, 3.75% w/v stacking gel) prepared as described elsewhere (214) and run alongside a protein standard (NativeMark Unstained Protein Standard, Thermo Fisher Scientific) at 25 mA for 3 h. For total protein staining, gels were incubated in AcquaStain Protein Gel Stain (Bulldog Bio) at 4 °C for 3 h. For CO dehydrogenase staining (259), gels were incubated in 50 mM Tris-HCl buffer containing 50 μM nitroblue tetrazolium chloride (NBT) and 100 μM phenazine methosulfate in an anaerobic jar (100% CO v/v atmosphere) at room temperature for 24 h. Weak bands corresponding to CO dehydrogenase activity were also observed for wild-type fractions after 4 h.

5.3.5 Gas chromatography

Gas chromatography was used to determine the kinetics and threshold of CO dehydrogenase activity of *M. smegmatis*. Briefly, 30 mL stationary-phase cultures of wild-type and Δ*coxL M. smegmatis* strains were grown in 120 mL serum vials sealed with butyl rubber stoppers. At 72 h post-OD$_{max}$, cultures were reaerated (1 h), resealed, and amended with CO (via 1% v/v CO in N$_2$ gas cylinder, 99.999% pure) to achieve headspace concentrations of ~200 ppmv. Cultures were agitated (150 rpm) for the duration of the incubation period to enhance CO transfer to the cultures and maintain an aerobic environment. Headspace samples of 1 mL were periodically collected using a gas-tight syringe to measure CO. Gas concentrations in samples were measured by gas chromatography using a pulsed discharge helium ionization detector (model TGA-6791-W-4U-2, Valco Instruments Company Inc.) as previously described (33). Concentrations of CO in each sample were regularly calibrated against ultra-pure CO gas standards of known concentrations to the limit of detection of 9 ppbv CO. Kinetic analysis was performed as described, except cultures were amended with six different starting concentrations of CO (4000, 2000, 1000, 500, 200, 50 ppmv) and oxidation was measured at up to five timepoints (0, 2, 4, 6, 8 h). Reaction velocity relative to the gas concentration was

calculated at each timepoint and plotted on a Michaelis–Menten curve. $V_{max\ app}$ and $K_{m\ app}$ values were derived through a non-linear regression model (GraphPad Prism, Michaelis–Menten, least squares fit) and linear regressions based on Lineweaver-Burk, Eadie-Hofstee, and Hanes-Woolf plots.

5.3.6   Respirometry measurements

For respirometry measurements, 30 mL cultures of wild-type and Δ*coxL M. smegmatis* were grown to mid-stationary phase (72 h post $OD_{max} \sim 0.9$) in 125 mL aerated conical flasks. Rates of O_2 consumption were measured before and after CO addition using a Unisense O_2 microsensor. Prior to measurement, the electrode was polarized at -800 mV for 1 h with a Unisense multimeter and calibrated with O_2 standards of known concentration. Gas-saturated PBS was prepared by bubbling PBS with 100% (v/v) of either O_2 or CO for 5 min. Initially, O_2 consumption was measured in 1.1 mL microrespiration assay chambers sequentially amended with *M. smegmatis* cell suspensions (0.9 mL) and O_2-saturated PBS (0.1 mL) that were stirred at 250 rpm at room temperature. After initial measurements, 0.1 mL of CO-saturated PBS was added into the assay mixture. Changes in O_2 concentrations were recorded using Unisense Logger Software (Unisense, Denmark). Upon observing a linear change in O_2 concentration, rates of consumption were calculated over a period of 20 s and normalized against total protein concentration.

5.3.7   Gene expression analysis

To assess CO dehydrogenase gene expression by qRT-PCR, synchronized 30 mL cultures of *M*. smegmatis were grown in triplicate in either 125 mL aerated conical flasks or 120 mL sealed serum vials supplemented with 1% (w/v) CO. Cultures were quenched at mid-exponential phase ($OD_{600} \sim 0.25$) or mid-stationary phase (3 days post-$OD_{max} \sim 0.9$) with 60 mL cold 3:2 glycerol:saline solution ($-20\,°C$). They were subsequently harvested by centrifugation ($20,000 \times g$, 30 min, $-9\,°C$), resuspended in 1 mL cold 1:1 glycerol:saline solution ($-20\,°C$), and further centrifuged ($20,000 \times g$, 30 min, $-9\,°C$). For cell lysis, pellets

were resuspended in 1 mL TRIzol Reagent, mixed with 0.1 mm zircon beads, and subjected to five cycles of bead-beating (4000 rpm, 30 s) in a Biospec Mini-Beadbeater. Total RNA was subsequently extracted using the phenol-chloroform method as per manufacturer's instructions (TRIzol Reagent User Guide, Thermo Fisher Scientific) and resuspended in diethylpyrocarbonate (DEPC)-treated water. RNA was treated with DNase using the TURBO DNA-free kit (Thermo Fisher Scientific) as per the manufacturer's instructions. RNA concentration, purity, and integrity were confirmed by using a NanoDrop ND-1000 spectrophotometer and running extracts on a 1.2% agarose gel. cDNA was then synthesized using SuperScript III First-Strand Synthesis System for qRT-PCR (Thermo Fisher Scientific) with random hexamer primers as per the manufacturer's instructions. qPCR was used to quantify the copy numbers of the target gene *coxL* and housekeeping gene *sigA* against amplicon standards of known concentration. A standard curve was created based on the cycle threshold (Ct) values of *coxL* and *sigA* amplicons that were serially diluted from 10^8 to 10 copies ($R^2 > 0.99$). The copy number of the genes in each sample was interpolated based on each standard curve and values were normalized to *sigA* expression in exponential phase in ambient air. For each biological replicate, all samples, standards, and negative controls were run in technical duplicate. All reactions were run in a single 96-well plate using the PowerUp SYBR Green Master Mix (Thermo Fisher Scientific) and LightCycler 480 Instrument (Roche) according to each manufacturers' instructions.

5.3.8 Growth and survival assays

For growth and survival assays, cultures were grown in 30 mL media in either 125 mL aerated conical flasks or 120 mL sealed serum vials containing an ambient air headspace amended with 20% (v/v) CO. Growth was monitored by measuring optical density at 600 nm (1 cm cuvettes; Eppendorf BioSpectrometer Basic); when OD_{600} was above 0.5, cultures were diluted ten-fold before measurement. All growth experiments were performed using three biological replicates. To count colony-forming units (CFU mL^{-1}), each culture was serially diluted in HdB (no carbon source) and spotted on to agar plates in technical quadruplicates.

Survival experiments were performed on two separate occasions using three biological replicates in the first experiment and six biological replicates in the second experiment. Percentage survival was calculated for each replicate by dividing the CFU mL^{-1} at each timepoint with the CFU mL^{-1} count at OD$_{max}$.

5.3.9 Glycerol quantification

Glycerol concentration in media was measured colorimetrically. Samples of 900 µL were taken periodically from triplicate cultures during growth, cells were pelleted (9500 × g, 2 min, room temperature) and the supernatant was collected and stored at −20 °C. Glycerol content for all supernatant samples was measured simultaneously in a single 96-well plate using a Glycerol Assay Kit (Sigma-Aldrich) as per manufacturer's instructions. Absorbance was measured at 570 nm using an Epoch 2 microplate reader (BioTek). A standard curve was constructed using four standards of glycerol (0 mM, 0.3 mM, 0.6 mM, and 1 mM; $R^2 > 0.99$). Glycerol concentration was interpolated from this curve. Samples were diluted either five-fold or two-fold in UltraPure water such that they fell within the curve. All samples, standards and blanks were run in technical duplicate.

5.3.10 Genome survey

We compiled the amino acid sequences of the catalytic subunits of all putative form I CO dehydrogenases (CoxL) represented in the National Center for Biotechnology Information (NCBI) Reference Sequence (RefSeq) (283). All sequences with greater than 55% sequence identity and 90% query coverage to CoxL sequences of *Oligotropha carboxidovorans* (WP_013913730.1), *Mycobacterum smegmatis* (WP_003892166.1), and *Natronorubrum bangense* (WP_006067999.1) were retrieved by protein BLAST (284). Homologous sequences with less than 55% sequence identity encoded form II CO dehydrogenases and hence were not retrieved. The dataset was manually curated to dereplicate sequences within species and remove incomplete sequences. The final dataset

contained a total of 709 CoxL sequences across 685 different bacterial and archaeal species (**Supplementary Table S13**).

5.3.11 Phylogenetic analysis

To construct phylogenetic trees, the retrieved sequences were aligned using ClustalW in MEGA7 (285). Initially, the phylogenetic relationships of 709 sequences were visualized on a neighbor-joining tree based on the Poisson correction method and bootstrapped with 500 replicates. Subsequently, the phylogenetic relationships of a representative subset of 94 sequences were visualized on a maximum-likelihood tree based on the Poisson correction method and bootstrapped with 200 replicates. Both trees were rooted with the protein sequences of five form II CO dehydrogenase catalytic subunit sequences (WP_012893108.1, WP_012950878.1, WP_013076571.1, WP_01359081.1, WP_013388721.1). We confirmed that trees of similar topology were produced upon using a range of phylogenetic methods, namely neighbor-joining, maximum-parsimony and maximum-likelihood in MEGA, Mr Bayes, phyml, and iqtree. In addition, equivalent trees were created by using the protein sequences of the CO dehydrogenase medium subunit (CoxM), small subunits (CoxS), or concatenations of all three subunits (CoxLMS). Varying the form II CO dehydrogenase sequence used also had no effect on the overall topology.

5.3.12 Metagenome and metatranscriptome analysis

Forty pairs of metagenomes and metatranscriptomes that encompassed a range of soil and marine sample types were selected and downloaded from the Joint Genome Institute (JGI) Integrated Microbial Genomes System (286) and the NCBI Sequence Read Archive (SRA) (287). **Supplementary Table S15** provides details of the datasets used. Raw metagenomes and metatranscriptomes were subjected to quality filtering using NGS QC Toolkit (288) (version 2.3.3, default settings, i.e., base quality score and read length threshold are 20 and 70%, respectively). SortMeRNA (289) (version 2.1, default settings and default rRNA databases) was used to removed ribosomal RNA (rRNA) reads from metatranscriptomes.

Each metagenome and metatranscriptome was subsampled to an equal depth of 5 million reads and 2 million reads, respectively, using seqtk (https://github.com/lh3/seqtk) seeded with parameter -s100. Subsampled datasets were then screened in DIAMOND (version 0.9.24.125, default settings, one maximum target sequence per query) (290) using the 709 CoxL protein sequences (**Supplementary Table S13**) and the 3261 hydrogenase catalytic subunit gene sequences from HydDB (100). Hits to CoxL were filtered with an amino acid alignment length over 40 residues and a sequence identity over 60%. Clade classification of the reads was based on their closest match to the CoxL sequence dataset. Hydrogenase hits were filtered with the same amino acid alignment length cutoff and a sequence identity over 50%. Group 4 [NiFe]-hydrogenase hits with a sequence identity below 60% were discarded.

5.4 Results

5.4.1 *Mycobacterium smegmatis* synthesizes carbon monoxide dehydrogenase in response to organic carbon starvation

We first performed a proteome analysis to gain a system-wide context of the levels of CO dehydrogenase during growth and survival of *M. smegmatis*. Shotgun proteomes were compared for triplicate cultures grown in glycerol-supplemented minimal media under two conditions: mid-exponential growth ($OD_{600} \sim 0.25$; 5.1 mM glycerol left in medium) and mid-stationary phase following carbon limitation (72 h post $OD_{max} \sim 0.9$; no glycerol detectable in medium) (**Figure 5.1a**). There was a major change in the proteome profile, with 270 proteins more abundant and 357 proteins less abundant by at least four-fold ($p < 0.05$) in the carbon-limited condition (**Figure 5.1b; Supplementary Table S12**).
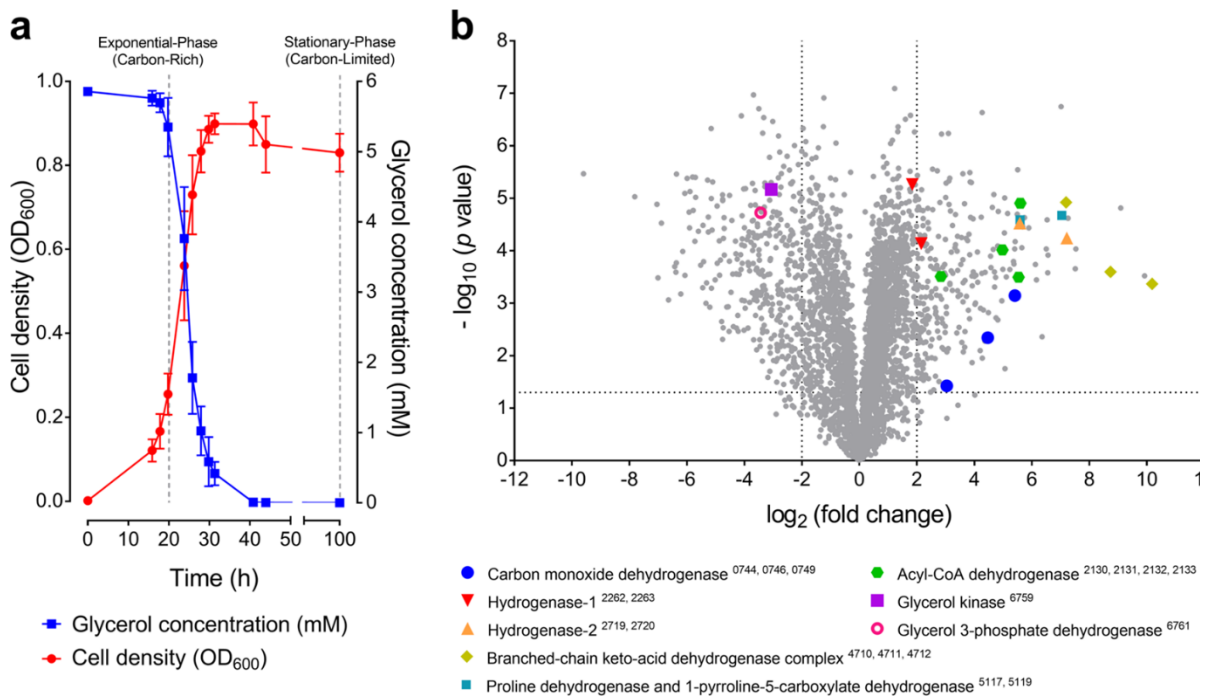
Figure 5.1. Comparison of proteome composition of carbon-replete and carbon-limited cultures of *Mycobacterium smegmatis*. a) Growth of *M. smegmatis* in Hartmans de Bont minimal medium supplemented with 5.8 mM glycerol. The glycerol concentration of the external medium is shown. Error bars show standard deviations of three biological replicates. Cells were harvested for proteomic analysis at $OD_{600} = 0.25$ (mid-exponential phase, glycerol-rich) and 3 days post OD_{max} (mid-stationary phase, glycerol-limited). **b)** Volcano plot showing relative expression change of genes following carbon limitation. Fold change was determined by dividing the relative abundance of each protein in three stationary phase proteomes with that in the three exponential phase proteomes (biological replicates). Each protein is represented by a gray dot. Structural subunits of selected metabolic enzymes, including the form I CO dehydrogenase, are highlighted and their locus numbers are shown in subscript in the legend.

The top 50 proteins with increased abundance included those involved in trace gas metabolism and amino acid catabolism. In line with our hypotheses, there was an increase in the structural subunits encoding a putative form I CO dehydrogenase, including a 54-fold increase in the catalytic subunit CoxL. Levels of the two uptake hydrogenases also increased, particularly the catalytic subunit of hydrogenase-2 (HhyL, 148-fold), in line with previous observations that mycobacteria persist on atmospheric H_2 (11, 195). There was also evidence that *M. smegmatis* generates additional reductant in this condition by catabolizing amino acid reserves: the three subunits of a branched-chain keto-acid dehydrogenase complex were the

most differentially abundant proteins overall and there was also a strong induction of the proline degradation pathway, including the respiratory proline dehydrogenase (**Figure 5.1b**).

The abundance of various enzymes mediating organic carbon catabolism decreased, including the respiratory glycerol 3-phosphate dehydrogenase (10-fold) and glycerol kinase (8-fold), in line with cultures having exhausted glycerol supplies (**Figure 5.1b**). The proteome also suggests that various energetically expensive processes, such as cell wall, ribosome, and DNA synthesis, were downregulated (**Supplementary Table S12**). Overall, these results suggest that *M. smegmatis* reduces its energy expenditure and expands its metabolic repertoire, including by oxidizing CO, to stay energized during starvation.

5.4.2 Carbon monoxide dehydrogenase mediates atmospheric CO oxidation and supports aerobic respiration

Having confirmed that a putative CO dehydrogenase is present in stationary-phase *M. smegmatis* cells, we subsequently confirmed its activity through whole-cell biochemical assays. To do so, we constructed a markerless deletion of the *coxL* gene (MSMEG_0746) (**Supplementary Figure S8**). Native polyacrylamide gels containing fractions of wild-type *M. smegmatis* harvested in carbon-limited stationary-phase cells strongly stained for CO dehydrogenase activity in a 100% CO atmosphere; the molecular mass of the band corresponds to the theoretical molecular mass of a dimer of CoxLMS subunits (~269 kDa). However, no activity was observed in the Δ*coxL* background (**Figure 5.2a**).

Gas chromatography measurements confirmed that *M. smegmatis* oxidized carbon monoxide at atmospheric concentrations. Stationary-phase cultures consumed the CO added to the headspace (~200 ppmv) to sub-atmospheric concentrations (46 ± 5 ppbv) within 100 h (**Figure 5.2b**). The apparent kinetic parameters of this activity ($V_{\text{max app}} = 3.13$ nmol g_{dw}^{-1} min^{-1}; $K_{\text{m app}} = 350$ nM; threshold $_{\text{app}} = 43$ pM) are consistent with a moderate-affinity, slow-acting enzyme (**Figure 5.2c; Supplementary Table S14**). Such rates are similar to those previously

measured for hydrogenase-2 (11). It is important to note, however, that measurements are based on whole-cell activities and may not reflect the kinetics of the purified enzyme. No change in CO mixing ratios was observed for the Δ*coxL* strain (**Figure 5.2b**), confirming that the form I CO dehydrogenase is the sole CO-oxidizing enzyme in *M. smegmatis* stationary phase cells. In turn, these results provide the first genetic proof that form I CO dehydrogenases mediate atmospheric CO oxidation.

We performed oxygen electrode experiments to confirm whether CO addition stimulated aerobic respiration. In stationary-phase cultures, addition of CO caused a 15-fold stimulation of respiratory O_2 consumption relative to background rates ($p < 0.0001$). This stimulation was observed in the wild-type strain, but not the Δ*coxL* mutant, demonstrating it is dependent on CO oxidation activity of the CO dehydrogenase (**Figure 5.2d, e**). Thus, while this enzyme is predominantly localized in the cytosol (**Figure 5.2a**), it serves as a *bona fide* respiratory dehydrogenase that supports aerobic respiration in *M. smegmatis*.
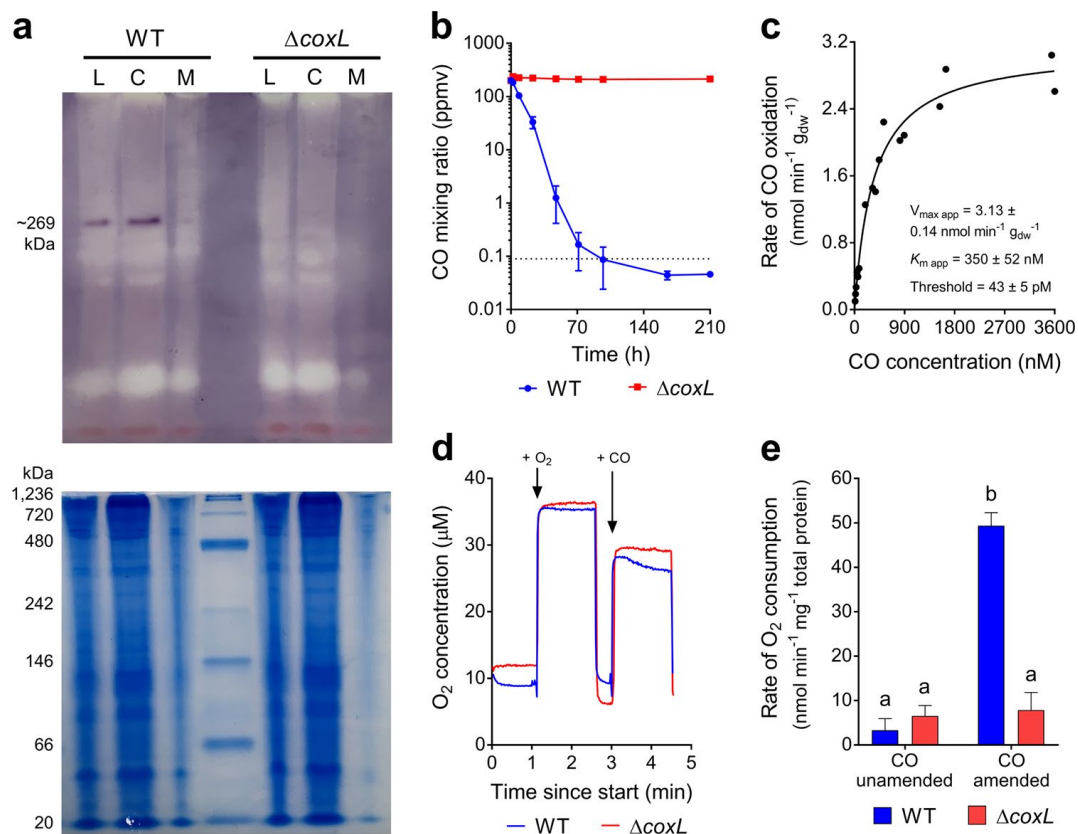
Figure 5.2. Comparison of carbon monoxide dehydrogenase activity of *Mycobacterium smegmatis* wild-type and Δ*coxL* cultures. a) Zymographic observation of CO dehydrogenase activity and localization. The upper gel shows enzyme activity stained with the artificial electron acceptor nitroblue tetrazolium chloride in a CO-rich atmosphere. The lower gel shows protein ladder and whole protein stained with Coomassie Blue. Results are shown for whole-cell lysates (L), cytosolic fractions (C), and membrane fractions (M) of wild-type (WT) and Δ*coxL* cultures. **b)** Gas chromatography measurement of CO oxidation to sub-atmospheric levels. Mixing ratios are displayed on a logarithmic scale, the dotted line shows the average atmospheric mixing ratios of CO (90 ppbv), and error bars show standard deviations of three biological replicates. **c)** Apparent kinetic parameters of CO oxidation by wild-type cultures. Curves of best fit and kinetic parameters were calculated based on a Michaelis–Menten non-linear regression model. $V_{\text{max app}}$ and $K_{\text{m app}}$ values derived from other models are shown in **Supplementary Table S14**. **d)** Examples of traces from oxygen electrode measurements. O_2 levels were measured before and after CO addition in both a wild-type and Δ*coxL* background. **e)** Summary of rates of O_2 consumption measured using an oxygen electrode. Center values show means and error bars show standard deviations from three biological replicates. For all values with different letters, the difference between means is statistically significant ($p < 0.001$) based on Student's *t*-tests.

5.4.3 Carbon monoxide is dispensable for growth and detoxification, but enhances survival during carbon starvation

We then performed a series of experiments to resolve the expression and importance of the CO dehydrogenase during growth and survival. Consistent with the proteomic analyses, expression levels of *coxL* were low in carbon-replete cultures (mid-exponential phase; 1.35×10^7 transcripts g_{dw}^{-1}) and increased 56-fold in carbon-limited cultures (mid-stationary phase; 7.48×10^8 transcripts g_{dw}^{-1}; $p < 0.01$). Addition of 1% CO did not significantly change *coxL* expression in either growing or stationary cultures (**Figure 5.3a**). These profiles suggest that *M. smegmatis* expresses CO dehydrogenase primarily to enhance survival by scavenging atmospheric CO, rather than to support growth on elevated levels of CO.

These inferences were confirmed by monitoring the growth of the wild-type and Δ*coxL* strains under different conditions. The strains grew identically on glycerol-supplemented minimal medium. Addition of 20% CO caused a slight increase in doubling time for both strains and

did not affect growth yield (**Figure 5.3b**). This suggests that *M. smegmatis* is highly tolerant of CO but does not require CO dehydrogenase to detoxify it. *M. smegmatis* did not grow chemolithoautotrophically on a minimal medium with 20% CO as the sole carbon and energy source (**Figure 5.3b**). While carboxydotrophic growth was previously reported for this strain, the authors potentially observed CO-tolerant heterotrophic or mixotrophic growth, given the reported media contained metabolizable organic carbon sources (151). Consistently, *M. smegmatis* lacks key enzymes of the Calvin–Benson cycle (e.g., RuBisCO, ribulose 1,5-bisphosphate carboxylase) typically required for carboxydotrophic growth.
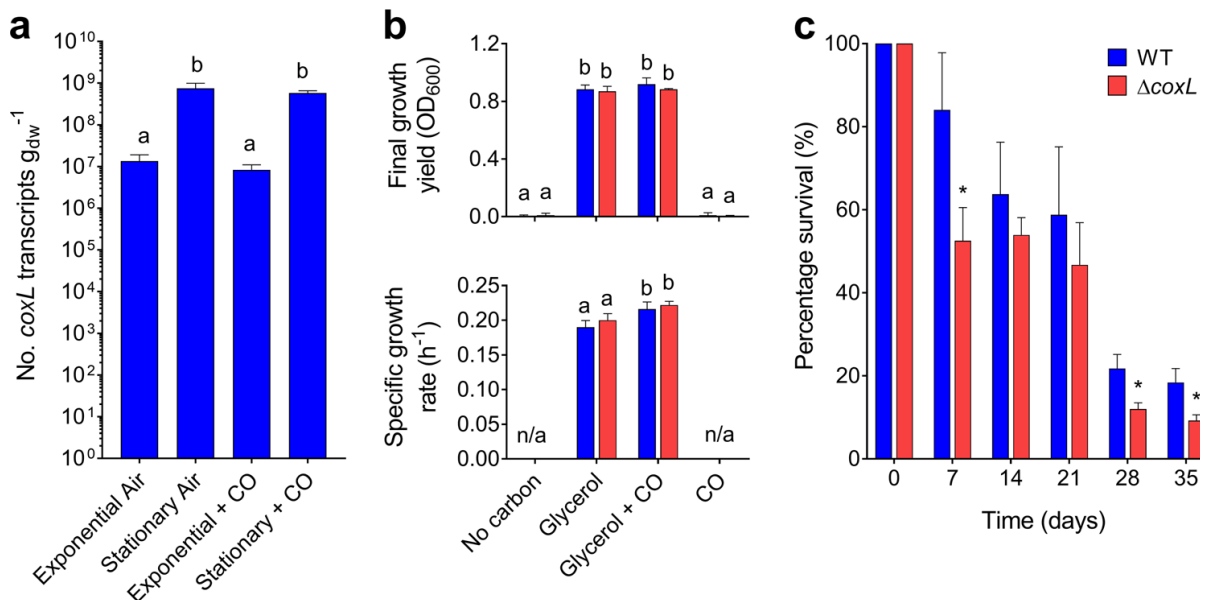
Figure 5.3. Expression and importance of carbon monoxide dehydrogenase during growth and survival of *Mycobacterium smegmatis*. a) Normalized number of transcripts of the CO dehydrogenase large subunit gene (*coxL*; MSMEG_0746) in wild-type cultures harvested during exponential phase (carbon-replete) and stationary phase (carbon-limited) in the presence of either ambient CO or 1% CO. Error bars show standard deviations of four biological replicates. For all values with different letters, the difference between means is statistically significant ($p < 0.01$) based on Student's *t*-tests. **b)** Final growth yields (OD_{max}) and specific growth rates wild-type and Δ*coxL* strains. Strains were grown on Hartmans de Bont minimal medium supplemented with either 5.5 mM glycerol, 20% CO, or both 5.5 mM glycerol and 20% CO. Values labeled with different letters are significantly different ($p < 0.05$) based on Student's *t*-tests. Error bars show standard deviations of three biological replicates. **c)** Long-term survival of wild-type and Δ*coxL* strains in Hartmans de Bont minimal medium supplemented

with either 5.5 mM glycerol. Percentage survival was calculated by dividing the colony-forming units (CFU mL^{-1}) at each timepoint with those counted at OD$_{max}$ (day 0). Error bars show standard deviations of nine biological replicates. For asterisked values, there was a significant difference in survival of Δ*coxL* strains compared to the wild-type ($p < 0.05$) based on Student's *t*-tests.

Finally, we monitored the long-term survival of the two strains after they reached maximum cell counts upon exhausting glycerol supplies (**Figure 5.1a**). The percentage survival of the Δ*coxL* strain was lower than the wild-type at all timepoints, including by 45% after 4 weeks and 50% after 5 weeks of persistence. These findings were reproducible across two independent experiments and were significant at the 98% confidence level (**Figure 5.3c**). Such reductions in relative percentage survival are similar to those previously observed for uptake hydrogenase mutants in *M. smegmatis* (47%) (36, 195) and *Streptomyces avermilitis* (74%) (34). These experiments, therefore, provide genetic evidence that atmospheric CO oxidation mediated by form I CO dehydrogenases enhances bacterial persistence. It should be noted that we did not attempt to complement the observed phenotypes, though whole-genome sequencing confirmed that no other substitutions were present in Δ*coxL* compared to the wild-type cells.

5.4.4 Atmospheric carbon monoxide oxidation is an ancient, taxonomically widespread and ecologically important process

We subsequently surveyed genomic, metagenomic, and metatranscriptomic datasets to gain insights into the taxonomic and ecological distribution of atmospheric CO oxidation. This yielded 709 amino acid sequences encoding large subunits of the form I CO dehydrogenases (CoxL) across some 685 species, 196 genera, 49 orders, and 25 classes of bacteria and archaea (**Supplementary Table S13**; **Figure 5.4a, b**). The retrieved sequences encompassed all sequenced species, across seven phyla (**Figure 5.4b**), that have previously been shown to mediate aerobic CO oxidation (**Supplementary Table S11**). We also detected *coxL* genes in nine other phyla where aerobic CO oxidation has yet to be

experimentally demonstrated (**Figure 5.4b**). Hence, the capacity for aerobic CO respiration appears to be a much more widespread trait among aerobic bacteria and archaea than previously reported (94, 129). It is particularly notable that *coxL* genes were detected in representatives of seven of the nine (281, 291) most dominant soil phyla, namely Proteobacteria, Actinobacteriota, Acidobacteriota, Chloroflexota, Firmicutes, Gemmatimonadota, and Bacteroidota (**Figure 5.4b**). While most species surveyed encoded a single copy, 16 actinobacterial species encoded two isozymes of CO dehydrogenase (**Supplementary Table S13**).
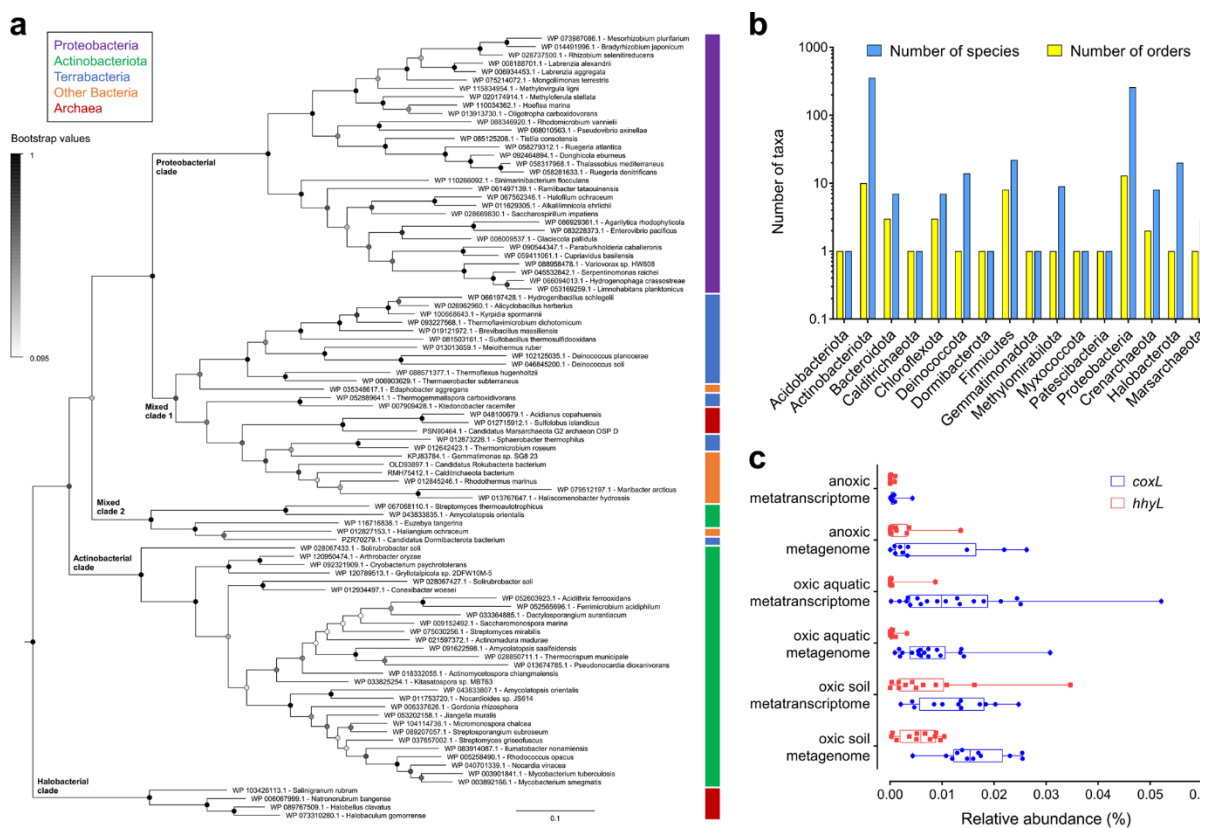
Figure 5.4. Distribution of carbon monoxide dehydrogenases in genomes, metagenomes, and metatranscriptomes. a) Maximum-likelihood phylogenetic tree showing the evolutionary history of the catalytic subunit of the form I CO dehydrogenase (CoxL). Evolutionary distances were computed using the Poisson correction model, gaps were treated by partial deletion, and the tree was bootstrapped with 200 replicates. The tree was constructed using a representative subset of 94 CoxL amino acid sequences from **Supplementary Table S13** and a neighbor-joining tree containing all 709 CoxL sequences retrieved in this study is provided in **Supplementary Figure S9**. The major clades of the tree are labeled, and the colored bars represent the phylum that each sequence is affiliated with. The tree was rooted with five form II

CO dehydrogenase sequences (not shown). **b)** Phylum-level distribution of the CoxL-encoding species and orders identified in this work. **c)** Abundance of *coxL* genes and transcripts in environmental samples. In total, 40 pairs of metagenomes and metatranscriptomes (20 aquatic, 20 terrestrial) were analyzed from a wide range of biomes (detailed in **Supplementary Table S15**). The abundance of *hhyL* genes and transcripts, encoding the high-affinity group 1h [NiFe]-hydrogenase, are shown for comparison. Box plots show the individual values and their mean, quartiles, and range for each dataset.

We constructed phylogenetic trees to visualize the evolutionary relationships of CoxL protein sequences (**Figure 5.4a; Supplementary Figure S9**). The trees contained five monophyletic clades that differed in phylum-level composition, namely actinobacterial, proteobacterial, and halobacterial clades, as well as mid-branching major (mixed 1) and minor (mixed 2) clades of mixed composition containing representatives from seven and three different phyla respectively. Clades were well-supported by bootstrap values, with exception of the mixed 2 clade (**Figure 5.4a; Supplementary Figure S9**). Trees with equivalent clades were produced when using seven distinct phylogenetic methods, using other CO dehydrogenase subunits (CoxM, CoxS, and CoxLMS concatenations), or varying the outgroup sequences. In all cases, major clades included CoxL proteins of at least one previously characterized carboxydotroph or carboxydovore (**Supplementary Table S11**). Surprisingly, all clades also contained species that have been previously shown to oxidize atmospheric CO (**Supplementary Table S11**). This suggests that atmospheric CO oxidation is a widespread and ancestral capability among CO dehydrogenases. In contrast, CO dehydrogenases known to support aerobic carboxydotrophic growth were sparsely distributed across the tree (**Figure 5.4a; Supplementary Table S11**).

To better understand the ecological significance of aerobic CO oxidation, we surveyed the abundance of *coxL* sequences across 40 pairs of metagenomes and metatranscriptomes (**Supplementary Table S11**). Genes and transcripts for *coxL* were detected across a wide range of biomes. They were particularly abundant in the oxic terrestrial and marine samples surveyed (1 in every 8000 reads), for example, grassland and rainforest soils, coastal and

mesopelagic seawater, and salt marshes (**Supplementary Table S16**). In contrast, they were expressed at very low levels in anaerobic samples (e.g., groundwater, deep subsurface, peatland) (**Supplementary Figure S10**). Across all surveyed metatranscriptomes, the majority of the *coxL* hits were affiliated with the mixed 1 (40%), proteobacterial (25%), and actinobacterial (25%) clades, with minor representation of the mixed 2 (8%) and halobacterial (2%) clades (**Supplementary Table S16**). The normalized transcript abundance of *coxL* was higher than the genetic determinants of atmospheric H_2 oxidation (*hhyL*; high-affinity hydrogenase) in most samples (18-fold in aquatic samples, 1.2-fold in terrestrial samples) (**Figure 5.4c**). Together, this suggests that CO oxidation is of major importance in aerated environments and is mediated by a wide range of bacteria and archaea.

5.5   Discussion

In this work, we validated that atmospheric CO oxidation supports bacterial survival during nutrient limitation. *M. smegmatis* increases the transcription and synthesis of a form I CO dehydrogenase by 50-fold in response to organic carbon limitation. Biochemical studies confirmed that this enzyme is kinetically adapted to scavenge atmospheric concentrations of CO and uses the derived electrons to support aerobic respiration. In turn, deletion of the genes encoding the enzyme did not affect growth under a range of conditions, but resulted in severe survival defects in carbon-exhausted cultures. These observations are reminiscent of previous observations that *M. smegmatis* expresses two high-affinity hydrogenases to persist by scavenging atmospheric H_2 (11, 36, 84, 195). In common with atmospheric H_2, atmospheric CO is a high-energy, diffusible, and ubiquitous trace gas (21), and is therefore a dependable source of energy to sustain the maintenance needs of bacteria during persistence. Overall, the proteome results suggest that *M. smegmatis* activates CO scavenging as a core part of a wider response to enhance its metabolic repertoire; the organism appears to switch from acquiring energy organotrophically during growth to mixotrophically during survival by scavenging a combination of inorganic and organic energy sources.

Despite this progress in resolving the physiological role of CO oxidation in this organism, detailed mechanistic studies are required to understand how *M. smegmatis* and other carboxydovores gain the energy from atmospheric CO oxidation. Firstly, it is unclear what enables CO dehydrogenase to bind and oxidize atmospheric CO. It is important to compare whole-cell kinetic parameters with those of the purified enzyme, given enzyme activity is likely to be influenced by both structural features and cellular context. While it is probable that structural adaptations of the enzyme contribute to high-affinity binding, the only solved structures of molybdenum–copper CO dehydrogenases to date are from the apparent low-affinity carboxydotroph *O. carboxidovorans* (53, 136). Secondly, it is unclear how CO dehydrogenase inputs electrons into the aerobic respiratory chain. Our study indicates that the CO dehydrogenase is primarily cytosolic, though it cannot be ruled out that it makes weak or transient associations with the cell membrane. The proteome data shows *M. smegmatis* expresses CoxG (MSMEG_0749), which is implicated as a membrane anchor for CO dehydrogenase in *O. carboxidovorans* (135, 292, 293). Thirdly, further studies are required to resolve how *M. smegmatis* couples CO oxidation to O_2 reduction, including with respect to reaction stoichiometry, electron flow, and terminal oxidase selectivity. In this regard, one discrepancy is that we observed a surprisingly high rate of O_2 reduction (oxygen electrode measurements) compared to CO oxidation (gas chromatography); side-by-side analyses are required to determine whether these findings are physiologically relevant or instead reflect methodological differences.

Looking more broadly, it is probable that CO supports the persistence of many other bacterial and archaeal species. Atmospheric CO oxidation is a common trait among all carboxydovores tested to date and has been experimentally demonstrated in 18 diverse genera of bacteria and archaea (33, 126, 262, 270, 271, 275, 280). In this regard, a recent study demonstrated that the hot spring bacterium *Thermomicrobium roseum* (phylum Chloroflexota) upregulates a form I CO dehydrogenase and oxidizes atmospheric CO as part of a similar response to

carbon starvation (33). It has also been demonstrated that the form I CO dehydrogenases of the known atmospheric CO scavenger *Ruegeria pomolori* (91) and a *Phaeobacter* isolate (92) from the marine *Roseobacter* clade (phylum Proteobacteria) are also highly upregulated under energy-limiting conditions. The capacity for atmospheric CO uptake has also been demonstrated in four halophilic archaeal genera (phylum Halobacterota) (271, 280) and may also extend to thermophilic archaea (phylum Crenarchaeota) (278, 279). Moreover, two cultured aerobic methanotrophs harbor the capacity for aerobic CO respiration (294, 295). Our study, by showing through a molecular genetic approach that CO oxidation enhances survival, provides a physiological rationale for these observations. Altogether, this suggests that most organisms encoding form I CO dehydrogenases use this enzyme to support survival rather than growth.

These results also have broader implications for understanding the biogeochemical cycling and microbial biodiversity at the ecosystem level. It is well-established that soil bacteria are major net sinks for atmospheric CO and marine bacteria mitigate geochemical oceanic emissions of this gas (257). This study, by confirming the enzymes responsible and demonstrating that their activities support bacterial persistence, has ramifications for modeling these biogeochemical processes. In turn, we propose that CO is an important energy source supporting the biodiversity and stability of aerobic heterotrophic communities in terrestrial and aquatic environments. The genomic survey supports this by demonstrating that form I CO dehydrogenases, most of which are predicted to support atmospheric CO oxidation, are encoded by 685 species and 16 phyla of bacteria and archaea. In turn, the metagenomic and metatranscriptomic analyses confirmed that *coxL* genes and transcripts are highly abundant in most aerated soil and marine ecosystems. The notably high abundance of *coxL* transcripts in pelagic samples of various depths suggests CO may be a major energy source for maintenance of marine bacteria. In soils, the oxidation of atmospheric CO may be of similar importance to atmospheric H_2; this is suggested by the strength of the soil sinks for these gases (6, 13), the abundance of *coxL* and *hhyL* genes in soil metagenomes, and the

distribution of these genes in the genomes of soil bacteria (49). Atmospheric CO may be especially important for sustaining communities in highly oligotrophic soils, as indicated by previous studies in polar deserts (29), volcanic deposits (94, 193, 296), and salt flats (271, 297, 298). Further work is now needed to understand which microorganisms mediate consumption of atmospheric CO in situ and how their activity is controlled by physicochemical factors.

Integrating these findings with the wider literature, we propose a new survival-centric model for the evolution of CO dehydrogenases. It was traditionally thought that aerobic CO oxidation primarily supports autotrophic and mixotrophic growth of microorganisms (19, 266). However, the majority of studied CO-oxidizing bacteria are, in fact, carboxydovores, of which those that have been kinetically characterized can oxidize CO at sub-atmospheric levels (**Supplementary Table S11**). In turn, our phylogenomic analysis revealed that atmospheric CO-oxidizing bacteria are represented in all five clades of the phylogenetic tree, suggesting that the common ancestor of these enzymes also harbored sufficient substrate affinity to oxidize atmospheric CO. On this basis, we propose that microorganisms first evolved a sufficiently high-affinity form I CO dehydrogenase to subsist on low concentrations of CO. The genes encoding this enzyme were then horizontally and vertically disseminated to multiple bacterial and archaeal genera inhabiting different environments. On multiple occasions, certain bacterial lineages evolved to support growth on CO in microenvironments where present at elevated concentrations. This would have required relatively straightforward evolutionary innovations, namely acquisition of Calvin–Benson cycle enzymes (e.g., RuBisCO) and their integration with CO dehydrogenase. The modulation of CO dehydrogenase kinetics was likely not a prerequisite, given these enzymes efficiently oxidize CO at a wide range of substrate concentrations (33, 262), but may have subsequently enhanced carboxydotrophic growth. In this regard, it remains to be explored whether some cultivated carboxydotrophs can also support persistence using trace concentrations of CO. These evolutionary inferences differ from hydrogenases, where high-affinity, oxygen-tolerant

enzymes appear to have evolved from low-affinity, oxygen-sensitive ones (49). However, it is probable that the processes of atmospheric CO and H_2 oxidation evolved due to similar physiological pressures and over similar evolutionary timescales.

5.6 Footnotes

Supplementary Information: The supplementary material for this chapter can be found in **Appendix D.**

Chapter 6

Discussion and Outlook

6.1 Discussion

6.1.1 H$_2$ oxidation is integrated with the mycobacterial respiratory chain during persistence

Current knowledge of the biochemistry of aerobic hydrogen metabolism has focused on organisms capable of autotrophic growth. For example, detailed studies have resolved how the membrane-bound hydrogenase in *Ralstonia eutropha* is integrated in the aerobic respiratory chain and tolerates oxygen poisoning (107, 120, 299–302). However, the most abundant H$_2$-oxidizing bacteria in soil ecosystems use H$_2$ to support persistence rather than growth, and this depends on phylogenetically and kinetically distinct hydrogenases (186, 303). Thus, new model systems for aerobic hydrogen metabolism need to be developed to understand the basis, regulation, and role of atmospheric H$_2$ oxidation. Using the soil saprophyte *M. smegmatis* as a model organism, we have illustrated in chapter 2 how uptake hydrogenases integrate with the respiratory chain during persistence. The respiratory complexes involved in central carbon metabolism that are usually abundant in carbon-replete conditions are downregulated in *M. smegmatis* upon carbon starvation (36). We show that mycobacteria remodel their respiratory chain to enable the use of alternative energy sources to sustain oxidative phosphorylation during carbon limitation. Consistent with previous reports, we found that uptake hydrogenases are upregulated and highly active in stationary phase and that these enzymes require O$_2$ to oxidize H$_2$ during starvation (11). Furthermore, we showed through fractionation experiments that the uptake hydrogenases are associated with the membrane, thus positioning them to facilitate possible electron transfer to the respiratory chain. These findings suggest that hydrogenases are physically and functionally integrated with the aerobic respiratory chain under carbon-limited conditions.

In *M. smegmatis*, it was postulated that the electrons from H$_2$ oxidation by Huc and Hhy enter the electron transport chain, thus maintaining the cellular proton gradient for ATP generation via oxidative phosphorylation (8, 11). Following this hypothesis, our work now provides the

first model on how this integration occurs. The oxygen dependence of both Huc and Hhy shows that these enzymes are obligately coupled to the aerobic respiratory chain during starvation. Through H_2 oxidation, they provide electrons to the menaquinone pool and the putative iron-sulfur proteins HucE and HhyE most probably function as the conduit for electron transfer to menaquinone. Other iron-sulfur proteins associated with H_2-oxidizing hydrogenase in other organisms are proposed to perform function similar to HucE and HhyE. For instance, HybA in *Escherichia coli* is a ferredoxin-type component of hydrogenase 2 involved in electron transfer between the hydrogenase and the quinone pool (304, 305). Similarly, HupX of *Dehalococcoides mccartyi* is part of an organohalide respiratory complex (OHR), consisting of several proteins including an uptake hydrogenase Hup (306, 307). The OHR is a complexome hypothesized to be a stand-alone fully functional respiratory chain and HupX is proposed to mediate the electron transfer from the hydrogenase within the complexome (306, 307). The putative function of HucE and HhyE as iron-sulfur proteins is based on their essentiality for the activity of the hydrogenases as shown in chapter 3 and their homology with other iron-sulfur proteins associated with group 2a and group 1h [NiFe]-hydrogenases, respectively (**Supplementary Figure S6**). However, it is possible that other hypothetical proteins could serve as the immediate electron acceptors of the hydrogenases to perform such function (190). From the menaquinone pool, the electrons feed into either the cytochrome *bcc-aa*$_3$ supercomplex or cytochrome *bd* oxidase. Huc seems to be obligately linked to the cytochrome *bcc-aa*$_3$, whereas Hhy feeds electrons to both terminal oxidases. This correlates with the function of the hydrogenases inferred from their expression profiles. The cytochrome *bcc-aa*$_3$ supercomplex is the main terminal oxidase during replicative growth and is significantly more efficient than cytochrome *bd* (152, 159–161). In contrast, cytochrome *bd* oxidase is expressed in preference to cytochrome *bcc-aa*$_3$ during hypoxia and carbon starvation (36, 164, 165). Thus, it is intuitive that Huc would donate electrons to cytochrome *bcc-aa*$_3$ supercomplex during transition from growth to stationary phase while Hhy, which is expressed predominantly during persistence, would also utilize the alternative terminal oxidase. The apparent obligate association of Huc with the cytochrome *bcc-aa*$_3$ oxidase could

have important bioenergetic implications. As Huc is also used during growth, proton-motive force could be efficiently generated through the cytochrome bcc-aa_3, which may help energize the cell during late exponential growth and early stages of persistence. Future studies are needed to determine the mechanistic basis of the association between the cytochrome bcc-aa_3 oxidase and Huc and to investigate whether such association is a broader feature of Huc-type hydrogenases.

Looking broadly, the integration of trace gas oxidation in aerobic respiration may help support persistence in other organisms. Respirometry measurements of H_2 consumption in the presence of different respiratory uncouplers have been demonstrated in other phyla such as Chloroflexi, Acidobacteria, and Verrucomicrobia (32, 33, 35). The observed change in their H_2 uptake in the presence of uncouplers suggests the interaction between H_2 oxidation and the respiratory chain of these organisms (32, 33, 35). This interaction may help maintain basic cellular functions by keeping the membrane energized and could be employed by the general microbial community to survive nutrient limitation.

6.1.2   Mycobacterial uptake hydrogenase is regulated by catabolite repression

We have shown in chapter 4 that catabolite repression plays a key role in regulating uptake hydrogenase genes expression and H_2 metabolism in mycobacteria. Catabolite repression has been previously shown to regulate various processes in mycobacteria and streptomycetes, though not in regulating hydrogenases (247, 308, 309). In streptomycetes, catabolite repression controls the expression of genes for the catabolism of alternative carbon sources (232, 310, 311), synthesis of antibiotics (312, 313), and morphological differentiation (313, 314). Mycobacteria have also been shown to regulate metabolic activities through catabolite repression, including pyrene biodegradation (308, 309, 315, 316). In this study, we show that *huc* expression is repressed by glycerol, thereby providing a direct link between organic carbon levels and the induction of alternative energy metabolism. This is mediated by GylR, a glycerol-responsive sensor that indirectly represses the expression of *huc*. This sensor

potentially interacts with a downstream regulator that can directly bind and regulate *huc* expression. CRP is a common regulator in catabolite repression used by many gram-negative bacteria and it has been demonstrated to activate hydrogenase genes expression in *Salmonella enterica* and *Escherichia coli* (80, 85, 87). *M. smegmatis*, unlike other gram-positive bacteria which employs a CcpA-system for catabolite repression, utilizes the CRP system (317–319). *M. smegmatis* has two CRP copies, CRP1 and CRP2, both of which are involved in regulating genes for carbon source transport and catabolism as well as genes encoding components of the respiratory chain (317). Additionally, CRP2 regulates genes implicated in the resuscitation of dormant cells and genes that are essential for growth on cholesterol (317, 320, 321). Although CRP1 and CRP2 are involved in regulating 239 and 58 genes, respectively, in *M. smegmatis* (317), they are not a plausible downstream regulator as suggested by our proteomic data where the CRPs are not upregulated in the *gylR* mutant and knockdown strain. However, other transcriptional regulators that are upregulated might play a key role in directly controlling *huc* expression.

Regulation of trace gas metabolism through catabolite repression could have significant implications. For instance, saprophytes living in environments where organic carbon availability is low or variable may sense organic carbon levels and express hydrogenases when starved. This may be particularly advantageous in desert ecosystems where organic carbon is typically extremely limited (322–324). They could adapt to and survive carbon limitation by expressing their uptake hydrogenases in order to consume the ubiquitous substrate H_2 instead. Aside from uptake hydrogenases, CO dehydrogenase may also be regulated via catabolite repression through distinct regulatory systems. Indeed, genes encoding CO dehydrogenase have been shown in different microorganisms to be upregulated during carbon starvation (33, 126, 209), though the exact signals and regulators responsible remain uncharacterized. Regulation of CO dehydrogenase, like uptake hydrogenases, may enhance the adaptability and survival of environmental microorganisms during carbon limitation.

6.1.3 CO oxidation supports persistence and not growth in mycobacteria and carboxydovores

The physiological role of CO oxidation in mycobacteria has been elucidated in chapter 5. We found that CO oxidation in *M. smegmatis* was solely mediated by a form I CO dehydrogenase and have shown for the first time that CO is oxidized to support mycobacterial survival and not growth. Previous studies have reported that mycobacteria, including *M. smegmatis*, can grow on CO as the sole carbon source, albeit very slowly (150, 151). It is possible that some mycobacteria are able to do this, as they have the enzymes necessary for carbon fixation (e.g. form I Rubisco) (325–327). However, our findings suggest *M. smegmatis* cannot grow on CO as the sole carbon and energy source, in line with it lacking enzymes for carbon fixation. Here we show aerobic CO dehydrogenase is expressed and active during stationary phase rather than during exponential growth and that *M. smegmatis* cultures were able to survive long-term organic carbon starvation by oxidizing CO. It may be important to note that we observed a residual low-level CO-oxidizing activity even in the absence of CO dehydrogenase. Such activity could be attributed to the cytochrome *bd* oxidase, which is resistant to poisoning from several compounds including CO (164, 166–168) and this terminal oxidase could have detoxifying effect on CO. Nevertheles, our findings strongly support a persistence-centric model for CO utilization in mycobacteria. Similar to H_2, CO is oxidized by *M. smegmatis* and may serve as a highly dependable energy source during nutrient limitation. Indeed, we found that *M. smegmatis* was able to oxidize CO at sub-atmospheric concentrations in line with a previous study (150).

More broadly, these findings suggest environmental carboxydovores may also persist using atmospheric CO. The aerobic CO dehydrogenase is widely distributed among environmental microorganisms. Our genomic and metagenomic surveys revealed that form I CO-dehydrogenase genes are encoded by more than 600 bacterial and archaeal species and is abundant in the oxic terrestrial and aquatic environments. These suggest that the capacity for

aerobic CO respiration is much more widespread among aerobic bacteria than previously reported (19, 129). While early studies largely centered on the role of CO in sustaining autotrophic growth of carboxydotrophs (19, 37, 41–43), subsequent studies have revealed that most CO-oxidizing bacteria are in fact carboxydovores (33, 46, 275, 280). It is likely that these bacteria, like *M. smegmatis*, also use atmospheric CO as an energy source to persist, rather than grow, in different environments. Reflecting this, the aerobic CO dehydrogenase of carboxydovores of marine Proteobacteria is upregulated during energy-limiting conditions (91, 92). Moreover, we have shown hot spring bacteria such as *Thermomicrobium roseum* are able to oxidize atmospheric CO in response to carbon limitation, similar to *M. smegmatis*(33). With these observations, our study provides a physiological explanation for atmospheric CO oxidation in carboxydovores.

Incorporating all the results in this study, the following summary of evidence demonstrate that trace gas oxidation supports mycobacterial persistence during organic carbon starvation: (i) the genes involved in trace gas metabolism are upregulated in stationary phase; (ii) both CO dehydrogenase and uptake hydrogenases are highly active during organic carbon limitation; (iii) wild type *M. smegmatis* has significantly higher long-term survival percentage than the CO dehydrogenase deletion mutants; (iv) deletion of structural subunits and putative iron-sulfur proteins of the uptake hydrogenases resulted in survival defect of *M. smegmatis*; and (v) expression of hydrogenase genes is directly regulated in response to organic carbon starvation. Uptake hydrogenases and CO dehydrogenases confer a survival advantage for mycobacteria, reflecting that atmospheric H_2 and CO are highly dependable substrates for bacteria to meet maintenance needs.

6.2   Outlook

6.2.1   Mechanism for high-affinity and oxygen tolerance

Microorganisms have the remarkable ability to oxidize H_2 and CO at atmospheric concentrations. This uptake of trace gases is essential for microbial long-term survival, as demonstrated in this work and previous studies (29, 31–33, 35, 83, 195). This capability depends on the high-affinity, oxygen tolerant hydrogenases and CO dehydrogenases. However, the mechanism for the high-affinity oxidation of H_2 and CO, as well the oxygen tolerance of these enzymes, still remains unresolved. Further work now needs to address: (i) how atmospheric H_2 and CO oxidation is catalyzed within the active sites of these enzymes; (ii) how the electrons are relayed within the enzyme and to the external redox partner; (iii) how atmospheric substrates travel into the catalytic center and the products out of the enzyme; (iv) which structural features confer high-affinity; and (v) which structural features contribute to oxygen tolerance.

To date, many [NiFe]-hydrogenases have been purified, their crystal structures solved, and catalytic cycles characterized (101–103, 105–110, 328). However, these hydrogenases have low affinity for H_2 and none can give insight to atmospheric H_2 oxidation. Similarly, the most extensively studied [MoCu]-CO dehydrogenase is from *Oligotropha carboxidovorans* but this carboxydotrophic enzyme has low affinity for CO and confers a physiologically different function than those found in carboxydovores (19, 43, 53, 140). Hence some structural characteristics and chemical behavior of this enzyme are likely to be different to those of high-affinity CO dehydrogenases. With respect to oxygen tolerance, structural studies have elucidated the basis for oxygen tolerance of several [NiFe]-hydrogenases and this relies on the ability of the active site to quickly recover from the oxidized state during the catalytic cycle (116, 120). In respiratory hydrogenases, this process depends largely on the structure of the iron-sulfur clusters that are proximally neighboring the active site (101, 106, 107, 121). However, this mechanism for oxygen tolerance is different between groups of hydrogenases.

As such, it will be invaluable to determine the mechanistic basis for both high-affinity and oxygen tolerance of hydrogenases such as Huc and Hhy.

Going forward, the fundamental structure and biochemical characteristics of the enzymes are needed to address the questions presented earlier. The first step to achieve this is by purifying the hydrogenases and CO dehydrogenase. Given recombinant production of membrane-associated multisubunit metalloenzymes such as hydrogenases is notoriously challenging (329–332), an alternative approach is to purify these enzymes by introducing chromosomal affinity tags (190). Our preliminary trials using this method on *M. smegmatis* Hhy resulted in the loss of activity and solubility of the enzyme. However, this can be circumvented in future experiments by optimizing the position of the tag in the enzymes or by purifying them natively. With the latter approach, we have attempted to purify Huc natively through a series of precipitation and column chromatography methods in the *gylR* mutant background, in which it is overproduced. These included ammonium sulfate precipitation, anion exchange chromatography, and size exclusion chromatography (**Figure 6.1**). While a considerable amount of progress has been achieved in this native purification effort, further optimization is required to achieve high yields. Nevertheless, native purification could be a better option for hydrogenases and CO-dehydrogenases as they are both multi-subunit membrane-associated metalloenzymes with multiple cofactors and complex assembly processes (40, 48, 53, 83). In this way, the loss of activity due to misfolding assembly would be prevented.
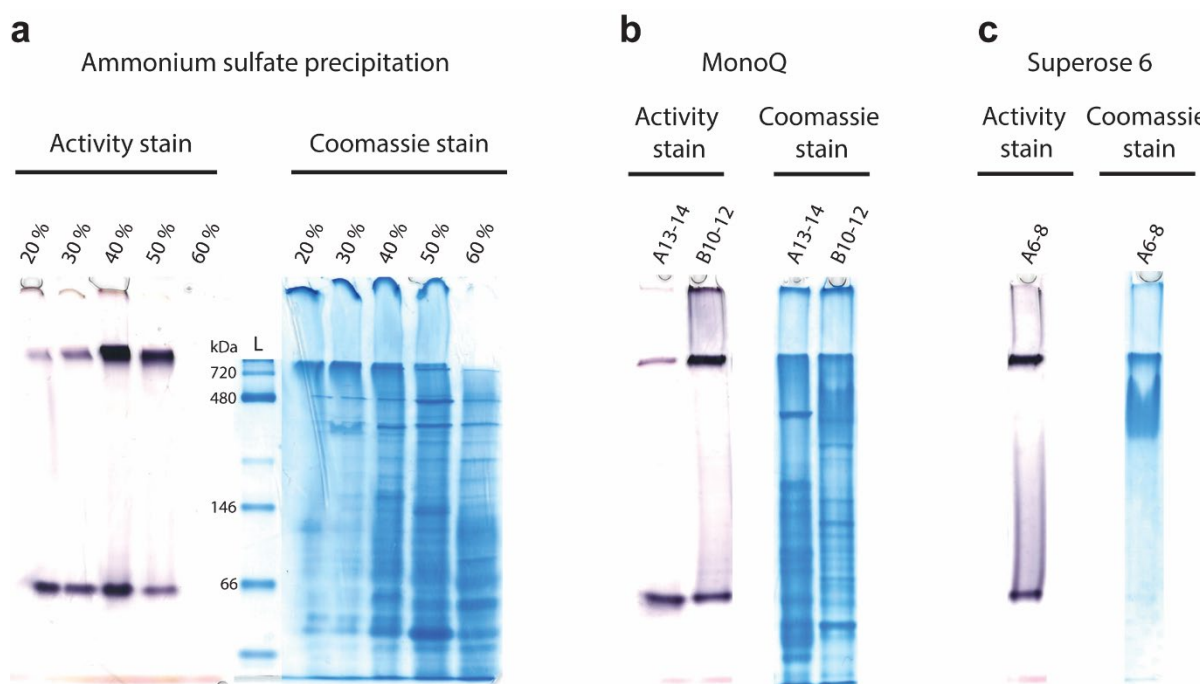
Figure 6.1. Native purification of Huc. Total protein and Huc activity staining after each purification step: **a)** Ammonium sulfate precipitation. Proteins are precipitated at different saturations of ammonium sulfate (shown as percentage above each lane), resulting in different fractions. **b)** Anion exchange chromatography using MonoQ; Huc is active in fractions A13-A14 and B10-B12. **c)** Size exclusion chromatography using Superose 6; Huc is active in fraction A6-A8. Huc activity staining is done in 7.5% native polyacrylamide gel. Artificial electron acceptor nitroblue tetrazolium chloride (500 µM) is used as chromogenic stain.

Upon purification, a series of biochemical and structural studies can be accomplished. For instance, protein electrochemistry will give insight on the redox states of the active site during catalysis, the redox states formed by the [NiFe] or [MoCu] metal centers in the presence or absence of oxygen, as well as the electron transfer relay between iron-sulfur clusters and between the enzyme and its physiological redox partner (333). Structural studies using cryo-electron microscopy or X-ray diffraction crystallography will provide atomic-resolution insights into the topology of the enzyme, show the specific amino acids that influence the chemistry of the active site, as well as the coordination of the metal co-factors and secondary structures in the enzyme (53, 106, 328). The insights derived from this structural study can be further investigated by site-directed mutagenesis to validate the specific residues conferring high

133

affinity and oxygen tolerance (328). Altogether, all these will help answer how high-affinity H_2 or CO oxidation takes place and how the enzymes avoid poisoning from O_2.

6.2.2 Integration in aerobic respiratory chain

H_2 oxidation has been demonstrated in chapter 2 to be associated with the aerobic respiratory chain of *M. smegmatis* during persistence, wherein the electrons are transferred from the hydrogenases to the terminal cytochrome oxidases via the menaquinone pool. However, a key inference remains to be biochemically validated: are the presumptive iron-sulfur proteins HucE and HhyE characterized in chapter 3 the actual immediate physiological redox partner of the uptake hydrogenases that facilitate electron transfer to menaquinone? Although it has been shown in this work that these proteins are important for the activity of the hydrogenases and the deletion of *hhyE* results in impaired survival of *M. smegmatis*, we have not established if these putative iron-sulfur proteins directly interact with the hydrogenases to accept electrons. Additionally, the findings fit the possibilities that these proteins could function either as a redox partner for H_2 oxidation or as an assembly protein involved in the maturation of the hydrogenases (230). Future studies should probe into the direct interaction between the putative iron-sulfur proteins and the hydrogenases. The integration of the iron-sulfur proteins with the respiratory chain could also be confirmed by examining if the electrons are transferred from these proteins to the menaquinone pool. Cross-linking mass spectrometry, respirometry assays in mutant backgrounds, and purifying the putative iron-sulfur proteins are the next steps to start teasing out the difference in their function, either as physiological electron acceptors that are integrated into the respiratory chain or maturation proteins. It would also be valuable to look into the function of other hypothetical proteins co-transcribed with *huc* and *hhy*, including the potential iron-sulfur protein HhaA (MSMEG_2717) (190).

Another part of the respiratory chain integration study that still remains unresolved is the nature of the high-MW species of Huc observed in chapter 2. It is unclear what forms this large complex. Is Huc assembled as part of a supercomplex together with other respiratory enzymes

or does it form an oligomer of itself? Forming supercomplexes is typical for many group 3 and 4 [NiFe]-hydrogenases (334, 335), for example the 13-subunit membrane-bound hydrogenase of *Pyrococcus furiosus* and the energy-converting hydrogenase A from *Methanobacterium thermoautotrophicum* (336–338). In contrast, supercomplex formation is not typical of group 1 and 2 [NiFe]-hydrogenases, though this does not rule out such possibility. Though we have demonstrated that Huc activity is coupled to aerobic respiration, future work should next address the nature of the high-MW species of Huc. This can be done by natively purifying the large complex using different chromatographic techniques discussed earlier in section **6.2.1**. The purified Huc can then be biochemically and structurally characterized to help figure out what constitutes the formation of the observed high-MW species. Demonstrating that Huc could exist as part of a larger multi-enzyme respiratory complex, in conjunction with its integration with aerobic respiration, would further enhance our understanding of how hydrogenases work.

Finally, the integration of CO oxidation with the electron transport chain has not been investigated. Respirometry measurements in a recent study shows that, during organic carbon starvation, electrons derived from CO oxidation can be funneled to both terminal oxidases of *M. smegmatis* (168). This already gives an indication of the interaction between CO-dehydrogenase and the respiratory chain. Future studies should then look at how the electrons derived from CO oxidation flow into the respiratory chain. In *O. carboxidovorans*, it has been reported that quinones serve as electron acceptors for the aerobic CO dehydrogenase (42). However, this study was done *in vitro* using purified CO dehydrogenase and quinone solutions which does not necessarily translate to how they physiologically function in whole cells. Moreover, this organism is capable of coupling CO oxidation with carbon fixation and hence the cellular integration of CO dehydrogenase from *O. carboxidovorans* would be different from that in *M. smegmatis*. Physiological investigations in whole cells must therefore be undertaken to know how the electrons from CO oxidation are utilized. For instance: (i) in carboxydovores, are the electrons directly donated to the quinone pool for aerobic respiration during

persistence; and (ii) in carboxydotrophs, if CO oxidation is also integrated to the respiratory chain, how would the electron transfer be deifferentiated for its use between oxidative phosphorylation and carbon fixation? A further question would be, if and how CO dehydrogenase is membrane-localized. Altogether, these will improve our comprehension of how CO dehydrogenase and CO oxidation are integrated to the respiratory chain.

6.2.3 Regulation

Further studies are needed to fully understand the regulation of uptake hydrogenase via catabolite repression in mycobacteria. In chapter 4, we have shown that GylR and glycerol indirectly repress *huc* expression but the key downstream regulator that GylR feeds into remains unresolved. In addition, GylR and glycerol are among many possible regulators and signal molecules that control expression of hydrogenase genes. Given that Huc activity was more pronounced in the stationary phase than in exponential phase when *M. smegmatis* was grown in glucose or acetate, these substrates may also have a role in repressing *huc* expression. Knocking down or out genes involved in the sensing of these organic substrates and looking at the Huc activity profile of these strains will help resolve this problem. The common downstream regulator that GylR, and probably the regulatory proteins for glucose and acetate catabolism, is feeding into could be identified by pulldown assays and comparing the results with proteomics. Our proteomic data have narrowed some possible candidates. Two of these are from the NarL/FixJ family and GntR family. Some regulators from these families have been involved in catabolite repression and expression of hydrogenase in response to oxygen level (75, 245). Studying these candidate regulators will help tease out if they have a role to play in Huc regulation.

With CO dehydrogenase, although we have shown it is regulated in stationary phase during carbon starvation, the regulators and sensors leading to its induction are still unknown. One clue to figuring this out is from a study implicating that mycobacteria can utilize CO dehydrogenase to combat nitrosative stress (339). CO dehydrogenase is reported to have

nitric oxide (NO)-oxidizing activity and that its expression is increased in response to exposure to reactive nitrogen species such as NO (339). Given this, the synthesis of CO dehydrogenase might be induced by a similar signaling cascade that is triggered by NO. In many bacteria and mammalian cells, NO has been shown to regulate the production of a secondary messenger molecule, bis-(3′,5′)-cyclic dimeric guanosine monophosphate (cyclic di-GMP) (340–342). This molecule regulates various cellular functions in bacteria including biofilm formation, motility, and quorum sensing (343–346). In mycobacteria, cyclic di-GMP regulates the expression of genes for lipid transport and metabolism, pathogenicity, dormancy, and long-term survival (347–351). It is plausible that this secondary messenger molecule could be used by mycobacteria to regulate the synthesis of CO dehydrogenase. For this to occur, the production of cyclic di-GMP would most possibly need to be induced by primary signal molecules and regulators. However, it would be unlikely that CO is the primary signal molecule given that the exposure of cultures in 1% CO did not significantly change the expression level of CO dehydrogenase compared to the cultures exposed only in air, and that CO dehydrogenase is upregulated during carbon limitation. Investigating the role of cyclic di-GMP in the expression of *coxLSM* and identifying the involved signals and regulators are the next steps to understanding CO dehydrogenase regulation in mycobacteria.

6.2.4 Implications for the persistence of mycobacterial pathogens

The ability of mycobacteria to persist using trace gases could have important implications on human mycobacterial diseases, particularly during the latent infection. Mycobacteria are notorious for their ability to establish latency during infection (144, 352). As a host defense strategy, macrophages through its heme oxygense-1 generate the toxic gas CO to kill invading pathogens (353). But despite this, mycobacterial pathogens, such *M. tuberculosis*, are able to persist under constant immune attack during latent infection and has been suggested to evade such immune response by sensing host-derived CO or by oxidizing the trace gas (150, 352, 354, 355). With our findings that CO oxidation supports long-term survival of *M. smegmatis*, *M. tuberculosis* could also employ this strategy during its dormancy inside the host. However,

this remains to be determined including if *M. tuberculosis* can oxidize CO at physiologically relevant concentrations and if so, whether it oxidizes CO as part of a broader detoxification strategy or to use it as energy source for persistence.

Another human mycobacterial pathogen that could employ trace gases for persistence is *M. marinum*. This opportunistic pathogen causes granulomatous skin infection and harbors both a group 1h [NiFe]-hydrogenase and a form I CO-dehydrogenase (100, 150, 356). It also has the ability to stay dormant during latent infection as demonstrated in zebrafish (357). Given its genetic capacity for trace gas oxidation and its capability for dormancy, *M. marinum* would have the enzymes to persist inside its host using H_2 and CO. In addition, our work has given insight into how the integration of trace gas oxidation with aerobic respiration may be employed by other mycobacteria to persist during dormancy. However, similar to *M. tuberculosis*, it remains to be resolved if *M. marinum* can oxidize H_2 and CO at concentrations that are physiologically relevant and whether it utilizes these trace gases to persist.

Future studies should examine how the enzymes for trace gas oxidation are utilized by mycobacterial pathogens, particularly to persist during latency. As some physiological characteristics differ between a saprophytic and a pathogenic mycobacteria, experimental data from *M. smegmatis* may not be always applicable for a generalization to *M. tuberculosis* or *M. marinum*; as such, studies directly looking at the pathogens *in vitro* and *in vivo* would be needed. Furthermore, if *M. smegmatis* can have impaired long-term survival without its hydrogenases or CO-dehydrogenase, it is worthwhile to examine this similar phenotype in *M. tuberculosis* or *M. marinum*. This could render the pathogen to be more vulnerable to antimicrobials upon losing its ability for prolonged survival in human host. *In vivo* studies of these pathogens on macrophages or animal models would therefore be crucial to demonstrate this. Collectively, these future endeavors would broaden our understanding of how mycobacterial persistence during latent infection works and how we can better combat mycobacterial diseases.

Appendices

Appendix A. Supplementary information for Chapter 2.

Table S1. Selected proteins identified in Huc and Hhy activity stain bands through mass spectrometry.

Gene ID (GenBank NCBI)	Protein	Log Probability	Number of unique peptides	Coverage (%)
Proteins in the "Huc" band				
4531215	HucL	27.27	6	15.89
4537735	QcrA	234.92	24	58.09
4535113	QcrB	168.88	18	32.97
4534034	QcrC	41.91	4	22.01
4534363	CtaA	7.75	2	4.12
4532360	CtaB	193.51	16	45.75
4535511	CtaC	13.50	1	6.90
Proteins in the "Hhy" band				
4535109	HhyS	25.86	2	8.83
4532665	HhyL	206.78	27	39.46

Table S2. All proteins identified in the high-MW band corresponding to Huc activity through mass spectrometry ([Excel file](#)).

Table S3. All proteins identified in the mid-sized MW band corresponding to Hhy activity through mass spectrometry ([Excel file](#)).

Table S4. Bacterial strains and plasmids used in this study.

Strain	Description	Source or reference
mc^{2}155	*Mycobacterium smegmatis* wild type strain	(212)
Huc-StrepII	mc^{2}155 with StrepII tag inserted at the C-terminus of MSMEG_2262 (*hucS-StrepII-hucL*)	This study
Hhy-StrepII	mc^{2}155 with StrepII tag inserted at the C-terminus of MSMEG_2720 (*hhyS-StrepII-hhyL*)	This study
Huc-only	mc^{2}155 with markerless deletions of MSMEG_2719, MSMEG_3931 (Δ*hhyL*Δ*hyhS*)	(83)
Hhy-only	mc^{2}155 with markerless deletions of MSMEG_2262, MSMEG_3931 Δ*hucS*Δ*hyhS*)	(83)
No Huc/Hhy	mc^{2}155 with markerless deletions of MSMEG_2262, MSMEG_2719, MSMEG_3931 (Δ*HucS*Δ*HhyL*Δ*hyhS*)	(83)

cyt *bcc-aa₃* -only	mc²155 with markerless deletions of cytochrome *bd* subunits (Δ*cydAB*)	(213)
cyt *bd*-only	mc²155 with markerless deletions of cytochrome *bcc-aa₃* subunits (Δ*qcrCAB*)	Gregory M. Cook (Otago University, NZ)
TOP10	*Escherichia coli* strain F- *mcrA* Δ(*mrr-hsd*RMS-*mcr*BC) Φ80*lacZ*ΔM15 Δ *lac*X74 *rec*A1 *ara*D139 Δ(*araleu*)7697 *gal*U *gal*K *rps*L (StrR) *end*A1 *nup*G	ThermoFischer

Plasmid	Description	Source or reference
pX33	Gmʳ, *sacB*, mycobacterial Ts *ori*, p15A *ori*, *xylE*	(210)
pHuc_StrepII	2656 bp *hucS₋StrepII-hucL* fragment in pX33	This study
pHhy_StrepII	3000 bp *hhyS₋StrepII-hhyL* fragment in pX33	This study

Table S5. List of primers used in this work.

Purpose	Primer name	Sequence (5' to 3')
Construction of pHuc_StrepII	HucF (*Spe*I restriction site)	AAA<u>ACTAGT</u>ATGGCATCGGTGCTTTGGTTC
	HucR (*Spe*I restriction site)	AAA<u>ACTAGT</u>TCACACCATCCCGTTGATCAC
Construction of pHhy_StrepII	HhyF (*Spe*I restriction site)	AAA<u>ACTAGT</u>ATGCCAACGGAGGCTGCAGT
	HhyR (*Spe*I restriction site)	AAA<u>ACTAGT</u>TCAGTCCCCGGTCGCGGA
Sequencing of constructs to verify cloning of insert	T7F	TAATACGACTCACTATAGGG
	pX33_SpeIR	AATAGATCATCGTCGCCG
	HucInt1	TACATGGGTCTGGCGGCGG
	HucInt2	CCAGGGCGTGGGCAACTAC
	HhyInt1	CACGGTGGCGGCATCGCG
	HhyInt2	GCTGGGGTGCTGGGGTTC
Screening of Huc-StrepII and Hhy-StrepII insertion mutants	Huc_chromF	AATCCGGCAGCAGCCCTG
	Huc_chromR	GACCGACCCCGTCGTCAC
	Hhy_chromF	GCGTCTTCACTCGGGACG
	Hhy_chromR	GTCAACGGGAACGTCGGC
	StrepR	GAACTGCGGGTGCGACCA
qRT-PCR of *hucL* (MSMEG_2263)	q2263F	ACCCTGATCCGCAACATCTG
	q2263R	GTCGTTCCAATGCTCCAGGA
qRT-PCR of *hhyL* (MSMEG_2719)	q2719F	AATCAGCACACCAACCCCAA
	q2719R	CCTCGAACTTCTCCCACGTC
	qsigAF	CTCAACGCCGAAGAAGAGGT

qRT-PCR of *sigA* (MSMEG_2758)	qsigAR	GCCCTTGGTGTAGTCGAACT
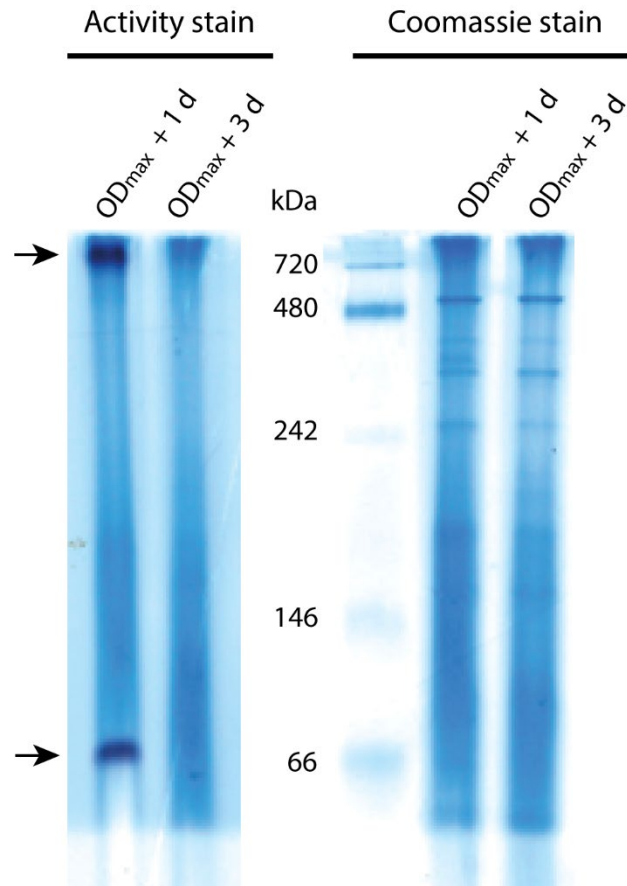
Figure S1. Hydrogenase activity staining in blue native PAGE. Differential native activity staining (left panel) of hydrogenases using whole-cell lysates of *M. smegmatis* WT strain harvested at either 1-d post-OD max (for Huc staining) or 3-d post-OD max (for Hhy staining). At 1-d post-OD max, the two bands (pointed by arrows) correspond to Huc activity. Both the high molecular weight (>700 kDa) and low molecular weight (>66 kDa) species are consistent with the bands seen in **Figure 2.2a**. No band corresponding to Hhy activity is observed in this blue native PAGE. The corresponding Coomassie stains of the total protein are shown at the right panel.
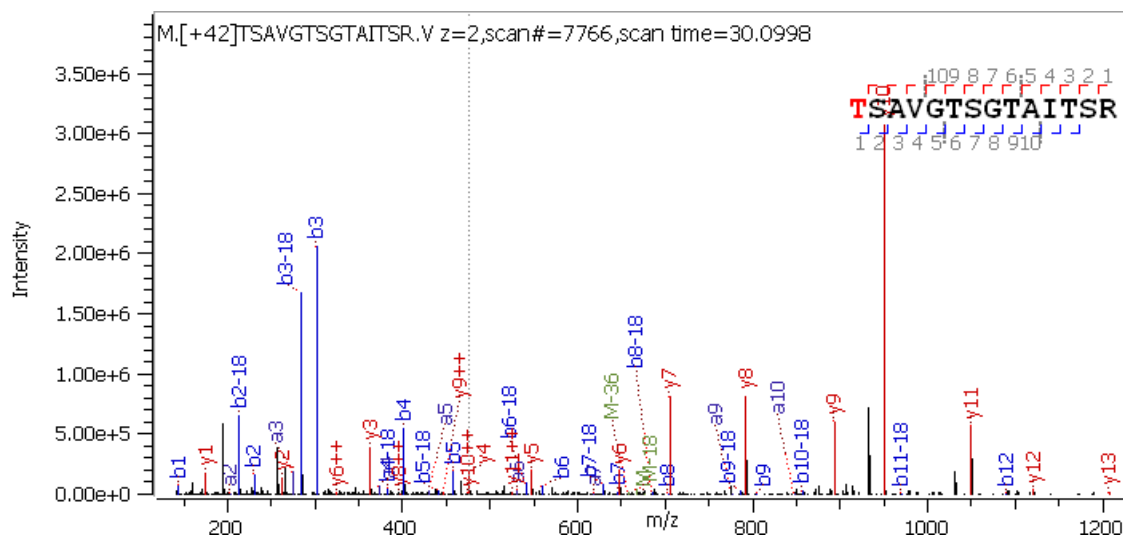
Figure S2. Spectrum of peptide sequence TSAVGTSGTAITSR at charge state of 2 from protein cytochrome C oxidase subunit 3 (CtaC) (Gene ID:4535511). The annotated b ions are shown in blue and the annotated y ions in red; x axis is the relative intensity and y axis is mass to charge (m/z) ratio; [+42] indicates protein N terminus is acetylated.

Appendix B. Supplementary information for Chapter 3.

Table S6. Bacterial strains and plasmids used in this study.

Strain	Description	Reference
mc²155	Electrocompetent, wild-type strain of *Mycobacterium smegmatis*	(212)
Δ*hucE*	mc²155 with markerless deletion of MSMEG_2268	This study
Δ*hhyE*	mc²155 with markerless deletion of MSMEG_2718	This study
Δ*hucE*Δ*hhyE*	mc²155 with markerless deletions of MSMEG_2268 and MSMEG_2718	This study
Δ*hucS*	mc²155 with markerless deletion of MSMEG_2262	(83)
Δ*hhyL*	mc²155 with markerless deletion of MSMEG_2719	(36)
Δ*hucS*Δ*hhyL*	mc²155 with markerless deletions of MSMEG_2262 and MSMEG_2719	(83)
DH5α	Chemically competent, wild-type strain of *Escherichia coli* F⁻ *endA1 glnV44 thi-1 recA1 relA1 gyrA96 deoR nupG purB20* φ80d*lacZ*ΔM15 Δ(*lacZYA-argF*)U169 *hsdR17*(rK⁻mK⁺) λ⁻	Thermo Fisher
TOP10	Chemically competent, wild-type strain of *E. coli* F⁻ *mcr*A Δ(*mrr-hsd*RMS-*mcr*BC) φ80*lacZ*ΔM15 Δ*lac*X74 *rec*A1 *ara*D139 Δ(*ara-leu*)7697 *gal*U *gal*K λ⁻ *rps*L(Str^R) *end*A1 *nup*G	Thermo Fisher

Plasmid	Description	Reference
pX33	Gm^r, *sacB*, mycobacterial Ts ori, p15A ori, *xylE*	(210)
pX33-*hucE*	pX33 harbouring the MSMEG_2268 deletion construct	This study
pX33-*hhyE*	pX33 harbouring the MSMEG_2718 deletion construct	This study
pMV261	Kan^r, mycobacterial oriM, pBR322 ori, P*hsp60* promoter	(225)
pMV*hucE*	pMV261 harbouring MSMEG_2268 gene insert	This study
pMV*hhyE*	pMV261 harbouring MSMEG_2718 gene insert	This study

Table S7. Primers used in this study.

Primer	Sequence (5' to 3')	Enzyme
del2268_fwd	aaa<u>ACTAGT</u>GTGTCAGGTTCGCATCGAC	*Spe*I
del2268_rvs	aaa<u>ACTAGT</u>TCACAACCGATCACGACCG	*Spe*I
2267_chrom_fwd	AGACCCTGTGCACGCGATC	
2269_chrom_rvs	CGGCGACCGCGTCGGAC	
del2718_fwd	aaa<u>ACTAGT</u>ATGACCACCACAGCTCCCAA	*Spe*I
del2718_rvs	aaa<u>ACTAGT</u>TCATGGGATGTCCTCCCGC	*Spe*I
2717_chrom_fwd	GCAGCGTCCTTCACGGA	

2719_chrom_rvs	GGTAACCCTCGTAGAGCA	
Pstl-2268_for	atacat<u>CTGCAG</u>AAATGACCGCGGCGGTCGAG	*Pst*I
HindIII-2268_rev	atacat<u>AAGCTT</u>CTCATCCGGTGACCCGCAC	*Hind*III
BamHI-2718_for	atacat<u>GGATCC</u>AATGGCGCCCGCCGTCACG	*BamH*I
HindIII-2718_rev	atacat<u>AAGCTT</u>CTCACGGTCCGGCCCCACC	*Hind*III
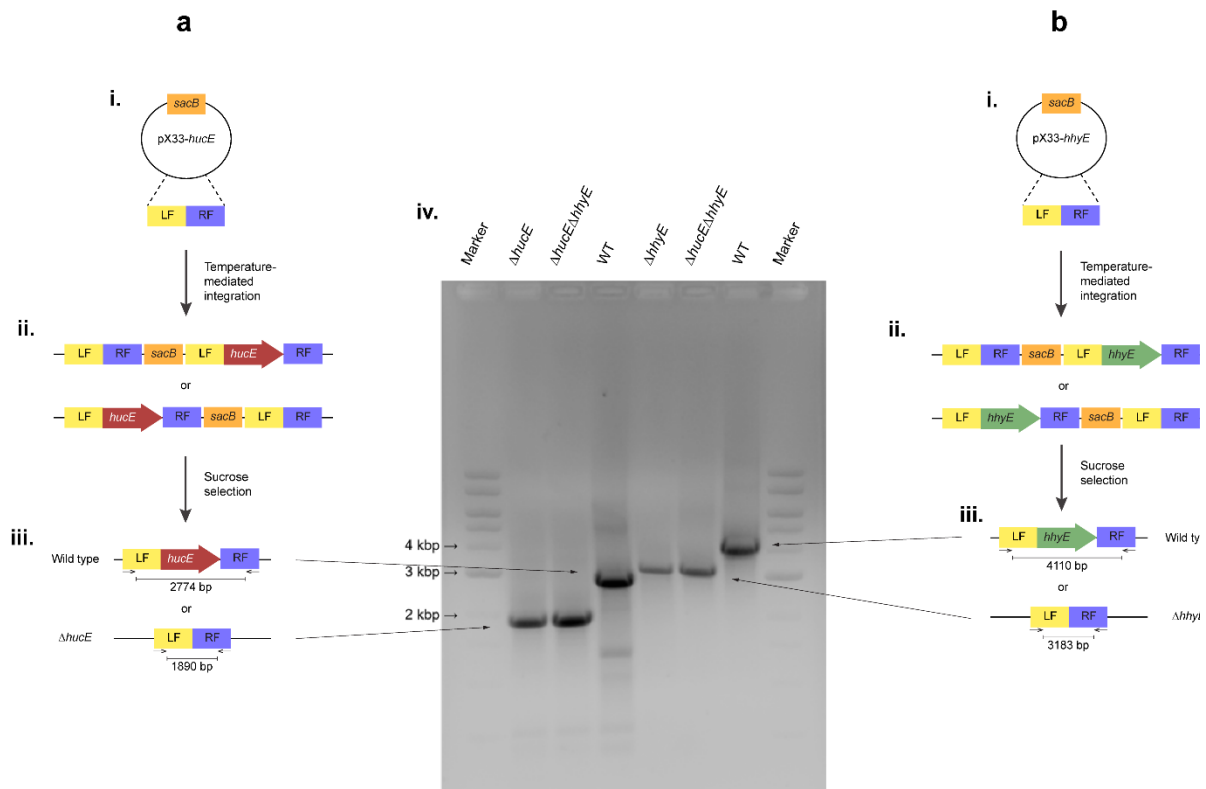
Figure S3. Deletion of the hucE and hhyE genes in *Mycobacterium smegmatis*. The schematic shows the four main steps that led to the production of knockouts of (a) *hucE* (MSMEG_2268) and (b) *hhyE* (MSMEG_2718). **(i)** Construction of the pX33-*hucE* / pX33- *hhyE* vectors containing a fused left flank (LF) and right flank (RF) of each gene. **(ii)** Temperature-mediated integration of the vector into the *M. smegmatis* chromosome via either the left flank or right flank of the chromosomal *hucE* / *hhyE* genes. **(iii)** Chromosomal excision of the vector due to sacB-mediated sucrose toxicity to either wild-type revertants or Δ*hucE* / Δ*hhyE* mutants. **(iv)** PCR-based screening through primers (2267_chrom_fwd, 2269_chrom_rvs, 2717_chrom_fwd, and 2719_chrom_rvs) targeting the flanks to confirm whether colonies are (a) wild-type revertant

(2774 bp product) or Δ*hucE* mutant (1890 bp product) and (b) wild-type revertant (4110 bp product) or Δ*hhyE* mutant (3183 bp product). Both primer sets were used to confirm the double mutant.
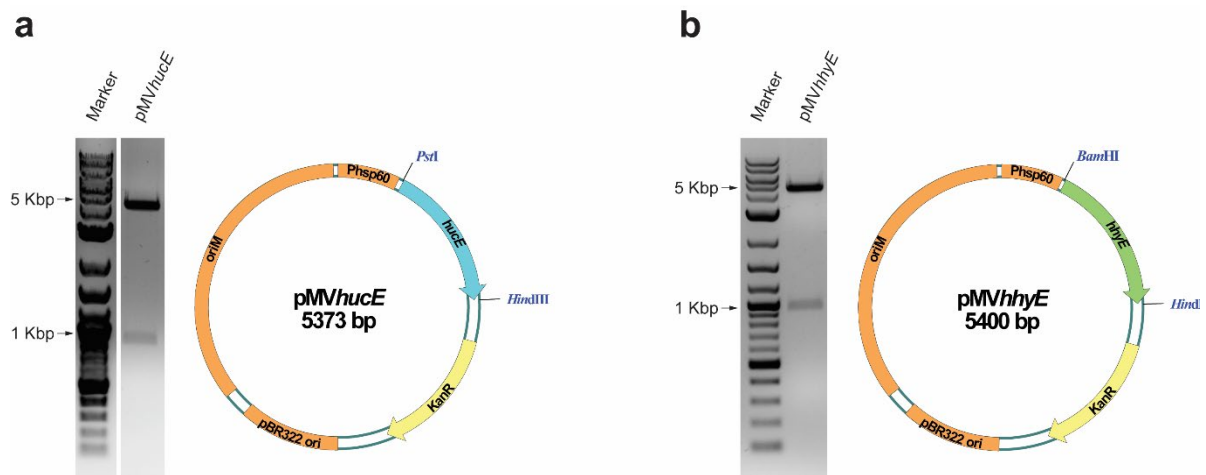
Figure S4 Construction of complementation vectors. a) pMV*hucE* digested with *Pst*I and *Hind*III (left side) produced two fragments (893 bp and 4480 bp) consistent with *hucE* insertion to the plasmid. Map of the plasmid is shown on the right side. **b)** pMV*hhyE* digested with *BamH*I and *Hind*III produced two fragments (932 bp and 4468 bp) consistent with *hhyE* insertion to the plasmid. Map of the plasmid is shown on the right side. The plasmids have an Escherichia coli pBR322 origin of replication, a mycobacterial OriM derived from pAL5000, a kanamycin resistance cassette (KanR), and a promoter P$_{hsp60}$.
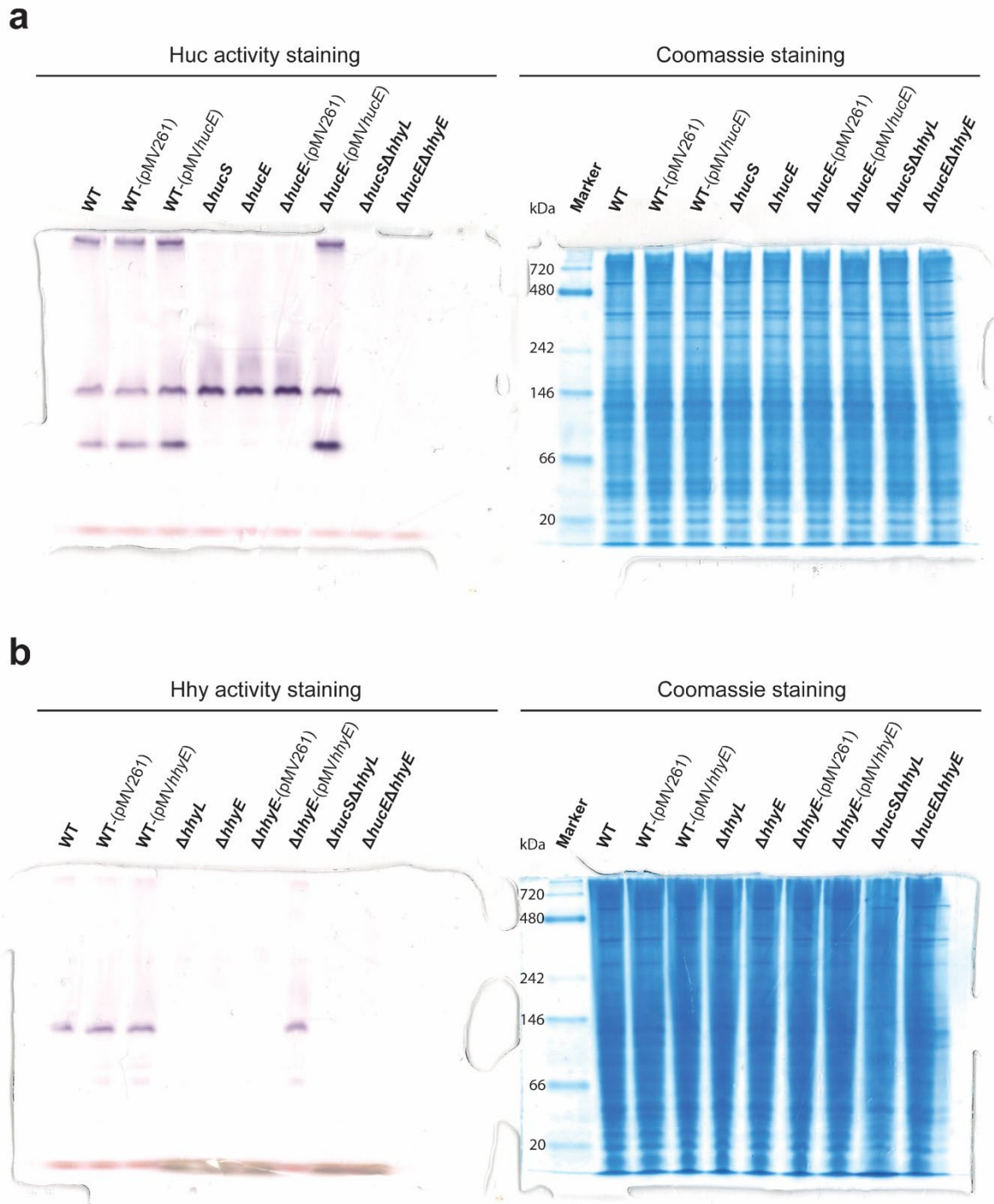
Figure S5 Original native polyacrylamide gels showing staining of hydrogenase activity.
a) Huc activity and **b)** Hhy activity. The left gels show hydrogenase activity stained with the artificial electron acceptor nitroblue tetrazolium in a H_2-rich atmosphere. The right gels show protein marker and total protein stained with Coomassie Blue.

146
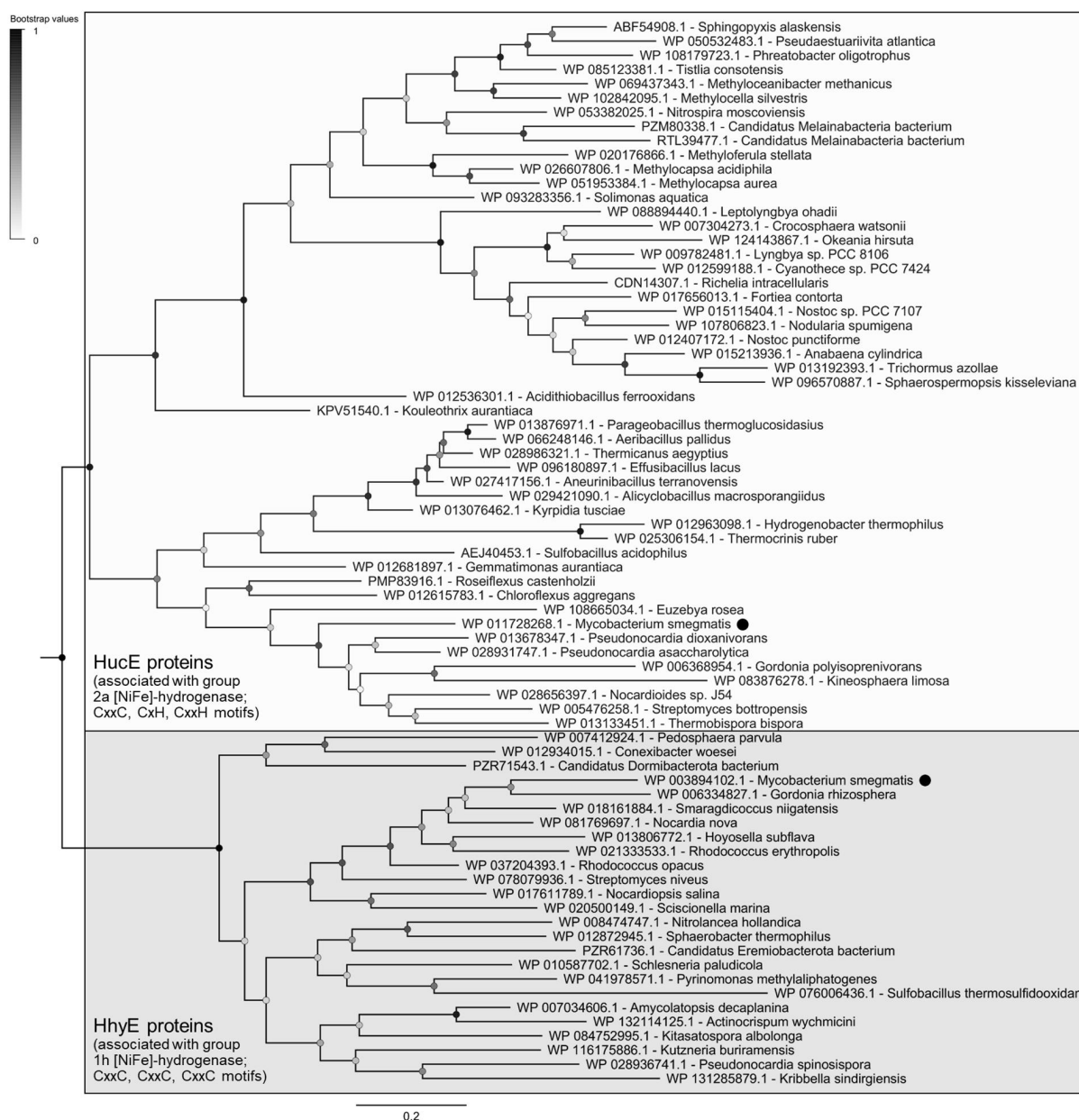
Figure S6. Phylogenetic tree of HucE and HhyE proteins associated with group 2a and 1h [NiFe]-hydrogenases. The tree visualizes the evolutionary relationships between a representative subset of 52 full-length HucE and 26 full-length HhyE sequences. The proteins encoded by *Mycobacterium smegmatis* are emphasized. The tree was constructed using the maximum-likelihood method (gaps treated with partial deletion), bootstrapped with 100 replicates, and rooted at the mid-point. Phylogenetic analysis was done by Zahra Islam.

Appendix C. Supplementary information for Chapter 4.

Table S8. Bacterial strains and plasmids used in this study.

Strain	Description	Reference
mc^{2}155	*Mycobacterium smegmatis* wild type strain; *ept-1*, efficient plasmid transformation mutant of mc^{2}6	Snapper et al., 1990
gylR mutant	mc^{2}155 with frameshift mutation in *gylR* (MSMEG_6757)	This study
gylR knockdown	mc^{2}155 with pLJR962_KDgylR	This study
DH5α	*Escherichia coli* F$^-$ φ80*lacZ*ΔM15 Δ(*lacZYA-arg*F)U169 *rec*A1 *end*A1 *hsd*R17(r$_K^-$, m$_K^+$) *pho*A *sup*E44 λ$^-$ *thi*-1 *gyr*A96 *rel*A1	Thermo Fischer

Plasmids	Description	Reference
pLJR962	Sth1 *dCas9*; Sth1 sgRNA scaffold; Tet repressor; L5-integrating backbone; ColE1 ori (*E. coli*); Kan^r	Rock et al., 2017
pLJR962_KDgylR	pLJR962 with sgRNA targeting *gylR* for repression	This study

Table S9. Primers used in this study.

Primers	Sequence (5' to 3')	Purpose
msmeg6757_KD1_fwd	GGGAATCCAGTTGGGTCGAACCGAG	sgRNA targeting *gylR* repression
msmeg6757_KD1_rev	AAACCTCGGTTCGACCCAACTGGAT	
pljr962_multi_SapI_fwd	GCTCTTCAGGATCTGACCAGGGAAAATAGCCCTC	Screening of strains harboring pLJR962_KDgylR
pljr962_multi_SapI_rev	GCTCTTCACTGAAAAAAATAAAAAAGGGGACCTCTA	
hucp_fw	CGACCAGACGCGCGGCCTC	Amplification of *huc* promoter for EMSA
hucp_rev	GACCGGCGAGATGTCTGGAAGTTC	
glpp_fw	GTAGCTGCAGTATCGCCGCGG	Amplification of *glpFKD* promoter for EMSA
glpp_rev	CACCCCGAACAGGATGAGGATGC	

Table S10. Relative intensities* of the Huc activity stain bands.

Different aTc concentration	Area	Percent	Relative intensity
WT	1903.1	1.2	1.0
gylR knockdown – 50 ng/mL	19003.8	12.1	10.0
gylR knockdown – 100 ng/mL	26336.3	16.8	13.8

gylR knockdown – 300 ng/mL	31104.6	19.8	16.3
gylR knockdown – 500 ng/mL	38111.5	24.3	20.0
gylR mutant	40579.7	25.8	21.3

Different OD - glycerol	Area	Percent	Relative intensity
WT OD 0.8	61.4	0.0	0.04
WT OD 1.5	478.3	0.3	0.28
WT ODmax	841.1	0.5	0.49
WT ODmax + 1d	1725.4	1.1	1.00
gylR mutant OD 0.8	15794.6	10.2	9.15
gylR mutant OD 1.5	18043.3	11.7	10.45
gylR mutant ODmax	23669.1	15.3	13.71
gylR mutant ODmax + 1d	25609.5	16.6	14.84
gylR knockdown OD 0.8	15369.2	9.9	8.91
gylR knockdown OD 1.5	19367.4	12.5	11.22
gylR knockdown ODmax	18423.7	11.9	10.67
gylR knockdown ODmax + 1d	15274.0	9.9	8.85

Different organic substrates	Area	Percent	Relative intensity
Gluc WT expo	5400.7	3.3	2.8
Gluc WT stat	18287.8	11.2	9.3
Succ WT expo	5645.9	3.5	2.9
Succ WT stat	5514.9	3.4	2.8
Acet WT expo	7914.6	4.8	4.0
Acet WT stat	16793.4	10.3	8.6
Gluc *gylR* mutant expo	19346.5	11.8	9.9
Gluc *gylR* mutant stat	7263.2	4.4	3.7
Succ *gylR* mutantstat	7916.3	4.8	4.0
Succ *gylR* mutant expo	1956.0	1.2	1.0
Acet *gylR* mutant expo	7333.8	4.5	3.7
Acet *gylR* mutant stat	16102.5	9.9	8.2
Gluc *gylR* knockdown expo	6079.0	3.7	3.1
Gluc *gylR* knockdown stat	11745.2	7.2	6.0
Succ *gylR* knockdown expo	4910.7	3.0	2.5
Succ *gylR* knockdown stat	4843.1	3.0	2.5
Acet *gylR* knockdown expo	5209.3	3.2	2.7
Acet *gylR* knockdown stat	11028.3	6.8	5.6

* Relative intensities of the band stains were analyzed using ImageJ (NIH, USA).
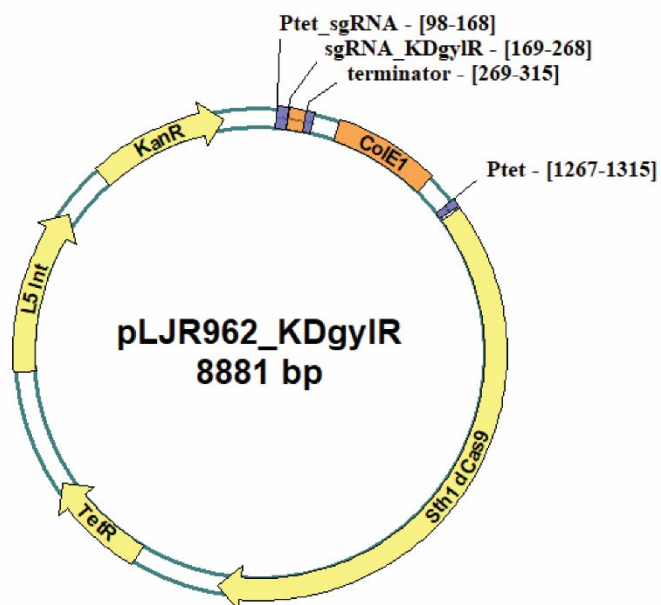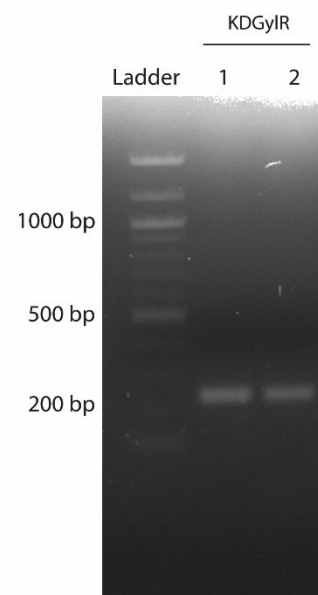
Figure S7. Plasmid and screening of *M. smegmatis gylR* knockdown strain. a) Plasmid construct for CRISPR interference of *gylR* . pLJR962_KDgylR contains Sth1 *dCas9* and *gylR*-targeting sgRNA scaffold (aTc-inducible), Tet repressor; L5-integrating backbone; ColE1 ori (*E. coli*); Kanamycin resistance cassette. **b)** PCR screening of *M. smegmatis* isolates (*gylR* knockdown 1 and 2) harboring pLJR962_KDgylR (amplicon size = 240 bp).

Appendix D. Supplementary information for Chapter 5.

Table S11. List of genera known to oxidize CO. The primary literature referenced was used to determine whether each genus has been reported to oxidize CO, grow chemolithoautotrophically on CO (column 3), or oxidize CO at atmospheric concentrations (column 4). Also listed is the phylogenetic clade that the CoxL sequences are affiliated with (column 6) based on the phylogenetic trees shown in **Figure 5.4a** and **Supplementary Figure S9.** Note that all taxonomic assignments are based on the genome taxonomy database (358) and hence may differ from those historically reported. In this regard, the carboxydotroph [*Streptomyces*] *thermautotrophicus* is now recognized as a distinct genus from *Streptomyces* and the former class Betaproteobacteria is now the order Betaproteobacteriales in the class Gammaproteobacteria.

Class (Phylum)	Genus	Growth on CO?	Ambient uptake?	Reference	Enzyme clade
Actinobacteria (Actinobacteriota)	[*Streptomyces*]	+	+	(262, 263)	Mixed 2
	Mycobacterium	?	+	(150, 151)	Actinobacterial
	Rhodococcus	?	?	(90, 272, 273)	Actinobacterial
Alphaproteobacteria (Proteobacteria)	*Oligotropha*	+	-	(43, 267)	Proteobacterial
	Bradyrhizobium	+/-	+	(126, 258, 259, 267)	Proteobacterial
	Carbophilus	+	?	(258)	Unsequenced
	Ruegeria	-	+	(47, 126, 127)	Proteobacterial
	Labrenzia	-	+	(46, 126)	Proteobacterial
	Mesorhizobium	-	+	(126)	Proteobacterial
	Aminobacter	-	+	(126)	Proteobacterial
	Roseobacter	-	?	(127)	Proteobacterial
	Roseovarius	-	?	(127)	Proteobacterial
	Dinoroseobacter	-	?	(127)	Proteobacterial
Bacilli (Firmicutes)	*Hydrogenibacillus*	+	-	(264)	Mixed 1
	Alicyclobacillus	?	?	(274)	Mixed 1
	Brevibacillus	?	?	(274)	Mixed 1
	Geobacillus	?	?	(274)	Mixed 1
	Anoxybacillus	?	?	(274)	Unsequenced
Chloroflexia (Chloroflexota)	*Thermomicrobium*	-	+	(33, 275, 276)	Mixed 1
	Sphaerobacter	?	?	(274)	Mixed 1
Deinococci (Deinococcota)	*Meiothermus*	?	?	(274)	Mixed 1
	Thermus	?	?	(274)	Mixed 1

Gammaproteobacteria (Proteobacteria)	*Hydrogenophaga*	+	-	(43, 44, 258, 267)	Proteobacterial
	Zavarzinia	+	?	(258, 261)	Proteobacterial
	Alkalispirillum	+	?	(260)	Proteobacterial
	Xanthomonas	+/-	+	(126)	Unsequenced
	Alkalilimnicola	+/-	+	(260, 268, 271)	Proteobacterial
	Burkholderia	-	+	(126, 269, 270)	Proteobacterial
	Paraburkholderia	-	+	(270)	Proteobacterial
	Stenotrophomonas	-	?	(126)	Unsequenced
Ktedonobacteria (Chloroflexota)	*Thermogemmatispora*	-	+	(33, 277)	Mixed 1
Halobacteria (Halobacterota)	*Halorubrum*	?	+	(271, 280)	Halobacterial
	Haloferax	?	+	(280)	Halobacterial
	Haloterrigena	?	+	(280)	Halobacterial
	Haloarcula	?	?	(280)	Halobacterial
	Natronorubrum	?	+	(271, 280)	Halobacterial
Thermoprotei (Crenarchaeota)	*Sulfolobus*	?	?	(279)	Mixed 1
	Aeropyrum	?	?	(278)	Mixed 1

Table S12. Summary of proteome data ([Excel file](#)). Results are shown for a shotgun proteomic experiment that compared relative protein content of three carbon-replete (mid-exponential phase) and three carbon-limited (mid-stationary phase) cultures of *Mycobacterium smegmatis*.

Table S13. List of carbon monoxide dehydrogenase sequences retrieved in this work ([Excel file](#)). A total of 709 sequences were retrieved of the form I CO dehydrogenase catalytic subunit (CoxL). Results are provided in table and FASTA format.

Table S14. Comparison of four methods to determine apparent kinetic parameters for CO oxidation for whole cells of *Mycobacterium smegmatis*.

Method	$V_{max\ app}$ CO (nmol min g_{dw}^{-1})	$K_{m\ app}$ CO (nM)
Nonlinear regression	3.13	209
Lineweaver-Burk plot	2.97	310
Hanes-Woolf plot	3.08	339
Eadie-Hofstee plot	2.90	291
Average	3.02	323

Table S15. Details of the metagenome and metatranscriptome samples analyzed in this work ([Excel file](#)).

Table S16. Relative abundance of carbon monoxide dehydrogenase and hydrogenase sequences in the analyzed metagenome and metatranscriptome datasets ([Excel file](#)). The relative abundance of CO dehydrogenase large subunit gene is shown by clade. The relative abundance of the hydrogenase large subunit genes, divided by subgroup, is also shown for comparison.

Table S17. List of bacterial strains and plasmids used in this work.

Name	Description	Reference
Mycobacterium smegmatis		
mc²155	*ept-1*, efficient plasmid transformation mutant of mc²6	(212)
Δ*coxL*	mc²155 with markerless deletion in *coxL* gene (MSMEG_0746)	This work
Escherichia coli		
TOP10	F- *mcrA* Δ(*mrr-hsd*RMS-*mcr*BC) Φ80*lacZ*ΔM15 Δ *lac*X74 *rec*A1 *ara*D139 Δ(*ara*leu)7697 *gal*U *gal*K *rps*L (StrR) *end*A1 *nup*G	Thermo Fisher
Plasmids		
pX33	Gm^r, *sacB*, mycobacterial Ts *ori*, p15A *ori*, *xylE*	(210)
pX33_coxL	2245 bp fragment of left and right flanks of *coxL* gene (MSMEG_0746) in pX33	This work

Table S18. List of primers used in this work.

Purpose	Primer name	Sequence	Tm (°C)
Sequencing of pX33_coxL to verify cloning of insert	Forward	TAATACGACTCACTATAGGG	52.0
	Reverse	AATAGATCATCGTCGCCG	51.9
Screening of Δ*coxL* (MSMEG_0746) mutant	Forward	CTGCCTATTGACGCTCGCG	58.9
	Reverse	ACCACATCGTCGACACCGC	60.4
qRT-PCR of *coxL* gene (MSMEG_0746)	Forward	CGTGGTGGTCAAACAGGAGA	57.2
	Reverse	GATCTCGCCGACCATGATGT	57.1
qRT-PCR of *sigA* gene (MSMEG_2758)	Forward	CTCAACGCCGAAGAAGAGGT	57.2
	Reverse	GCCCTTGGTGTAGTCGAACT	57.0
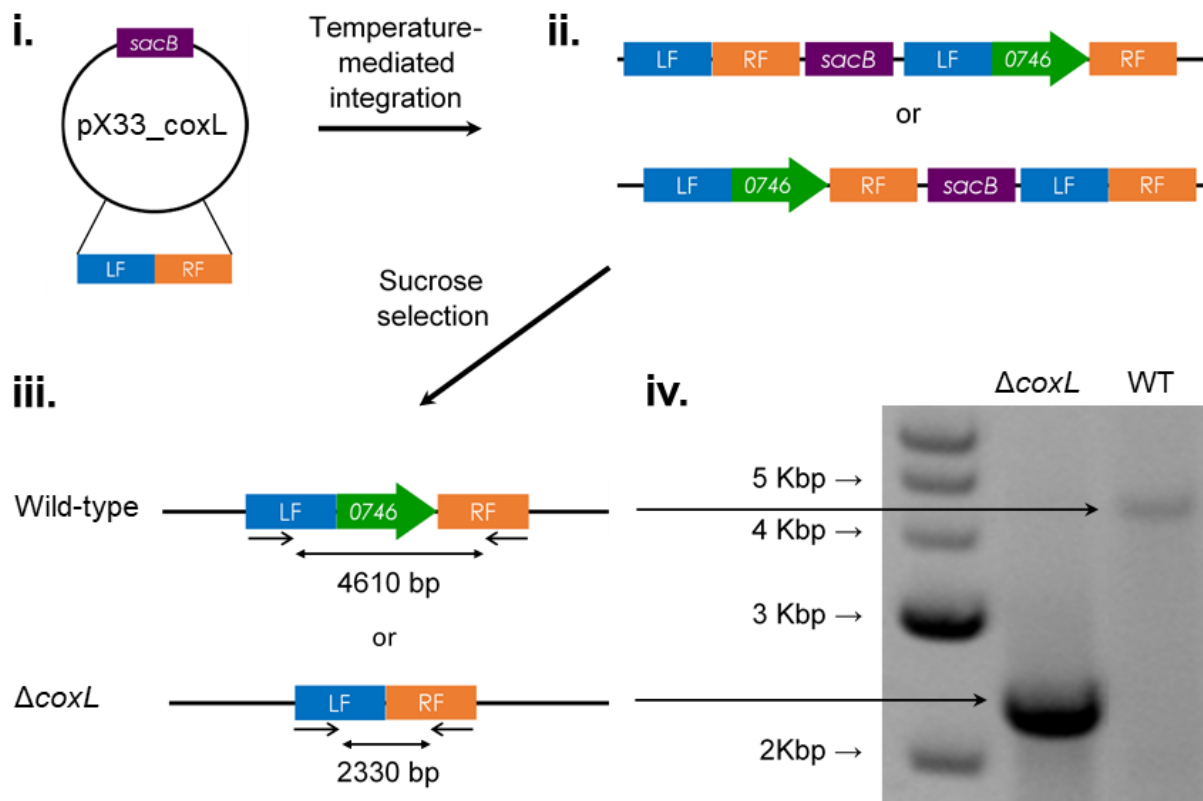
Figure S8. Deletion of the *coxL* gene in *Mycobacterium smegmatis*. The schematic shows the four main steps that led to the production of a knockout of the *coxL* gene (MSMEG_0746). (**i**) Construction of the pX33_coxL vector containing a fused left flank (LF) and right flank (RF) of the *coxL* gene. (**ii**) Temperature-mediated integration of the vector into the *M. smegmatis* chromosome via either the left flank or right flank of the chromosomal *coxL* gene. (**iii**) Chromosomal excision of the vector due to *sacB*-mediated sucrose toxicity to either wild-type revertants or Δ*coxL* mutants. (**iv**) PCR-based screening through primers targeting the flanks to confirm whether colonies are wild-type revertants (4610 bp product) or Δ*coxL* mutants (2330 bp product).

Figure S9 (tif). Neighbor-joining phylogenetic tree showing the evolutionary history of the catalytic subunit of the form I carbon monoxide dehydrogenase (CoxL). Evolutionary distances were computed using the Poisson correction model, gaps were treated by partial deletion, and the tree was bootstrapped with 500 replicates. The tree was constructed using all 709 CoxL sequences retrieved in this study as shown in **Supplementary Table S13**. The tree is divided into five clades as per the maximum-likelihood tree (**Figure 5.4a**): Proteobacterial Clade (**a**), Mixed Clade 1 (**b**), Halobacterial Clade (**c**), Mixed Clade 2 (**d**), and

Actinobacterial Clade (**e**). The tree was rooted with five form II CO dehydrogenase sequences (not shown). As the figure is too large to be embedded, it should be directly downloaded as a .tif file.
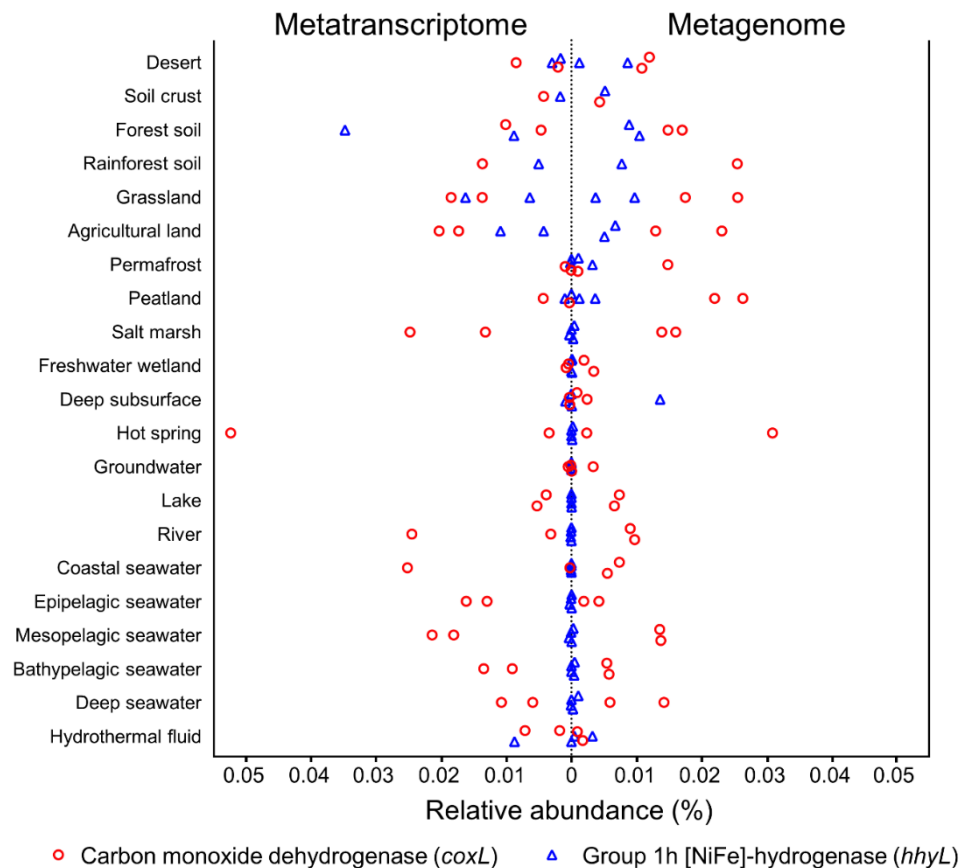
Figure S10. Mirror diagram showing the abundance of genes and transcripts encoding the carbon monoxide dehydrogenase large subunit (*coxL*) by ecosystem type. In total, 40 pairs of metagenomes and metatranscriptomes (20 aquatic, 20 terrestrial) were analyzed from a wide range of biomes (detailed in **Supplementary Table S15**). The abundance of *hhyL* genes and transcripts, encoding the high-affinity group 1h [NiFe]-hydrogenase, are shown for comparison.
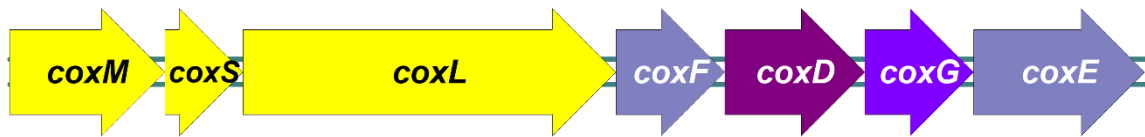
Figure S11. Organization of genes associated with CO dehydrogenase of *Mycobacterium smegmatis*. Genes encode the medium, small, and large structural subunits (*coxMSL*); proteins that are homologous to those in *O. carboxidovorans* including an ATPase (*coxD*); maturation proteins (*coxE* and *coxF*); membrane anchor (*coxG*) (292, 359, 360).

References

1. Mason, A. S. (1977) Atmospheric HT and HTO: 4. Estimation of atmospheric hydrogen residence time from interhemispheric tritium gas transport. *J. Geophys. Res.* **82**, 5913–5916

2. Liu, S. C., and Donahue, T. M. (1974) The aeronomy of hydrogen in the atmosphere of the Earth. *J. Atmos. Sci.* **31**, 1118–1136

3. Hunten, D. M., and Strobel, D. F. (1974) Production and escape of terrestrial hydrogen. *J. Atmos. Sci.* **31**, 1–8

4. Novelli, P. C., Lang, P. M., Masarie, K. A., Hurst, D. F., Myers, R., and Elkins, J. W. (1999) Molecular hydrogen in the troposphere: Global distribution and budget. *J. Geophys. Res.* **104**, 427–430

5. Rhee, T. S., Brenninkmeijer, C. A. M., and Rockmann, T. (2006) The overwhelming role of soils in the global atmospheric hydrogen cycle. *Atmos. Chem. Phys.* **6**, 1611–1625

6. Ehhalt, D. H., and Rohrer, F. (2009) The tropospheric cycle of H2: A critical review. *Tellus, Ser. B Chem. Phys. Meteorol.* **61**, 500–535

7. Constant, P., Poissant, L., and Villemur, R. (2009) Tropospheric H_2 budget and the response of its soil uptake under the changing environment. *Sci. Total Environ.* **407**, 1809–1823

8. Greening, C., Constant, P., Hards, K., Morales, S. E., Oakeshott, J. G., Russell, R. J., Taylor, M. C., Berney, M., Conrad, R., and Cook, G. M. (2015) Atmospheric hydrogen scavenging: From enzymes to ecosystems. *Appl. Environ. Microbiol.* **81**, 1190–1199

9. Conrad, R., and Seiler, W. (1981) Decomposition of atmospheric hydrogen by soil microorganisms and soil enzymes. *Soil Biol. Biochem.* **13**, 43–49

10. Constant, P., Poissant, L., and Villemur, R. (2008) Isolation of *Streptomyces* sp. PCB7, the first microorganism demonstrating high-affinity uptake of tropospheric H_2. *ISME J.* **2**, 1066–1076

11. Greening, C., Berney, M., Hards, K., Cook, G. M., and Conrad, R. (2014) A soil actinobacterium scavenges atmospheric H_2 using two membrane-associated, oxygen-dependent [NiFe] hydrogenases. *Proc. Natl. Acad. Sci.* **111**, 4257–4261

12. Meredith, L. K., Rao, D., Bosak, T., Klepac-Ceraj, V., Tada, K. R., Hansel, C. M., Ono, S., and Prinn, R. G. (2014) Consumption of atmospheric hydrogen during the life cycle of soil-dwelling actinobacteria. *Environ. Microbiol. Rep.* **6**, 226–238

13. Khalil, M. A. ., and Rasmussen, R. A. (1990) The global cycle of carbon monoxide: Trends and mass balance. *Chemosphere.* **20**, 227–242

14. Logan, J. A., Prather, M. J., Wofsy, S. C., and Mcelroy, M. B. (1981) Tropospheric

chemistry: A global perspective. **86**, 7210–7254

15. Fishman, J., and Crutzen, P. J. (1978) The origin of ozone in the troposphere. *Nature*. **274**, 855–858

16. Zheng, B., Chevallier, F., Yin, Y., Ciais, P., Fortems-Cheiney, A., Deeter, M. N., Parker, R. J., Wang, Y., Worden, H. M., and Zhao, Y. (2019) Global atmospheric carbon monoxide budget inferred from multi-species atmospheric inversions. *Earth Syst. Sci. Data*. **1**, 1–42

17. Feilberg, K. L., Sellåg, S. R., Nielsen, C. J., Griffith, D. W. T., and Johnson, M. S. (2002) CO + OH → CO 2 + H: The relative reaction rate of five CO isotopologues. *Phys. Chem. Chem. Phys.* **4**, 4687–4693

18. Lu, Y., and Khalil, M. A. K. (1993) Ethane and carbon monoxide in oh chemistry: the effects of feedbacks and reservoirs generated by the reactive products. *Chemosphere*. **26**, 641–655

19. King, G. M., and Weber, C. F. (2007) Distribution, diversity and ecology of aerobic CO-oxidizing bacteria. *Nat. Rev. Microbiol.* **5**, 107–118

20. Seiler, W. (1974) The cycle of atmospheric CO. *Tellus*. **26**, 116–135

21. Conrad, R. (1996) Soil microorganisms as controllers of atmospheric trace gases (H_2, CO, CH_4, OCS, N_2O, and NO). *Microbiol. Rev.* **60**, 609–640

22. Schwartz, E., Fritsch, J., and Friedrich, B. (2013) H_2-metabolizing prokaryotes. in *The Prokaryotes: Prokaryotic Physiology and Biochemistry* (Rosenberg, E., DeLong, E. F., Lory, S., Stackebrandt, E., and Thompson, F. eds), pp. 119–199, Springer, Berlin/Heidelberg, Germany

23. Morita, R. Y. (1999) Is H_2 the universal energy source for long-term survival? *Microb. Ecol.* **38**, 307–320

24. Vignais, P. M., and Billoud, B. (2007) Occurrence, classification, and biological function of hydrogenases: An overview. *Chem. Rev.* **107**, 4206–4272

25. Kawasumi, T., Igarashi, Y., Kodama, T., and Minoda, Y. (1984) *Hydrogenobacter thermophilus* gen. nov., sp. nov., an extremely thermophilic, aerobic, hydrogen-oxidizing bacterium. *Int. J. Syst. Bacteriol.* **34**, 5–10

26. Nishihara, H., Igarashi, Y., and Kodama, T. (1991) *Hydrogenovibrio marinus* gen. nov., sp. nov., a marine obligately chemolithoautotrophic hydrogen-oxidizing bacterium. *Int. J. Syst. Bacteriol.* **41**, 130–133

27. Hanus, F. J., Maier, R. J., and Evans, H. J. (1979) Autotrophic growth of H_2-uptake-positive strains of *Rhizobium japonicum* in an atmosphere supplied with hydrogen gas. *PNAS*. **76**, 1788–92

28. Paoli, G. C., and Tabita, F. R. (1998) Aerobic chemolithoautotrophic growth and RubisCO function in *Rhodobacter capsulatus* and a spontaneous gain of function

mutant of *Rhodobacter sphaeroides*. *Arch. Microbiol.* **170**, 8–17

29. Ji, M., Greening, C., Vanwonterghem, I., Carere, C., Bay, S., Steen, J., Montgomery, K., Lines, T., Beardall, J., Dorst, J. van, Snape, I., Stott, M., Hugenholtz, P., and Ferrari, B. (2017) Atmospheric trace gases support primary production in Antarctic desert ecosystems. *Nature*. **552**, 400–403

30. Lynch, R. C., Darcy, J. L., Kane, N. C., Nemergut, D. R., and Schmidt, S. K. (2014) Metagenomic evidence for metabolism of trace atmospheric gases by high-elevation desert actinobacteria. *Front. Microbiol.* **5**, 1–13

31. Islam, Z. F., Welsh, C., Bayly, K., Grinter, R., Southam, G., Gagen, E. J., and Greening, C. (2020) A widely distributed hydrogenase oxidises atmospheric H_2 during bacterial growth. *ISME J.* https://doi.org/10.1038/s41396-020-0713-4

32. Carere, C. R., Hards, K., Houghton, K. M., Power, J. F., Mcdonald, B., Collet, C., Gapes, D. J., Sparling, R., Boyd, E. S., Cook, G. M., Greening, C., and Stott, M. B. (2017) Mixotrophy drives niche expansion of verrucomicrobial methanotrophs. *ISME J.* **11**, 2599–2610

33. Islam, Z. F., Cordero, P. R. F., Feng, J., Chen, Y., Bay, S. K., Jirapanjawat, T., Gleadow, R. M., Carere, C. R., Stott, M. B., Chiri, E., and Greening, C. (2019) Two Chloroflexi classes independently evolved the ability to persist on atmospheric hydrogen and carbon monoxide. *ISME J.* **13**, 1801–1813

34. Liot, Q., and Constant, P. (2016) Breathing air to save energy - new insights into the ecophysiological role of high-affinity [NiFe]-hydrogenase in *Streptomyces avermitilis*. *Microbiologyopen*. **5**, 47–59

35. Greening, C., Carere, C. R., Rushton-Green, R., Harold, L. K., Hards, K., Taylor, M. C., Morales, S. E., Stott, M. B., and Cook, G. M. (2015) Persistence of the dominant soil phylum Acidobacteria by trace gas scavenging. *Proc. Natl. Acad. Sci.* **112**, 10497–10502

36. Berney, M., and Cook, G. M. (2010) Unique flexibility in energy metabolism allows mycobacteria to combat starvation and hypoxia. *PLoS One*. **5**, e8614

37. Ragsdale, S. W. (2004) Life with carbon monoxide. *Crit. Rev. Biochem. Mol. Biol.* **39**, 165–195

38. Alonso, J. R., Cardellach, F., López, S., Casademont, J., and Miró, Ò. (2003) Carbon monoxide specifically inhibits cytochrome C oxidase of human mitochondrial respiratory chain. *Pharmacol. Toxicol.* **93**, 142–146

39. Barton, L. L. (2004) Electron transport and coupled phosphorylation. in *Structural and Functional Relationships in Prokaryotes* (Barton, L. L. ed), pp. 397–467, Springer, New York, NY

40. Jeoung, N., Fesseler, J., Goetzl, S., and Dobbek, H. (2014) Carbon monoxide. Toxic

gas and fuel for anaerobes and aerobes: Carbon monoxide dehydrogenases. in *The Metal-Driven Biogeochemistry of Gaseous Compounds in the Environment, Metal Ions in Life Sciences* (Kroneck, P. M. H., and Torres, M. E. S. eds), pp. 37–69, Springer Netherlands, 10.1007/978-94-017-9269-1

41. Kim, Y. M., and Hegeman, G. D. (1981) Electron transport system of an aerobic carbon monoxide-oxidizing bacterium. *J. Bacteriol.* **148**, 991–994

42. Wilcoxen, J., Zhang, B., and Hille, R. (2011) The reaction of the molybdenum- and copper-containing carbon monoxide dehydrogenase from *Oligotropha carboxydovorans* with quinones. *Biochemistry.* **50**, 1910–1916

43. Meyer, O., and Schlegel, H. G. (1978) Reisolation of the carbon monoxide utilizing hydrogen bacterium *Pseudomonas carboxydovorans* (Kistner) comb. nov. *Arch. Microbiol.* **118**, 35–43

44. Kiessling, M., and Meyer, O. (1982) Profitable oxidation of carbon monoxide or hydrogen during heterotrophic growth of Pseudomonas carboxydoflava. *FEMS Microbiol. Lett.* **13**, 333–338

45. Kim, Y. J., and Kim, Y. M. (1989) Induction of carbon monoxide dehydrogenase during heterotrophic growth of *Acinetobacter* sp. strain JC1 DSM 3803 in the presence of carbon monoxide. *FEMS Microbiol. Lett.* **59**, 207–210

46. Weber, C. F., and King, G. M. (2007) Physiological, ecological, and phylogenetic characterization of *Stappia*, a marine CO-oxidizing bacterial genus. *Appl. Environ. Microbiol.* **73**, 1266–1276

47. Cunliffe, M. (2013) Physiological and metabolic effects of carbon monoxide oxidation in the model marine bacterioplankton *Ruegeria pomeroyi* DSS-3. *Appl. Environ. Microbiol.* **79**, 738–740

48. Lubitz, W., Ogata, H., Ruediger, O., and Reijerse, E. (2014) Hydrogenases. *Chem. Rev.* **114**, 4081–4148

49. Greening, C., Biswas, A., Carere, C. R., Jackson, C. J., Taylor, M. C., Stott, M. B., Cook, G. M., and Morales, S. E. (2016) Genomic and metagenomic surveys of hydrogenase distribution indicate H_2 is a widely utilised energy source for microbial growth and survival. *ISME J.* **10**, 761–777

50. Thauer, R. K., Kaster, A.-K., Goenrich, M., Schick, M., Hiromoto, T., and Shima, S. (2010) Hydrogenases from methanogenic archaea, nickel, a novel cofactor, and H_2 storage. *Annu. Rev. Biochem.* **79**, 507–536

51. Zirngibl, C., Hedderich, R., and Thauer, R. K. (1990) N5,N10-Methylenetetrahydromethanopterin dehydrogenase from *Methanobacterium thermoautotrophicum* has hydrogenase activity. *FEBS Lett.* **261**, 112–116

52. Dobbek, H. (2019) Mechanism of Ni,Fe-Containing carbon monoxide dehydrogenases.

Struct. Bond. **179**, 153–166

53. Dobbek, H., Gremer, L., Meyer, O., and Huber, R. (1999) Crystal structure and mechanism of CO dehydrogenase, a molybdo iron-sulfur flavoprotein containing S-selanylcysteine. *Proc. Natl. Acad. Sci. U. S. A.* **96**, 8884–8889

54. Meyer, O., Gremer, L., Ferner, R., Ferner, M., Dobbek, H., Gnida, M., Meyer-Klaucke, W., and Huber, R. (2000) The role of Se, Mo and Fe in the structure and function of carbon monoxide dehydrogenase. *Biol. Chem.* **381**, 865–876

55. Dobbek, H., Svetlitchnyi, V., Gremer, L., Huber, R., and Meyer, O. (2001) Crystal structure of a carbon monoxide dehydrogenase reveals a [Ni-4Fe-5S] cluster. *Science (80-.).* **293**, 1281–1285

56. Doukov, T. I., Iverson, T. M., Seravalli, J., Ragsdale, S. W., and Drennan, C. L. (2002) A Ni-Fe-Cu center in a bifunctional carbon monoxide dehydrogenase/acetyl-CoA synthase. *Science (80-.).* **298**, 567–572

57. Gong, W., Hao, B., Wei, Z., Ferguson, D. J., Tallant, T., Krzycki, J. A., and Chan, M. K. (2008) Structure of the α2ε2 Ni-dependent CO dehydrogenase component of the Methanosarcina barkeri acetyl-CoA decarbonylase/synthase complex. *Proc. Natl. Acad. Sci. U. S. A.* **105**, 9558–9563

58. Ragsdale, S. W., and Wood, H. G. (1985) Acetate biosynthesis by acetogenic bacteria. *J. Biol. Chem.* **260**, 3970–3977

59. Ljungdahl, L. G. (1986) the Autotrophic Pathway of acetate synthesis in acertogenic bacteria. *Annu. Rev. Microbiol.* **40**, 415–450

60. Ragsdale, S. W., and Pierce, E. (2008) Acetogenesis and the Wood-Ljungdahl pathway of CO_2 fixation. *Biochim. Biophys. Acta - Proteins Proteomics.* **1784**, 1873–1898

61. Stupperich, E., Hammel, K. E., Fuchs, G., and Thauer, R. K. (1983) Carbon monoxide fixation into the carboxyl group of acetyl coenzyme A during autotrophic growth of Methanobacterium. *FEBS Lett.*

62. DeRose, V. J., Telser, J., Anderson, M. E., Lindahl, P. A., and Hoffman, B. M. (1998) A multinuclear ENDOR study of the C-cluster in CO dehydrogenase from *Clostridium thermoaceticum*: Evidence for H(x)O and histidine coordination to the [Fe4S4] center. *J. Am. Chem. Soc.* **120**, 8767–8776

63. Lindahl, P. A., and Ragsdale, S. W. (1990) CO dehydrogenase from *Clostridium*. *J. Biol. Chem.* **265**, 3873–3879

64. Hofmann, M., Kassube, J. K., and Graf, T. (2005) The mechanism of Mo-/Cu-dependent CO dehydrogenase. *J. Biol. Inorg. Chem.* **10**, 490–495

65. Elsen, S., Colbeau, A., Chabert, J., and Vignais, P. M. (1996) The *hupTUV* operon is involved in negative control of hydrogenase synthesis in *Rhodobacter capsulatus*. *J. Bacteriol.* **178**, 5174–5181

66. Lenz, O., and Friedrich, B. (1998) A novel multicomponent regulatory system mediates H$_2$ sensing in *A. eutrophus. Proc. Natl. Acad. Sci.* **95**, 12474–12479

67. Rey, F. E., Oda, Y., and Harwood, C. S. (2006) Regulation of uptake hydrogenase and effects of hydrogen utilization on gene expression in *Rhodopseudomonas palustris. J. Bacteriol.* **188**, 6143–6152

68. Vignais, P. M. (2009) Regulation of hydrogenase gene expression. in *Advances in Photosynthesis and Respiration: The Purple Phototrophic Bacteria* (Hunter, C. N., Dalda, F., Thurnaues, M. C., and Beatty, J. T. eds), pp. 743–757, **28**, 743–757

69. Kleihues, L., Lenz, O., Bernhard, M., Buhrke, T., and Friedrich, B. (2000) The H$_2$ sensor of *Ralstonia* eutropha is a member of the subclass of regulatory [NiFe] hydrogenases. *J. Bacteriol.* **182**, 2716–2724

70. Durmowicz, M. C., and Maier, R. J. (1997) Roles of HoxX and HoxA in biosynthesis of hydrogenase in *Bradyrhizobium japonicum. J. Bacteriol.* **179**, 3676–3682

71. Buhrke, T., Lenz, O., Porthun, A., and Friedrich, B. (2004) The H$_2$-sensing complex of *Ralstonia eutropha*: Interaction between a regulatory [NiFe] hydrogenase and a histidine protein kinase. *Mol. Microbiol.* **51**, 1677–1689

72. Black, L. K., Fu, C., and Maier, R. J. (1994) Sequences and characterization of *hupU* and *hupV* genes of *Bradyrhizobium japonicum* encoding a possible nickel-sensing complex involved in hydrogenase expression. *J. Bacteriol.* **176**, 7102–7106

73. Sciotti, M. A., Chanfon, A., Hennecke, H., and Fischer, H. M. (2003) Disparate oxygen responsiveness of two regulatory cascades that control expression of symbiotic genes in *Bradyrhizobium japonicum. J. Bacteriol.* **185**, 5639–5642

74. Nellen-Anthamatten, D., Rossi, P., Preisig, O., Kullik, I., Babst, M., Fischer, H. M., and Hennecke, H. (1998) *Bradyrhizobium japonicum* FixK2, a crucial distributor in the FixLJ-dependent regulatory cascade for control of genes inducible by low oxygen levels. *J. Bacteriol.* **180**, 5251–5255

75. Durmowicz, M. C., and Maier, R. J. (1998) The FixK2 protein is involved in regulation of symbiotic hydrogenase expression in *Bradyrhizobium japonicum. J. Bacteriol.* **180**, 3253–3256

76. Bates, D. M., Popescu, C. V., Khoroshilova, N., Vogt, K., Beinert, H., Münck, E., and Kiley, P. J. (2000) Substitution of leucine 28 with histidine in the *Escherichia coli* transcription factor FNR results in increased stability of the [4Fe-4S]2+ cluster to oxygen. *J. Biol. Chem.* **275**, 6234–6240

77. Kiley, P. J., and Beinert, H. (1998) Oxygen sensing by the global regulator, FNR: The role of the iron-sulfur cluster. *FEMS Microbiol. Rev.* **22**, 341–352

78. Kovács, Á. T., Rákhely, G., Browning, D. F., Fülöp, A., Maróti, G., Busby, S. J. W., and Kovács, K. L. (2005) An FNR-type regulator controls the anaerobic expression of Hyn

hydrogenase in *Thiocapsa roseopersicina*. *J. Bacteriol.* **187**, 2618–2627

79. Messenger, S. L., and Green, J. (2003) FNR-mediated regulation of hyp expression in *Escherichia coli*. *FEMS Microbiol. Lett.* **228**, 81–86

80. Zbell, A. L., Benoit, S. L., and Maier, R. J. (2007) Differential expression of NiFe uptake-type hydrogenase genes in *Salmonella enterica* serovar Typhimurium. *Microbiology*. **153**, 3508–3516

81. Elsen, S., Swem, L. R., Swem, D. L., and Bauer, C. E. (2004) RegB/RegA, a highly conserved redox-responding global two-component regulatory system. *Microbiol. Mol. Biol. Rev.* **68**, 263–279

82. Elsen, S., Dischert, W., Colbeau, A., and Bauer, C. E. (2000) Expression of uptake hydrogenase and molybdenum nitrogenase in *Rhodobacter capsulatus* is coregulated by the RegB-RegA two-component regulatory system. *J. Bacteriol.* **182**, 2831–2837

83. Berney, M., Greening, C., Hards, K., Collins, D., and Cook, G. M. (2014) Three different [NiFe] hydrogenases confer metabolic flexibility in the obligate aerobe *Mycobacterium smegmatis*. *Environ. Microbiol.* **16**, 318–330

84. Berney, M., Greening, C., Conrad, R., Jacobs, W. R., and Cook, G. M. (2014) An obligately aerobic soil bacterium activates fermentative hydrogen production to survive reductive stress during hypoxia. *Proc. Natl. Acad. Sci.* **111**, 11479–11484

85. Jamieson, D. J., Sawers, R. G., Rugman, P. A., Boxer, D. H., and Higgins, C. F. (1986) Effects of anaerobic regulatory mutations and catabolite repression on regulation of hydrogen metabolism and hydrogenase isoenzyme composition in *Salmonella typhimurium*. *J. Bacteriol.* **168**, 405–411

86. Deutscher, J. (2008) The mechanisms of carbon catabolite repression in bacteria. *Curr. Opin. Microbiol.* **11**, 87–93

87. Richard, D. J., Sawers, R. G., Sargent, F., McWalter, L., and Boxer, D. H. (1999) Transcriptional regulation in response to oxygen and nitrate of the operons encoding the [NiFe] hydrogenases 1 and 2 of *Escherichia coli*. *Microbiology*. **145**, 2903–2912

88. Atlung, T., Knudsen, K., Heerfordt, L., and BrØndsted, L. (1997) Effects of σ(s) and the transcriptional activator AppY on induction of the *Escherichia coli hya* and *cbdAB-appA* operons in response to carbon and phosphate starvation. *J. Bacteriol.* **179**, 2141–2146

89. Pinske, C., McDowall, J. S., Sargent, F., and Sawers, R. G. (2012) Analysis of hydrogenase 1 levels reveals an intimate link between carbon and hydrogen metabolism in *Escherichia coli* K-12. *Microbiology*. **158**, 856–868

90. Patrauchan, M. A., Miyazawa, D., LeBlanc, J. C., Aiga, C., Florizone, C., Dosanjh, M., Davies, J., Eltis, L. D., and Mohn, W. W. (2012) Proteomic analysis of survival of *Rhodococcus jostii* RHA1 during carbon starvation. *Appl. Environ. Microbiol.* **78**, 6714–6725

91. Christie-Oleza, J. A., Fernandez, B., Nogales, B., Bosch, R., and Armengaud, J. (2012) Proteomic insights into the lifestyle of an environmentally relevant marine bacterium. *ISME J.* **6**, 124–135

92. Muthusamy, S., Lundin, D., Mamede Branca, R. M., Baltar, F., González, J. M., Lehtiö, J., and Pinhassi, J. (2017) Comparative proteomics reveals signature metabolisms of exponentially growing and stationary phase marine bacteria. *Environ. Microbiol.* **19**, 2301–2319

93. King, G. M., Weber, C. F., Nanba, K., Sato, Y., and Ohta, H. (2008) Atmospheric CO and hydrogen uptake and CO oxidizer phylogeny for Miyake-Jima, Japan volcanic deposits. *Microbes Environ.* **23**, 299–305

94. King, G. M., and Weber, C. F. (2008) Interactions between bacterial carbon monoxide and hydrogen consumption and plant development on recent volcanic deposits. *ISME J.* **2**, 195–203

95. Constant, P., Chowdhury, S. P., Hesse, L., and Conrad, R. (2011) Co-localization of atmospheric H_2 oxidation activity and high affinity H_2-oxidizing bacteria in non-axenic soil and sterile soil amended with Streptomyces sp. PCB7. *Soil Biol. Biochem.* **43**, 1888–1893

96. Constant, P., Chowdhury, S. P., Pratscher, J., and Conrad, R. (2010) Streptomycetes contributing to atmospheric molecular hydrogen soil uptake are widespread and encode a putative high-affinity [NiFe]-hydrogenase. *Environ. Microbiol.* **12**, 821–829

97. Bothe, H., Schmitz, O., Yates, M. G., and Newton, W. E. (2010) Nitrogen fixation and hydrogen metabolism in cyanobacteria. *Microbiol. Mol. Biol. Rev.* **74**, 529–551

98. Papen, H., Kentemich, T., Schmülling, T., and Bothe, H. (1986) Hydrogenase activities in cyanobacteria. *Biochimie*. **68**, 121–132

99. Tamagnini, P., Axelsson, R., Lindberg, P., Oxelfelt, F., Wünschiers, R., and Lindblad, P. (2002) Hydrogenases and hydrogen metabolism of cyanobacteria. *Microbiol. Mol. Biol. Rev.* **66**, 1–20

100. Søndergaard, D., Pedersen, C. N. S., and Greening, C. (2016) HydDB : A web tool for hydrogenase classification and analysis. *Sci. Rep.* 10.1038/srep34212

101. Fritsch, J., Scheerer, P., Frielingsdorf, S., Kroschinsky, S., Friedrich, B., Lenz, O., and Spahn, C. M. T. (2011) The crystal structure of an oxygen-tolerant hydrogenase uncovers a novel iron-sulphur centre. *Nature*. **479**, 249–252

102. Higuchi, Y., Yagi, T., and Yasuoka, N. (1997) Unusual ligand structure in Ni – Fe active center and an additional Mg site in hydrogenase revealed by high resolution X-ray structure analysis. *Structure*. **5**, 1671–1680

103. Matias, P. M., Soares, C. M., Saraiva, L. M., Coelho, R., Morais, J., Le Gall, J., and Carrondo, M. A. (2001) [NiFe] hydrogenase from *Desulfovibrio desulfuricans* ATCC

27774: Gene sequencing, three-dimensional structure determination and refinement at 1.8 Å and modelling studies of its interaction with the tetrahaem cytochrome c_3. *J. Biol. Inorg. Chem.* **6**, 63–81

104. Ogata, H., Hirota, S., Nakahara, A., Komori, H., Shibata, N., Kato, T., Kano, K., and Higuchi, Y. (2005) Activation process of [NiFe] hydrogenase elucidated by high-resolution X-ray analyses: Conversion of the ready to the unready state. *Structure*. **13**, 1635–1642

105. Pierik, A. J., Roseboom, W., Happe, R. P., Bagley, K. A., Albracht, S. P. J., and Lacey, D. (1999) Carbon monoxide and cyanide as intrinsic ligands to iron in the active site of [NiFe]-hydrogenases. *J. Biol. Chem.* **274**, 3331–3337

106. Schäfer, C., Bommer, M., Hennig, S. E., Jeoung, J. H., Dobbek, H., and Lenz, O. (2016) Structure of an actinobacterial-type [NiFe]-hydrogenase reveals insight into O_2-tolerant H_2 oxidation. *Structure*. **24**, 285–292

107. Shomura, Y., Yoon, K.-S., Nishihara, H., and Higuchi, Y. (2011) Structural basis for a [4Fe-3S] cluster in the oxygen-tolerant membrane-bound [NiFe]-hydrogenase. *Nature*. **479**, 253–256

108. Shomura, Y., Tai, H., Nakagawa, H., Ikeda, Y., Ishii, M., Igarashi, Y., Nishihara, H., Ogo, S., Hirota, S., and Higuchi, Y. (2017) Structural basis of the redox switches in the NAD^+-reducing soluble [NiFe]-hydrogenase. *Science (80-.).* **357**, 928–932

109. Wagner, T., Koch, J., Ermler, U., and Shima, S. (2017) Methanogenic heterodisulfide reductase (HdrABC-MvhAGD) uses two noncubane [4Fe-4S] clusters for reduction. *Science (80-.).* **357**, 699–703

110. Volbeda, A., Garcin, E., Piras, C., De Lacey, A. L., Fernandez, V. M., Hatchikian, E. C., Frey, M., and Fontecilla-Camps, J. C. (1996) Structure of the [NiFe] hydrogenase active site: Evidence for biologically uncommon Fe ligands. *J. Am. Chem. Soc.* **118**, 12989–12996

111. Montet, Y., Amara, P., Volbeda, A., Vernede, X., Hatchikian, E. C., Field, M. J., Frey, M., and Fontecilla-Camps, J. C. (1997) Gas access to the active site of Ni-Fe hydrogenases probed by X-ray crystallography and molecular dynamics. *Nat. Struct. Biol.* **4**, 523–526

112. Topin, J., Rousset, M., Antonczak, S., and Golebiowski, J. (2012) Kinetics and thermodynamics of gas diffusion in a NiFe hydrogenase. *Proteins Struct. Funct. Bioinforma.* **80**, 677–682

113. Ogata, H., Lubitz, W., and Higuchi, Y. (2016) Structure and function of [NiFe] hydrogenases. *J. Biochem.* **160**, 251–258

114. Stein, M., and Lubitz, W. (2002) Quantum chemical calculations of [NiFe] hydrogenase. *Curr. Opin. Chem. Biol.* **6**, 243–249

115. Volbeda, A., Martin, L., Cavazza, C., Matho, M., Faber, B. W., Roseboom, W., Albracht, S. P. J., Garcin, E., Rousset, M., and Fontecilla-Camps, J. C. (2005) Structural differences between the ready and unready oxidized states of [NiFe] hydrogenases. *J. Biol. Inorg. Chem.* **10**, 239–249

116. Ogata, H., Lubitz, W., and Higuchi, Y. (2009) [NiFe] hydrogenases: structural and spectroscopic studies of the reaction mechanism. *Dalt. Trans.* **9226**, 7577

117. Volbeda, A., Charon, M.-H., Piras, C., Hatchikian, E. C., Frey, M., and Fontecilla-Camps, J. C. (1995) Crystal structure of the nickel–iron hydrogenase from *Desulfovibrio gigas*. *Nature*. **373**, 580–587

118. Petrenko, A., and Stein, M. (2017) Distal [FeS]-Cluster coordination in [NiFe]-Hydrogenase facilitates intermolecular electron transfer. *Int. J. Mol. Sci.* **18**, 1–10

119. Fdez Galván, I., Volbeda, A., Fontecilla-Camps, J. C., and Field, M. J. (2008) A QM/MM study of proton transport pathways in a [NiFe] hydrogenase. *Proteins*. **73**, 195–203

120. Fritsch, J., Lenz, O., and Friedrich, B. (2013) Structure, function and biosynthesis of O_2-tolerant hydrogenases. *Nat. Rev. Microbiol.* **11**, 106–114

121. Lauterbach, L., and Lenz, O. (2013) Catalytic production of hydrogen peroxide and water by oxygen-tolerant [NiFe]-hydrogenase during H_2 cycling in the presence of O_2. *J. Am. Chem. Soc.* **135**, 17897–17905

122. Marques, M. C., Coelho, R., De Lacey, A. L., Pereira, I. A. C., and Matias, P. M. (2010) The three-dimensional structure of [nifese] hydrogenase from desulfovibrio vulgaris hildenborough: A hydrogenase without a bridging ligand in the active site in its oxidised, "as-isolated" state. *J. Mol. Biol.* **396**, 893–907

123. Pandelia, M.-E., Nitschke, W., Infossi, P., Giudici-Orticoni, M.-T., Bill, E., and Lubitz, W. (2011) Characterization of a unique [FeS] cluster in the electron transfer chain of the oxygen tolerant [NiFe] hydrogenase from Aquifex aeolicus. *Proc. Natl. Acad. Sci. U. S. A.* **108**, 6097–6102

124. Roessler, M. M., Evans, R. M., Davies, R. A., Harmer, J., and Armstrong, F. A. (2012) EPR spectroscopic studies of the Fe-S clusters in the O_2-tolerant [NiFe]-hydrogenase hyd-1 from *Escherichia coli* and characterization of the unique [4Fe-3S] cluster by HYSCORE. *J Am Chem Soc.* **134**, 15581–15594

125. Buhrke, T., Lenz, O., Krauss, N., and Friedrich, B. (2005) Oxygen tolerance of the H_2-sensing [NiFe] hydrogenase from *Ralstonia eutropha* H16 is based on limited access of oxygen to the active site. *J. Biol. Chem.* **280**, 23791–23796

126. King, G. M. (2003) Molecular and culture-based analyses of aerobic carbon monoxide oxidizer diversity. *Appl. Environ. Microbiol.* **69**, 7257–7265

127. Cunliffe, M. (2011) Correlating carbon monoxide oxidation with cox genes in the abundant Marine *Roseobacter Clade*. *ISME J.* **5**, 685–691

128. Lalonde, I., and Constant, P. (2016) Identification of unknown carboxydovore bacteria dominant in deciduous forest soil via succession of bacterial communities, coxl genotypes, and carbon monoxide oxidation activity in soil microcosms. *Appl. Environ. Microbiol.* **82**, 1324–1333

129. Quiza, L., Lalonde, I., Guertin, C., and Constant, P. (2014) Land-use influences the distribution and activity of high affinity CO-oxidizing bacteria associated to type I-*coxL* genotype in soil. *Front. Microbiol.* **5**, 1–15

130. Cunliffe, M., Schäfer, H., Harrison, E., Cleave, S., Upstill-Goddard, R., and Murrell, J. C. (2008) Phylogenetic and functional gene analysis of the bacterial and archaeal communities associated with the surface microlayer of an estuary. *ISME J.* **2**, 776–789

131. Venter, J. C., Remington, K., Heidelberg, J. F., Halpern, A. L., Rusch, D., Eisen, J. A., Wu, D., Paulsen, I., Nelson, K. E., Nelson, W., Fouts, D. E., Levy, S., Knap, A. H., Lomas, M. W., Nealson, K., White, O., Peterson, J., Hoffman, J., Parsons, R., Baden-Tillson, H., Pfannkoch, C., Rogers, Y. H., and Smith, H. O. (2004) Environmental genome shotgun sequencing of the Sargasso sea. *Science (80-.).* **304**, 66–74

132. Dunfield, K. E., and King, G. M. (2004) Molecular analysis of carbon monoxide-oxidizing bacteria associated with recent Hawaiian volcanic deposits. *Appl. Environ. Microbiol.* **70**, 4242–4248

133. Weber, C. F., and King, G. M. (2010) Distribution and diversity of carbon monoxide-oxidizing bacteria and bulk bacterial communities across a succession gradient on a Hawaiian volcanic deposit. *Environ. Microbiol.* **12**, 1855–1867

134. Yang, J., Zhou, E., Jiang, H., Li, W., Wu, G., Huang, L., Hedlund, B. P., and Dong, H. (2015) Distribution and diversity of aerobic carbon monoxide-oxidizing bacteria in geothermal springs of China, the Philippines, and the United States. *Geomicrobiol. J.* **32**, 903–913

135. Santiago, B., Schübel, U., Egelseer, C., and Meyer, O. (1999) Sequence analysis, characterization and CO-specific transcription of the cox gene cluster on the megaplasmid pHCG3 of *Oligotropha carboxidovorans*. *Gene.* **236**, 115–124

136. Dobbek, H., Gremer, L., Kiefersauer, R., Huber, R., and Meyer, O. (2002) Catalysis at a dinuclear [CuSMo(=O)OH] cluster in a CO dehydrogenase resolved at 1.1-Å resolution. *Proc. Natl. Acad. Sci. U. S. A.* **99**, 15971–15976

137. Gnida, M., Ferner, R., Gremer, L., Meyer, O., and Meyer-Klaucke, W. (2003) A novel binuclear [CuSMo] cluster at the active site of carbon monoxide dehydrogenase: Characterization by x-ray absorption spectroscopy. *Biochemistry.* **42**, 222–230

138. Zhang, B., Hemann, C. F., and Hille, R. (2010) Kinetic and spectroscopic studies of the molybdenum-copper CO dehydrogenase from *Oligotropha carboxidovorans*. *J. Biol. Chem.* **285**, 12571–12578

139. Siegbahn, P. E. M., and Shestakov, A. F. (2005) Quantum chemical modeling of CO oxidation by the active site of molybdenum CO dehydrogenase. *J. Comput. Chem.* **26**, 888–898

140. Xu, K., and Hirao, H. (2018) Revisiting the catalytic mechanism of Mo-Cu carbon monoxide dehydrogenase using QM/MM and DFT calculations. *Phys. Chem. Chem. Phys.* **20**, 18938–18948

141. Brennan, P. J., and Nikaido, H. (1995) The envelope of mycobacteria. *Annu. Rev. Biochem.* **64**, 29–63

142. Hartmans, S., Bont, J. A. M. De, and Stackebrandt, E. (2006) The Genus *Mycobacterium* — Nonmedical. in *The Prokaryotes* (Dworkin, M., Falkow, S., Rosenberg, E., Schleifer, K.-H., and Stackebrandt, E. eds), pp. 889–918, Springer, New York, NY

143. Magee, J. G., and Ward, A. C. (2015) *Mycobacterium*. in *Bergey's Manual of Systematics of Archaea and Bacteria* (Whitman, W. B., DeVos, P., Dedysh, S., Hedlund, B., Kämpfer, P., Rainey, F., Trujillo, M. E., Bowman, J. P., Brown, D. R., Glöckner, F. O., Oren, A., Paster, B. J., Wade, W., Ward, N., Busse, H.-J., and Reysenbach, A.-L. eds), pp. 1–81, John Wiley & Sons, Inc., 10.11400/kekkaku1923.33.260

144. Saviola, B., and Bisha, W. (2006) The Genus *Mycobacterium* - Medical. in *The Prokaryotes* (Dworkin, M., Falkow, S., Rosenberg, E., Schleifer, K.-H., and Stackebrandt, E. eds), pp. 741–754, Springer, New York, NY, 10.1007/0-387-30744-3

145. Grange, J. M. (1996) The biology of the genus *Mycobacterium*. *Soc. Appl. Bacteriol. Symp. Ser.* **25**, 1–9

146. Wayne, L. G., and Lin, K. Y. (1982) Glyoxylate metabolism and adaptation of *Mycobacterium tuberculosis* to survival under anaerobic conditions. *Infect. Immun.* **37**, 1042–1049

147. Dick, T., Lee, B. H., and Murugasu-Oei, B. (1998) Oxygen depletion induced dormancy in *Mycobacterium smegmatis*. *FEMS Microbiol. Lett.* **163**, 159–164

148. Heitkamp, M. A., Franklin, W., and Cerniglia, C. E. (1988) Microbial metabolism of polycyclic aromatic hydrocarbons: Isolation and characterization of a pyrene-degrading bacterium. *Appl. Environ. Microbiol.* **54**, 2549–2555

149. Urakami, T., and Yano, I. (1989) Methanol-utilizing *Mycobacterium* strains isolated from soil. **133**, 125–133

150. King, G. M. (2003) Uptake of carbon monoxide and hydrogen at environmentally relevant concentrations by mycobacteria? Uptake of carbon monoxide and hydrogen at environmentally relevant concentrations by mycobacteria. *Appl. Environ. Microbiol.* **69**, 7266–7272

151. Park, S. W., Hwang, E. H., Park, H., Kim, J. A., Heo, J., Lee, K. H., Song, T., Kim, E., Ro, Y. T., Kim, S. W., and Kim, Y. M. (2003) Growth of mycobacteria on carbon monoxide and methanol. *J. Bacteriol.* **185**, 142–147

152. Cook, G. M., Hards, K., Vilchèze, C., Hartman, T., and Berney, M. (2013) Energetics of respiration and oxidative phosphorylation in mycobacteria. *Microbiol. Spectr.* **2**, 1–30

153. Mitchell, P. (1961) Coupling of phosphorylation to electron and hydrogen transfer by a chemi-osmotic type of mechanism. *Nature.* **191**, 144–148

154. Nicholls, D. G., and Ferguson, S. J. (2013) *Bioenergetics, 4th edition*, Academic Press, Cambridge, Massachusetts, USA

155. Collins, M. D., and Jones, D. (1981) Distribution of isoprenoid quinone structural types in bacteria and their taxonomic implications. *Microbiol. Rev.* **45**, 316–354

156. Rao, M., Streur, T. L., Aldwell, F. E., and Cook, G. M. (2001) Intracellular pH regulation by *Mycobacterium smegmatis* and *Mycobacterium bovis* BCG. *Microbiology.* **147**, 1017–1024

157. Preiss, L., Langer, J. D., Yildiz, Ö., Eckhardt-Strelau, L., Guillemont, J. E. G., Koul, A., and Meier, T. (2015) Structure of the mycobacterial ATP synthase Fo rotor ring in complex with the anti-TB drug bedaquiline. *Sci. Adv.* **1**, 1–9

158. Lu, P., Lill, H., and Bald, D. (2014) ATP synthase in mycobacteria: Special features and implications for a function as drug target. *Biochim. Biophys. Acta - Bioenerg.* **1837**, 1208–1218

159. Megehee, J. A., Hosler, J. P., and Lundrigan, M. D. (2006) Evidence for a cytochrome *bcc-aa*$_3$ interaction in the respiratory chain of *Mycobacterium smegmatis*. *Microbiology*. **152**, 823–829

160. Matsoso, L. G., Kana, B. D., Crellin, P. K., Lea-smith, D. J., Pelosi, A., Powell, D., Dawes, S. S., Rubin, H., Coppel, R. L., and Mizrahi, V. (2005) Function of the Cytochrome. *J. Bacteriol.* **187**, 6300–6308

161. Wiseman, B., Nitharwal, R. G., Fedotovskaya, O., Schäfer, J., Guo, H., Kuang, Q., Benlekbir, S., Sjöstrand, D., Ädelroth, P., Rubinstein, J. L., Brzezinski, P., and Högbom, M. (2018) Structure of a functional obligate complex III2IV2 respiratory supercomplex from *Mycobacterium smegmatis*. *Nat. Struct. Mol. Biol.* **25**, 1128–1136

162. Cook, G. M., and Poole, R. K. (2016) A bacterial oxidase like no other? *Science (80-.).* **352**, 518–519

163. D'Mello, R., Hill, S., and Poole, R. K. (1996) The cytochrome bd quinol oxidase in *Escherichia coli* has an extremely high oxygen affinity and two oxygen-binding haems: Implications for regulation of activity in vivo by oxygen inhibition. *Microbiology*. **142**, 755–763

164. Kana, B. D., Weinstein, E. A., Avarbock, D., Dawes, S. S., Rubin, H., and Mizrahi, V.

(2001) Characterization of the *cydAB*-encoded cytochrome *bd* oxidase from *Mycobacterium smegmatis*. *J Bacteriol*. **183**, 7076–7086

165. Aung, H. L., Berney, M., and Cook, G. M. (2014) Hypoxia-activated cytochrome bd expression in *Mycobacterium smegmatis* is cyclic AMP receptor protein dependent. *J. Bacteriol.* **196**, 3091–3097

166. Forte, E., Borisov, V. B., Davletshin, A., Mastronicola, D., Sarti, P., and Giuffrè, A. (2013) Cytochrome *bd* oxidase and hydrogen peroxide resistance in *Mycobacterium tuberculosis*. *MBio*. **4**, 2013

167. Saini, V., Chinta, K. C., Reddy, V. P., Glasgow, J. N., Stein, A., Lamprecht, D. A., Rahman, M. A., Mackenzie, J. S., Truebody, B. E., Adamson, J. H., Kunota, T. T. R., Bailey, S. M., Moellering, D. R., Lancaster, J. R., and Steyn, A. J. C. (2020) Hydrogen sulfide stimulates *Mycobacterium tuberculosis* respiration, growth and pathogenesis. *Nat. Commun.* **11**, 1–17

168. Bayly, K., Cordero, P. R. F., Huang, C., Schittenhelm, R., Grinter, R., and Greening, C. (2020) Mycobacteria tolerate carbon monoxide by remodelling their respiratory chain. *bioRxiv*. 10.1101/2020.04.08.032912

169. Lu, P., Heineke, M. H., Koul, A., Andries, K., Cook, G. M., Lill, H., Van Spanning, R., and Bald, D. (2015) The cytochrome bd-type quinol oxidase is important for survival of Mycobacterium smegmatis under peroxide and antibiotic-induced stress. *Sci. Rep.* **5**, 10333:1–10

170. Kalia, N. P., Hasenoehrl, E. J., Ab Rahman, N. B., Koh, V. H., Ang, M. L. T., Sajorda, D. R., Hards, K., Grüber, G., Alonso, S., Cook, G. M., Berney, M., and Pethe, K. (2017) Exploiting the synthetic lethality between terminal respiratory oxidases to kill *Mycobacterium tuberculosis* and clear host infection. *Proc. Natl. Acad. Sci.* **114**, 7426–7431

171. Small, J. L., Park, S. W., Kana, B. D., Ioerger, T. R., Sacchettini, J. C., and Ehrt, S. (2013) Perturbation of cytochrome *c* maturation reveals adaptability of the respiratory chain in Mycobacterium tuberculosis. *MBio*. **4**, 1–8

172. Weinstein, E. A., Yano, T., Li, L. S., Avarbock, D., Avarbock, A., Helm, D., McColm, A. A., Duncan, K., Lonsdale, J. T., and Rubin, H. (2005) Inhibitors of type II NADH:menaquinone oxidoreductase represent a class of antitubercular drugs. *Proc. Natl. Acad. Sci. U. S. A.* **102**, 4548–4553

173. Yano, T., Lin-Sheng, L., Weinstein, E., Teh, J. S., and Rubin, H. (2006) Steady-state kinetics and inhibitory action of antitubercular phenothiazines on *Mycobacterium tuberculosis* Type-II NADH-menaquinone oxidoreductase (NDH-2). *J. Biol. Chem.* **281**, 11456–11463

174. Vilchèze, C., Weinrick, B., Leung, L. W., and Jacobs, W. R. (2018) Plasticity of

Mycobacterium tuberculosis NADH dehydrogenases and their role in virulence. *Proc. Natl. Acad. Sci. U. S. A.* **115**, 1599–1604

175. Rao, S. P. S., Alonso, S., Rand, L., Dick, T., and Pethe, K. (2008) The protonmotive force is required for maintaining ATP homeostasis and viability of hypoxic, nonreplicating *Mycobacterium tuberculosis*. *Proc. Natl. Acad. Sci. U. S. A.* **105**, 11945–11950

176. Miesel, L., Weisbrod, T. R., Marcinkeviciene, J. A., Bittman, R., and Jacobs, W. R. (1998) NADH dehydrogenase defects confer isoniazid resistance and conditional-lethality in *Mycobacterium smegmatis*. *J. Bacteriol.* **180**, 2459–2467

177. Pecsi, I., Hards, K., Ekanayaka, N., Berney, M., Hartman, T., Jacobs, W. R. J., and M.Cook, G. (2014) Essentiality of succinate dehydrogenase in *Mycobacterium smegmatis*. *MBio.* **5**, 1–14

178. Hartman, T., Weinrick, B., Vilchèze, C., Berney, M., Tufariello, J., Cook, G. M., and Jacobs, W. R. (2014) Succinate dehydrogenase is the regulator of respiration in *Mycobacterium tuberculosis*. *PLoS Pathog.* 10.1371/journal.ppat.1004510

179. Eoh, H., and Rhee, K. Y. (2013) Multifunctional essentiality of succinate metabolism in adaptation to hypoxia in *Mycobacterium tuberculosis*. *Proc. Natl. Acad. Sci. U. S. A.* **110**, 6554–6559

180. Berney, M., Weimar, M. R., Heikal, A., and Cook, G. M. (2012) Regulation of proline metabolism in mycobacteria and its role in carbon metabolism under hypoxia. *Mol. Microbiol.* **84**, 664–681

181. Tanner, J. J. (2008) Structural biology of proline catabolism. *Amino Acids*. **35**, 719–730

182. Betts, J. C., Lukey, P. T., Robb, L. C., McAdam, R. A., and Duncan, K. (2002) Evaluation of a nutrient starvation model of *Mycobacterium tuberculosis* persistence by gene and protein expression profiling. *Mol. Microbiol.* **43**, 717–731

183. Nicholson, W. L., Munakata, N., Horneck, G., Melosh, H. J., and Setlow, P. (2000) Resistance of *Bacillus* endospores to extreme terrestrial and extraterrestrial environments. *Microbiol. Mol. Biol. Rev.* **64**, 548–572

184. Gray, D. A., Dugar, G., Gamba, P., Strahl, H., Jonker, M. J., and Hamoen, L. W. (2019) Extreme slow growth as alternative strategy to survive deep starvation in bacteria. *Nat. Commun.* **10**, 1–12

185. Watson, S. P., Clements, M. O., and Foster, S. J. (1998) Characterization of the starvation-survival response of *Staphylococcus aureus*. *J. Bacteriol.* **180**, 1750–1758

186. Greening, C., Grinter, R., and Chiri, E. (2019) Uncovering the metabolic strategies of the dormant microbial majority: towards Integrative Approaches. *mSystems*. **4**, 1–5

187. Friedrich, B., Buhrke, T., Burgdorf, T., and Lenz, O. (2005) A hydrogen-sensing multiprotein complex controls aerobic hydrogen metabolism in *Ralstonia eutropha*.

Biochem. Soc. Trans. **33**, 97–101

188. Schwartz, E. (2008) Megaplasmids of aerobic hydrogenotrophic and carboxidotrophic bacteria. in *Microbial Megaplasmids. Microbial Monographs* (Schwartz, E. ed), pp. 239–270, Springer-Verlag Berlin Heidelberg, 10.1007/7171

189. Burgdorf, T., Lenz, O., Buhrke, T., Van Der Linden, E., Jones, A. K., Albracht, S. P. J., and Friedrich, B. (2006) [NiFe]-hydrogenases of *Ralstonia eutropha* H16: Modular enzymes for oxygen-tolerant biological hydrogen oxidation. *J. Mol. Microbiol. Biotechnol.* **10**, 181–196

190. Schäfer, C., Friedrich, B., and Lenz, O. (2013) Novel, oxygen-insensitive group 5 [NiFe]-hydrogenase in *Ralstonia eutropha*. *Appl. Environ. Microbiol.* **79**, 5137–5145

191. Frielingsdorf, S., Schubert, T., Pohlmann, A., Lenz, O., and Friedrich, B. (2011) A trimeric supercomplex of the oxygen-tolerant membrane-bound [NiFe]-hydrogenase from *Ralstonia eutropha* H16. *Biochemistry*. **50**, 10836–10843

192. Volbeda, A., Darnault, C., Parkin, A., Sargent, F., Armstrong, F. A., and Fontecilla-Camps, J. C. (2013) Crystal structure of the O_2-tolerant membrane-bound hydrogenase 1 from *Escherichia coli* in complex with its cognate cytochrome *b*. *Structure*. **21**, 184–190

193. King, G. M. (2003) Contributions of atmospheric CO and hydrogen uptake to microbial dynamics on recent Hawaiian volcanic deposits. *Appl. Environ. Microbiol.* **69**, 4067–4075

194. Schmidt, U. (1974) Molecular hydrogen in the atmosphere. *Tellus A*. **26**, 78–90

195. Greening, C., Villas-Bôas, S. G., Robson, J. R., Berney, M., and Cook, G. M. (2014) The growth and survival of *Mycobacterium smegmatis* is enhanced by co-metabolism of atmospheric H_2. *PLoS One*. **9**, e103034

196. Piché-Choquette, S., Khdhiri, M., and Constant, P. (2018) Dose-response relationships between environmentally-relevant H_2 concentrations and the biological sinks of H_2, CH_4 and CO in soil. *Soil Biol. Biochem.* **123**, 190–199

197. Bay, S., Ferrari, B., and Greening, C. (2018) Life without water: How do bacteria generate biomass in desert ecosystems? *Microbiol. Aust.* **39**, 28–32

198. Kanno, M., Constant, P., Tamaki, H., and Kamagata, Y. (2015) Detection and isolation of plant-associated bacteria scavenging atmospheric molecular hydrogen. *Environ. Microbiol.* **18**, 2495–2506

199. Kessler, A. J., Chen, Y.-J., Waite, D. W., Hutchinson, T., Koh, S., Popa, M. E., Beardall, J., Hugenholtz, P., Cook, P. L. M., and Greening, C. (2019) Bacterial fermentation and respiration processes are uncoupled in anoxic permeable sediments. *Nat. Microbiol.* **4**, 1014–1023

200. Khdhiri, M., Hesse, L., Popa, M. E., Quiza, L., Lalonde, I., Meredith, L. K., Röckmann,

T., and Constant, P. (2015) Soil carbon content and relative abundance of high affinity H_2-oxidizing bacteria predict atmospheric H_2 soil uptake activity better than soil microbial community composition. *Soil Biol. Biochem.* **85**, 1–9

201. Piché-Choquette, S., Khdhiri, M., and Constant, P. (2017) Survey of high-affinity H_2-oxidizing bacteria in soil reveals their vast diversity yet underrepresentation in genomic databases. *Microb. Ecol.* **74**, 771–775

202. Ferrari, B. C., Bissett, A., Snape, I., Dorst, J. Van, Palmer, A. S., Ji, M., Siciliano, S. D., Stark, J. S., Winsley, T., and Brown, M. V (2016) Geological connectivity drives microbial community structure and connectivity in polar , terrestrial ecosystems. **18**, 1834–1849

203. Price, P. B., and Sowers, T. (2004) Temperature dependence of metabolic rates for microbial growth, maintenance, and survival. *Proc. Natl. Acad. Sci.* **101**, 4631–4636

204. Myers, M. R., and King, G. M. (2016) Isolation and characterization of *Acidobacterium ailaaui* sp. nov., a novel member of Acidobacteria subdivision 1, from a geothermally heated Hawaiian microbial mat. *Int. J. Syst. Evol. Microbiol.* **66**, 5328–5335

205. Tran, S. L., and Cook, G. M. (2005) The F_1F_o-ATP synthase of *Mycobacterium smegmatis* is essential for growth. *J. Bacteriol.* **187**, 5023–5028

206. Edwards, S. E., Loder, C. S., Wu, G., Corker, H., Bainbridge, B. W., Hill, S., and Poole, R. K. (2000) Mutation of cytochrome *bd* quinol oxidase results in reduced stationary phase survival, iron deprivation, metal toxicity and oxidative stress in *Azotobacter vinelandii. FEMS Microbiol. Lett.* **185**, 71–77

207. Safarian, S., Rajendran, C., Müller, H., Preu, J., Langer, J. D., Hirose, T., Kusumoto, T., Sakamoto, J., Michel, H., and Ovchinnikov, S. (2016) Structure of a *bd* oxidase indicates similar mechanisms for membrane-integrated oxygen reductases. *Science (80-.).* **352**, 583–586

208. Borisov, V. B., Gennis, R. B., Hemp, J., and Verkhovsky, M. I. (2011) The cytochrome *bd* respiratory oxygen reductases. *Biochim. Biophys. Acta.* **1807**, 1398–1413

209. Cordero, P. R. F., Bayly, K., Leung, P. M., Huang, C., Islam, Z. F., Schittenhelm, R. B., King, G. M., and Greening, C. (2019) Atmospheric carbon monoxide oxidation is a widespread mechanism supporting microbial survival. *ISME J.*

210. Gebhard, S., Tran, S. L., and Cook, G. M. (2006) The Phn system of Mycobacterium smegmatis: A second high-affinity ABC-transporter for phosphate. *Microbiology.* **152**, 3453–3465

211. Green, M. R., and Sambrook, J. (2012) *Molecular cloning: a laboratory manual*, 4th Ed., Cold Spring Harbor Laboratory Press, Cold Spring Harbor, New York, USA

212. Snapper, S. B., Melton, R. E., Mustafa, S., Kieser, T., and Jr, W. R. J. (1990) Isolation and characterization of efficient plasmid transformation mutants of *Mycobacterium*

smegmatis. *Mol. Microbiol.* **4**, 1911–1919

213. Lu, X., Williams, Z., Hards, K., Tang, J., Cheung, C. Y., Aung, H. L., Wang, B., Liu, Z., Hu, X., Lenaerts, A., Woolhiser, L., Hastings, C., Zhang, X., Wang, Z., Rhee, K., Ding, K., Zhang, T., and Cook, G. M. (2019) Pyrazolo[1,5- a]pyridine inhibitor of the respiratory cytochrome *bcc* complex for the treatment of drug-resistant tuberculosis. *ACS Infect. Dis.* **5**, 239–249

214. Walker, J. M. (2009) Nondenaturing polyacrylamide gel electrophoresis of proteins. in *The Protein Protocols Handbook*, 3rd Ed., pp. 171–176, Humana Press, Totowa, New Jersey, USA

215. Heikal, A., Nakatani, Y., Dunn, E., Weimar, M. R., Day, C. L., Baker, E. N., Lott, J. S., Sazanov, L. A., and Cook, G. M. (2014) Structure of the bacterial type II NADH dehydrogenase: A monotopic membrane protein with an essential role in energy generation. *Mol. Microbiol.* **91**, 950–964

216. Piché-Choquette, S., and Constant, P. (2019) Molecular hydrogen, a neglected key driver of soil biogeochemical processes. *Appl. Environ. Microbiol.* **85**, 1–19

217. Kim, M., Jang, J., Binte, N., Rahman, A. B., Pethe, X. K., and Berry, X. E. A. (2015) Isolation and characterization of a hybrid respiratory supercomplex consisting of *Mycobacterium tuberculosis* cytochrome *bcc* and *Mycobacterium smegmatis* cytochrome *aa*$_3$. *J. Biol. Chem.* **290**, 14350–14360

218. Cook, G. M., Greening, C., Hards, K., and Berney, M. (2014) Energetics of pathogenic bacteria and opportunities for drug development. in *Advances in Microbial Physiology* (Poole, R. K. ed), pp. 1–65, Academic Press, Cambridge, Massachusetts, USA

219. Dhiman, R. K., Mahapatra, S., Slayden, R. A., Boyne, M. E., Lenaerts, A., Hinshaw, J. C., Angala, S. K., Chatterjee, D., Biswas, K., Narayanasamy, P., Kurosu, M., and Crick, D. C. (2009) Menaquinone synthesis is critical for maintaining mycobacterial viability during exponential growth and recovery from non-replicating persistence. *Mol. Microbiol.* **72**, 85–97

220. Matsuno-Yagi, A., and Hatefi, Y. (2002) Ubiquinol-Cytochrome *c* Oxidoreductase . *J. Biol. Chem.* **271**, 6164–6171

221. Nicholls, D. G., and Ferguson, S. J. (2013) Ion transport across energy-conserving membranes. in *Bioenergetics*, 4th Ed., pp. 13–25, Academic Press, Cambridge, Massachusetts, USA

222. Greening, C., and Cook, G. M. (2014) Integration of hydrogenase expression and hydrogen sensing in bacterial cell physiology. *Curr. Opin. Microbiol.* **18**, 30–38

223. Cordero, P. R. F., Grinter, R., Hards, K., Cryle, M. J., Warr, C. G., Cook, G. M., and Greening, C. (2019) Two uptake hydrogenases differentially interact with the aerobic respiratory chain during mycobacterial growth and persistence. *J. Biol. Chem.* **294**,

18980–18991

224. Hartmans, S., and De Bont, J. A. M. (1992) Aerobic vinyl chloride metabolism in *Mycobacterium aurum* L1. *Appl. Environ. Microbiol.* **58**, 1220–1226

225. Stover, C. K., Cruz, V. F. D. I., Fuerst, T. R., Burlein, J. E., Benson, L. A., Bennett, L. T., Bansal, G. P., Young, J. F., Lee, M. H., Hatfull, G. F., Snapper, S. B., Barletta, R. G., Jacobs, W. R. J., and Bloom, B. R. (1991) New use of bcg for recombinant vaccines. **351**, 456–460

226. Smith, P. K., Krohn, R. I., Hermanson, G. T., Mallia, A. K., Gartner, F. H., Provenzano, M. D., Fujimoto, E. K., Goeke, N. M., Olson, B. J., and Klenk, D. C. (1985) Measurement of protein using bicinchoninic acid. *Anal. Biochem.* **150**, 76–85

227. Schmidt, C. L., and Shaw, L. (2001) A comprehensive phylogenetic analysis of rieske and rieske-type iron-sulfur proteins. *J. Bioenerg. Biomembr.* **33**, 9–26

228. Brown, E. N., Friemann, R., Karlsson, A., Parales, J. V., Couture, M. M. J., Eltis, L. D., and Ramaswamy, S. (2008) Determining Rieske cluster reduction potentials. *J. Biol. Inorg. Chem.* **13**, 1301–1313

229. Pinske, C., Jaroschinsky, M., Sargent, F., and Sawers, R. G. (2012) Zymographic differentiation of [NiFe]-Hydrogenases 1, 2 and 3 of *Escherichia coli* K-12. *BMC Microbiol.* **12**, 1–12

230. Fritsch, J., Siebert, E., Priebe, J., Zebger, I., Lendzian, F., Teutloff, C., Friedrich, B., and Lenz, O. (2014) Rubredoxin-related maturation factor guarantees metal cofactor integrity during aerobic biosynthesis of membrane-bound [NiFe] hydrogenase. *J. Biol. Chem.* **289**, 7982–7993

231. Bong, H.-J., Ko, E.-M., Song, S.-Y., Ko, I.-J., and Oha, J.-I. (2019) Tripartite regulation of the *glpFKD* operon involved in glycerol catabolism by GylR, Crp, and SigF in *Mycobacterium smegmatis*. **201**, 1–15

232. Hindle, Z., and Smith, C. P. (1994) Substrate induction and catabolite repression of the *Streptomyces coelicoior* glycerol operon are mediated through the GylR protein. *Mol. Microbiol.* **12**, 737–745

233. Yang, B., Gerhardt, S. G., and Larson, T. J. (1997) Action at a distance for glp repressor control of *glpTQ* transcription in *Escherichia coli* K-12. *Mol. Microbiol.* **24**, 511–521

234. Spoering, A. L., Vulić, M., and Lewis, K. (2006) GlpD and PlsB participate in persister cell formation in *Escherichia coli*. *J. Bacteriol.* **188**, 5136–5144

235. Rock, J. M., Hopkins, F. F., Chavez, A., Diallo, M., Chase, M. R., Gerrick, E. R., Pritchard, J. R., Church, G. M., Rubin, E. J., Sassetti, C. M., Schnappinger, D., and Fortune, S. M. (2017) Programmable transcriptional repression in mycobacteria using an orthogonal CRISPR interference platform. *Nat. Microbiol.* **2**, 1–9

236. Cox, J., and Mann, M. (2008) MaxQuant enables high peptide identification rates,

individualized p.p.b.-range mass accuracies and proteome-wide protein quantification. *Nat. Biotechnol.* **26**, 1367–1372

237. Tyanova, S., Temu, T., Sinitcyn, P., Carlson, A., Hein, M. Y., Geiger, T., Mann, M., and Cox, J. (2016) The Perseus computational platform for comprehensive analysis of (prote)omics data. *Nat. Methods.* **13**, 731–740

238. Safi, H., Gopal, P., Lingaraju, S., Ma, S., Levine, C., Dartois, V., Yee, M., Li, L., Blanc, L., Liang, H. P. H., Husain, S., Hoque, M., Soteropoulos, P., Rustad, T., Sherman, D. R., Dick, T., and Alland, D. (2019) Phase variation in Mycobacterium tuberculosis *glpK* produces transiently heritable drug tolerance. *Proc. Natl. Acad. Sci. U. S. A.* **116**, 19665–19674

239. Qi, L. S., Larson, M. H., Gilbert, L. A., Doudna, J. A., Weissman, J. S., Arkin, A. P., and Lim, W. A. (2013) Repurposing CRISPR as an RNA-guided platform for sequence-specific control of gene expression. *Cell.* **152**, 1173–1183

240. Hünnefeld, M., Persicke, M., Kalinowski, J., and Frunzke, J. (2019) The MarR-Type regulator MalR is involved in stress-responsive cell envelope remodeling in *Corynebacterium glutamicum*. *Front. Microbiol.* **10**, 1–15

241. Ellison, D. W., and Miller, V. L. (2006) Regulation of virulence by members of the MarR/SlyA family. *Curr. Opin. Microbiol.* **9**, 153–159

242. Rodríguez-Moya, J., Argandõa, M., Reina-Bueno, M., Nieto, J. J., Iglesias-Guerra, F., Jebbar, M., and Vargas, C. (2010) Involvement of EupR, a response regulator of the NarL/FixJ family, in the control of the uptake of the compatible solutes ectoines by the halophilic bacterium *Chromohalobacter salexigens*. *BMC Microbiol.* 10.1186/1471-2180-10-256

243. Noriega, C. E., Lin, H.-Y., Chen, L.-L., Williams, S. B., and Stewart, V. (2010) Asymmetric cross regulation between the nitrate-responsive NarX-NarL and NarQ-NarP two-component regulatory systems from *Escherichia coli* K-12. *Mol. Microbiol.* **75**, 394–412

244. Pellicer, M. T., Badía, J., Aguilar, J., and Baldomà, L. (1996) *glc* locus of *Escherichia coli*: Characterization of genes encoding the subunits of glycolate oxidase and the glc regulator protein. *J. Bacteriol.* **178**, 2051–2059

245. Hooper, L. V., Xu, J., Falk, P. G., Midtvedt, T., and Gordon, J. I. (1999) A molecular sensor that allows a gut commensal to control its nutrient foundation in a competitive ecosystem. *Proc. Natl. Acad. Sci. U. S. A.* **96**, 9833–9838

246. Reizer, A., Deutscher, J., Saier, M. H., and Reizer, J. (1991) Analysis of the gluconate gnt operon of *Bacillus* subtilis. *Mol. Microbiol.* **5**, 1081–1089

247. Romero-Rodríguez, A., Rocha, D., Ruiz-Villafán, B., Guzmán-Trampe, S., Maldonado-Carmona, N., Vázquez-Hernández, M., Zelarayán, A., Rodríguez-Sanoja, R., and

Sánchez, S. (2017) Carbon catabolite regulation in *Streptomyces*: new insights and lessons learned. *World J. Microbiol. Biotechnol.* **33**, 1–11

248. Weissenborn, D. L., Wittekindtn, N., and Larsonsii, T. J. (1992) Structure and regulation of the *glpFK* operon encoding glycerol. *Biochemistry.* **267**, 6122–6131

249. Novelli, P. C., Masarie, K. A., and Lang, P. M. (1998) Distributions and recent changes of carbon monoxide in the lower troposphere. *J. Geophys. Res. Atmos.* **103**, 19015–19033

250. Chi, X., Winderlich, J., Mayer, J. C., Panov, A. V., Heimann, M., Birmili, W., Heintzenberg, J., Cheng, Y., and Andreae, M. O. (2013) Long-term measurements of aerosol and carbon monoxide at the ZOTTO tall tower to characterize polluted and pristine air in the Siberian taiga. *Atmos. Chem. Phys.* **13**, 12271–12298

251. Petrenko, V. V., Martinerie, P., Novelli, P., Etheridge, D. M., Levin, I., Wang, Z., Blunier, T., Chappellaz, J., Kaiser, J., Lang, P., Steele, L. P., Hammer, S., Mak, J., Langenfelds, R. L., Schwander, J., Severinghaus, J. P., Witrant, E., Petron, G., Battle, M. O., Forster, G., Sturges, W. T., Lamarque, J. F., Steffen, K., and White, J. W. C. (2013) A 60 yr record of atmospheric carbon monoxide reconstructed from Greenland firn air. *Atmos. Chem. Phys.* **13**, 7567–7585

252. Bartholomew, G. W., and Alexander, M. (1981) Soil as a sink for atmospheric carbon monoxide. *Appl. Environ. Microbiol.* **212**, 1389–1391

253. Inman, R. E., Ingersoll, R. B., and Levy, E. A. (2011) Soil : A natural sink for carbon monoxide. *Science.* **172**, 1229–1231

254. Kirschke, S., Bousquet, P., Ciais, P., Saunois, M., Canadell, J. G., Dlugokencky, E. J., Bergamaschi, P., Bergmann, D., Blake, D. R., Bruhwiler, L., Cameron-Smith, P., Castaldi, S., Chevallier, F., Feng, L., Fraser, A., Heimann, M., Hodson, E. L., Houweling, S., Josse, B., Fraser, P. J., Krummel, P. B., Lamarque, J. F., Langenfelds, R. L., Le Quéré, C., Naik, V., O'doherty, S., Palmer, P. I., Pison, I., Plummer, D., Poulter, B., Prinn, R. G., Rigby, M., Ringeval, B., Santini, M., Schmidt, M., Shindell, D. T., Simpson, I. J., Spahni, R., Steele, L. P., Strode, S. A., Sudo, K., Szopa, S., Van Der Werf, G. R., Voulgarakis, A., Van Weele, M., Weiss, R. F., Williams, J. E., and Zeng, G. (2013) Three decades of global methane sources and sinks. *Nat. Geosci.* **6**, 813–823

255. Swinnerton, A. J. W., Linnenbom, V. J., and Lamontagne, R. A. (1970) The Ocean : A natural source of carbon monoxide. *Science.* **167**, 984–986

256. Xie, H., Bélanger, S., Demers, S., Vincent, W. F., and Papakyriakou, T. N. (2009) Photobiogeochemical cycling of carbon monoxide in the southeastern Beaufort Sea in spring and autumn. *Limnol. Oceanogr.* **54**, 234–249

257. Zafiriou, O. C., Andrews, S. S., and Wang, W. (2003) Concordant estimates of oceanic

carbon monoxide source and sink processes in the Pacific yield a balanced global "blue-water" CO budget. *Global Biogeochem. Cycles*. 10.1029/2001GB001638

258. Zavarzin, G. A., and Nozhevnikova, A. N. (1977) Aerobic carboxydobacteria. *Microb. Ecol.* **3**, 305–326

259. Lorite, M. J., Tachil, J., Sanjuán, J., Meyer, O., and Bedmar, E. J. (2000) Carbon monoxide dehydrogenase activity in *Bradyrhizobium japonicum*. *Appl. Environ. Microbiol.* **66**, 1871–1876

260. Sorokin, D. Y., Tourova, T. P., Kovaleva, O. L., Kuenen, J. G., and Muyzer, G. (2010) Aerobic carboxydotrophy under extremely haloalkaline conditions in *Alkalispirillum/Alkalilimnicola* strains isolated from soda lakes. *Microbiology*. **156**, 819–827

261. Cypionka, H., Meyer, O., and Schlegel, H. G. (1980) Physiological characteristics of various species of strains of carboxydobacteria. *Arch. Microbiol.* **127**, 301–307

262. Gadkari, D., Schricker, K., Acker, G., Kroppenstedt, R. M., and Meyer, O. (1990) *Streptomyces thermoautotrophicus* sp. nov., a thermophilic CO- and H$_2$-oxidizing obligate chemolithoautotroph. *Appl. Environ. Microbiol.* **56**, 3727–3734

263. Kim, S. B., Falconer, C., Williams, E., and Goodfellow, M. (1998) *Streptomyces thermocarboxydovorans* sp. nov. and *Streptomyces thermocarboxydus* sp. nov., two moderately thermophilic carboxydotrophic species from soil. *Int. J. Syst. Bacteriol.*

264. Krüger, B., and Meyer, O. (1984) Thermophilic Bacilli growing with carbon monoxide. *Arch. Microbiol.* **139**, 402–408

265. Kraut, M., and Meyer, O. (1988) Plasmids in carboxydotrophic bacteria: physical and restriction analysis. *Arch. Microbiol.* **149**, 540–546

266. Meyer, O., and Schlegel, H. G. (1983) Biology of aerobic carbin monoxide bacteria. *Annu. Rev. Microbiol.* **37**, 277–310

267. Conrad, R., Meyer, O., and Seiler, W. (1981) Role of carboxydobacteria in consumption of atmospheric carbon monoxide by soil. *Appl. Environ. Microbiol.* **42**, 211–215

268. Hoeft, S. E., Blum, J. S., Stolz, J. F., Tabita, F. R., Witte, B., King, G. M., Santini, J. M., and Oremland, R. S. (2007) Alkalilimnicola ehrlichii sp. nov., a novel, arsenite-oxidizing haloalkaliphilic gammaproteobacterium capable of chemoautotrophic or heterotrophic growth with nitrate or oxygen as the electron acceptor. *Int. J. Syst. Evol. Microbiol.* **57**, 504–512

269. Weber, C. F., and King, G. M. (2012) The phylogenetic distribution and ecological role of carbon monoxide oxidation in the genus *Burkholderia*. *FEMS Microbiol. Ecol.* **79**, 167–175

270. Weber, C. F., and King, G. M. (2017) Volcanic soils as sources of novel CO-oxidizing *Paraburkholderia* and *Burkholderia*: *Paraburkholderia hiiakae* sp. nov.,

Paraburkholderia metrosideri sp. nov., *Paraburkholderia paradisi* sp. nov., *Paraburkholderia peleae* sp. nov., and *Burkholderia alpina* sp. . *Front. Microbiol.* **8**, 1–10

271. King, G. M. (2015) Carbon monoxide as a metabolic energy source for extremely halophilic microbes: Implications for microbial activity in Mars regolith. *Proc. Natl. Acad. Sci. U. S. A.* **112**, 4465–4470

272. Yano, T., Yoshida, N., and Takagi, H. (2012) Carbon monoxide utilization of an extremely oligotrophic bacterium, *Rhodococcus erythropolis* N9T-4. *J. Biosci. Bioeng.* **114**, 53–55

273. Bartholomew, G. W., and Alexander, M. (1979) Microbial metabolism of carbon monoxide in culture and in soil. *Appl. Environ. Microbiol.* **37**, 932–937

274. King, C. E. (2013) *Diversity and activity of aerobic thermophilic carbon monoxide-oxidizing bacteria on Kilauea volcano, Hawaii*. Ph.D. thesis, Louisiana State University, USA

275. King, C. E., and King, G. M. (2014) *Thermomicrobium carboxidum* sp. nov., and *Thermorudis peleae* gen. nov., sp. nov., carbon monoxide-oxidizing bacteria isolated from geothermally heated biofilms. *Int. J. Syst. Evol. Microbiol.* **64**, 2586–2592

276. Wu, D., Raymond, J., Wu, M., Chatterji, S., Ren, Q., Graham, J. E., Bryant, D. A., Robb, F., Colman, A., Tallon, L. J., Badger, J. H., Madupu, R., Ward, N. L., and Eisen, J. A. (2009) Complete genome sequence of the aerobic CO-oxidizing thermophile *Thermomicrobium roseum*. *PLoS One*. 10.1371/journal.pone.0004207

277. King, C. E., and King, G. M. (2014) Description of *Thermogemmatispora carboxidivorans* sp. nov., a carbon-monoxideoxidizing member of the class Ktedonobacteria isolated from a geothermally heated biofilm, and analysis of carbon monoxide oxidation by members of the class Ktedonobacteria. *Int. J. Syst. Evol. Microbiol.* **64**, 1244–1251

278. Nishimura, H., Nomura, Y., Iwata, E., Sato, N., and Sako, Y. (2010) Purification and characterization of carbon monoxide dehydrogenase from the aerobic hyperthermophilic archaeon *Aeropyrum pernix*. *Fish. Sci.* **76**, 999–1006

279. Sokolova, T. G., Yakimov, M. M., Chernyh, N. A., Lun'kova, E. Y., Kostrikina, N. A., Taranov, E. A., Lebedinskii, A. V., and Bonch-Osmolovskaya, E. A. (2017) Aerobic carbon monoxide oxidation in the course of growth of a hyperthermophilic archaeon, *Sulfolobus* sp. ETSY. *Microbiol. (Russian Fed.* **86**, 539–548

280. McDuff, S., King, G. M., Neupane, S., and Myers, M. R. (2016) Isolation and characterization of extremely halophilic CO-oxidizing Euryarchaeota from hypersaline cinders, sediments and soils and description of a novel CO oxidizer, *Haloferax namakaokahaiae* Mke2.3T, sp. nov. *FEMS Microbiol. Ecol.* **92**, 1–8

281. Delgado-Baquerizo, M., Oliverio, A. M., Brewer, T. E., Benavent-gonzález, A., Eldridge, D. J., Bardgett, R. D., Maestre, F. T., Singh, B. K., and Fierer, N. (2018) Bacteria found in soil. *Science.* **325**, 320–325

282. Walsh, C. M., Gebert, M. J., Delgado-Baquerizo, M., Maestre, F. T., and Fierer, N. (2019) A global survey of mycobacterial diversity in soil. *bioRxiv*. **85**, 1–14

283. Pruitt, K. D., Tatusova, T., and Maglott, D. R. (2007) NCBI reference sequences (RefSeq): A curated non-redundant sequence database of genomes, transcripts and proteins. *Nucleic Acids Res.* **35**, 61–65

284. Altschul, S. F., Gish, W., Miller, W., Myers, E. W., and Lipman, D. J. (1990) Basic local alignment search tool. *J. Mol. Biol.* **215**, 403–410

285. Kumar, S., Stecher, G., and Tamura, K. (2016) MEGA7: Molecular Evolutionary Genetics Analysis Version 7.0 for Bigger Datasets. *Mol. Biol. Evol.* **33**, 1870–1874

286. Markowitz, V. M., Chen, I. M. A., Palaniappan, K., Chu, K., Szeto, E., Grechkin, Y., Ratner, A., Jacob, B., Huang, J., Williams, P., Huntemann, M., Anderson, I., Mavromatis, K., Ivanova, N. N., and Kyrpides, N. C. (2012) IMG: The integrated microbial genomes database and comparative analysis system. *Nucleic Acids Res.* **40**, 115–122

287. Leinonen, R., Sugawara, H., and Shumway, M. (2011) The sequence read archive. *Nucleic Acids Res.* **39**, 2010–2012

288. Patel, R. K., and Jain, M. (2012) NGS QC toolkit: A toolkit for quality control of next generation sequencing data. *PLoS One*. 10.1371/journal.pone.0030619

289. Kopylova, E., Noé, L., and Touzet, H. (2012) SortMeRNA : Fast and accurate filtering of ribosomal RNAs in metatranscriptomic data . To cite this version : HAL Id : hal-00748990 SortMeRNA : Fast and accurate filtering of ribosomal RNAs in metatranscriptomic data. *Bioinformatics*. **00**, 1–7

290. Buchfink, B., Xie, C., and Huson, D. H. (2014) Fast and sensitive protein alignment using DIAMOND. *Nat. Methods*. **12**, 59–60

291. Janssen, P. H. (2006) Identifying the dominant soil bacterial taxa in libraries of 16S rRNA and 16S rRNA Genes. **72**, 1719–1728

292. Fuhrmann, S., Ferner, M., Jeffke, T., Henne, A., Gottschalk, G., and Meyer, O. (2003) Complete nucleotide sequence of the circular megaplasmid pHCG3 of *Oligotropha carboxidovorans*: Function in the chemolithoautotrophic utilization of CO, H_2 and CO_2. *Gene*. **322**, 67–75

293. Pelzmann, A. M., Mickoleit, F., and Meyer, O. (2014) Insights into the posttranslational assembly of the Mo-, S- and Cu-containing cluster in the active site of CO dehydrogenase of *Oligotropha carboxidovorans*. *J. Biol. Inorg. Chem.* **19**, 1399–1414

294. Vorobev, A. V., Baani, M., Doronina, N. V., Brady, A. L., Liesack, W., Dunfield, P. F.,

and Dedysh, S. N. (2011) *Methyloferula stellata* gen. nov., sp. nov., an acidophilic, obligately methanotrophic bacterium that possesses only a soluble methane monooxygenase. *Int. J. Syst. Evol. Microbiol.* **61**, 2456–2463

295. Tveit, A. T., Hestnes, A. G., Robinson, S. L., Schintlmeister, A., Dedysh, S. N., Jehmlich, N., Von Bergen, M., Herbold, C., Wagner, M., Richter, A., and Svenning, M. M. (2019) Widespread soil bacterium that oxidizes atmospheric methane. *Proc. Natl. Acad. Sci. U. S. A.* **116**, 8515–8524

296. Weber, C. F., and King, G. M. (2009) Water stress impacts on bacterial carbon monoxide oxidation on recent volcanic deposits. *ISME J.* **3**, 1325–1334

297. King, G. M. (2007) Microbial carbon monoxide consumption in salt marsh sediments. *FEMS Microbiol. Ecol.* **59**, 2–9

298. Myers, M. R., and King, G. M. (2017) Perchlorate-coupled carbon monoxide (CO) oxidation: Evidence for a plausible microbe-mediated reaction in Martian brines. *Front. Microbiol.* **8**, 1–8

299. Bernhard, M., Benelli, B., Hochkoeppler, A., Zannoni, D., and Friedrich, B. (1997) Functional and structural role of the cytochrome b subunit of the membrane-bound hydrogenase complex of *Alcaligenes eutrophus* H16. *Eur. J. Biochem.* **248**, 179–186

300. Burgdorf, T., Lenz, O., Buhrke, T., Van Der Linden, E., Jones, A. K., Albracht, S. P. J., and Friedrich, B. (2006) [NiFe]-hydrogenases of *Ralstonia eutropha* H16: Modular enzymes for oxygen-tolerant biological hydrogen oxidation. *J. Mol. Microbiol. Biotechnol.* **10**, 181–196

301. Lenz, O., Ludwig, M., Schubert, T., Bürstel, I., Ganskow, S., Goris, T., Schwarze, A., and Friedrich, B. (2010) H_2 conversion in the presence of O_2 as performed by the membrane-bound [NiFe]-Hydrogenase of *Ralstonia eutropha*. *ChemPhysChem*. **11**, 1107–1119

302. Saggu, M., Zebger, I., Ludwig, M., Lenz, O., Friedrich, B., Hildebrandt, P., and Lendzian, F. (2009) Spectroscopic insights into the oxygen-tolerant membrane-associated [NiFe] hydrogenase of *Ralstonia eutropha* H16. *J. Biol. Chem.* **284**, 16264–16276

303. Bay, S. K., Dong, X., Bradley, J. A., Leung, P.-M., Grinter, R., Jirapanjawat, T., Arndt, S. K., Cook, P. L. M., LaRowe, D., Nauer, P. A., Chiri, E., and Greening, C. (2020) Trace gas oxidizers are widespread and active members of soil microbial communities. *Nat. Microbiol.*

304. Beaton, S. E., Evans, R. M., Finney, A. J., Lamont, C. M., Armstrong, F. A., Sargent, F., and Carr, S. B. (2018) The structure of hydrogenase-2 from *Escherichia coli*: Implications for H_2-driven proton pumping. *Biochem. J.* **475**, 1353–1370

305. Pinske, C., Jaroschinsky, M., Linek, S., Kelly, C. L., Sargent, F., and Sawers, R. G.

(2015) Physiology and bioenergetics of [NiFe]-hydrogenase 2-catalyzed H2-consuming and H2-producing reactions in Escherichia coli. *J. Bacteriol.* **197**, 296–306

306. Kublik, A., Deobald, D., Hartwig, S., Schiffmann, C. L., Andrades, A., Bergen, M. von, Sawers, R. G., and Adrian, L. (2016) Identification of a multi-protein reductive dehalogenase complex in *Dehalococcoides mccartyi* strain CBDB1 suggests a protein-dependent respiratory electron transport chain obviating quinone involvement. *Environ. Microbiol.* **18**, 3044–3056

307. Seidel, K., Kühnert, J., and Adrian, L. (2018) The complexome of *Dehalococcoides mccartyi* reveals its organohalide respiration-complex is modular. *Front. Microbiol.* **9**, 1–14

308. Zhang, C., and Anderson, A. J. (2013) Utilization of pyrene and benzoate in *Mycobacterium* isolate KMS is regulated differentially by catabolic repression. *J. Basic Microbiol.* **53**, 81–92

309. De Carvalho, L. P. S., Fischer, S. M., Marrero, J., Nathan, C., Ehrt, S., and Rhee, K. Y. (2010) Metabolomics of *Mycobacterium tuberculosis* reveals compartmentalized co-catabolism of carbon substrates. *Chem. Biol.* **17**, 1122–1131

310. Kayali, H. A., Tarhan, L., Sazak, A., and Sahin, N. (2011) Carbohydrate metabolite pathways and antibiotic production variations of a novel *Streptomyces* sp. M3004 depending on the concentrations of carbon sources. *Appl. Biochem. Biotechnol.* **165**, 369–381

311. Brawner, M. E., Mattern, S. G., Babcock, M. J., and Westpheling, J. (1997) The *Streptomyces* galP1 promoter has a novel RNA polymerase recognition sequence and is transcribed by a new form of RNA polymerase in vitro. *J. Bacteriol.* **179**, 3222–3231

312. Ruiz, B., Chávez, A., Forero, A., García-Huante, Y., Romero, A., Snchez, M., Rocha, D., Snchez, B., Rodríguez-Sanoja, R., Sánchez, S., and Langley, E. (2010) Production of microbial secondary metabolites: Regulation by the carbon source. *Crit. Rev. Microbiol.* **36**, 146–167

313. Romero-Rodríguez, A., Ruiz-Villafán, B., Tierrafría, V. H., Rodríguez-Sanoja, R., and Sánchez, S. (2016) Carbon catabolite regulation of secondary metabolite formation and morphological differentiation in *Streptomyces coelicolor*. *Appl. Biochem. Biotechnol.* **180**, 1152–1166

314. Seo, J. W., Ohnishi, Y., Hirata, A., and Horinouchi, S. (2002) ATP-binding cassette transport system involved in regulation of morphological differentiation in response to glucose in *Streptomyces griseus*. *J. Bacteriol.* **184**, 91–103

315. Pimentel-Schmitt, E. F., Thomae, A. W., Amon, J., Klieber, M. A., Roth, H. M., Muller, Y. A., Jahreis, K., Burkovski, A., and Titgemeyer, F. (2006) A glucose kinase from *Mycobacterium smegmatis*. *J. Mol. Microbiol. Biotechnol.* **12**, 75–81

316. Dass, B. K. M., Sharma, R., Shenoy, A. R., Mattoo, R., and Visweswariah, S. S. (2008) Cyclic AMP in mycobacteria: Characterization and functional role of the Rv1647 ortholog in *Mycobacterium smegmatis*. *J. Bacteriol.* **190**, 3824–3834

317. Aung, H. L., Dixon, L. L., Smith, L. J., Sweeney, N. P., Robson, J. R., Berney, M., Buxton, R. S., Green, J., and Cook, G. M. (2015) Novel regulatory roles of cAMP receptor proteins in fast-growing environmental mycobacteria. *Microbiol. (United Kingdom)*. **161**, 648–661

318. Sharma, R., Zaveri, A., Gopalakrishnapai, J., Thiruneelakantan, S., Varshney, U., and Visweswariah, S. S. (2014) Paralogous cAMP receptor proteins in *Mycobacterium smegmatis* show biochemical and functional divergence. *Biochemistry*. **53**, 7765–7776

319. Warner, J. B., and Lolkema, J. S. (2003) CcpA-Dependent Carbon Catabolite Repression in Bacteria. *Microbiol. Mol. Biol. Rev.* **67**, 475–490

320. Griffin, J. E., Gawronski, J. D., DeJesus, M. A., Ioerger, T. R., Akerley, B. J., and Sassetti, C. M. (2011) High-resolution phenotypic profiling defines genes essential for mycobacterial growth and cholesterol catabolism. *PLoS Pathog.* **7**, 1–9

321. Kana, B. D., Gordhan, B. G., Downing, K. J., Sung, N., Vostroktunova, G., Machowski, E. E., Tsenova, L., Young, M., Kaprelyants, A., Kaplan, G., and Mizrahi, V. (2008) The resuscitation-promoting factors of *Mycobacterium tuberculosis* are required for virulence and resuscitation from dormancy but are collectively dispensable for growth in vitro. *Mol. Microbiol.* **67**, 672–684

322. Wuest, S. (2014) Seasonal variation in soil organic carbon. *Soil Sci. Soc. Am. J.* **78**, 1442–1447

323. Ontl, T. A., and Schulte, L. A. (2012) Fundamentals of soil organic carbon soil carbon storage. *Nat. Educ. Knowl.* **3**, 35

324. Jordaan, K., Lappan, R., Dong, X., Aitkenhead, I. J., Bay, S. K., Chiri, E., Wieler, N., Meredith, L. K., Cowan, D. A., Chown, S. L., and Greening, C. (2020) Hydrogen-oxidizing bacteria are abundant in desert soils and strongly stimulated by hydration. *mSystems*. **5**, 1–19

325. Lee, J. H., Park, D. O., Park, S. W., Hwang, E. H., Oh, J. Il, and Kim, Y. M. (2009) Expression and regulation of ribulose 1,5-bisphosphate carboxylase/oxygenase genes in *Mycobacterium* sp. strain JC1 DSM 3803. *J. Microbiol.* **47**, 297–307

326. Park, S. W., Hwang, E. H., Jang, H. S., Lee, J. H., Kang, B. S., Oh, J. Il, and Kim, Y. M. (2009) Presence of duplicate genes encoding a phylogenetically new subgroup of form I ribulose 1,5-bisphosphate carboxylase/oxygenase in *Mycobacterium* sp. strain JC1 DSM 3803. *Res. Microbiol.* **160**, 159–165

327. Tiago, I., Alarico, S., Maranha, A., Coelho, C., Pereira, S. G., and Empadinhas, N. (2019) High-quality draft genome sequences of rare nontuberculous *Mycobacteria*

isolated from surfaces of a Hospital. *Microbiol. Resour. Announc.* **8**, 23–25

328. Vansuch, G. E., Wu, C.-H., Haja, D. K., Blair, S. A., Chica, B., Johnson, M. K., Adams, M. W. W., and Dyer, R. B. (2020) Metal–ligand cooperativity in the soluble hydrogenase-1 from Pyrococcus *furiosus* . *Chem. Sci.* **11**, 8572–8581

329. Fan, Q., Neubauer, P., Lenz, O., and Gimpel, M. (2020) Heterologous hydrogenase overproduction systems for biotechnology—an overview. *Int. J. Mol. Sci.* **21**, 1–25

330. Lenz, O., Gleiche, A., Strack, A., and Friedrich, B. (2005) Requirements for heterologous production of a complex metalloenzyme: The membrane-bound [NiFe] hydrogenase. *J. Bacteriol.* **187**, 6590–6595

331. Kim, J. Y. H., Jo, B. H., and Cha, H. J. (2010) Production of biohydrogen by recombinant expression of [NiFe]-hydrogenase 1 in *Escherichia coli*. *Microb. Cell Fact.* **9**, 1–10

332. Sun, J., Hopkins, R. C., Jenney, F. E., McTernan, P. M., and Adams, M. W. W. (2010) Heterologous expression and maturation of an NADP-dependent [NiFe]-Hydrogenase: A key enzyme in biofuel production. *PLoS One*. 10.1371/journal.pone.0010526

333. Flanagan, L. A., and Parkin, A. (2016) Electrochemical insights into the mechanism of NiFe membrane-bound hydrogenases. *Biochem. Soc. Trans.* **44**, 315–328

334. Mills, D. J., Vitt, S., Strauss, M., Shima, S., and Vonck, J. (2013) De novo modeling of the F_{420}-reducing [NiFe]-hydrogenase from a methanogenic archaeon by cryo-electron microscopy. *Elife*. **2013**, 1–21

335. Allegretti, M., Mills, D. J., McMullan, G., Kühlbrandt, W., and Vonck, J. (2014) Atomic model of the F_{420}-reducing [NiFe] hydrogenase by electron cryo-microscopy using a direct electron detector. *Elife*. **3**, 1–20

336. Sapra, R., Verhagen, M. F. J. M., and Adams, M. W. W. (2000) Purification and characterization of a membrane-bound hydrogenase from the hyperthermophilic archaeon *Pyrococcus furiosus*. *J. Bacteriol.* **182**, 3423–3428

337. Marreiros, B. C., Batista, A. P., Duarte, A. M. S., and Pereira, M. M. (2013) A missing link between complex i and group 4 membrane-bound [NiFe] hydrogenases. *Biochim. Biophys. Acta - Bioenerg.* **1827**, 198–209

338. Tersteegen, A., and Hedderich, R. (1999) Methanobacterium thermoautotrophicum encodes two multisubunit membrane- bound [NiFe] hydrogenases. Transcription of the operons and sequence analysis of the deduced proteins. *Eur. J. Biochem.* **264**, 930–943

339. Park, S. W., Song, T., Kim, S. Y., Kim, E., Oh, J. Il, Eom, C. Y., and Kim, Y. M. (2007) Carbon monoxide dehydrogenase in mycobacteria possesses a nitric oxide dehydrogenase activity. *Biochem. Biophys. Res. Commun.* **362**, 449–453

340. Furchgott, R. F., and Jothianahdan, D. (1991) Endothelium-dependent and -independent vasodilation involving cyclic GMP: Relaxation induced by nitric oxide,

carbon monoxide and light. *Blood Vessels*. **28**, 52–61

341. Rinaldo, S., Giardina, G., Mantoni, F., Paone, A., and Cutruzzolà, F. (2018) Beyond nitrogen metabolism: Nitric oxide, cyclic-di-GMP and bacterial biofilms. *FEMS Microbiol. Lett.* **365**, 1–9

342. Barraud, N., Schleheck, D., Klebensberger, J., Webb, J. S., Hassett, D. J., Rice, S. A., and Kjelleberg, S. (2009) Nitric oxide signaling in *Pseudomonas aeruginosa* biofilms mediates phosphodiesterase activity, decreased cyclic di-GMP levels, and enhanced dispersal. *J. Bacteriol.* **191**, 7333–7342

343. Simm, R., Morr, M., Kader, A., Nimtz, M., and Römling, U. (2004) GGDEF and EAL domains inversely regulate cyclic di-GMP levels and transition from sessibility to motility. *Mol. Microbiol.* **53**, 1123–1134

344. Thormann, K. M., Duttler, S., Saville, R. M., Hyodo, M., Shukla, S., Hayakawa, Y., and Spormann, A. M. (2006) Control of formation and cellular detachment from *Shewanella oneidensis* MR-1 biofilms by cyclic di-GMP. *J. Bacteriol.* **188**, 2681–2691

345. Ueda, A., and Wood, T. K. (2009) Connecting quorum sensing, c-di-GMP, pel polysaccharide, and biofilm formation in *Pseudomonas aeruginosa* through tyrosine phosphatase TpbA (PA3885). *PLoS Pathog.* **5**, 1–15

346. Ryan, R. P., Fouhy, Y., Lucey, J. F., and Dow, J. M. (2006) Cyclic di-GMP signaling in bacteria: Recent advances and new puzzles. *J. Bacteriol.* **188**, 8327–8334

347. Hong, Y., Zhou, X., Fang, H., Yu, D., Li, C., and Sun, B. (2013) Cyclic di-GMP mediates *Mycobacterium tuberculosis* dormancy and pathogenecity. *Tuberculosis*. **93**, 625–634

348. Zhang, H. N., Xu, Z. W., Jiang, H. W., Wu, F. L., He, X., Liu, Y., Guo, S. J., Li, Y., Bi, L. J., Deng, J. Y., Zhang, X. E., and Tao, S. C. (2017) Cyclic di-GMP regulates *Mycobacterium tuberculosis* resistance to ethionamide. *Sci. Rep.* **7**, 1–12

349. Sharma, I. M., Prakash, S., Dhanaraman, T., and Chatterji, D. (2014) Characterization of a dual-active enzyme, DcpA, Involved in cyclic diguanosine monophosphate turnover in *Mycobacterium smegmatis*. *Microbiol. (United Kingdom)*. **160**, 2304–2318

350. Bharati, B. K., Sharma, I. M., Kasetty, S., Kumar, M., Mukherjee, R., and Chatterji, D. (2012) A full-length bifunctional protein involved in c-di-GMP turnover is required for long-term survival under nutrient starvation in *Mycobacterium smegmatis*. *Microbiol. (United Kingdom)*. **158**, 1415–1427

351. Li, W., and He, Z. G. (2012) LtmA, a novel cyclic di-GMP-responsive activator, broadly regulates the expression of lipid transport and metabolism genes in *Mycobacterium smegmatis*. *Nucleic Acids Res.* **40**, 11292–11307

352. Flynn, J. L., and Chan, J. (2001) Tuberculosis: Latency and reactivation minireview. *Infect. Immun.* **69**, 4195–4201

353. Vijayan, V., Wagener, F. A. D. T. G., and Immenschuh, S. (2018) The macrophage

heme-heme oxygenase-1 system and its role in inflammation. *Biochem. Pharmacol.* **153**, 159–167

354. Zacharia, V. M., and Shiloh, M. U. (2012) Effect of carbon monoxide on *Mycobacterium tuberculosis* pathogenesis. *Med. Gas Res.* **2**, 30

355. Shiloh, M. U., Manzanillo, P., and Cox, J. S. (2008) *Mycobacterium tuberculosis* senses host-derived carbon monoxide during macrophage infection. *Cell Host Microbe.* **3**, 323–330

356. Vega-lópez, F. (2012) *Mycobacterium marinum Infection: Fish Tank Granuloma*, 10th Ed. (Ryan, E. T., Hill, D. R., Solomon, T., Aronson, N. E., and Endy, T. P. eds), Elsevier Inc., 10.1016/B978-0-323-55512-8.00064-8

357. Parikka, M., Hammarén, M. M., Harjula, S. K. E., Halfpenny, N. J. A., Oksanen, K. E., Lahtinen, M. J., Pajula, E. T., Iivanainen, A., Pesu, M., and Rämet, M. (2012) *Mycobacterium marinum* causes a latent infection that can be reactivated by gamma irradiation in adult zebrafish. *PLoS Pathog.* 10.1371/journal.ppat.1002944

358. Parks, D. H., Chuvochina, M., Waite, D. W., Rinke, C., Skarshewski, A., Chaumeil, P.-A., and Hugenholtz, P. (2018) A standardized bacterial taxonomy based on genome phylogeny substantially revises the tree of life. *Nat. Biotechnol.* **36**, 996–1004

359. Song, T., Park, S. W., Park, S. J., Kim, J. H., Yu, J. Y., Oh, J., and Kim, Y. M. (2010) Cloning and expression analysis of the duplicated genes for carbon monoxide dehydrogenase of *Mycobacterium* sp. strain JC1 DSM 3803. *Microbiology*. **156**, 999–1008

360. Neumann, M., and Leimkühler, S. (2011) The role of system-specific molecular chaperones in the maturation of molybdoenzymes in bacteria. *Biochem. Res. Int.* **850924**, 1–13